Stimuli-Sensitive Hydrogel Materials for Sensing and Drug Delivery

by

Nicky Mac Kenna B.Sc.

Thesis Submitted for the Degree of Doctor of Philosophy

Supervisor:

Dr. Aoife Morrin

School of Chemical Sciences

Sept 2015

Declaration:

I hereby certify that this material, which I now submit for assessment on the programme of study leading to the award of PhD, is entirely my own work, that I have exercised reasonable care to ensure that the work is original, and does not to the best of my knowledge breach any law of copyright, and has not been taken from the work of others save and to the extent that such work has been cited and acknowledged within the text of my work.

Signed: _____

(Candidate) ID No.: _____

Date: _____

Table of Contents

Chapter 2

Impedimetric Transduction of Swelling in Glucose-Sensitive Hydrogels

Chapter 3

Impedimetric Transduction of Swelling for Detection of β-D-glucuronidase

Chapter 4

Electro-Stimulated Release from a Reduced Graphene Oxide Composite Hydrogel

Abbreviations

ΔEp	peak potential separation
ϕ	phase curve
4-MUG	4-methylumbelliferyl-β-D-glucuronide
4-NP	4-nitrophenol
4-NPG	4-nitrophenol-β-D-glucuronide
A	electrode area
AA	acrylic acid
AAPBA	3-acrylamidophenylboronic acid
Ab	antibody
Ag	antigen
AuNPs	gold nanoparticles
Ag/AgCl	silver/silver chloride
ANOVA	analysis of variance
BSA	bovine serum albumin
C	concentration of redox active species in bulk solution
C.albicans	candida albicans
CFU	colony forming units
CNTs	carbon nanotubes

CPE	constant phase element
CV	cyclic voltammetry
D	diffusion coefficient
DI	deionised
ECHs	electroconductive hydrogels
E.coli	escherichia coli
EIS	electrochemical impedance spectroscopy
Ep	peak potential
Epa	anodic peak potential
Epc	cathodic peak potential
EPA	environmental protection agency
FAD	flavin adenine dinucleotide
GO	graphene oxide
GOx	glucose oxidase
GUS	β-D-glucuronidase
HA	hyaluronic acid
HARC	hexaaminеruthenium (III) chloride
HRP	horse-radish peroxidase
ICPs	inherently conducting polymers

IgG	immunoglobulin G
$i_{p,a}$	anodic peak current
$i_{p,c}$	cathodic peak current
ISF	interstitial fluid
LCST	lower critical solution temperature
LOx	lactate oxidase
M	length of the elastic chains
MA	maleic acid
MEMS	microelectromechanical systems
Mn	number average molecular weight
MO	methyl orange
n	number of electrons transferred
NIPAM	N-isopropylacrylamide
NSAIDS	non-steroidal anti-inflammatory drugs
OCP	open circuit potential
OEGMA	oligo(ethylene glycol) methacrylate
PAA	poly(acrylic acid)
PAAm	poly(acrylamide)
PBS	phosphate buffer saline

PC	photonic crystal
PEG	poly(ethylene glycol)
PEGDA	poly(ethylene glycol) diacrylate
PEGDGE	poly(ethylene glycol) diglycidyl ether
PEGDMA	poly (ethylene glycol)-dimethacrylate
PEGMA	poly(ethylene glycol) methyl ether methacrylate
pHEMA	poly(hydroxyethylmethacrylate)
pMMA	poly(methyl methacrylate)
PPy	polypyrrole
PVA	poly(vinyl alcohol)
PVI-dmeOs	poly(vinylimidazole)- $Os(4,4'\text{-dimethylbpy})_2Cl$
PVME	poly(vinyl methyl ether)
Q	equilibrium swelling degree
QCM	quartz crystal microbalance
rGO	reduced graphene oxide
Rcc	carbon cloth resistance
R_{ct}	electron transfer resistance
Rgel	gel resistance
Rs	solution resistance

S.aureus	staphylococcus aureus
SEM	scanning electron microscope
SDS	sodium n-dodecyl sulfonate
SPHs	superporous hydrogels
SPRi	surface plasmon resonance imaging
TEGDA	tetraethylene glycol diacrylate
UCST	upper critical solution temperature
υ	scan rate
V_O	volume of dry polymer network
Wdry	weight of gel dry
Wwet	weight of gel after immersion in solution
Z	total impedance

Acknowledgments

First and foremost I would like to thank my supervisor Dr. Aoife Morrin for her consistent support, guidance, enthusiasm and sense of humour throughout the past few years. Thank you for all the opportunities you afforded me, especially all the great trips away!

I would like to thank the Irish Research Council without whose financial support I would not have been able to pursue my research.

I was lucky to spend some time in the Intelligent Polymer Research Institute in Wollongong and wish to thank everyone that made this a possibility, especially Prof. Simon Moulton. Thanks to everyone I met over there that made my trip even more enjoyable.

I am grateful to the chemistry department in DCU, especially the technical staff, who I could always count on for help. I would like to thank my lab buddies over the past few years for their advice, support and putting up with all my music choices.

I must say a huge thank you to all my postgrad friends for all the laughs and support during my time in DCU- especially Brian, Orla, Leeanne, Sean and Dr. Boss. Thanks for being there throughout the highs and lows. I'll miss our long lunches (particularly bar Fridays), DVD nights and sneaky midweek McGowans!

I would also like to thank my family for their support and everything they've done for me throughout my many years in college.

A special thanks to Dave for all his patience, encouragement and love. Thanks for always being there, listening to my rants and our weekly Eddie Rockets. I can't thank you enough for all you've done.

List of Publications and Presentations

Publications

- N. Mac Kenna, P. Calvert, A. Morrin, G. G. Wallace and S. E. Moulton, *Electro-stimulated release from a reduced graphene oxide composite hydrogel*, J. Mater. Chem. B, 2015, 3, 2530-2537.
- N. Mac Kenna, P. Calvert, A. Morrin, *Impedimetric transduction of swelling in pH-responsive hydrogels*, Analyst, 2015, 140(9), 3003-3011.
- N. Mac Kenna, A. Morrin, *Detection of β-D-glucuronidase based on pH-sensitive hydrogel swelling*, 2015 (manuscript in preparation for Biosensors and Bioelectronics).
- N. Mac Kenna, A. Morrin, *Development of a pH-sensitive superporous hydrogel prepared via the catalytic decomposition of H_2O_2 by Ag nanoparticles*, 2015 (manuscript in preparation for RSC Advances).

Oral presentations

- *Development of a Hydrogel-based Impedimetric Biosensor*, COST Action Meeting (IC1208: *Integrating devices and materials: a challenge for new instrumentation in ICT*), Santarém, Portugal, March 2014.
- *Development of an Impedimetric Biosensor Based on the Swelling Response of a Hydrogel*, 9th Postgraduate Research Topics Meeting in Electroanalysis and Sensing, London, England, November 2014.
- *Electrically Controlled Drug Delivery from a Reduced Graphene Oxide Composite Hydrogel*, 16th Topical ISE Meeting, Angra dos Reis, Brazil, March 2015.

Poster presentations

- *Development of a Rigid Conducting Polymer Epoxy Composite for Use as a Robust Sensor Transducer,* Smart Surfaces 2012, Dublin, Ireland, March 2012.
- *Fabrication and Characterisation of Glucose-Sensitive Hydrogels***,** 17th EuroAnalysis 2013, Warsaw, Poland, August 2013**.**
- *Electrochemical Impedimetric Biosensor: Swelling Response of a pH Sensitive Hydrogel*, Biosensors 2014, Melbourne, Australia, May 2014.

Abstract

The application of stimuli-sensitive hydrogels in the fabrication of smart devices has become increasingly popular with many research groups and industries. In addition to their ability to experience large reversible transitions in their swelling behaviour due to small physiological or environmental changes, they are also often highly biocompatible, versatile and possess a high storage capacity for the immobilisation of biomolecules. Several transduction methods are currently employed for monitoring the swelling response of these materials, frequently these are based on optical and mechanical methods. Electrochemical transduction has not been investigated as thoroughly but would offer significant benefits in terms of direct coupling with microelectronics, reliability and the possibility of mass production of low-cost disposable electrode devices amenable to miniaturisation. This work demonstrates that electrochemical impedance spectroscopy can be used to track hydrogel swelling in response to target analytes. Highly sensitive detection was achieved based on resistance changes of a pH-sensitive hydrogel in response to glucose. As it demonstrated good potential as a sensing platform, the applicability of this system for detecting other analytes which can elicit a pH change and are challenging in terms of limit of detection requirements was subsequently investigated. The hydrogel was modified to detect β-D-glucuronidase, a marker compound for *E.coli*.

Intelligent materials are also highly desirable for controlled drug delivery applications. In comparison with traditional routes of drug administration (i.e. oral and injection methods), on-demand drug delivery offers safer, more effective medical treatment by enabling site-specific administration with on-off regulation in real time. Consequently, the synthesis and characterisation of a novel electroactive hydrogel

composite and its potential application in electro-stimulated drug delivery were explored.

Finally, numerous strategies were investigated to improve the swelling rate to overcome the slow response time associated with the hydrogel system. A new fabrication route for superporous hydrogels was investigated and shown for the first time to be a viable synthesis method for hydrogel systems which may be limited by pH or templating restrictions. A dramatic reduction in response time, from hours to seconds, was demonstrated. If coupled with impedimetric transduction, rapid, highly sensitive analyte detection could be achieved which would offer significant benefits and advance the application of hydrogels in smart devices.

Chapter 1

Stimuli-Sensitive Hydrogels in Sensing and Drug Delivery

1.1 Hydrogels: General introduction

Hydrogels were first introduced in 1960 in a seminal paper by Wichterle and Lim as novel biomaterials for ophthalmology [1]. They are three-dimensional polymeric networks capable of absorbing large amounts of water whilst maintaining structural stability. It has previously been stated that a hydrogel can imbibe a water content up to 99% of its dry weight, and swell greater than 10 times in volume, without dissolution [2]. Due to their high water content and unique swelling properties, hydrogels are soft, pliable materials which often exhibit excellent biocompatibility. They possess many biological traits resembling natural living tissue both compositionally and mechanically [3]. Throughout the past few decades, application of these impressive materials has rapidly expanded to areas including sensing, drug delivery, tissue engineering and regenerative medicine.

Upon immersion into an aqueous environment the polymer network will imbibe water until it reaches a swollen equilibrium state, whereby the osmotic force solvating the repeating units of the macromolecular chains is counter-balanced by the elastic force of the cross-linked structure. The presence of chemical or physical cross-links in the network structure are essential in retaining the three-dimensional integrity of the swollen polymer network. In chemically cross-linked hydrogels, cross-linking agents are utilised to covalently bind the polymer chains. Once formed, these gels possess permanent properties (shape, size etc.) and are no longer soluble. Alternatively, in physically cross-linked hydrogels polymer chains are held together via non-covalent interactions such as hydrogen bonding, hydrophobic interactions, van der Waals forces, chain entanglements and ionic interactions. Consequently physically cross-linked gels can undergo conformational changes and possess sol-gel reversibility [4-6]. This means that these polymers can display liquid or solid behaviour depending

on environmental conditions. For example, monomers containing hydrophobic groups, such as N-isopropylacrylamide (NIPAM), will aggregate above a certain temperature and dissolve below that temperature generating a phase transition from a hydrogel to a hydrosol (no cross-linking). These polymers are generally non-toxic and formed under milder reaction conditions, favouring them when polymerisation is required *in situ* such as injectable hydrogel formulations used in biomedical applications. However, they are typically mechanically weaker than chemically cross-linked gels and external environmental changes may cause undesired network disruption [7-9].

Several alternative classifications of hydrogels exist. These include categorisation according to source: natural or synthetic; method of preparation: homopolymers, copolymers or interpenetrating polymers; ionic charge: non-ionic or ionic (anionic, cationic or ampholytic); biodegradability: non-biodegradable or biodegradable and physical properties: stimulus-sensitive or –insensitive [10, 11].

Synthesis of chemically cross-linked hydrogels is primarily based upon the reaction of hydrophilic monomers, initiators and crosslinkers. Common methods of preparation involve copolymerisation or free radical polymerisation using monomers such as polyethylene glycol, acrylic acid and methacrylic acid. Aqueous solutions, such as water, are commonly used as diluents to control the heat of polymerisation and the final hydrogel properties [12]. The connecting of the macromolecular chains together to form a progressively larger branched polymer is referred to as gelation and the ‘gel point’ is the first appearance of this structure. Choice of monomer, cross-linker, ratio of monomer to cross-linker, reaction time and reaction temperature are all important factors in determining the overall properties of the hydrogel and are therefore selected carefully to tailor gels for specialised applications [13]. Recently, hybrid gel materials have been synthesised to confer unique properties.

Functionalising the polymer backbone with complementary pairs can be used to generate self-assembling affinity hydrogels based on specific interactions between antibody-antigen, aptamer-substrate and peptide-peptide pairs [14-16]. A highly selective swelling response can be induced due to competitive binding upon exposure to unbound species. Ionogels can be produced by generating the polymer network in the presence of an ionic liquid to alter the viscosity, density or conductivity of the resulting network [17]. Many other types of gels exist including organogels [18], xerogels [19] and aerogels [20].

The swelling behaviour of hydrogel systems is another important factor in hydrogel design. The amount of space in the network structure that can accommodate water dictates the swelling capacity. As hydrophilic monomers are commonly utilised in hydrogel synthesis water uptake occurs firstly at the hydrophilic, polar groups. This causes the network to swell, exposing hydrophobic sites and leading to hydrophobic interactions. Furthermore, if ionic groups are present in the polymer chains the electroneutrality of the hydrogel system with its surrounding solution is disturbed and osmosis is generated by the migration of counter ions into the gel matrix to balance the charge. This osmotic pressure results in additional swelling. Finally, electrostatic forces exerted by adjacent ionised groups generate significant expansions in the network allowing for increased swelling. The swelling is opposed by the elastic retraction force of the chemical and physical cross-linking junctions as depicted in Fig 1.1 [13, 21, 22].

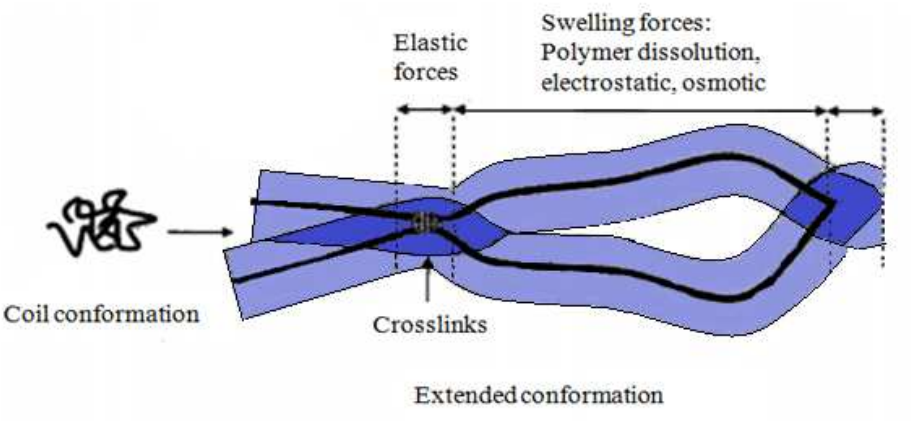

Figure 1.1. Swelling mechanism in hydrogels. Partially redrawn from [13].

Considerable interest has emerged in the area of hydrogel-based drug delivery systems [23-27]. Their three-dimensional structure allows immobilisation of protein, peptide and DNA-based drugs. Hydrogels can be injected at the target site, creating localised drug delivery while their viscoelastic nature minimises damage to the host. After administration, the gel can polymerise *in situ*, with the active reagent incorporated, by environmental stimuli (temperature, pH, light etc.). For example, methylcellulose-based hydrogels are used in *in situ* gelling systems as they aggregate due to hydrophobic interactions between methyl groups upon heating to physiological temperature [28]. Shear-thinning hydrogels can also polymerise *in situ* as they are liquid under shear-stress but self-heal into hydrogels after removal of the stress after injection [29]. Once implanted the hydrogel can swell or biodegrade and release the drug. If cell microencapsulation techniques are utilised the active drug component will be protected from triggering an immune response [10, 30].

The application of hydrogels in the area of tissue engineering is extensive [10, 31-33]. Hydrogels are being investigated as both temporary and permanent solutions

for tissue regeneration and restoration. These gels have a high water content and their permeability allows for the flux of nutrients and excreted metabolites. They possess mechanical strength similar to that of natural tissue and growth factors and other bioactive reagents are often incorporated to aid the proliferation of healthy cells. Tissue scaffolds are also being created using highly porous hydrogels containing living cells or biodegradable hydrogels, including fibrin, collagen and chitosan [13, 21, 34, 35]. Biodegradable hydrogels can be designed to degrade slowly, thereby allowing time for cells to migrate and generate new extracellular matrix, promoting more successful long-term regeneration [36].

Additional biomedical applications include use as soft contact lenses [37], wound dressings [38] and prevention of post-surgical scars [39] due to their biocompatibility, non-antigenic and non-thrombogenic properties. They have been used in arterial [40] and spinal cord repair to bridge the gap between legions [41]. Applications outside the biomedical field are also being explored, such as in the hygiene industry in products like diapers and sanitary towels [42]. This requires hydrogels with fast swelling capabilities and good stability, as well as being low-cost and safe materials. They are also used in the agricultural industry for the controlled release of pesticides and fertilisers [43].

In recent years, hydrogels have received considerable attention as attractive materials in sensing and diagnostic applications. They are frequently employed as a passive support material for the immobilisation of biomaterials. Their 3D matrix increases analyte loading capacity versus 2D immobilisation, whilst providing protection and stability to the active part of the sensor. Sensor components may also be coated with hydrogel to prevent undesirable interactions with proteins, cells and other biological molecules which are too large to penetrate the gel [44]. Alternatively,

their specific properties including swelling, phase transitions and associated properties are also exploited in sensing [45]. These types of hydrogels are classified as stimuli-sensitive or responsive hydrogels and are discussed in detail in the next section.

1.2 Stimuli-sensitive hydrogels in sensing applications

Stimuli-sensitive hydrogels have gained considerable interest over the past few years. Also known as smart or intelligent hydrogels, these gels experience large reversible transitions in their swelling behaviour due to small environmental changes. The hydrogel can be designed to respond to a wide variety of chemical stimuli including pH [46], temperature [47], light [48], specific ions [49], humidity or solvents [50], electric or magnetic fields [51, 52], chemical or biological agents [53] etc. Some hydrogels have multiple sensitivities [54-56]. This induced swelling produces conformational changes which alter many properties of the hydrogel system; including network structure, permeability, refractive index, interfacial tension and mechanical strength [57]. Therefore, stimuli-sensitive hydrogels can sense an external signal, assess it and induce a measureable structural change, thereby displaying sensor, processor and actuator functionalities. This behaviour is extremely attractive in the development of intelligent, selective, low-cost sensing devices.

1.2.1 pH-sensitive hydrogels

pH-sensitive hydrogels are polyelectrolytes that contain weak acidic or weak basic pendant groups in their network structure. These acidic or basic groups can accept or release protons, undergoing ionisation, in response to environmental pH. As previously stated, electrostatic repulsion between adjacent ionised groups and the

osmotic pressure generated by mobile counterions produces an increase in the hydrodynamic volume of the network. The hydrogel can be designed to undergo reversible phase transitions in a desired pH range by selection of an ionisable moiety with a pKa matching this range. In general, pH-sensitive hydrogels cannot be used as universal pH sensors as they typically possess a working range of 2-3 pH units. Richter *et al*. have displayed sensitivity in the order of 10^{-3} to 10^{-5} pH units using a poly(vinyl alcohol)-poly(acrylic acid) (PVA-PAA) hydrogel coated quartz crystal, demonstrating that these hydrogels can be designed for specialised applications [58, 59].

Acidic hydrogels, or anionic hydrogels, are unswollen at low pH as the acidic groups are protonated and unionised. Swelling is initiated when the environmental pH rises above the characteristic pKa of the acidic group and the gel becomes ionised by deprotonation. Alternatively, basic hydrogels, or cationic hydrogels, exhibit the opposite swelling trend. Swelling occurs when the environmental pH falls below the pKa of the cationic groups and the gel is ionised by protonation. Once the hydrogel has reached maximum ionisation the network will stop swelling. Any additional increase in pH will only increase the ionic strength, which will reduce osmotic pressure and result in deswelling or compression of the gel [59]. Examples of acidic polymers are poly(carboxylic acids), poly(acrylic acids) and poly(methacrylic acids) and examples of basic polymers include poly(etheramines), poly(lysine) and chitosan. Amphiphilic hydrogels contain both acidic and basic groups and therefore display two phase transitions as illustrated in Fig 1.2.

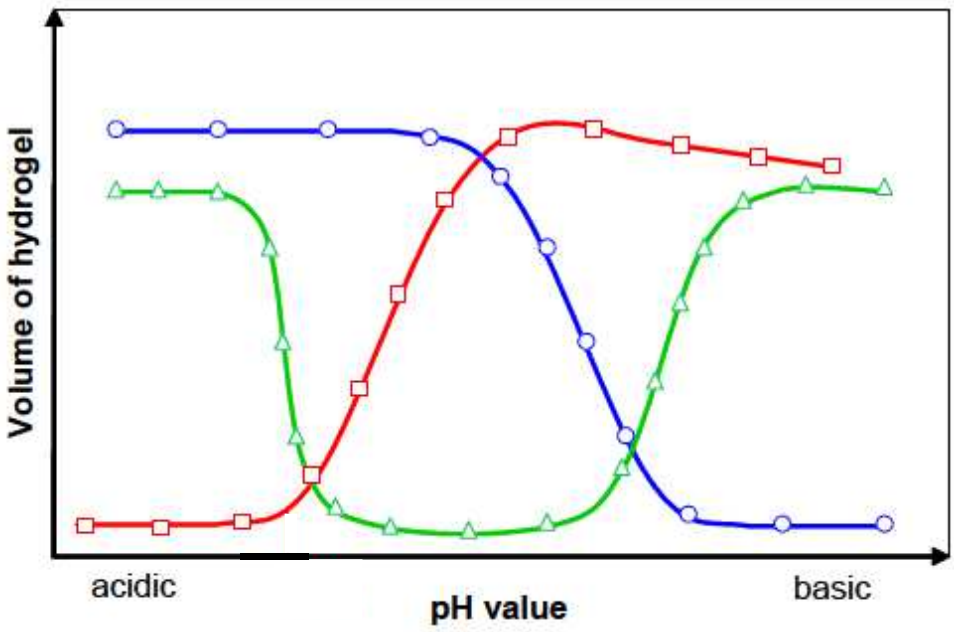

Figure 1.2. Phase transition behaviour of polyelectrolyte hydrogels: Acidic hydrogels (), basic hydrogels () and amphiphilic hydrogels (). Adapted from [59].

Recently, Sun *et al.* [60] reported fabrication of pH gated core-shell hybrid nanoparticles for glucose sensing and controlled insulin release. They utilised a mesoporous silica nanoparticle, as the insulin carrier, coated with a pH-sensitive polymer shell containing 3-acrylamidophenylboronic acid (AAPBA) cross-linked with NIPAM. In aqueous medium phenylboronic acid exists in equilibrium between its charged and uncharged forms. They determined that when environmental pH was near the pKa of the phenylboronic acid, stable phenylborate-glucose complexes were formed. These complexes were anionically charged and as the concentration of glucose was increased, the equilibrium was shifted towards a higher number of charged forms, thereby increasing the hydrophilicity of the gel. This resulted in swelling of the core shell and subsequent insulin release. They observed 20% insulin release at both pH 1.0 and pH 5.0, 33% at pH 6.3, 65% at pH 7.4 and finally, 77% at pH 8.5. Release

rates were seen to increase when the cross-linking was removed from the shell structure.

Herber *et al*. [61] developed a carbon dioxide gas sensor based on the swelling response of a cationic hydrogel. A thin hydrogel layer was encapsulated on a pressure sensor and generated pressure by swelling as the pH decreased upon exposure to CO_2. Changes in the partial pressure of CO_2 as small as 0.5 kPa were detected and the 90% response time was achieved in less than 5 min.

Beebe *et al.* [62] designed a self-regulated valve system inside microfluidic channels for separating solutions according to pH. As shown in Fig 1.3 below, the device consisted of a 'T'-shaped channel with different hydrogels positioned at the entrances to the branches. One hydrogel swells at low pH and contracts at high pH, while the other hydrogel is designed to exhibit the inverse behaviour. Solution flow is then automatically directed down either branch depending on its pH. Both channels can also be sealed in a certain pH range. Therefore, these pH-sensitive hydrogels can sense, actuate and regulate flow which often requires multiple discrete components.

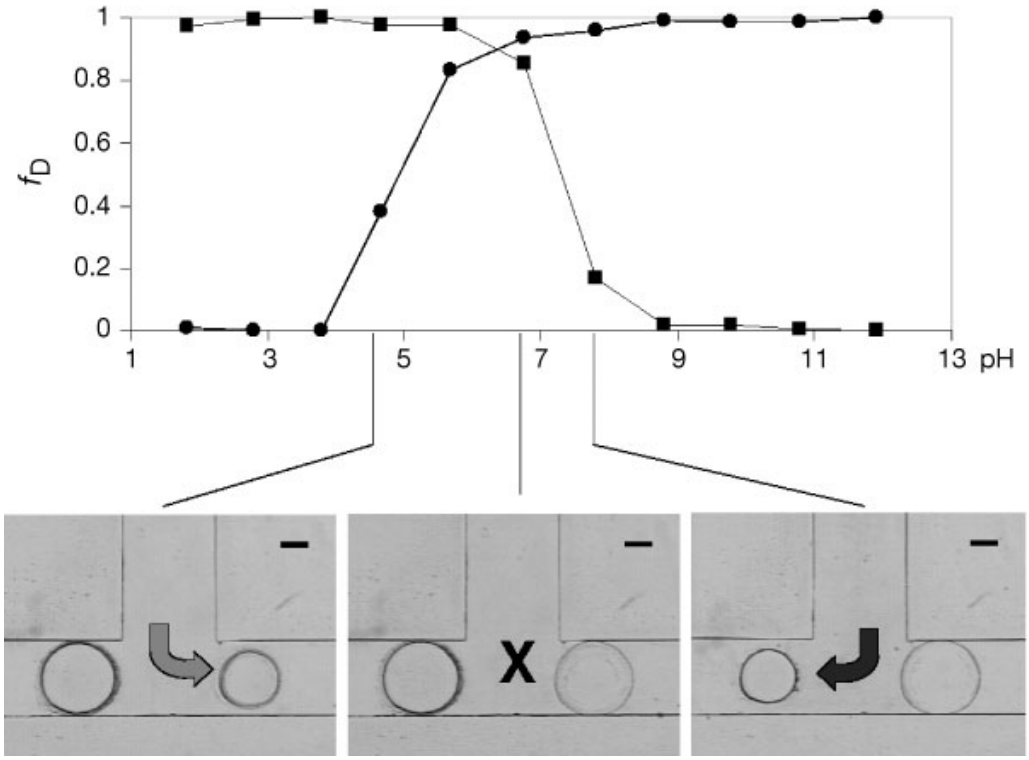

Figure 1.3 Graph of the fractional change in diameter (f_D) of two different hydrogels with pH and corresponding image of the pH-sensitive valve system. Taken from [62].

1.2.2 Temperature-sensitive hydrogels

Temperature-sensitive hydrogels are prepared from polymers with the ability to reversibly swell and contract, or undergo sol-gel transitions, in response to environmental temperature. These hydrogels may be divided into two classes; those that swell if the temperature falls below a critical point, a lower critical solution temperature (LCST), and those that swell if the temperature rises above a critical point, an upper critical solution temperature (UCST). Hydrogels exhibiting a LCST, such as those containing NIPAM and poly(vinyl methyl ether) (PVME), imbibe water and form hydrogen bonds with water molecules below the critical temperature. Once environmental temperature rises above this point, hydrophobic interactions between

hydrophobic groups in solution and the polymer backbone begin to dominate, contracting the polymer network and expelling water. Hydrogels exhibiting a UCST, including PAA and poly(acrylamide) (PAAm), produce insoluble hydrogen-bond complexes which are disrupted at higher temperatures, allowing the gel to swell [63-65]. The critical transition temperature of these polymers can be altered if desired by adjusting the overall hydrophilicity of the system via copolymerising with other monomers [66].

Yang *et al*. [67] immobilised fluorescent molecules in temperature-sensitive pNIPAM-co-AA brushes for the detection of Cr(VI). As temperature was increased from 4 to 70^{O}C the photoluminescence intensity of the brushes decreased. They attributed this to non-consistent shrinking of the polymer brushes enlarging the distance between fluorescent molecules, thereby decreasing restrictions on the intermolecular rotations. A linear and reversible response was observed from 4 to 60^{O}C with a detection limit of 0.5 ppm.

A Cu^{2+} sensor based on a thermoresponsive pNIPAM microgel with fluorescence reporter moieties was reported by Yin *et al*. [68].The hydrogels were labelled with a metal-chelate acceptor to selectively bind Cu^{2+} which resulted in quenching of the fluorescence emission intensity. Application of elevated temperatures collapsed the microgel and improved detection sensitivity from ~46 nM at 20^{O}C to ~8 nM at 45^{O}C. This was attributed to more efficient capture of Cu^{2+} ions by decreasing the distance between metal-chelate acceptor molecules and enhancing cooperative complexation effects. Also due to the spatial closeness in the collapsed network, the Cu^{2+} complex could quench the fluorescence emission of nearby fluorescing moieties. Many other examples of temperature-sensitive hydrogels in therapeutic applications are present in literature, including several recent reviews on

use of biodegradable block copolymers [69, 70], thermoresponsive microgels [71, 72] and polysaccharide hydrogels [73].

Due to their physiological significance, pH- and temperature-sensitive hydrogels are the most commonly studied classes of stimuli-sensitive hydrogels. However, as stated previously various alternative stimuli are employed in hydrogel systems. A brief overview of the effect of these stimuli on hydrogel networks is provided in Table 1.1 below.

Table 1.1 Overview of other stimuli and hydrogel responses. Adapted from [74].

Stimulus	Hydrogel type	Response	Additional reference
Ionic strength	Ionic	Changes in ionic strength alter the concentration of ions inside the gel resulting in swelling/deswelling	[75]
Chemical species	Electron-accepting groups	Electron-donating compounds cause charge transfer between active sites changing the swelling behaviour	[76]
Enzyme/ Substrate	Immobilised enzymes/ substrates	Products of enzyme-substrate reactions or enzyme hydrolysis of polymer network can initiate swelling	[77, 78]
Magnetic	Embedded magnetic particles	Applied magnetic fields can cause re-arrangement of embedded particles which can change pore size and influence swelling behaviour	[79]
Electrical	Polyelectrolyte	Applied electric fields alter the charge balance and induce ion fluxes changing the swelling behaviour	[80]
Ultrasound	pNIPAM-AA	Ultrasound irradiation breaks hydrogel bonds inducing swelling	[81]
Unbound complementary species	Crosslinking based on complementary pairs	Swelling is induced by competitive binding upon exposure to unbound species	[82]

1.3 Transduction methods for hydrogel-based sensors

In cases where the hydrogel properties are being monitored a tranducer is required to convert the non-electrical (e.g. swelling) signals into measurable optical or electrical signals. They function by detecting changes in the properties of the polymer network, including cross-linking density, volume and tensile strength, or on the mechanical work produced by the swelling mechanism [59]. Current approaches include optical, mechanical, microgravimetry and electrochemical methods.

Several research groups have nanostructured hydrogels to transduce their swelling mechanism based on the diffraction or interference of light. Numerous hydrogel sensors have been fabricated using hydrogel diffraction gratings by monitoring the diffraction efficiency upon swelling [83-85]. Wang *et al*. [86] designed hydrogel diffraction gratings for the detection of human thrombin (Fig 1.4). A thrombin-binding aptamer and its complementary sequence were functionalised as physical cross-linking points in the polymer backbone. Swelling was induced when the binding was disrupted upon exposure to human thrombin, thereby increasing the trough depth and the diffraction efficiency of the grating.

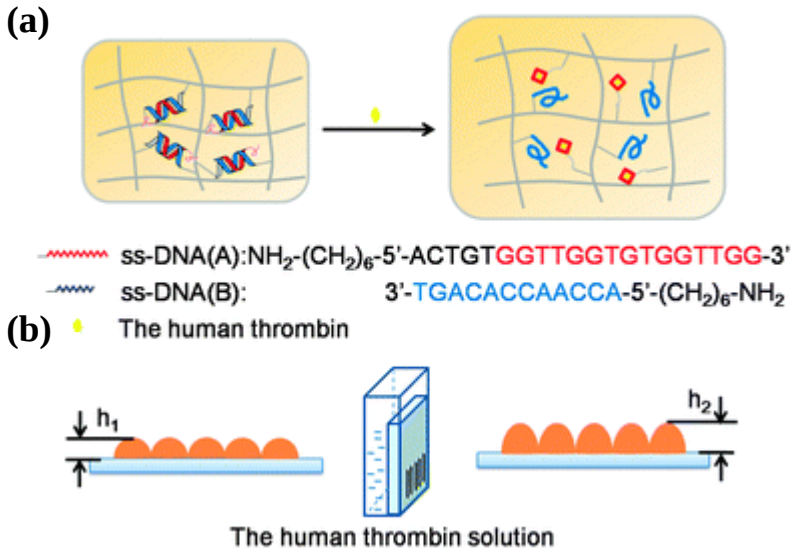

Figure 1.4 (a) Schematic illustration of the hydrogel diffraction grating swelling when exposed to human thrombin and (b) increase in trough height. Taken from [86].

Many diffraction-based hydrogel sensors are fabricated using either colloidal crystal arrays/photonic crystals (PC) of hydrogel spheres or holographic Bragg gratings with embedded silver nanoparticles. Under white light illumination, both approaches produce a characteristic spectral peak with a wavelength determined by the crystal lattice spacing or the holographic fringes, according to Braggs law. Kang *et al.* [87] designed a poly(hydroxyethylmethacrylate)-co-methyl methacrylate p(HEMA-co-MMA) PC hydrogel which exhibited a strong reflection at 2.1 μm based on Braggs law. The reflectance peak was red-shifted to 2.22 μm upon swelling in water. A pH-sensitive 1-D PC prepared by spincoating thin films of titanium dioxide, graphene oxide and poly(ethylene glycol) (PEG)-cross-linked poly((methyl vinyl ether)-co-maleic acid) (PMVE-co-MA) was studied by Yao *et al.* [88]. They observed a shift in the photonic stopband from 468 nm to 490 nm by swelling the hydrogel in an alkali solution (unspecified) at pH 14. The stopband was reversed back to 468 nm

upon deswelling in a pH 7 solution. Volumetric changes of 2-D PC hydrogels in response to glucose [89] and lectin concanavalin A [90] have recently been studied by monitoring changes in the Debye diffraction ring diameter due to changes in neighbouring particles spacing in the crystal array. Yetisen *et al*. [91] developed a pH-sensitive holographic p(HEMA-co-MMA) hydrogel which swells upon deprotonation as the pH increases from pH 4-8. As seen in Fig 1.5, this induced swelling increases the spacing of the silver nanoparticles and shifts the peak wavelength from 495 nm to 815 nm. Several other holographic hydrogel-based sensors have been reported including for detection of glucose [92], humidity [93] and bacterial growth [94].

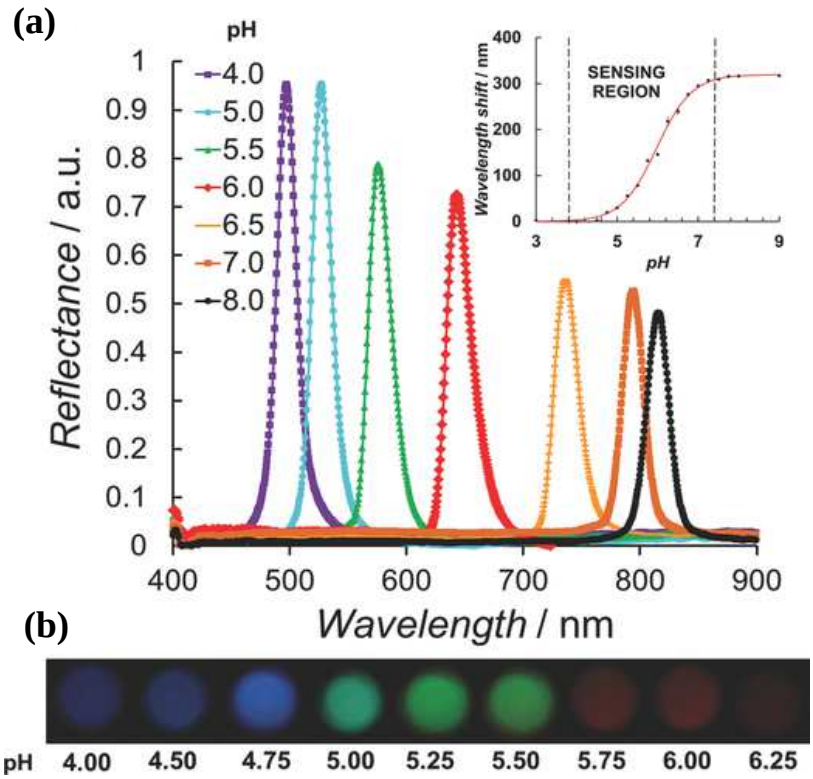

Figure 1.5 (a) Diffraction spectra of a holographic hydrogel swollen in phosphate buffers of different pH values. Inset: Data expressed as sensor response (n=3) and (b) Photographs of the holographic hydrogels recorded under white light illumination upon immersion into pH 4 to pH 6.25 phosphate buffers. Taken from [91].

An interference-based optical sensor was developed by Zhang *et al*. [95] to track glucose-induced swelling by using the hydrogel as a Fabry Perot cavity. Incident light was reflected at the air-gel and gel-substrate interfaces, creating an interference pattern whose phase depends on the optical pathlength within the hydrogel. They calculated the optical pathlength from the reflection spectra shown in Fig 1.6 and determined that it increased linearly upon swelling in the presence of glucose.

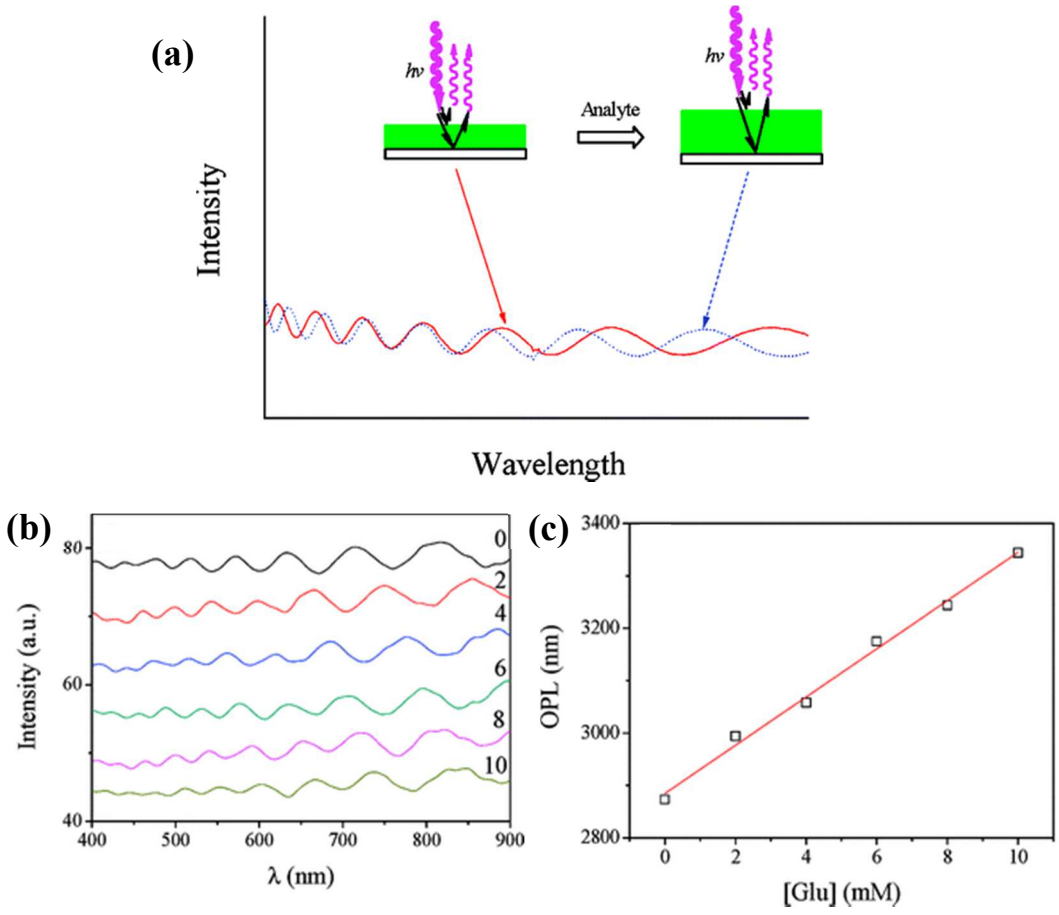

Figure 1.6 (a) Schematic illustration of the shift in Fabry-Perot fringes in response to analyte induced hydrogel swelling, (b) Reflectance spectra of PVA/P(AAm-AAPBA) hydrogel film in various concentrations of glucose (mM) (in 0.05 M pH 8.5 phosphate buffer) and (c) Calculated optical path length as a function of glucose concentration. Taken from [95]

Mechanical transduction exploits the hydrogel swelling response to strain or deform a mechanical transduction element and alter its properties. The two main classes of mechanical signal transduction are microcantilevers and bending plate transducers. Peng *et al*. [96] developed a microcantilever sensor modified with chitosan/gelatin hydrogels for the detection of fluoride ions. A bending deflection of the microcantilever was induced as the hydrogel swelled upon exposure to fluoride ions and was measured using an optical beam deflection method. As illustrated in Fig 1.7, bending plate transducers utilise a piezoresistive sensing diaphragm to detect changes in the mechanical pressure applied to the sensor. The hydrogel is typically confined between a porous membrane, which allows analyte diffusion, and a piezoresistive diaphragm as pressure transducer. As the hydrogel swells, the pressure and voltage output increases [97-99]. Sorber *et al* [100] spincoated a PAA/PVA hydrogel on a commercially available pressure sensor chip to convert the bending plate deflections into an output voltage. pH-sensitivity was observed as the output voltage increased (20-160 mV) as the hydrogel swelled in NaOH (pH 12). The voltage then decreased (160-20 mV) as the hydrogel deswelled when placed in HCl (pH 2).

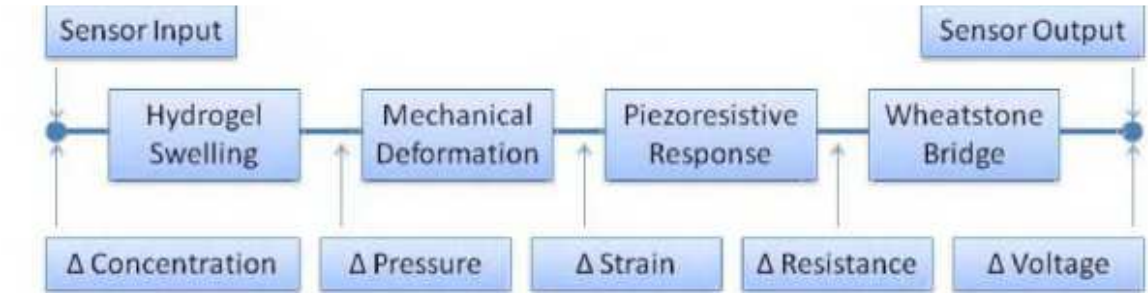

Figure 1.7 Schematic of piezoresistive signal transduction. Analyte induced hydrogel swelling deforms the piezoresistive diaphragm producing a piezoresistive response. A Wheatstone bridge is incorporated to change the mechanical signal into a voltage output, which is analysed to determine the sensor response. Taken from [101]

Hydrogels have been coated on quartz crystal microbalances (QCM) for microgravimetric signal transduction. The QCM experiences a change in surface resonance frequency as the surface load changes upon swelling/deswelling. Wang *et al*. [102] investigated the swelling response of an aptamer hydrogel for the detection of avian influenza virus H5N1. The hydrogel network was generated by cross-linking ssDNA and an aptamer with specificity against the surface protein of the virus. Swelling was induced upon exposure to the target virus as cross-links dissolved when the aptamer preferentially bound with the virus. A decrease in resonance frequency shift was detected as the hydrogel swelled upon exposure to H5N1. Titer values of 1.28, 0.64 and 0.128 HAU corresponded to a decrease in resonance frequency of 90, 51 and 25 Hz respectively. A detection limit of 0.0128 HAU was achieved with the optimised formulation.

Electrochemical transduction has many advantages including its reliability, the impressive capabilities of electrochemical techniques, direct coupling with microelectronics, facilitated quantitative control and ease of interfacing with intricate systems. A conductimetric sensor has been developed by Sheppard *et al*. [103] based upon conductivity measurements of a pH-sensitive hydrogel. A planar interdigitated electrode array was coated with a thin layer of cationic hydrogel which swells (/deswells) in response to local pH changes producing an increase (/decrease) in ion mobility partitioned by the gel. A change in resistance of up to 45% per pH unit was detected. Guan et al. [104] monitored the swelling mechanism of gels in a microelectromechanical systems (MEMS) microfluidic platform with embedded conductometric sensing and simple optical methods. As shown in Fig 1.8, a ruler was deposited on the bottom of the channel enabling optical readings and pairs of sensing electrodes were patterned along the channel walls for measuring the change in

conductance. An undisclosed hydrogel was utilised for proof-of-concept testing of the MEMS device. A 200% increase in surface area and 35% decrease in resistance were observed when fully swollen in water.

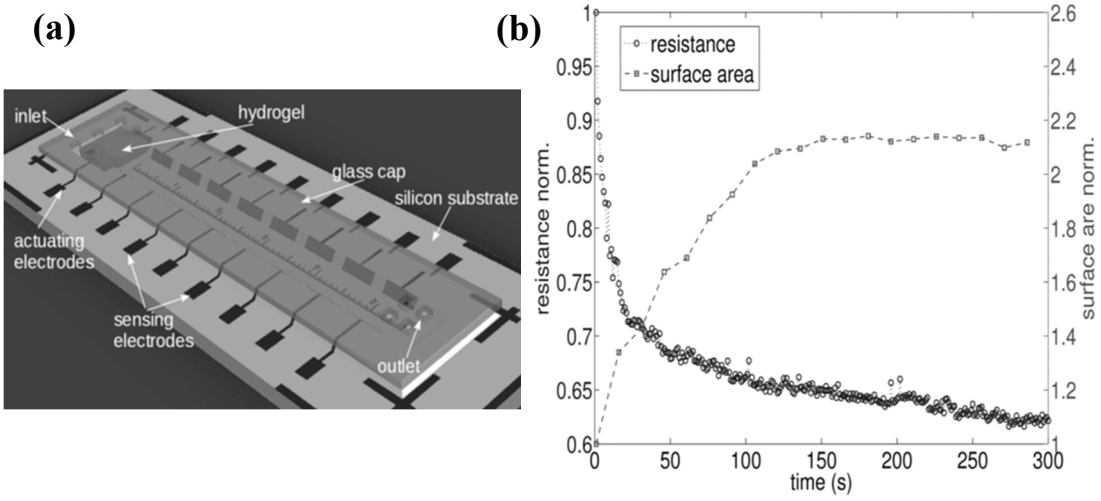

Figure 1.8 (a) 3D Schematic of the MEMS device and (b) Conductometric and optical dependence on the swelling time of an unspecified Pluronic®-based electroactive hydrogel. Reproduced from [104].

Additionally, amperometric sensors have been fabricated which exploit the hydrogel swelling. A redox polymer, poly(vinylimidazole) was reacted with Os(4,4'-dimethylbpy)2Cl (PVI-dmeOs) and electrodeposited on carbon nanotubes (CNTs) to detect the activity of redox enzymes such as GOx and lactate oxidase (LOx) [105]. The mobility of the polymer chains increases when swollen in solution, thereby increasing the rate of electron-transferring collisions between redox centres and the electronic conductivity of the gel. It was determined that the redox hydrogel enhanced the detection sensitivity, as the redox centres of the enzymes were connected or "wired" through the redox centres of the polymer backbone to the CNT electrodes.

Redox hydrogels have also been cross-linked with enzymes for amperometric detection of glycerol [106] and glucose [107].

Single frequency impedance (4 kHz) was used by Justin *et al*. [108] to investigate the pH sensitivity of a p(HEMA)-PEG-tetraethyleneglycol diacrylate (TEGDA) hydrogel coated on a micro-disc electrode array. They determined that the hydrogel exhibited a repeatable response to step changes in pH. A 20% decrease in real impedance was observed as the pH was increased from pH 6.1-8.8.

However, electrochemical transduction is employed much less frequently than optical and mechanical methods to transduce hydrogel swelling. In electrochemical sensing platforms, alternative properties of hydrogels are exploited more commonly instead of their swelling response. Applications include use as a 3D biocompatible matrix suitable for high loading of biomolecules [109], a protection or particle adhesive layer [110] and for interference suppression [111]. In most examples in the literature, hydrogels are used purely as an encapsulation medium for biomolecules to ensure their proximity close to the electrode surface.

1.4 Electroconductive hydrogels for drug delivery

1.4.1 Drug delivery from hydrogels

Hydrogels have also generated extensive interest as drug delivery systems [112]. As stated previously, they display excellent biocompatibility, hydrophilicity and flexibility. Their versatility in design permits loading of a wide range of drugs. Drugs as small as NSAIDS (non-steroidal anti-inflammatory drugs) and DNA-based drugs, or as sizable as peptides and proteins have been immobilised in gel matrices.

Depending on the monomer selection, drugs with various chemical compositions, degrees of hydrophobicity/hydrophilicity and associated charge can be incorporated. Muco- or bio-adhesiveness can be integrated to facilitate drug targeting and promote adsorption in mucosal tissues (e.g. buccal, nasal, rectal and ocular cavities etc.) [113, 114]. Hydrogel 'stealth' characteristics *in vivo* have been observed through evasion of triggering an immune response and decreasing phagocytic activity, thus prolonging circulation time [115, 116].

Drug delivery from hydrogels can be classified according to the rate-limiting step of the release mechanism i.e. diffusion, swelling or chemically controlled. Diffusion controlled release is the most common and is typically modelled using Fick's laws of diffusion. Swelling controlled release arises when the rate of release is dependent on the hydrogel swelling rate and is heavily based on the polymer relaxation time. Chemically controlled release occurs when drug release results from reactions occurring inside the hydrogel network, such as bond cleavage or degradation of polymer chains [117]. However, these release profiles are rather idealistic and rarely mutually exclusive. Many different mathematical models and simulations have been developed for these release mechanisms over the last 30 years and reviewed several times [117-122].

1.4.2 Controlled drug delivery from hydrogels

Traditional routes of drug administration, including oral and injection methods, commonly supply a maximum dose of drug initially which rapidly decreases over time. However, intelligent drug carriers capable of on-demand drug delivery have aroused much interest in recent years. Controlled drug release would provide safer, more efficient drug distribution by enabling site-specific drug delivery with on-off

regulation in real time. Adverse side-effects would be dramatically reduced and patient compliance would increase. This precision could result in improved medical treatment of illnesses such as diabetes as well as personalised treatment plans for individual patients.

Numerous studies have shown that stimuli-sensitive hydrogels can be used to modulate drug release in response to physiological variations based on their swelling response. These intelligent hydrogels are capable of an auto-feedback mechanism whereby the drug is released only when needed and release is suspended at normal state [123-126]. Many pH- and temperature-sensitive drug delivery systems have been designed based on this principle. For example, Ali *et al*. [127] showed pH-dependant release of venlafaxine, a water-soluble anti-depressant, from a PVA-based hydrogel. Release was retarded at pH 1.2 but increased significantly upon swelling at pH 7.4. Similarly, a pNIPAM-co-vinyl terminated poly(dimethylsiloxane)-co-AA hydrogel permitted release at pH 7.4 but suspended release at pH 1.4 for the delivery of indomethacin through the gastrointestinal tract [128]. Patton and Palmer [129] demonstrated fabrication of pNIPAM hydrogel nanoparticles encapsulating bovine haemoglobin as novel oxygen carriers. These gels were designed to swell when body temperature is abnormally low ($< 36^{O}C$), helping to prevent hypoxia in conditions such as hypothermia by increasing oxygen delivery. Thermo-sensitive hydrogels are also frequently used in the controlled release of antipyretics and anti-inflammatory therapeutics. These gels are designed to swell and release their active drug based on small temperature changes in the body [130, 131].

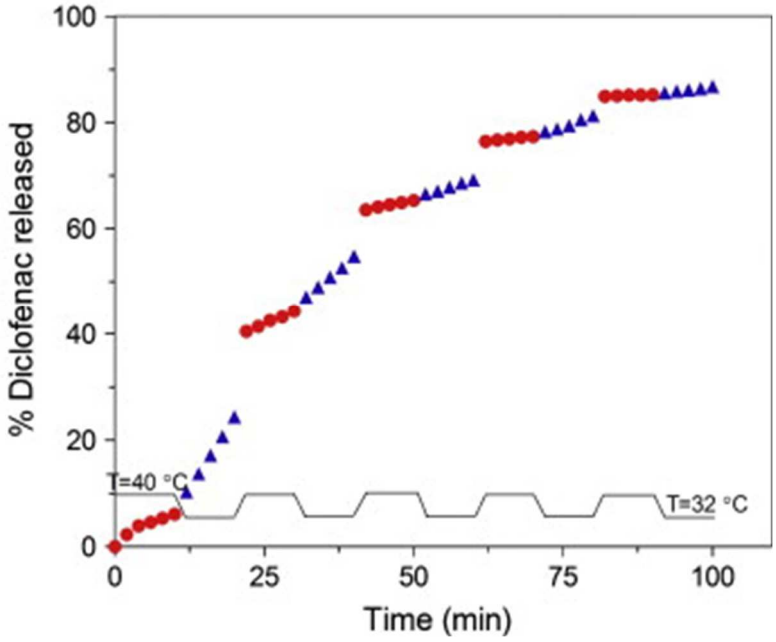

Figure 1.9 Temperature-stimulated release of diclofenac from a poly (NIPAM-co-β-cyclodextrin) hydrogel into PBS at pH 7.4. Temperature was cycled between 32^{O}C and 40^{O}C. Taken from [131].

Recent advances in polymer chemistry and hydrogel design have promoted the development of injectable hydrogels [123, 132-136] and biodegradable hydrogels [137-139] for drug delivery. Injectable hydrogels are designed to undergo sol-gel transformations upon exposure to physiological conditions, most frequently using thermo-sensitive polymers which polymerise at body temperature. They can be administered in a minimally invasive manner, eliminating the inconvenience, cost and potential risks associated with surgery. Biodegradable hydrogels are designed to degrade in clinically relevant timescales and eliminate the need for additional surgery to recover the implant. These are both extremely attractive attributes in a smart drug delivery system.

Several regulating systems for insulin delivery for diabetic patients have been developed. These include pH-sensitive polymers, such as 2-hydroxyethyl methacrylate-co-N,N-dimethylaminoethyl methacrylate, containing immobilised glucose oxidase which catalyses the conversion of glucose to gluconic acid, initiating swelling and subsequent insulin release [140, 141]. Other polymer systems containing phenylboronic acid groups have been utilised for their reversible complex formation with glucose, enabling on-off regulation [142, 143]. These systems permit self-regulated, site-specific drug delivery at a specific rate, circumventing the need for multiple injections, specialised personnel and continuous monitoring.

1.4.2.1 Electro-stimulated drug delivery

Various external stimuli have been employed recently to initiate drug release from responsive materials *in vivo*. These include use of ultrasound, radiofrequency, light, NIR and laser radiation, magnetic and electric fields [144, 145]. Use of an electric field as an applied stimulus has many advantages, including reliability and precise control of magnitude, duration and intervals of pulses. The application or removal of an electrical field can trigger drug release similar to the pulsatile release of numerous endogenous chemicals *in vivo* including insulin, oestrogen and growth hormones. Electric fields can be generated by applying an electro-conducting patch to the skin above the implanted gel. Electrodes are then connected to the patch and the electric field is switched on. Iontophoresis and electroporation have been utilised for drug delivery *in vivo* [146-148].

However, many hydrogels are inherently non-electroactive and require the addition of an electroconductive component. These electroconductive hydrogels (ECHs) can be prepared by producing the gel directly from conducting polymers [149,

150], incorporating inherently conducting polymers (ICPs) [151, 152] or conductive particles into the hydrogel network [153-155]. When composited together, these materials aim to integrate the unique properties of their constituents i.e. the swellability, high water content, biocompatibility and 3D matrix of hydrogels with the electrical conductivity, electrochemical redox properties and switchable electrical and optical properties of the selected conductive materials. Thus, this new class of advanced materials possess many technologically significant properties for electro-stimulated drug delivery.

In general, when synthesising ECHs, the hydrogel is the primary component and the electroactive component is polymerised within it. However, it is possible to polymerise the hydrogel within an ICP. As illustrated in Fig 1.10, the ICP and hydrogel monomers can be reacted with free radical initiators. The pre-polymer solution can subsequently be drop-coated onto electrodes or other substrates, cast into membranes or spun as fibres, depending on the chosen application [156]. If electrochemical polymerisation is desired, the hydrogel is deposited onto a metallic or semi-conducting electrode which is placed in an electrolyte solution containing the ICP monomer and a potential is applied, initiating polymerisation. Alternatively, chemical polymerisation can be utilised, whereby the hydrogel structure is immersed in a monomer solution with an initialising oxidant. Enzymes and other small molecules can be immobilised within the ECH when dispersed in the aqueous solution via electropolymerisation.

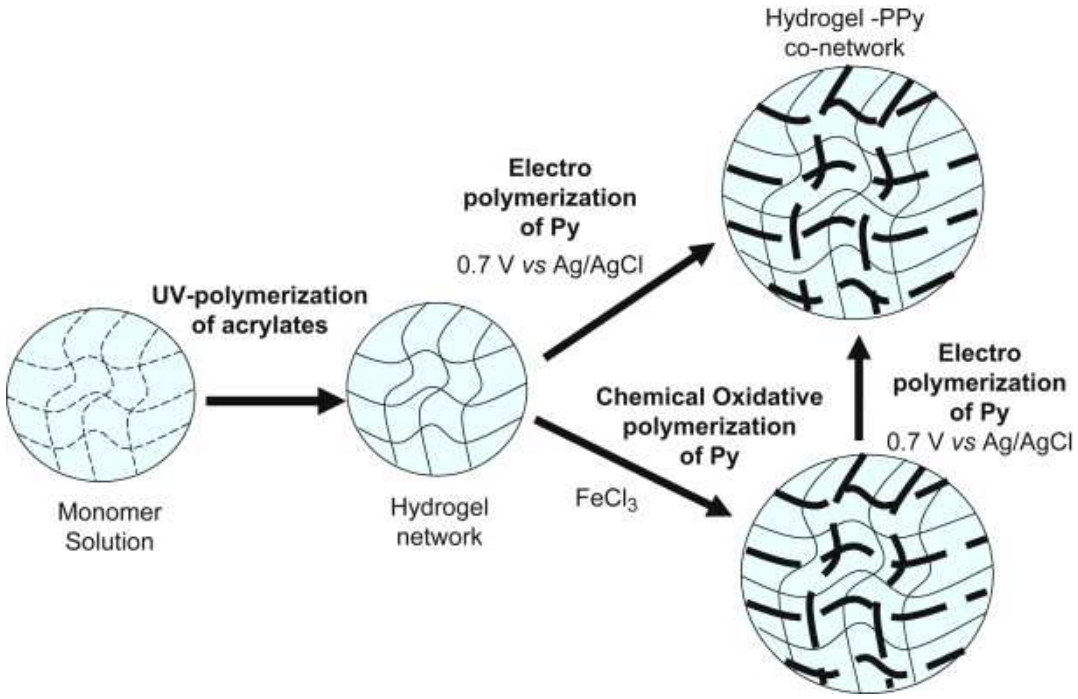

Figure 1.10 Schematic representation of a polypyrrole (PPy) ECH synthesis. Taken from [156].

Application of an electrical stimulus can switch the oxidation state of conducting polymers. Redox reactions involve polymer charging and discharging and is accompanied by ion migration in and out of the bulk polymer. Córdoba de Torresi *et al.* [157] demonstrated electro-stimulated release of safranin as a model drug from a polyaniline-PAAm composite. The amount and rate of release of safranin was increased when an oxidising potential was applied (+ 0.6 V) compared with a reducing potential (-0.2 V). The drug can also be incorporated as a dopant molecule to maintain charge neutrality on the ICP backbone. Niamlang *et al.* [158] doped a poly(p-phenylene vinylene)-PAAm hydrogel with aloin and exhibited its release profile at various electric field strengths (0-0.1 V). Accelerated release was observed as the electric field strength increased due to the stronger reduction reaction increasing polymer-drug electrostatic interactions, expanding the PPV chains and electroporation

of the matrix pore size. Cyclic potential stimulation can also trigger controlled drug release based upon reversible swelling/deswelling of the ICP produced by the movement of ions and water in and out of the bulk polymer. Wadhwa *et al*. [159] utilised this process as a pump for the release of dexamethasone from a PPy film and detected linear correlation between the number of CV cycles and amount released.

Another commonly used release mechanism is electro-induced deswelling of the hydrogel. The process of deswelling can generate forced convection which ejects or 'squeezes' the drug from the hydrogel matrix. Ali *et al.* [160] showed electro-stimulated release of theophylline from a 2-acrylamido-2-methyl propane sulfonic acid (AMPS)-AA hydrogel based on hydrogel deswelling. Rapid release was observed upon application of a 1 V electric field, which retarded once it was switched off. Similarly, Liu *et al.* [161] observed accelerated release of Vitamin B12 from a chitosan-montmorillonite hydrogel with applied potential (5 V) based on deswelling.

Alternatively, the opposite trend (i.e. electro-induced swelling) is generally required for the delivery of macromolecules. Sawahata *et al.* [162] demonstrated pulsatile release of insulin from a weakly basic poly(dimethylaminopropyl)-acrylamide hydrogel. Upon electrical stimulation the hydrogel swelled permitting insulin diffusion, however diffusion was inhibited when the stimulus was removed and the gel shrank. Insulin delivery has also been exhibited from hydrogels designed to erode upon electrical stimulation [146]. Kwon *et al*. [163] demonstrated pulsatile release of approximately 70% of their insulin loading from a poly(ethyloxazoline)-poly(methacrylic acid) hydrogel.

1.5 Response times- a limitation of hydrogel systems

One of the principal limitations of hydrogel-based systems is their rate of response. Many hydrogels require hours or days for equilibrium swelling in a new environment. While a slow response may be desirable in some situations, such as long-term drug delivery, many applications require rapid swelling. Fast response times are necessary in sensing and drug delivery applications when rapid intervention may be required. Use of hydrogels as self-actuating pumps and valves in MEMS microfluidic devices also necessitates fast swelling for efficient flow control. Hygiene products such as diapers and sanitary towels also require rapid swelling to quickly imbibe large volumes of fluid.

As stated previously, the swelling rate is primarily diffusion controlled. Consequently, reducing the diffusion path length through production of smaller or thinner hydrogels is often the simplest method to achieve faster swelling rates. Many literature sources refer to an early paper by Tanaka and Filmore [164], which states that the diffusion rate is inversely proportional to the square of the characteristic length of the gel. However, this theory is not without some criticism [165]. Baldi *et al*. [166] showed that as they reduced the thickness of their phenylboronic acid-based hydrogel microvalve from 500 µm to 30 µm the opening time reduced from over 4 h to 7 min in their MEMS device. Bates *et al*. [167] reduced the response time of their piezoresistive pressure sensor from 20 h to 0.34 h by reducing hydrogel thickness from 400 µm to 50 µm. Micro-spheres and nanogels exhibit fast response times due to their three-dimensional size reduction [50, 168-170]. However, reducing the size of the hydrogel may not be desirable or practical for use as it can reduce the loading capacity of drugs, compromise mechanical strength of a hydrogel valve etc.

An alternative approach to improving the response rate has been preparation of comb-type polymers by grafting freely mobile chains onto the polymer backbone. This method has proven capable of increasing the rate of deswelling. Xia *et al.* [171] grafted linear pNIPAM chains on their nanogels. They attributed their rapid shrinking to the freely mobile ends of the grafted chains aggregating and leaving interconnected microporous spaces for water to diffuse out of the gel. Zhang *et al*. [172] also demonstrated rapid deswelling of comb-type grafted poly (NIPAM-co-N,N-dimethylamino ethyl methacrylate) hydrogels in response to temperature and pH stimuli. The structure and deswelling of these gels are shown in Fig 1.11. They reported that once the grafted chains were dehydrated subsequent hydrophobic reactions between the chains would accelerate deswelling.

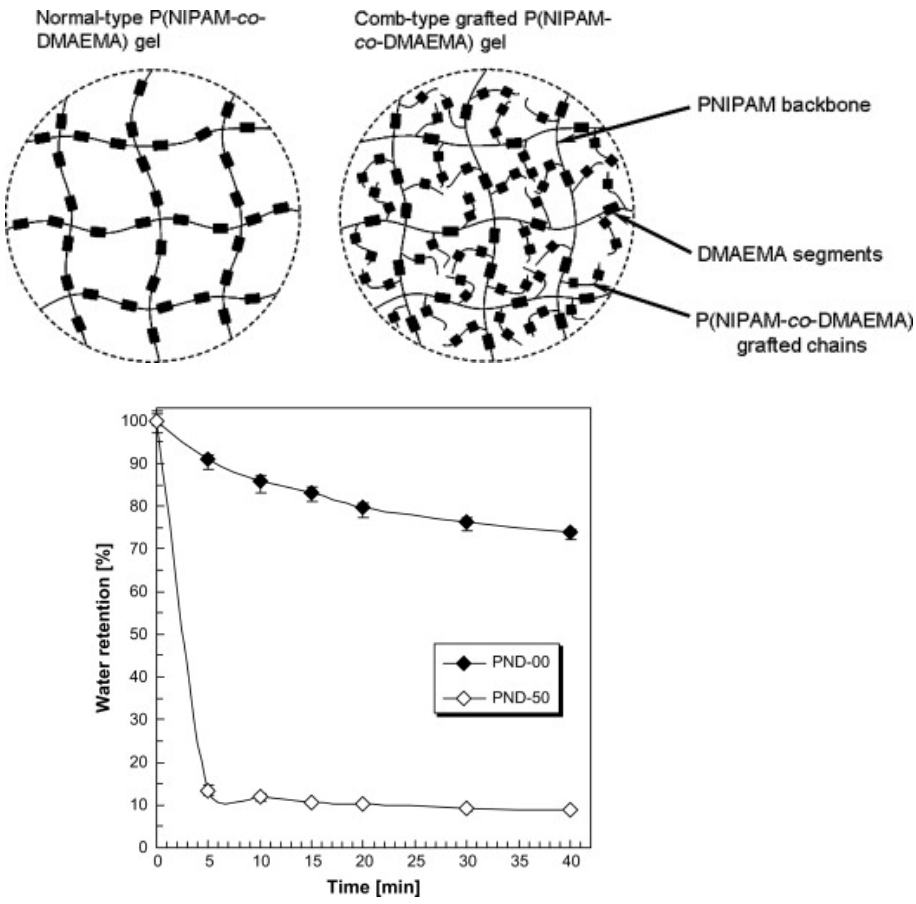

Figure 1.11 Schematic and deswelling of normal- (PND-00) and comb-type grafted (PND-50) p(NIPAM-co-DMAEMA) hydrogels. Deswelling is shown in pH 11.0 buffer (unspecified) at 44^{O}C (increased suddenly from 18^{O}C) Taken from [172].

Increasing the porosity of a hydrogel can achieve faster solution uptake and expulsion. Fabrication of micro/macroporous hydrogel materials can be accomplished by introducing a pore-forming agent [173] or using freeze-drying techniques [174]. However, these hydrogels are still primarily diffusion dependant. Superporous hydrogels (SPHs) contain an interconnecting pore system and can absorb water by capillary action through the open channels, exhibiting significantly faster response times than diffusion dependant systems. The pores are in the range of 100 μm to 1000 μm and are often formed utilising gas blowing techniques. A common method of

synthesis involves generating carbon dioxide bubbles by reacting Na_2CO_3 or $NaHCO_3$ with acid to initiate foaming. Surfactants are generally incorporated as foam stabilisers to sustain the gas bubbles for longer periods of time and improve homogeneity in the gel. [165]

SPHs are commonly used as gastric retention devices to extend the gastric residence time of drugs. Halim *et al.* [175] developed a gastric retention device by loading chromium picolinate into a SPH composite. The hydrogel showed that gastric retention persisted for 24 h during *in vivo* studies in dogs. Kumar *et al*. [176] designed AA-based hydrogels for gastric retention devices which swelled in 3 min and released almost 98% of the metformin loaded. Yang *et al*. [177] prepared poly(acrylic acid) SPH microparticles to prepare fast-melting ketoprofen tables. The microspheres possessed a high swelling ratio (80 times dry weight) and disintegrated in 15 (± 2) s under 63 MPa pressure. SPHs have also be used in the development of biomedical devices for treating aneurysms. They can swell at the aneurysm site and clot the blood without compromising the parent artery [178]. Due to their fast and extensive swelling, SPHs have been suggested in a variety of other applications including oral delivery of insulin [179], diet aids [178], topical vaginal delivery [180], bone tissue-engineering [181] and delivery of growth factors [182].

1.6 Electroanalytical techniques

Central to this thesis is the fabrication and characterisation of novel hydrogel materials. Cyclic voltammetry and EIS were the primary electrochemical techniques utilised to characterise and transduce hydrogel swelling. An introduction to these techniques is provided in this section.

1.6.1 Cyclic voltammetry

Cyclic voltammetry (CV) is a powerful and widely used electrochemical technique for initial electrochemical studies of new systems. Information regarding the thermodynamics of redox processes, kinetics of electron transfer reactions and adsorption processes can be acquired. Redox potentials of electroactive species can be rapidly located and the interfacial properties of electrodes, and modified electrodes, can be evaluated. It is a potentiodynamic measurement which consists of linearly scanning the working electrode potential at a particular scan rate to a maximum set potential and then reversing the scan in the opposite direction to the initial potential. A schematic of a voltammogram for a reversible redox species is illustrated in Fig 1.12. The forward scan generates a peak in current as the analyte is reduced (or oxidised depending on the scan direction). The current increases as the voltage approaches the reduction potential of the analyte and then decreases as the concentration of electroactive species in proximity with the electrode surface depletes. The product of the initial reduction or oxidation is then oxidised or reduced, respectively, upon reversing the scan direction. Theoretical analysis of the wave shape leads to the Randles-Sevcik equation which describes the effect of scan rate on peak current;

$$i_p = 2.69 \times 10^5 n^{3/2} A D^{1/2} C \upsilon^{1/2} \qquad \text{Equation 1.1}$$

where i_p is the peak current, n is the number of electrons transferred, A is the electrode area (cm^2), D is the diffusion coefficient ($cm^2\ s^{-1}$), C in the concentration of redox active species in bulk solution (mol cm^{-3}), and υ is scan rate ($V\ s^{-1}$).

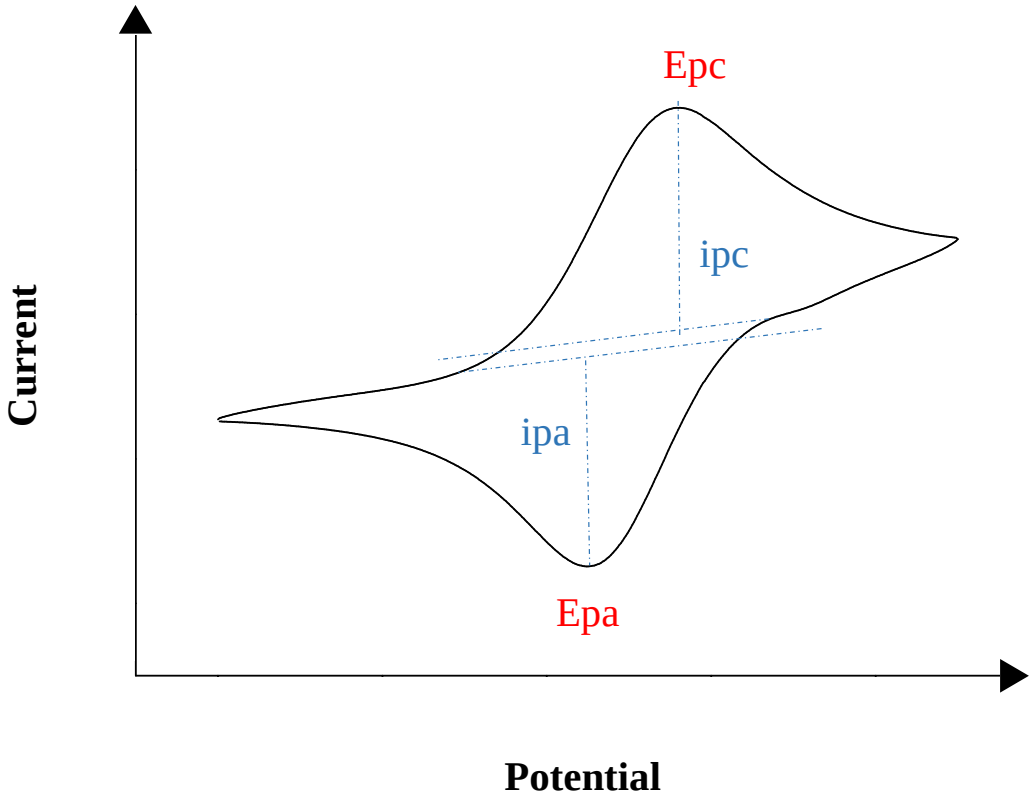

Figure 1.12 Schematic of a cyclic voltammogram of a reversible reaction. E_{pa} and E_{pc} represent the anodic and cathodic peak potentials, respectively, and i_{pa} and i_{pa} represent the anodic and cathodic peak current heights, respectively.

Reversible couples will display a ratio of the anodic peak current and cathodic peak current that is near unity ($1 = i_{pa}/i_{pc}$) and separation of peak maxima of 59 mV/n. However, in practice, many systems are not always ideally reversible due to slower kinetics and hence the peak ratio will decrease and the separation of peak maxima will increase. These systems are termed quasi-reversible. Completely irreversible systems will display only one peak and no reverse peak will be noted [183].

While CV is an excellent technique for investigating the mechanism of electrode reactions, it is used less frequently for quantitative measurements as the limits of detection achieved are typically not very low (~10^{-5} M) [184]. This is due to

the relative contributions of the Faradaic and non-Faradaic currents (double-layer charging, redox-surface processes etc.). Thus, CV is generally not used for sensing applications, but rather for characterisation purposes.

1.6.2 Electrochemical impedance spectroscopy

Electrochemical impedance spectroscopy (EIS) is a highly sensitive and efficient electrochemical technique for investigating a wide variety of chemical, electrochemical and surface reactions. EIS involves measurement of impedance (complex resistance) (Z) over a wide range of frequencies, permitting acquisition of a broad range of information as the response of the system changes with frequency.

Similar to resistance, impedance is a measure of the ability of a circuit to resist the flow of electrical current. Resistance is defined by Ohm's law which states that;

$$R = V/I \qquad \text{Equation 1.2}$$

where R is resistance (ohms), V is dc voltage (volts) and I is current (amperes). However, this relationship is only valid for an ideal resistor which follows Ohms law at all current and voltage levels, has a resistance independent of frequency and possesses in phase AC current and voltage signals. Impedance is a more realistic measurement for many systems as it is not limited by these properties.

As depicted in Fig 1.13, impedance measurements consist of applying a small AC excitation potential to an electrochemical cell and recording the current and phase difference of the concomitant electrical current which develops across it. The excitation voltage can be expressed as;

$$E_t = E_o \sin(\omega t) \qquad \text{Equation 1.3}$$

where E_t is the potential at time t (V), E_o is the potential amplitude (V), ω is radial frequency (rad/s) and t is time (s). The sinusoidal current response has a phase shift (Φ) and different amplitude (I_O). It is expressed as;

$$I_t = I_O \sin(\omega t + \Phi) \qquad \text{Equation 1.4}$$

where I_t is the current at time t (A), I_O is the current amplitude (A) and Φ is the phase shift (rad). Consequently, analogous with Ohm's Law, impedance can then be calculated as follows;

$$Z = \frac{E}{I} = \frac{Eo \sin(\omega t)}{I_O \sin(\omega t + \Phi)} = Z_O \frac{Eo \sin(\omega t)}{I_O \sin(\omega t + \Phi)} \qquad \text{Equation 1.5}$$

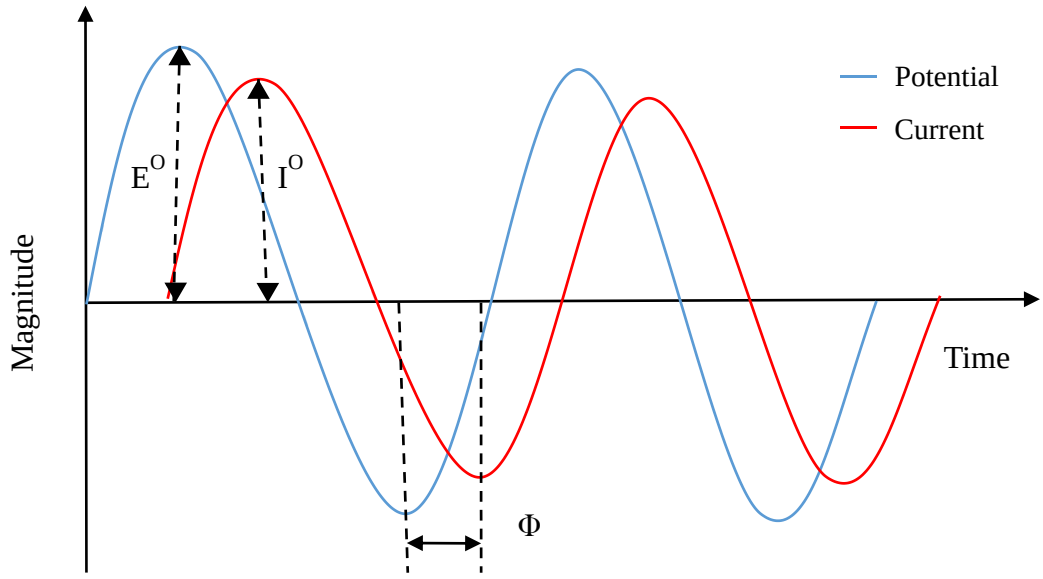

Figure 1.13 Schematic of sinusoidal applied potential and the current response as a function of time. E^O and I^O represent the potential and current amplitude respectively, and Φ represents the phase shift.

Nyquist and Bode plots are the two most common methods of displaying the generated data. The Nyquist plot shows the data as real (Z') versus imaginary (Z''),

with every point providing the characteristics of the complex impedance per frequency. However, the primary disadvantage with this plot is that the frequency is not explicitly shown. In comparison, the Bode plot shows the phase and amplitude over the frequency range analysed and allows small impedances to be identified in the presence of larger impedances.

EIS is emerging as a powerful transduction method for biosensors. Limits of detection as low as 10^{-17} M have previously been achieved [185]. These biosensors can be classified as Faradaic or non-Faradaic biosensors depending on if a redox species is incorporated. Non-Faradaic biosensors have been described as being more amenable to point-of-care applications as no additional reagent is required [186]. The sensing principle is often based upon resistance or capacitance changes of a particular element in the system. Electrical equivalent circuits are designed for data fitting to extract equivalent resistance and capacitance values for each system element. These values are then correlated with analyte concentration. It is important that the elements of the model have a physical basis, as although additional circuit components will improve the fit, they may not be realistic. Alternatively, the total impedance at a particular frequency can be exploited. In this instance, the frequency must be selected carefully as it can contain information about a combination of circuit elements or be dictated primarily by one element.

1.7 Conclusion

As detailed above hydrogels are extremely versatile and unique materials. They display great potential for use in many fields, including sensing and drug delivery, with applications varying from providing a simple inert protective coating, to use as an intelligent drug delivery system capable of sensing physiological changes and auto-titrating a drug. Many research groups have developed novel hydrogels for the detection of clinically important analytes encompassing wide linear ranges, low detection limits and high selectivity. Controlled drug release has been achieved with systems displaying on-off regulation in real time. Application of hydrogel-based electrochemical sensing platforms and electro-responsive drug delivery have yet to be fully explored. Further research is required into the reliability, specificity, material design and release kinetics of these materials before becoming commercially viable, particularly for *in vivo* applications.

1.8 Thesis outline

The purpose of this work was to develop new stimuli-sensitive hydrogel materials for sensing and controlled drug delivery applications. The applicability of EIS as a sensitive transduction method for hydrogel swelling in response to an analyte will be explored, in addition to various strategies to improve the response time of these materials.

Chapter 2 will report on the fabrication and optimisation of a pH-sensitive PEGDGE-Jeffamine® hydrogel for the detection of glucose. Hydrogel modified carbon cloth electrodes will be utilised to investigate the feasibility of employing EIS to measure changes in gel resistance upon swelling with increasing glucose concentration. Sensitive detection was achieved with a limit of detection of 0.08 μM, thus demonstrating EIS to be a viable transduction method for monitoring hydrogel swelling.

The applicability of this system for detecting other analytes which can elicit a pH change and are challenging in terms of limit of detection requirements was investigated in Chapter 3. Consequently, the pH-sensitive hydrogel was modified to detect β-D-glucuronidase, a marker compound for *E.coli*. Similar low limits of detection were achieved despite altering various aspects of the system including the placement of the enzyme and use of elevated temperature.

Chapter 4 investigates the synthesis and characterisation of a novel electroactive hydrogel composite and its potential application in electro-stimulated drug delivery. Incorporation of reduced graphene oxide attributed new properties and enhanced the inherent characteristics of the PEGDGE-Jeffamine® hydrogel system.

Through variation of the rGO content, electrode polarity and magnitude, a wide number of drug release profiles were observed, ranging from slow release of low dosages to rapid release of high dosages.

To overcome the slow response time associated with the PEGDGE-Jeffamine® hydrogel, and indeed many hydrogel systems, numerous strategies were explored to improve the swelling rate in Chapter 5. These included reduction of hydrogel size, templating with porogens and inducing macroporosity with gas blowing methods. A new fabrication route for superporous hydrogels was investigated, as well as its implications on swelling rate when measured gravimetrically and impedimetrically. Conclusions and recommendations for future work arising from this thesis are discussed in Chapter 6.

Chapter 2

Impedimetric Transduction of Swelling in Glucose-Sensitive Hydrogels

2.1 Introduction

Approximately 345 million people worldwide suffer with diabetes mellitus, a group of metabolic diseases resulting from insulin deficiency and hyperglycaemia. This condition is associated with blood glucose levels outside the normal range of 80-120 mg/dl (4.4-6.6 mM). Chronic hyperglycaemia can lead to dysfunction and failure of the heart, kidneys, eyes and nerves. Stringent glycaemic control is necessary to reduce the risk of these illnesses. This requires vigilant daily monitoring of blood glucose concentration; rendering glucose the most commonly tested analyte. Around 85% of the biosensor market is composed of glucose biosensors [187]. Accordingly, a substantial amount of research focuses on the development of reliable clinically accurate devices for diabetes management. However, despite the numerous impressive advances in glucose sensing in the past 50 years, challenges still remain regarding the achievement of stable, accurate, sensitive glucose measurements.

Due to the associated discomfort, cost and inconvenience with the conventional finger prick method, recent research has focused on developing minimally invasive and non-invasive technologies for collecting and measuring glucose. This would improve compliance with monitoring glucose levels and management of diabetes and its secondary complications (vision impairment, amputation, renal failure etc.). While blood is the most understood matrix for diagnostic measurements, other readily accessible biological fluids are becoming attractive targets for non-invasive glucose measurements. Recent research has shown that glucose can be measured in low concentrations (μM) in sweat [188, 189], interstitial fluid (ISF) [190, 191], saliva [192, 193] and tears [194, 195].

The application of hydrogels as a sensing platform for glucose has gained considerable interest in the past few years. As discussed in Chapter 1, the high water content and biocompatibility of hydrogels provide a suitable environment for the preservation of enzyme activity, whilst permitting diffusion of the analyte or substrate. Additionally, the 3D nature of the polymer network enables a high loading capacity of enzyme molecules in close proximity with the electrode surface. The high swelling responsive and tunable nature of stimuli-sensitive gels is also very attractive for designing sensitive, selective biosensors with fast response times. Combining this with electrochemical transduction offers the possibility of mass-production of low-cost, disposable electrode devices amenable to miniaturisation and widespread application.

Three distinct classes of glucose-sensitive hydrogels exist; phenylboronic acid-containing, lectin-loaded and glucose-oxidase loaded hydrogels [13]. Many researchers have exploited the high affinity of phenylboronic acid for complexing with glucose [196-198]. However, phenylboronic acid is often most sensitive to glucose in alkaline conditions and can potentially be unstable at physiological pH. Several other investigations have focussed on the complementary binding of a lectin, concanavalin A, to glucose [199-201]. Lectin systems can be limited by the leaching of concanavalin A however, leading to a progressive loss in activity and immunotoxicity issues [202].

This work describes the fabrication and characterisation of a glucose biosensor based on the swelling response of a pH-responsive hydrogel. The hydrogel comprises an aliphatic diamine cross-linked with polyethylene glycol diglycidyl ether (PEGDGE) in a single simple polymerisation step, generating a polymeric network with pendant basic groups. GOx was entrapped within the ionisable gel network to target glucose as a model analyte. The enzymatic catalysis of glucose produces gluconic acid as follows:

$$\text{Glucose} + O_2 + H_2O \xrightarrow{\text{GOx}} \text{Gluconic acid} + H_2O_2 \qquad \text{Equation 2.1}$$

The protons produced by the partial dissociation of gluconic acid ionise the pendant basic groups of the hydrogel network and generate charge along the polymer backbone. Electrostatic repulsion forces between adjacent ionised groups create a large swelling force altering the hydrodynamic volume and permeability of the gel. Additionally, gluconate anions migrate into the gel matrix to balance the charge, producing additional osmotic pressure and increasing the swelling capacity further. A schematic representation of this process is displayed below in Fig 2.1. In this work, the swelling response of the glucose-sensitive hydrogel is tracked and optimised for the detection of glucose using weight-based swelling studies. Subsequently, an appropriate electrode material was selected for investigating the electrochemical response of the hydrogel upon exposure to glucose using voltammetry of a bulk solution redox probe and non-Faradaic EIS. The feasibility of using EIS as a sensitive transduction method for monitoring hydrogel swelling in response to an analyte was explored.

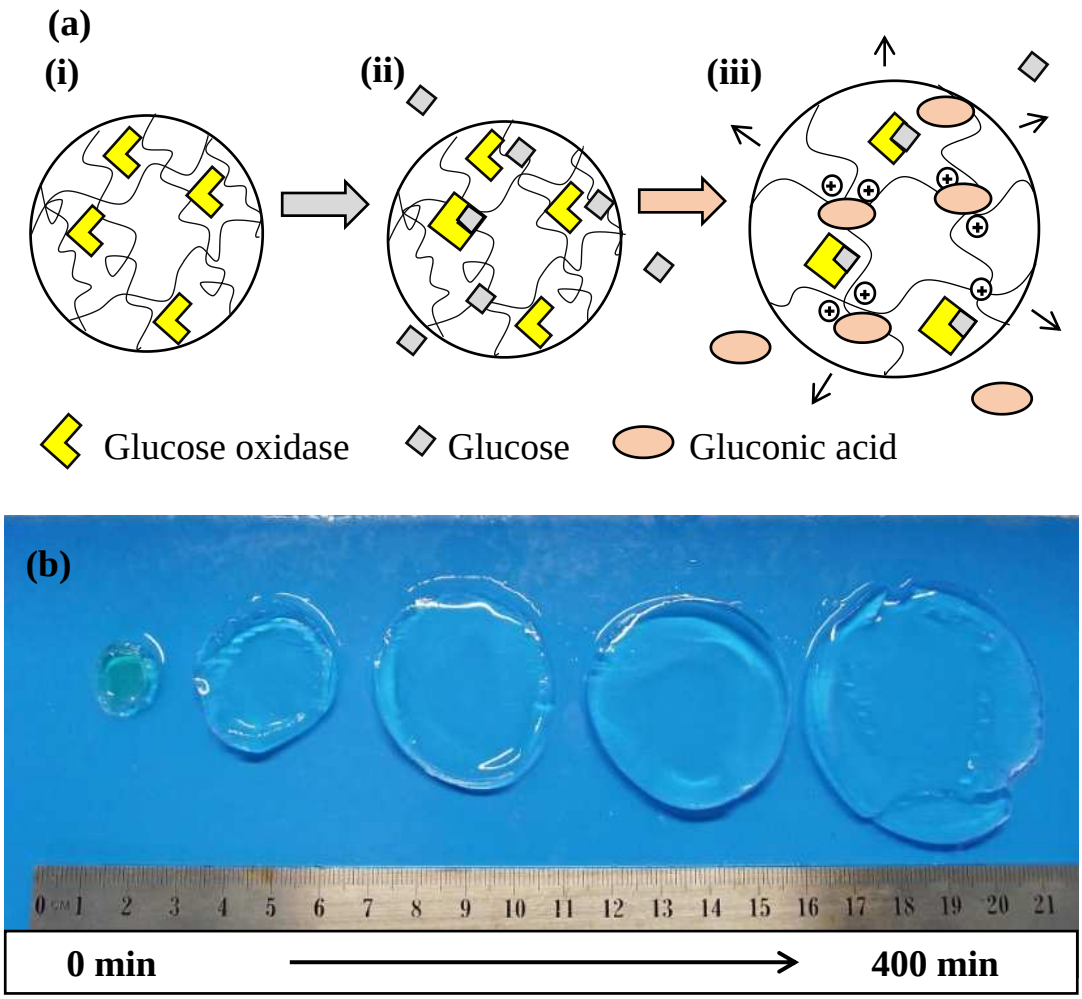

Figure 2.1 (a) Schematic of the swelling mechanism: (i) Glucose oxidase immobilised within a polymer network, (ii) glucose diffusion and (iii) production of gluconic acid/network ionisation. (b) Photograph of the swelling response of glucose-sensitive hydrogels in glucose (10 mM) over time (After equilibrium swelling in DI water overnight).

2.2 Experimental

2.2.1 Materials

Poly (ethylene glycol) diglycidyl ether (PEGDGE, average Mn 526), glucose oxidase from *Aspergillus niger* (GOx, 17,300 U/g), catalase from *Aspergillus niger* (480,947 U/g) and potassium ferrocyanide (II) trihydrate ($K_4[Fe(CN)_6] \cdot 3H_2O$) were purchased from Sigma-Aldrich (Ireland). Jeffamine® EDR-148 polyetheramine was obtained from Huntsman Corporation (US). D-glucose anhydrous was obtained from BDH Limited (UK). Untreated carbon cloth (44 x 48 yarns/inch, 99% carbon) was purchased from Fuel Cell Store (US) and phosphate buffer saline (PBS) tablets were purchased from Applichem (Germany). All chemicals were used as purchased and all aqueous solutions were prepared using deionised (DI) water (18 MΩ cm @ 298 K). The Ag/AgCl reference electrode and Pt gauze auxiliary electrode were purchased from CH Instruments, Inc. (UK) and Sigma-Aldrich (Ireland) respectively.

2.2.2 Instrumentation

All electrochemical protocols were performed on a CH potentiostat (CHI660C), using cyclic voltammetry (CV) or AC impedance modes. Voltammetric studies were conducted in a potassium ferricyanide solution (2 mM) in KCl (1 M). The potential of the working electrode was cycled from -0.1 to 0.6 V vs. Ag/AgCl at a scan rate of 0.05 Vs^{-1}.

Electrochemical impedance spectroscopy (EIS) was performed in PBS (10 mM; pH 7.4) using the AC impedance mode of the CHI660C electrochemical workstation. A perturbation signal of 10 mV was applied across a frequency range of 0.1 to 1 x 10^4 Hz. An external Ag/AgCl reference electrode and a platinum mesh

auxiliary electrode were utilised. All spectra were recorded at 0 V vs Ag/AgCl and modelled using ZView software (version 3.3e, Scribner Associates, US).

Scanning electron micrographs were obtained using a Hitachi S3400V scanning electron microscope at an accelerating voltage of 20 kV. All samples were gold-sputtered for 90 s using a Quorum Technologies sputter coater (750T).

2.2.3 Synthesis of glucose-sensitive hydrogel

The glucose-sensitive hydrogels were prepared by cross-linking Jeffamine® EDR-148 polyetheramine and PEGDGE in DI water. The molar ratio of epoxide to amine was adjusted as summarised in Table 1. Unless otherwise stated, a 1.0:1.0 molar ratio of PEGDGE to Jeffamine® EDR-148 was utilised with 1% w/w GOx dissolved in the epoxy-amine precursor solution. These precursor solutions were inverted several times until the enzymes were fully dissolved. Where stated, catalase was also incorporated at an enzyme ratio of 9.4 units catalase per unit GOx.

Table 2.1 Synthesis of PEGDGE-Jeffamine® (epoxy-amine) networks

Mole ratio of amine-epoxy	Jeffamine® EDR-148	PEGDGE	DI H_2O
1.2:1.0	0.1129 g 0.763 mmol	0.3344 g 0.636 mmol	0.5527 g
1.0:1.0	0.0982 g 0.636 mmol	0.3491g 0.636 mmol	0.5527 g
1.0:1.2	0.0849 g 0.574 mmol	0.3623g 0.688 mmol	0.5527 g
1.0:1.5	0.0706 g 0.477 mmol	0.3766g 0.716 mmol	0.5527 g
1.0:2.0	0.0546 g 0.369 mmol	0.3882 g 0.738 mmol	0.5527 g

2.2.4 Gravimetric characterisation of the swelling response

The swelling behaviour of the hydrogel was determined gravimetrically. 4 mL of the hydrogel precursor solution was poured into petri-dishes (53 mm internal diameter) and were placed in the refrigerator (4^{o}C) overnight to cure. Cylindrical gel discs (11.6 mm diameter) were cut from the polymerised hydrogel membrane using a core sampler. Each disc was weighed (W_{dry}) before immersion into the desired aqueous solution. At specific time intervals, the swollen discs were removed from solution, blotted dry with filter paper and weighed (W_{wet}). The swelling ratio at various time intervals was calculated using the following relationship:

$$\text{Swelling ratio} = \frac{W_{wet} - W_{dry}}{W_{dry}} \qquad \text{Equation 2.2}$$

2.2.5 Electrochemical optimisation of the swelling response

Carbon cloth strips (4 x 1 cm) were cut from a large sheet of carbon cloth. Off-the-shelf nail varnish was applied to the cloth to define the working electrode area (0.5 x 0.5 cm) and prevent solution from travelling up through the cloth via capillary action. The carbon cloth electrodes were then dip-coated into a solution of the hydrogel precursors to apply the hydrogel. When additional coats of hydrogel were required, electrodes were allowed to polymerise for 2 h between dip-coats to ensure polymerisation. Prior to all electrochemical experiments, hydrogel modified electrodes were swollen in electrolyte solution for 24 h.

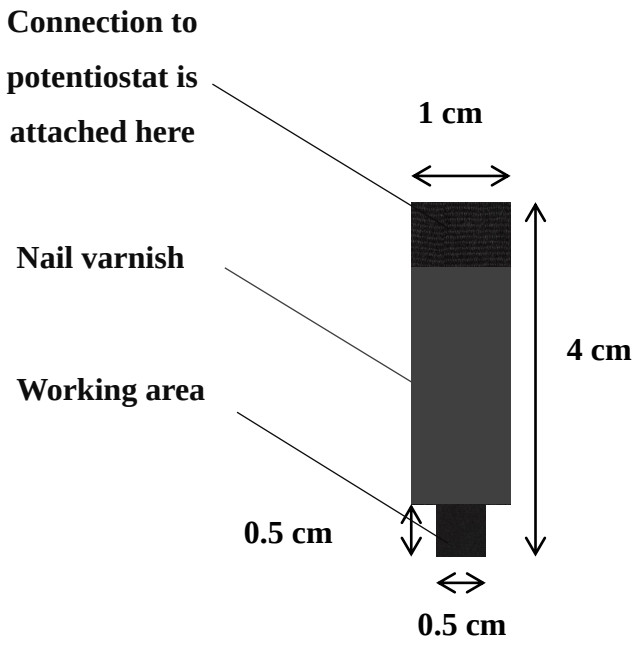

Figure 2.2. Schematic of the carbon cloth electrode.

2.2.6 Quantitative analysis of the swelling response

The glucose calibration curve using the gravimetric method was prepared with gel discs containing 5% w/w GOx and catalase incorporated. Each disc was weighed (W_{dry}) before immersion into distilled water for 24 h. After 24 h, each disc was re-weighed (W_{wet}) to quantify the swelling ratio due to water uptake using Equation 2.2 before immersion into a stirred glucose solution. After 100 min, the swollen discs were removed from solution, blotted dry and weighed (W_{wet}). The swelling ratio due to glucose at 100 min was calculated using Equation 2.2. The overall swelling response of the gel discs was calculated as follows;

Swelling response =

$$\text{Swelling ratio}_{\text{glucose @ 100 min}} - \text{Swelling ratio}_{\text{water uptake}} \qquad \text{Equation 2.3}$$

2.3 Results & Discussion

2.3.1 Gravimetric characterisation of the glucose-sensitive hydrogels

Polyfunctional amines are commonly utilised as curatives for epoxy resins. As displayed in Fig 2.3, an addition reaction occurs between the primary amines of the Jeffamine® EDR-148 and the epoxide groups of the PEGDGE, producing a secondary amine and hydroxyl group (a). Depending on the stoichiometry of the reaction, the secondary amine can react further with another epoxide group, forming a tertiary amine and a second hydroxyl group (b). If the temperature is sufficiently high, the system will change from a liquid to a three-dimensional thermoset structure. It is noteworthy that due to steric hindrance, the secondary amines are less reactive than the primary amines. Thus, the majority of the remaining amine hydrogens will exist as secondary amines in the final network.

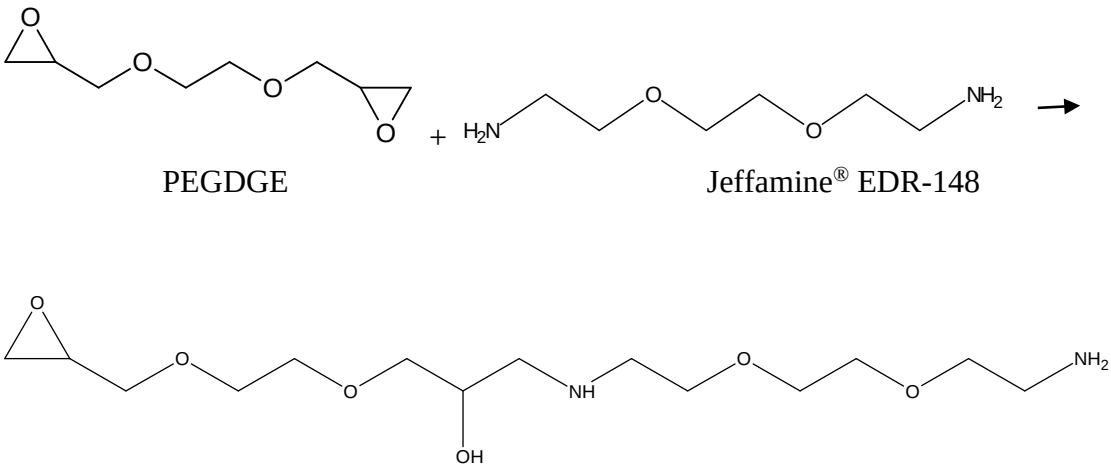

Figure 2.3 (a) Hydrogel formation chemistry.

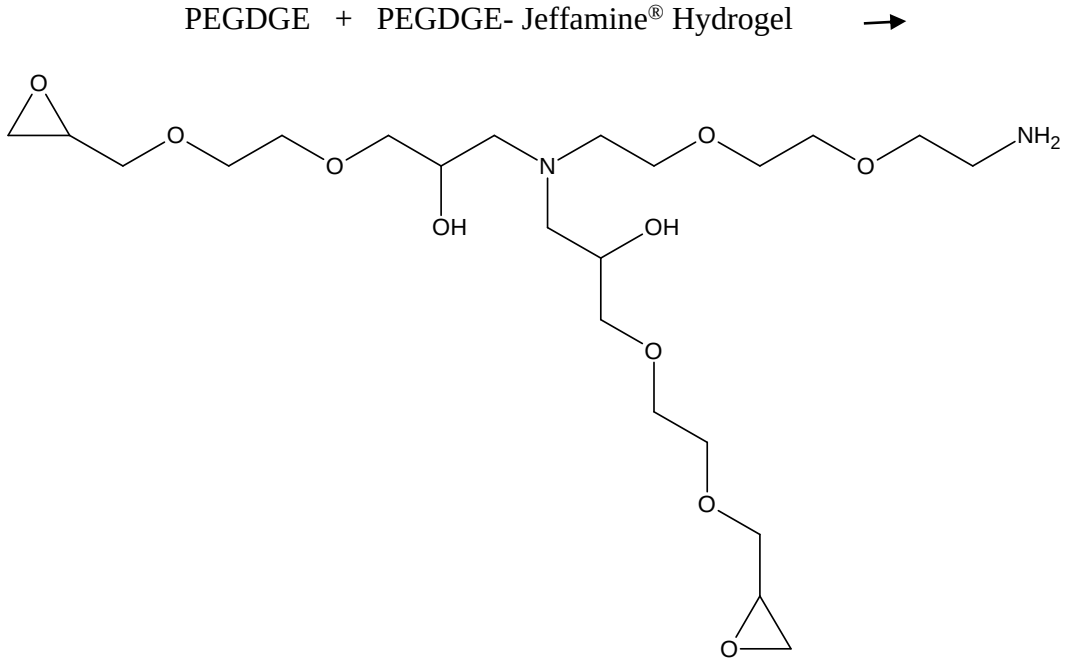

Figure 2.3 (b) PEGDGE-Jeffamine® reaction schematic with excess PEGDGE.

The choice of amine will affect many properties of the polymerised network, including reactivity, viscosity, mechanical strength and temperature resistance. For example, aliphatic amines possess higher reactivity and temperature resistance than aromatic amines but aromatic amines can achieve superior mechanical strength. Yoshioka and Calvert [203] have previously prepared a series of hydrogels based on the reaction of water-soluble polyamines with aqueous solutions of ethyleneglycol diglycidyl ether. They demonstrated that the gels produced a strong swelling response in acidic solutions which could be tuned based upon the ratio of amine to epoxy, as well as displaying good mechanical strength. This result was confirmed by Teodorescu *et al*. [204, 205] using aliphatic primary diamines and diepoxy-terminated PEG gels. Additionally, they determined that the swelling response could be enhanced by increasing the molecular weight of PEG (from 600-4000 Da) and using shorter amines as the hydrophilicity of the gel is increased. In this work Jeffamine® EDR-148 is

utilised as an epoxy curative. Jeffamine® EDR-148 is a water-soluble aliphatic diamine that cures at room temperature. It possesses 4 amine hydrogen atoms potentially available for cross-linking.

The aliphatic diamine was successfully cross-linked with PEGDGE in a single simple polymerisation step, generating a polymeric network with pendant basic groups containing entrapped GOx. The degree of swelling is related closely to the 3-D network structure of the hydrogel. In an acidic environment, charge is generated along the amine-epoxy polymer backbone due to electrostatic repulsion between the amines of the Jeffamine®, leading to an increase in the hydrodynamic volume of the polymer. A series of gels were prepared in which the molar ratio of Jeffamine®:PEGDGE (amine:epoxide) was adjusted as summarised in Table 2.1. The relationship between the amine:epoxide molar ratio and the swelling behaviour of the hydrogel in glucose (10 mM) was investigated gravimetrically (Fig 2.4). It is evident that the 1.2:1.0 Jeffamine®:PEGDGE network produced the greatest swelling response. This is attributed to the high amount of hydrophilic amines available for ionisation and the low cross-linking density achieved. The swelling response was seen to decrease as the degree of cross-linking increased. The polymer network prepared with a stoichiometric ratio of reactants (1:1) aimed to produce a model network-type structure. A model network is homogeneous and exhibits a known, constant functionality of branch points. Ideally, every polymer chain is connected at each end to different branch points and the cross-linking density is therefore consistent throughout [206]. However, real polymer networks tend to deviate from the ideal due to imperfections arising from pre-existing order, inhomogeneities or network defects. Networks formed with an even higher epoxy content, such as 1.0:1.5 Jeffamine®:PEGDGE and 1.0:2.0 Jeffamine®:PEGDGE, yielded very poor swelling responses. This behaviour is

attributed to the high cross-linking density and poor ionisation. As the network structure becomes tighter, ionisation is impaired by electrostatic effects exerted by adjacent ionised amines. Furthermore, excess epoxy groups can lead to the formation of defects in the network structure in the form of meshes, chain entanglements and grafts [207] which could possibly restrict the swelling response.

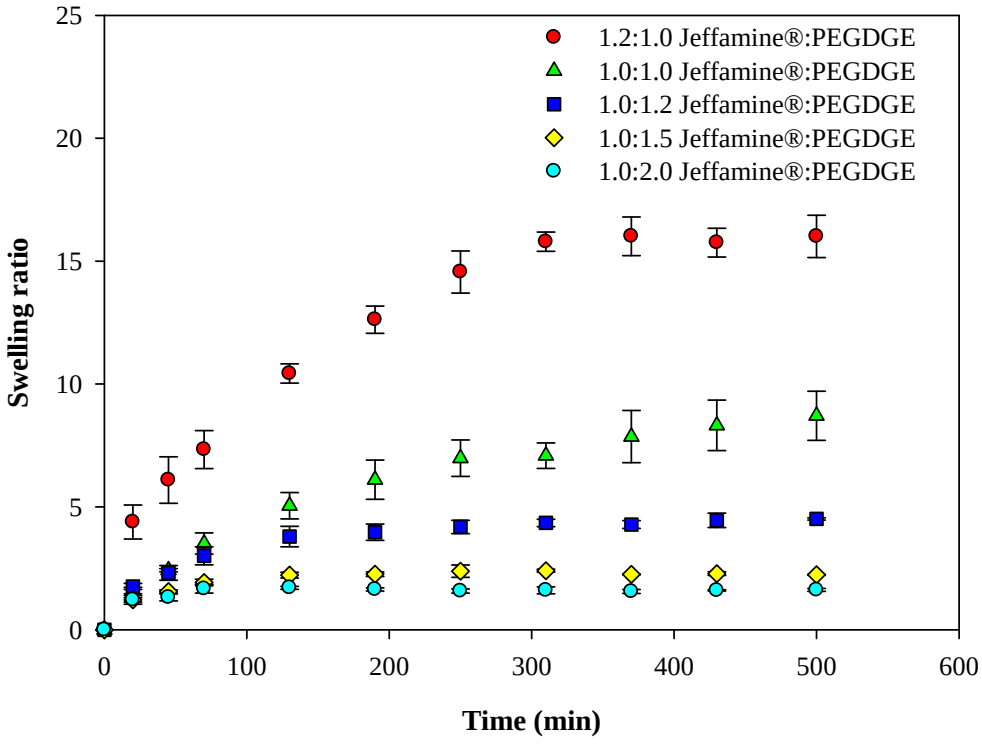

Figure 2.4 Swelling behaviour of glucose-sensitive hydrogels prepared with different Jeffamine®:PEGDGE ratios in glucose (10 mM).

Although the 1.2:1.0 Jeffamine®:PEGDGE hydrogels generated the highest swelling ratio which would likely produce the highest response in a hydrogel-based biosensor, elevated temperatures were required to complete polymerisation. Consequently, all hydrogels were prepared using 1.0:1.0 molar ratio to avoid heating as this could potentially denature incorporated enzymes.

The ratio of amine to epoxy also affected the elasticity of the system. The elastic modulus of gels and swollen rubbers is highly dependent on the cross-linking density and ratio of polymer to swelling medium, among other parameters. The 1:1 Jeffamine®:PEGDGE hydrogels displayed high flexibility. As the cross-linking density of the hydrogels increased from 1:1 Jeffamine®:PEGDGE to 1:2 Jeffamine®:PEGDGE, it was observed that the elastic modulus increased and the system became more rigid, this may be a desirable attribute depending on the application of the system. However, as the aim of this work is to determine the suitability of the system for a sensor application based on its swelling response, this did not necessitate further investigation.

The influence of several other factors on swelling response were also investigated including the effect of solution stirring, GOx loading and the addition of catalase. Optimum enzyme kinetics are paramount for achieving good response times in enzyme-based biosensors. Fig 2.5 shows the effect of solution stirring on the swelling behaviour of glucose-sensitive hydrogels. Stirring, as expected, can be seen to dramatically accelerate the enzyme kinetics. After 100 min, the swelling response has risen 35% in the stirred solutions compared with the unstirred solutions. This increases further to 187% after 500 min. It is evident that without stirring, GOx activity is diffusion limited. Thus, the system relies upon the mass transport of glucose molecules and water to the gel surface by natural diffusion governed by Fick's first law. Additionally, an external diffusion layer (Nernst diffusion layer) can be present at the surface in which concentration polarisation occurs, whereby the solution at the membrane surface becomes depleted in the permeating solute and enriched in this solute on the permeate side. The mechanical agitation produces forced convection in the surrounding solution. This reduces the thickness of the diffusion layer which is

known to be dependent on the nature and stirring speed of the solution, with more rapid stirring corresponding to a thinner diffusion layer [202]. Consequently, the collision frequency of GOx with substrate molecules is increased, thereby improving the hydrogel response time.

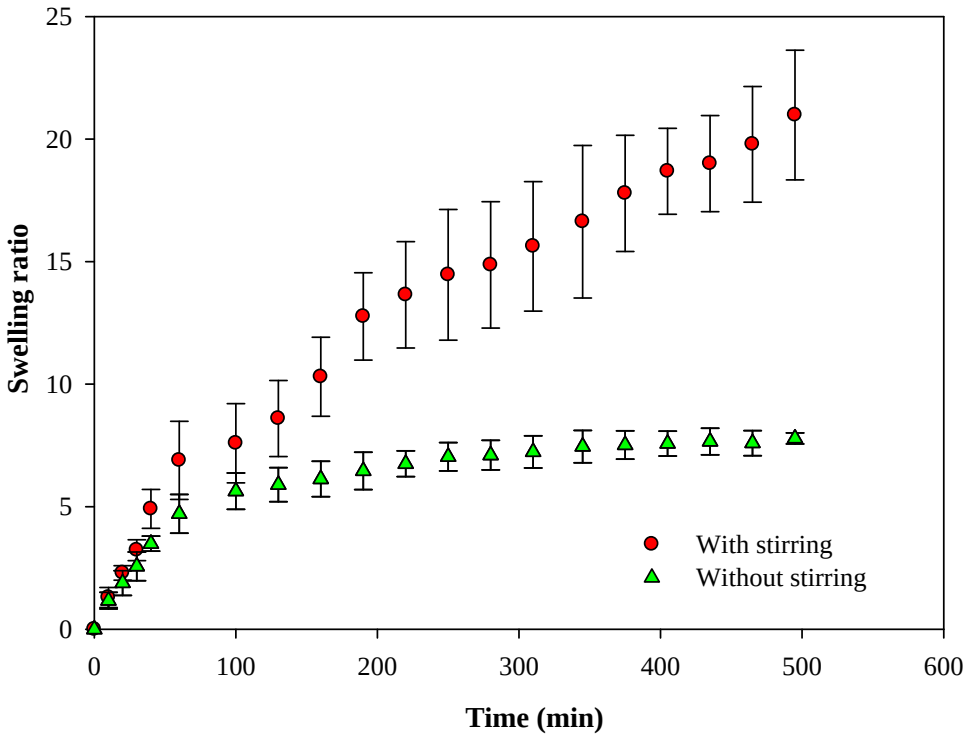

Figure 2.5 Swelling behaviour of glucose-sensitive hydrogels with and without stirring in glucose (10 mM). (n=3)

Enzyme loading was investigated by preparing GOx-modified hydrogels in which the GOx loading was varied from 0.1% to 5% total enzyme (GOx and catalase). The ratio of catalase:GOx content was held constant, to optimise the GOx loading. The swelling response to glucose (10 mM) is displayed in Fig 2.6. Substrates and product can diffuse in and out of the gel network whilst enzymes, which are immobilised via matrix entrapment are retained due to their large size. Additionally, as the isoelectric

point of GOx is 4.2 [208] the surface of the enzyme was negatively charged when the hydrogel in swollen in DI water or in PBS and thus, the enzyme may also be retained by ionic interactions with the cationic polymer network. It was observed that as the enzyme loading was increased from 0.1% to 5%, the swelling response to glucose substrate increased. After 100 min the swelling ratio increased by almost 3-fold, from 5 (± 0.118) to 14 (± 0.637). This is due to each GOx molecule functioning as a reaction site for the catalysed oxidation of glucose into gluconic acid. Therefore, a higher GOx content leads to a greater production of gluconic acid, increasing ionisation of the polymeric network and hence the swelling capacity. A similar behaviour has been reported previously whereby GOx activity increased in pHEMA hydrogel membranes upon increasing the GOx loading up to 15-20 mg per gram of gel [206, 207].

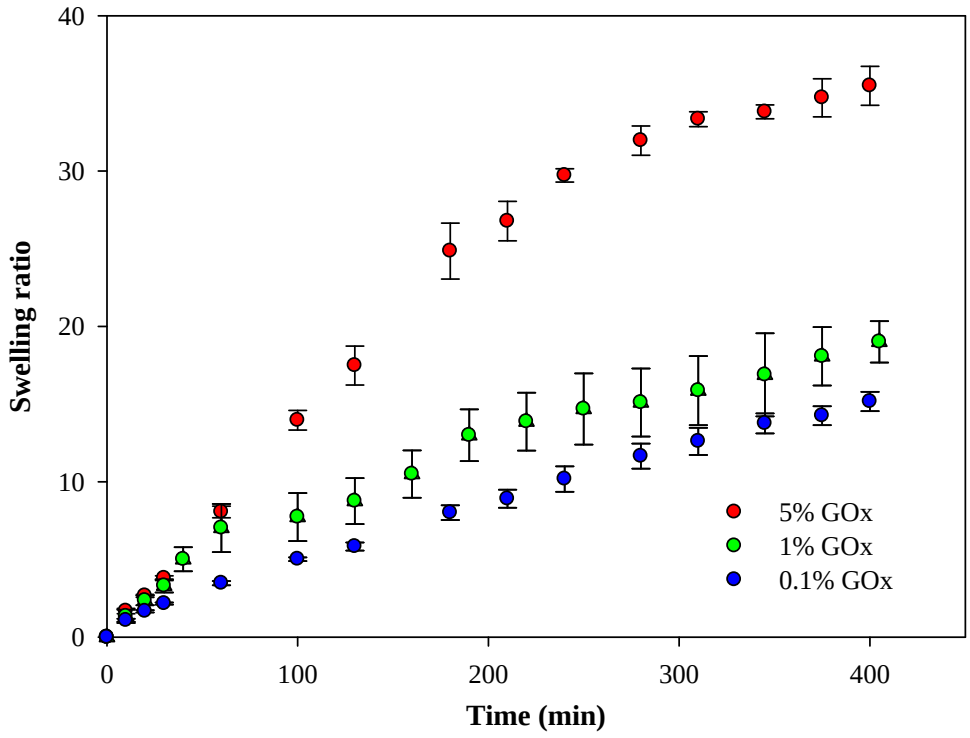

Figure 2.6 Swelling behaviour of glucose-sensitive hydrogels containing 0.1%, 1% and 5% total enzyme loading (GOx and catalase) in stirred glucose solutions (10 mM). (n=3)

Finally, the swelling behaviour of glucose-sensitive hydrogels with and without entrapped catalase was studied. Two inherent limitations of glucose-based sensors can be at least partially overcome by the inclusion of catalase. Oxygen availability is one of these limitations because of the low solubility of oxygen in aqueous-based solutions. As seen in Equation 2.1, one mole of oxygen is required to react with one mole of glucose in the enzymatic catalysis of glucose. Additionally, hydrogen peroxide production during the catalysis is known to inhibit the activity of GOx [208]. Catalase can catalyse hydrogen peroxide and produce oxygen according to Equation 2.4:

$$H_2O_2 \xrightarrow{\text{Catalase}} \frac{1}{2}O_2 + H_2O \qquad \text{Equation 2.4}$$

According to this equation, catalase produces half a mole of oxygen reducing the oxygen limitation of the GOx enzymatic reaction and the hydrogen peroxide inhibition. This enhancement is necessary for long-term glucose monitoring. As such, the incorporation of catalase into this system was studied. As can be seen in Fig 2.7, greater swelling responses are achieved for the hydrogels that have catalase incorporated. This differentiation in the swelling responses becomes apparent after 160 min. It is likely that at this time the oxygen supply is beginning to deplete and the concentration of hydrogen peroxide is increasing in the gels without catalase, inhibiting glucose catalysis and hence restricting the swelling response. After 525 min in glucose, hydrogels without catalase produced a swelling ratio of 15 (± 2.12) whereas gels with catalase resulted in a response of 23 (± 2.75), an increase of 65%. Additionally, after 525 min of swelling, gels with immobilised catalase are continuing to swell while those without are reaching steady-state. This corresponds with the

increased oxygen supply and improved glucose oxidase stability by the removal of hydrogen peroxide via the catalase reaction.

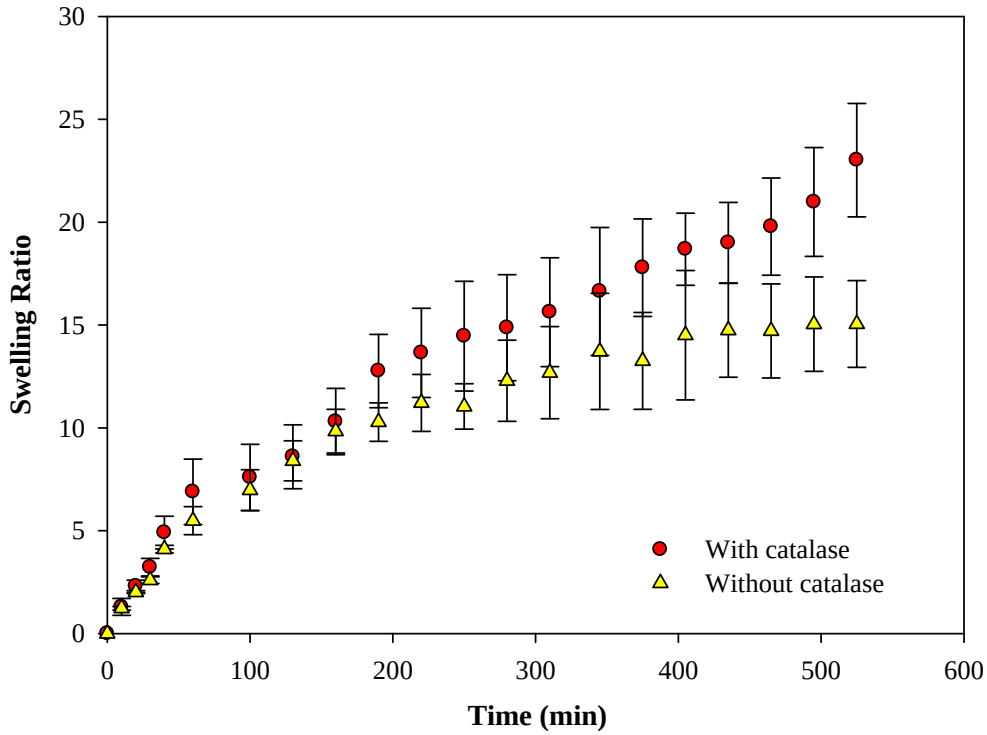

Figure 2.7 Swelling behaviour of glucose-sensitive hydrogels with and without catalase present in stirred glucose (10 mM). (n=3)

2.3.2 Electrochemical optimisation of the glucose-sensitive hydrogels

In this section, it was investigated whether the swelling response of the gels could be converted into measurable electrical signals using non-Faradaic EIS as a transduction method. Tracking the swelling response of hydrogels has routinely been done via optical or piezo-electric measurements [45]. However, little research has been done to date on using an electrochemical or electrical transduction method to track hydrogel swelling in response to a particular analyte for a sensor application. Volume

changes of the polymer network produced by the swelling mechanism upon exposure to glucose were detected and monitored using cyclic voltammetry and EIS.

Carbon cloth was selected as a suitable electrode material for investigating the swelling response of the hydrogel due to its high porosity and flexibility. These characteristics provide extra support to the swollen hydrogel, reducing the risk of delamination from the electrode surface, without restricting the swelling response. With a carbon content of 99%, the fabric also has the electrochemical properties of other carbon-based electrodes i.e. high electric conductivity, gas permeability, corrosion resistance and high tensile strength [209].

Fig 2.8 depicts SEM images of (a-b) bare carbon cloth, (c-d) 1 coat of hydrogel, (e-f) 2 coats of hydrogel and (g-h) 5 coats of hydrogel applied via dip-coating into a hydrogel pre-cursor solution. As the electrode material is porous, hydrogel polymerisation occurs three-dimensionally with the hydrogel penetrating the cloth fibres instead of only coating the surface. The numerous individual fibres are evident in images (a) and (b) showing a high surface area. This is advantageous in an electrode material as it can produce high responses due to the increased surface area of electroactive material. Images (c) and (d) show that 1 coating of gel is sufficient to coat all the fibres of the cloth. As the loading of gel was increased, the topography became smoother and, after 5 coats, the individual carbon fibres were no longer visible (Fig 2.8, e,f).

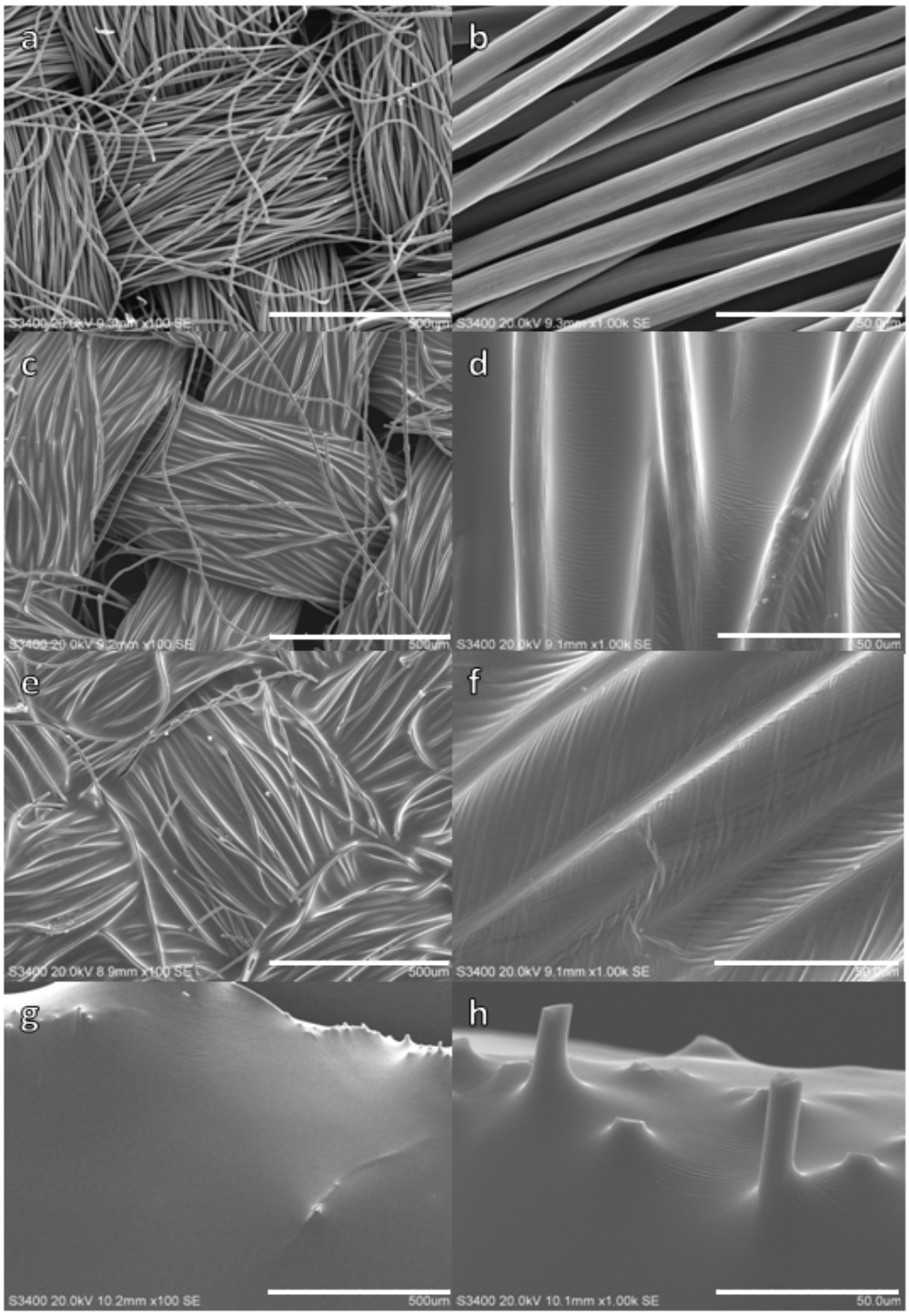

Figure 2.8 SEM images of carbon cloth dip-coated in hydrogel. The right-hand column contains the low magnification (100 X) images (500 µm scale bars) and the left-hand column contains the high magnification (1000 X) images (50 µm scale bars) (a)-(b) bare carbon cloth electrode, (c)-(d) 1 coat of gel, (e)-(f) 2 coats of gel and (g)-(h) 5 coats of gel.

The voltammetric performance of the hydrogel modified carbon cloth was explored using the ferri/ferrocyanide redox couple. CVs of the redox couple at the bare carbon cloth and with a number of hydrogel coatings were recorded (Fig 2.9). The thickness of the hydrogel layer had a profound effect on the voltammetric properties of the carbon cloth. The peak potential separation (ΔEp) increased and the anodic ($i_{p,a}$) and cathodic ($i_{p,c}$) peak currents decreased, as increasing numbers of coats of hydrogel precursors were applied. 5 coats of hydrogel completely inhibited the redox probe from accessing the electrode surface over the timescale of the experiment. This behaviour was attributed to the very thick hydrogel film (Fig 2.8 g,h) which impeded the diffusion of the redox probe to the electrode surface. The electrode with a single coat of gel demonstrated a linear dependence on the square root of scan rate $(\upsilon)^{½}$, (r^2= 0.9928, Fig A-1.1), suggesting a diffusion controlled process was occurring through the hydrogel.

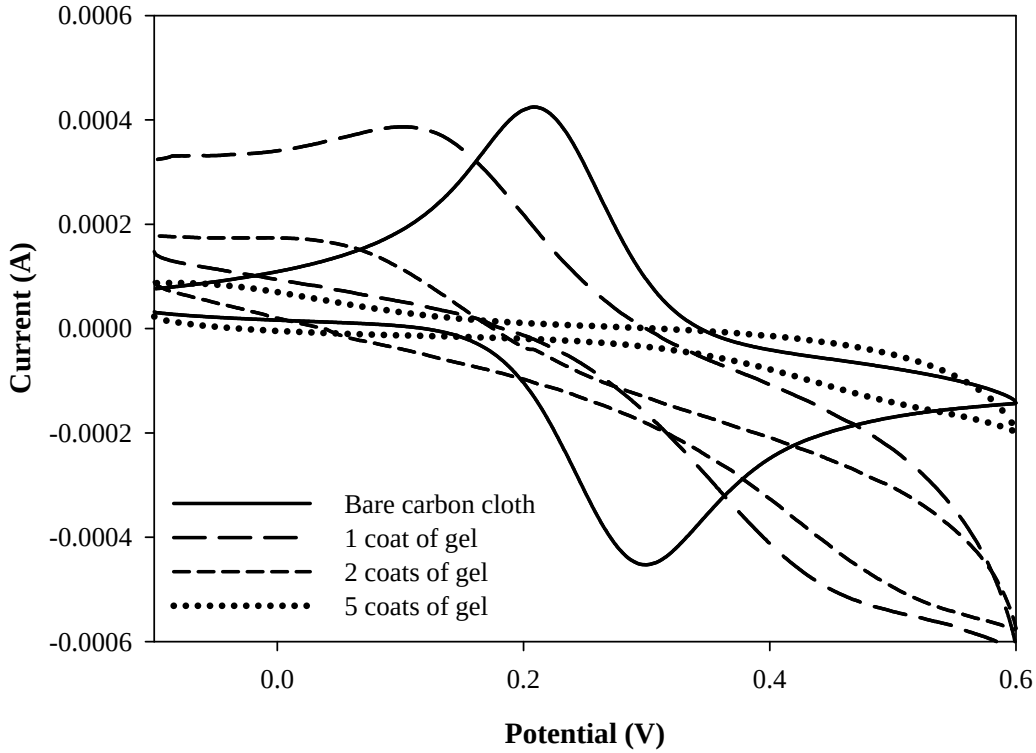

Figure 2.9 Cyclic voltammograms of different hydrogel loadings on carbon cloth electrodes in potassium ferrocyanide (2 mM) in KCl (1 M).

2.3.3 Tracking hydrogel swelling in response to glucose via redox voltammetry

Cyclic voltammetry was employed to investigate the electrochemical response of the glucose-sensitive hydrogel upon exposure to glucose. 1 coat of hydrogel (5 % GOx) was applied to carbon cloth electrodes. Each electrode was allowed reach equilibrium swelling in glucose, within the known physiological range, before measurements were recorded. In order to study the voltammetric performance of the system, electrodes were removed from glucose and placed in bulk potassium ferrocyanide solutions (2 mM). Fig 2.10 displays the response of the ferri/ferrocyanide redox couple through the swollen gels. It was evident that exposing the glucose-sensitive hydrogel to glucose had a very significant influence on the diffusion properties of the hydrogel. The bulk solution Fe^{2+}/Fe^{3+} reversibility improved with increasing glucose concentration. For example, the redox couple gave a ΔEp value of 298 mV after immersion in 10 mM glucose, compared to 512 mV and 403 mV for 1 mM and 2 mM glucose, respectively. The i_p values also increased with glucose concentration. This behaviour was attributed to the ionisation of the hydrogel matrix by the catalysis of glucose to gluconic acid via Equation 2.1. As stated previously, the swelling force generated is proportional to glucose concentration. It is apparent that this swelling force alters the hydrodynamic volume and permeability of the gel, resulting in lower electric resistance and enhanced charge transfer properties.

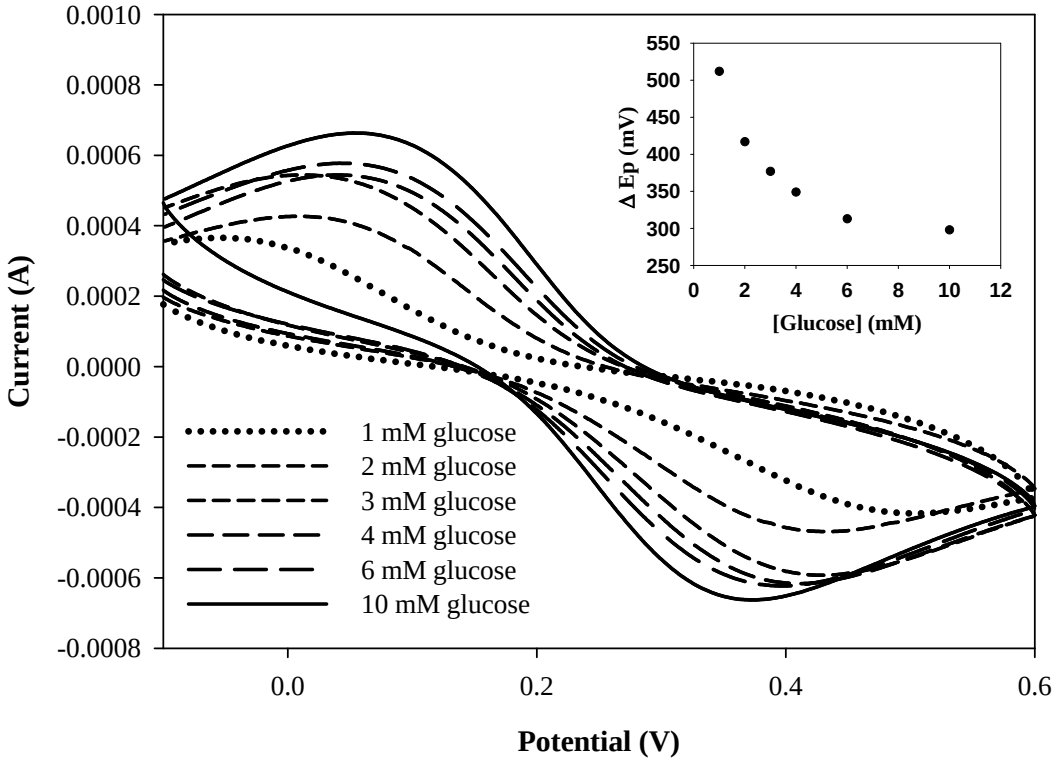

Figure 2.10 Cyclic voltammograms of GOx hydrogel after exposure to glucose in ferri/ferrocyanide (2 mM) in KCl (1 M). Inset figure represents the relationship between ΔEp and glucose concentration.

2.3.4 Tracking hydrogel swelling in response to glucose via EIS

Non-Faradaic EIS was employed as an alternate means to track hydrogel swelling. Fig 2.11 represents typical Nyquist (-Z" vs. Z') plots for the hydrogel modified carbon cloth electrodes with a single coat of gel applied. The Nyquist impedance spectra show the relationship between the real and imaginary components of complex impedance of the hydrogel in response to glucose induced swelling. The spectra are dominated by the presence of capacitive lines. They comprise a high frequency intercept on the real Z' axis and the beginning of a semi-circular arc across the high to low frequency range. The high frequency intercept is representative of a

combination of electrolyte ionic resistance and the resistance of the contacts to the potentiostat. The semi-circular arc, which becomes more visible with increasing glucose concentration, corresponds primarily to changes in capacitance and resistance at the electrode interface. It is evident that swelling of the hydrogel alters the capacitance and diffusional properties of the gel network. The imaginary part of the impedance (-Z") decreases with increasing concentrations of glucose suggesting an increase in capacitance and decrease in gel resistance. This decrease in -Z'' is attributed to the transition of the hydrogel network from a compressed state to an expanded state via ionisation of the polymer backbone and increased osmotic pressure. Thus, hydrogel porosity increases and the diffusion rate through the gel network is accelerated.

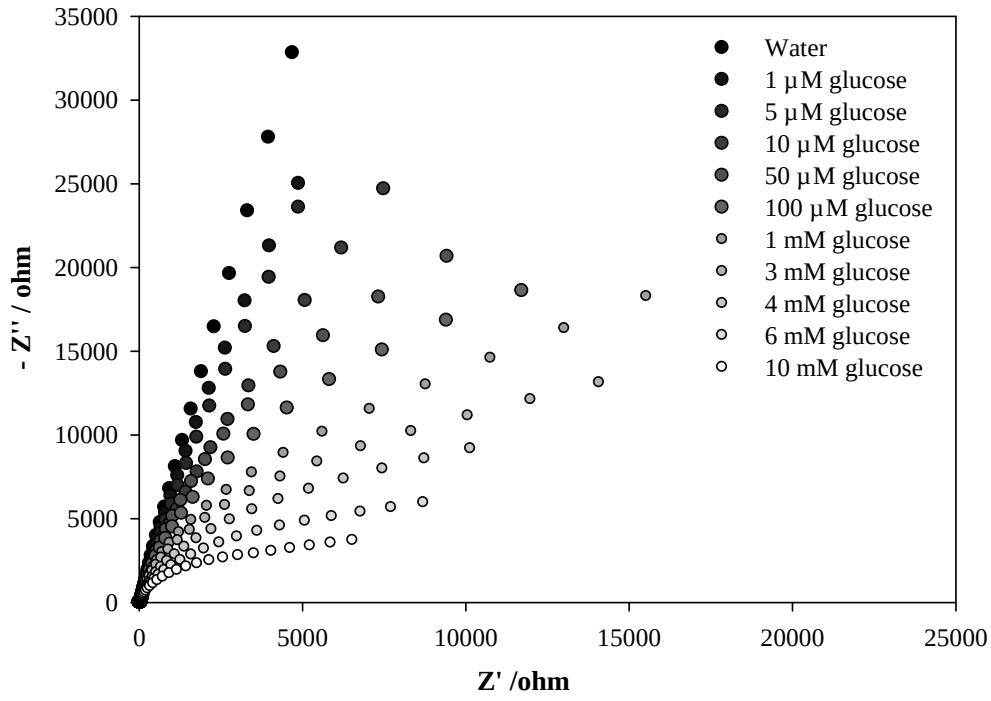

Figure 2.11 Nyquist plot of GOx-modified hydrogels after swelling in various concentrations of glucose for 24 h (in 10 mM PBS).

Fig 2.12 shows combined Bode plots of the modulus of impedance (Z) and the phase curve (ϕ) of the glucose-sensitive hydrogels as a function of the frequency range scanned. They can be divided into frequency regions indicative of the dominant kinetics within that domain. The horizontal domain at high frequencies (>0.4 kHz) with low phase shows resistive behaviour, while the mid-frequency domain (100 Hz to 0 Hz) shows the capacitive behaviour of the hydrogel in the form of line with a slope of -1, with a phase of -80 degrees and finally, the low frequency domain (<0 Hz) where the capacitive behaviour persists. Z is seen to decrease with increasing glucose concentration across the frequency region, resulting again from the increase in the porosity of the hydrogel via ionisation-induced swelling.

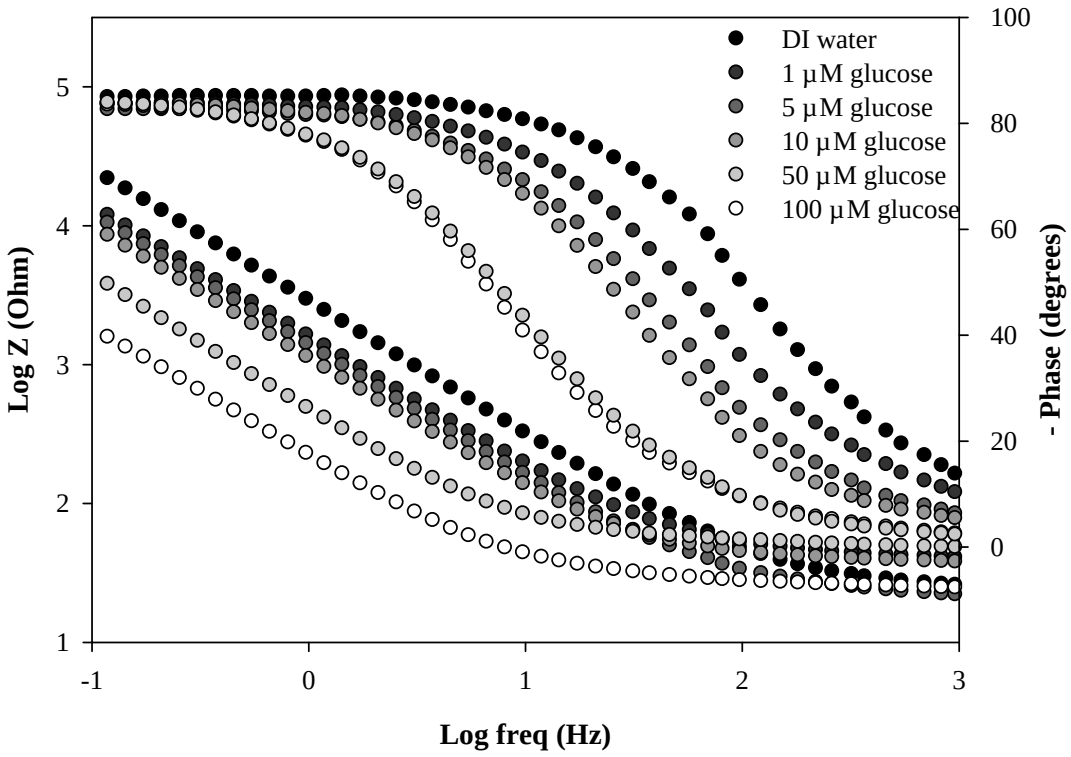

Figure 2.12 Bode plots showing impedance of GOx hydrogels after swelling in various concentrations of glucose for 24 h (in 10 mM PBS).

2.3.5 Quantitative glucose analysis

The swelling response of the optimised hydrogel in glucose was quantitatively tracked using both gravimetry and EIS. Utilising gravimetry, the swelling response of glucose-sensitive hydrogel discs was linear in the range 1 to 20 mM glucose (18-360 mg/dL) with a correlation coefficient of 0.9946 and detection limit of 0.33 mM (Fig 2.13). This detection limit was calculated based on the swelling response of hydrogel discs in DI water. This response was equated to 0.33 mM using the equation of the line generated by the calibration curve with three times the standard deviation added. Hydrogels without GOx incorporated were also swollen in glucose (10 mM) to verify that glucose alone was not altering the swelling response. Hydrogels in the presence of glucose produced a swelling profile equivalent to hydrogels swollen in water indicating that glucose was not interacting with the polymer network (Fig A-1.2).

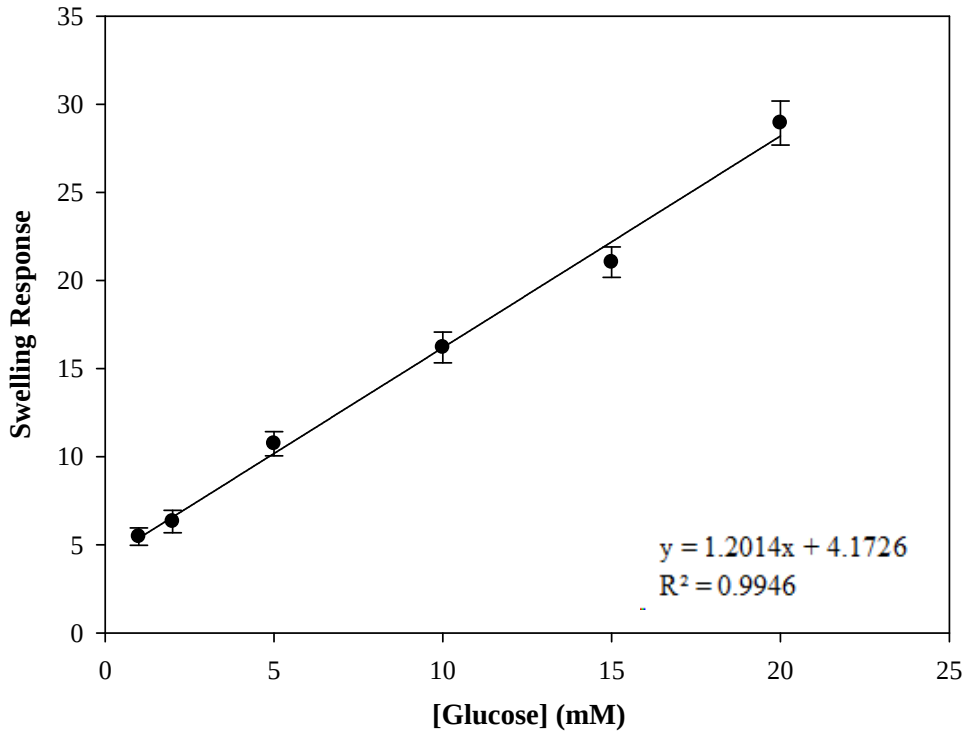

Figure 2.13 Gravimetric calibration curve of glucose-sensitive hydrogel discs after swelling for 100 min in glucose (1-20 mM). (n=3)

A second calibration curve was prepared based on the impedimetric data. EIS can distinguish the individual contributions of each circuit component by modelling the data using an electrical equivalent circuit representative of the system under investigation. The circuit displayed in Fig 2.14 (a) produced the best fit to the experimental data. It is a simple circuit that can be divided up by its individual elements. It comprises the solution resistance (Rs) in series with a parallel combination of a constant phase element (CPE1) and the intrinsic resistance of the carbon cloth substrate (Rcc), connected in series to a CPE (CPE2) and resistance (Rgel) from the hydrogel coating. CPEs were utilised in lieu of pure capacitors to compensate for non-homogeneity in the system. They are sometimes referred to as 'leaky' capacitors and are a realistic model for rough, porous materials such as these [210, 211]. An example

of the fit obtained for these gels in present in Fig A-1.3. Chi-squared (χ^2) values with magnitude of $10^{-4}/10^{-5}$ were observed for all samples which indicated good agreement between the experimental data and the model data obtained from the equivalent circuit. A linear decrease in gel resistance (Rgel) corresponding to the swelling response was detected in the range 1 to 100 µM with a correlation coefficient of 0.9980 and a detection limit of 0.08 µM (Fig 2.14 (b)). The limit of detection was calculated based on the swelling response of GOx-modified hydrogels in PBS (10 mM). The average Rgel value of the hydrogel modified carbon cloth electrodes in PBS equated to 0.08 µM using the equation of the line generated by the calibration curve with three times the standard deviation added. A negative slope in the semi-log plot of glucose concentration versus Rgel indicated first-order reaction kinetics. This was unsurprising as the reaction of glucose and glucose oxidase has been reported previously to follow Michaelis-Menten kinetics (Km = 33 mM) [212].

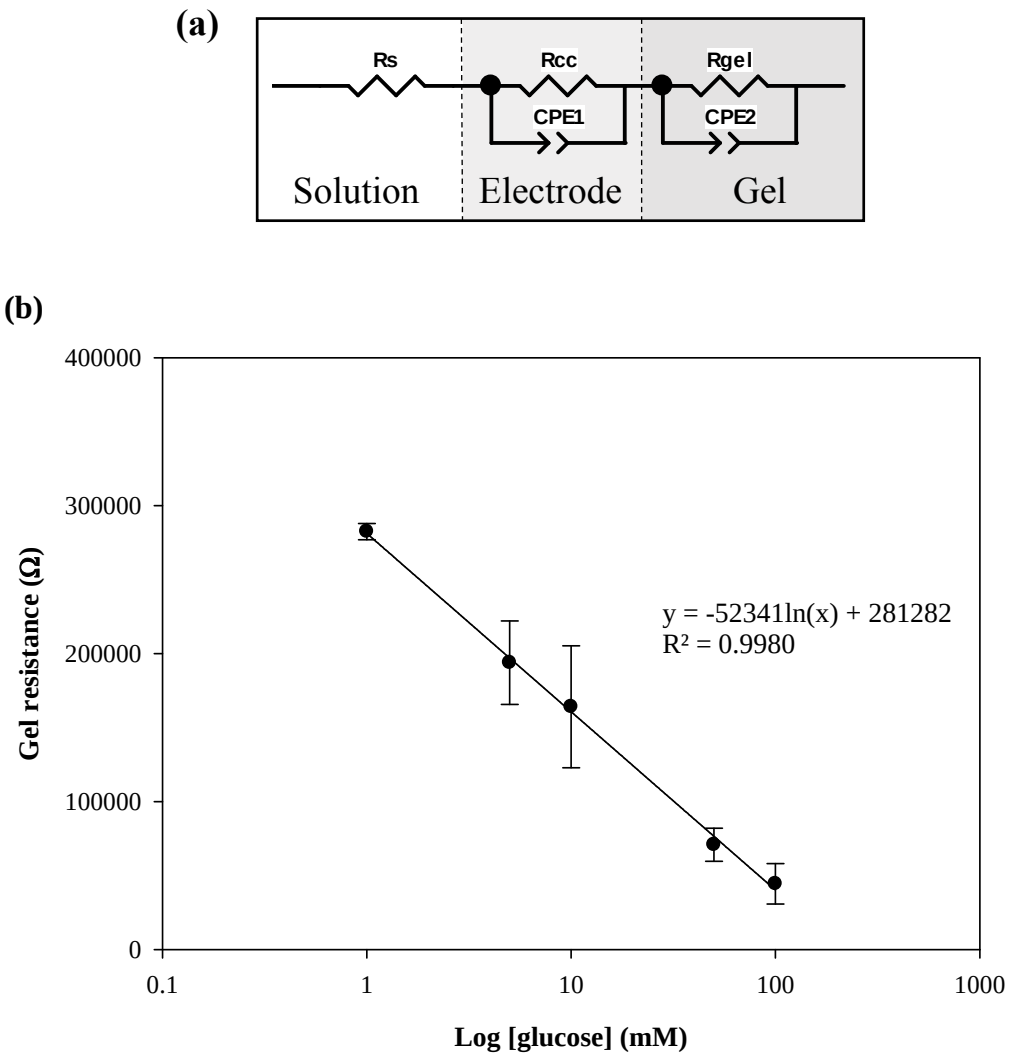

Figure 2.14 (a) Electrical equivalent circuit used for glucose-sensitive hydrogel modified carbon cloth electrodes and (b) EIS calibration curve of GOx-modified hydrogels in glucose using the resistance values obtained from the 'Rgel' component of the electrical equivalent circuit (in 10 mM PBS).

In comparison with the gravimetric method, the linear range has increased by three orders of magnitude and the limit of detection by six orders of magnitude using EIS. This substantial increase in sensitivity, coupled with the textile-based electrode substrate approach introduces the possibility of measuring glucose concentration via

the skin in sweat or ISF - a much less invasive approach to glucose monitoring than blood measurements. Indeed, electrochemical transduction would have significant advantages given its reliability, simplicity and facile coupling with low-cost microelectronics. The choice of a conducting textile opens up the possibility of a wearable glucose sensor, whereas gravimetric measurements are not practical for biosensing, particularly in the area of wearable sensors. As shown in Table 2 the linear range and limit of detection of this work compare favourably with other low glucose concentration biosensors targeting skin analysis.

Table 2.2. Linear range and limit of detection comparison with other low glucose concentration biosensors for skin analysis.

Sensor	Principle	Linear Range	Limit of Detection
GOx-Prussian Blue amperometric biosensor [213]	Temporary tattoo-based system which uses reverse iontophoresis to extract ISF	0-100 µM	3 µM
GOx-Carbon nanotubes amperometric biosensor [214]	3-electrode transducer which uses reverse iontophoresis to extract ISF	3-15 mM	*3 mM
GOx-Ferrocene amperometric biosensor [215]	3-electrode transducer which uses reverse iontophoresis to extract ISF	3-15 mM	*3 mM
Fluorophore-labelled glucose binding protein [216]	Fluorescence intensity decreases with increasing glucose concentration (Unspecified biological matrix)	0-5 µM	0.08 µM
This work	Hydrogel swelling in PBS	1-100 µM	0.08 µM

*In absence of limit of detection lowest standard concentration is given.

2.4 Conclusion

This study demonstrates a rapid, facile, single step method for the fabrication of a glucose-sensitive hydrogel. The 3D nature of the polymer network allowed a high enzyme loading in a biocompatible environment. Initial characterisation of the swelling response using weight-based swelling studies determined that the response could be tailored by variation of the cross-linking density of the network and the enzyme loading. Additionally, the thickness of the hydrogel coating on the carbon cloth had a great impact on its voltammetric properties and suggested a diffusion controlled process was occurring through the hydrogel. EIS measurements showed a decrease in impedance with increasing glucose concentration.

Both gravimetry and EIS were used as quantitative approaches to measure the swelling effect of glucose on these gels. Direct gravimetric measurement gave a sensitivity down to 0.33 mM glucose. In this case of EIS, the limit of detection improves dramatically by approx. 6-fold. This provides strong evidence that non-Faradaic EIS can be used to sensitively track hydrogel swelling in response to a target analyte.

This work establishes for the first time, a simple approach for developing impedimetric biosensors based on the swelling of stimuli-sensitive hydrogels. Possible interference effects remain to be explored, including common organic acids found in sweat such as lactic and pyruvic acid. While the swelling of bulk gels is slow, it is likely that this time will be significantly reduced as the thickness of the gel layers and the scale of the electrodes is reduced. The volume of sample required for analysis will also be reduced following this miniaturisation, providing a viable method for glucose monitoring in wearable sweat or ISF sensors.

Chapter 3

Impedimetric Transduction of Swelling for Detection of β-D-glucuronidase

3.1 Introduction

As detailed in Chapter 2, a pH-sensitive hydrogel has been developed, based on the entrapment of GOx within a PEGDGE-Jeffamine® hydrogel, which swells in response to glucose concentration. Electrochemical transduction was successfully implemented to convert the non-electrical swelling signals into measurable electrical signals. As this system demonstrated good potential as a sensing platform, the next step is to investigate the applicability of this system for other relevant analytes that could be challenging in terms of limit of detection requirements.

The pH-sensitive hydrogel will be developed as a novel sensing platform for the detection of *Escherichia Coli* (*E.coli*) in environmental water samples. *E.coli* is a gram-negative, facultatively anaerobic bacterium which is commonly found in the intestines of people and animals. While the majority of *E.coli* strains are innocuous, some serotypes such as O157:H7 can lead to serious infections when ingested including urinary tract infections, sepsis and gastro-intestinal infections. Therefore, in many countries health departments will routinely screen for *E.coli* in food and water. Early detection and identification of pathogens is highly important for clinical diagnosis, food safety and water analysis [217]. Additionally, *E.coli* has been employed as an indicator microorganism for faecal pollution for numerous years. Recently, there has been renewed interest in the enumeration *of E.coli* in bathing and recreational waters. The European Union introduced a new Bathing Water Directive (2006/7/EC) which was transposed to Irish bathing water regulations in 2008 (S.I. 79 of 2008) and came into operation in 2011. The regulations classify water quality as ‘excellent’, ‘good’ or ‘sufficient’ using *E.coli* and intestinal enterococci as contamination indicators.

Traditional microbiological strategies for screening water samples to determine the concentration of indicator organisms include multiple-tube fermentation, membrane filtration and plate counting [218]. These standard methods are highly accurate and inexpensive, but are labour intensive and time-consuming as the conventional incubation requires 24 to 48 h. As a result, the design of rapid, simple and sensitive methods of *E.coli* detection still remains a challenge. Recently, new methods have emerged which utilise immunoassays, optical and electrochemical detection. Krishnan *et al.* [219] developed an optical immunosensor functionalised with silver-silica core-shell nanoparticles covalently bound with a fluorescent dye and anti-*E.coli* antibody. They achieved a limit of detection of 5 CFU/mL using a sandwich-type assay and photoluminescence spectroscopy detection. Huang *et al.* [220] demonstrated use of antibody-modified graphene to detect *E.coli* as low as 10 CFU/mL based on changes in conductance. Mondani *et al*. [221] designed an antibody microarray which could detect 100-1000 CFU/mL using surface plasmon resonance imaging (SPRi) in complex food matrices (milk and round beef) in approximately 7 h. Maalouf *et al.* [222] compared use of SPR and non-Faradaic EIS for *E.coli* detection with biotinylated anti-*E.coli* linked to neutravidin on a gold electrode. They obtained a detection limit of 10^7 CFU/mL using SPR and 10 CFU/mL whole bacteria with EIS (10^3 CFU/mL lysed *E.coli*), with the EIS signal based upon changes in polarisation resistance which was obtained by fitting the Nyquist spectra with an equivalent circuit.

Frequently, sensing technologies employ synthetic enzyme substrates or fluorogenic dyes, leading to faster, more-specific detection. Enzymes β-galactosidase and β-D-glucuronidase (GUS), produced by *E.coli* are commonly used as marker compounds. They catalyse the hydrolysis of β-glucuronides into D-glucuronic acid and aglycons. Usually the signal will derive from the production of the aglycon which

is detected spectrophotometrically, such as with glucoside o-nitrophenyl-beta-D-galactose and 5-bromo-6-chloro-3-indolyl-β-D-glucuronide, or using fluorimetry, such as 4-methylumbelliferyl-β-D-glucuronide (4-MUG) and carboxyumbelliferyl-B-D-glucuronide [223]. For example, Geary *et al.* [224] detected low concentrations of GUS from *E.coli,* 1.0 x 10^3 CFU/mL, in 230 (± 15.1) min based on the fluorescence of 3-carboxyumbelliferone from carboxyumbelliferyl-B-D-glucuronide. Huang *et al.* [225] developed a biochip with a detection limit of 10^6 CFU/mL and analysis time of 12 h using 4-MUG as a fluorogenic substrate. Electrochemical techniques including amperometry can also be employed. Zhang *et al.* [218] developed an amperometric sensor based on electroanalysis of 4-nitrophenol (4-NP) generated by GUS hydrolysis of 4-nitrophenyl β-D-glucuronide. A linear range of 1.5 x 10^2 to 1.0 x 10^6 CFU/mL and detection limit of 100 CFU/mL were achieved for the 3 h assay based on the reduction of 4-NP using a bismuth nano-film modified glassy carbon electrode. Other groups have investigated the amperometric response of 4-NP in environmental water samples [226] and spiked food samples [227], obtaining detection of 1.0 CFU/mL after 10 h and 4 x 10^4 cells/mL after 1.5 h respectively. Another approach involves modifying the surface of the working electrode with *Moraxella* species which degrades 4-NP into hydroquinone which can be subsequently oxidised and detected using amperometry [228, 229]. An enzyme-based hydrogel using electrochemical transduction has not yet been investigated, to the author's knowledge.

In addition to *E.coli* analysis, detection and quantification of the enzyme GUS is also important in other areas of environmental and clinical analysis. For instance, GUS is frequently used as a reporter gene for monitoring gene expression in plant and mammalian cells. GUS identification is therefore important for determination of spatial and temporal expression of the target gene [230-232]. In humans, deficiency of

GUS can result in the metabolic disease Mucopolysaccharidosis VII (Sly syndrome) [233]. It also has been identified as a possible marker for colon cancer and can be used to measure the degree of differentiation and invasiveness of colorectal cancer cells [234, 235].

This chapter investigates GUS detection based on electrochemical detection of the swelling response of the pH-sensitive hydrogel. As illustrated in Fig 3.1, 4-MUG will be immobilised in the PEGDGE-Jeffamine® hydrogel initially. Network ionisation, and therefore swelling, will be induced when the hydrogel is immersed in an aqueous solution of GUS due to the production of D-glucuronic acid. Similar to D-gluconic acid, D-glucuronic acid will ionise the pendent amine groups of the network, generating charge along the polymer backbone. Electrostatic repulsion forces between the adjacent ionised groups will create a large osmotic swelling force altering the hydrodynamic volume and permeability of the gel proportionally with enzyme concentration.

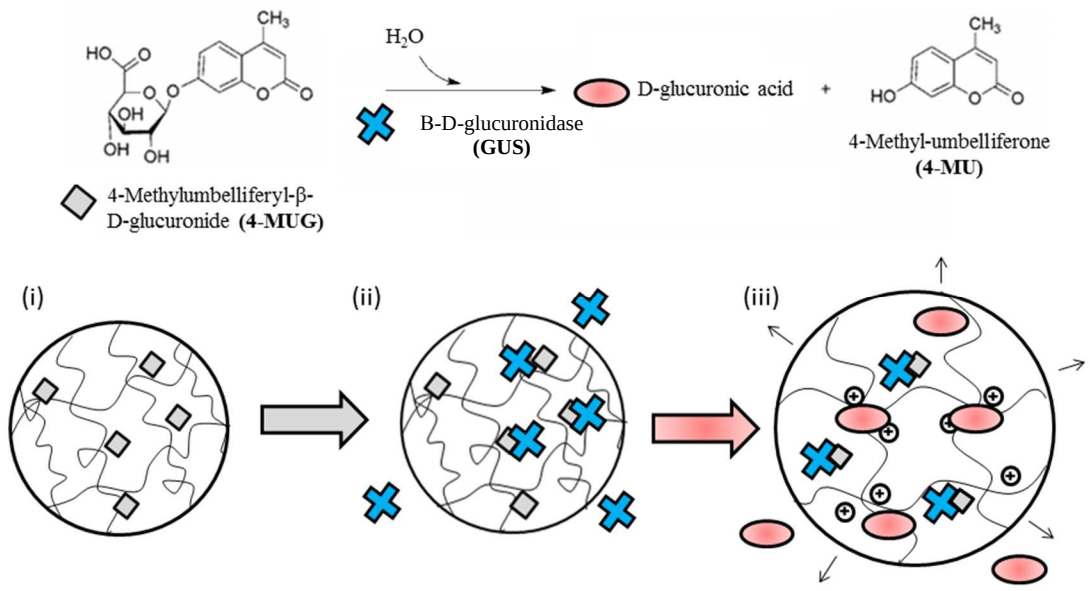

Figure 3.1. Schematic of the swelling mechanism: (i) 4-MUG immobilised within the pH-sensitive polymer network, (ii) GUS diffusion and (iii) production of glucuronic acid/network ionisation.

3.2 Experimental

3.2.1 Materials

As per Materials Section 2.2.1 with the following additions: β-glucuronidase from *Escherichia coli*, 4-methylumbelliferyl-β-D-glucuronide hydrate (4-MUG), 4-nitrophenol β-D-glucuronide (4-NPG) and 4-nitrophenol (4-NP) were purchased from Sigma-Aldrich (Ireland). All chemicals were used as purchased and all aqueous solutions were prepared using DI water (18 MΩ cm @ 298 K).

3.2.2 Instrumentation

As per Instrumentation Section 2.2.2.

3.2.3 4-MUG hydrogel synthesis

4-MUG hydrogels were prepared by cross-linking PEGDGE and Jeffamine® EDR-148 polyetheramine in a 1.0:1.0 molar ratio in DI water. 0.5% w/w 4-MUG was added into the hydrogel precursor solution and inverted several times until it was fully dissolved.

3.2.4 GUS hydrogel synthesis

GUS hydrogels were prepared by cross-linking PEGDGE and Jeffamine® EDR-148 polyetheramine in a 1.0:1.0 molar ratio in DI water. 0.5% w/w GUS was added into the hydrogel precursor solution and inverted several times until it was fully dissolved.

3.2.5 Gravimetric characterisation of the swelling response

Cylindrical discs of 4-MUG and GUS hydrogels were prepared by pouring 4 mL of the hydrogel precursor solution into petri-dishes (53 mm internal diameter) and

placing them in the refrigerator (4^{O}C) overnight to polymerise. Cylindrical discs (3.5 mm diameter) were cut from the polymerised membrane with a Harris Uni-Core™ core sampler. Their swelling ratio in DI water was measured at regular time intervals and calculated as per Section 2.2.4. If stated that temperature was applied, the swelling solutions, containing the gels, were placed in a heated water bath at the desired temperature for the duration of the experiment.

3.2.6 Impedimetric analysis of swelling

Carbon cloth electrodes were cut and insulated as per Section 2.2.5. Single dip coats of GUS hydrogels were applied to the working area of the electrodes and they were placed in the refrigerator (4^{O}C) overnight to polymerise. The GUS-modified carbon cloth electrodes were swollen in solutions of 4-MUG (5 mM) or 4-NPG (5 mM) in water baths at 37^{O}C and the impedance spectra were recorded after 500 min using the parameters outlined in Section 2.2.2. If stated, open circuit potential (OCP) measurements were also recorded for 300 s and the impedance spectra were then performed at the final OCP reading after this time period. The calibration curves were prepared by fitting the data with an appropriate electrical equivalent circuit.

When investigating the effect of temperature on the impedimetric measurements, 1:1 PEGDGE-Jeffamine® hydrogel modified carbon cloth electrodes were prepared. Impedance spectra were recorded without prior swelling to obtain the initial resistance of the hydrogels. The hydrogels were then swollen in DI water in water baths at room temperature, 37^{O}C or 50^{O}C. Impedance spectra were recorded after 300 min and 500 min of swelling. Statistical analysis was performed using the Analysis ToolPak in Microsoft Excel 2013. Data were compared using one-way

analysis of variance (ANOVA). p values lower than 0.05 indicate that the populations are significantly different with 95% confidence.

3.2.7 Cyclic voltammetry in 4-NP

Voltammograms of bare carbon cloth electrodes were recorded in 1 mM 4-NP (10 mM PBS) by cycling between -0.8 and 1.2 V at 0.05 V/s vs. Ag/AgCl.

3.3 Results & Discussion

3.3.1 Gravimetric swelling analysis of 4-MUG hydrogels in GUS

4-MUG hydrogels were fabricated by dissolving 4-MUG in the PEGDGE-Jeffamine® precursor solution. As illustrated in Fig 3.1, 4-MUG is hydrolysed to D-glucuronic acid by GUS producing an acidic environment which ionises the pendant basic groups of the cationic network and generating charge along the polymer backbone. Electrostatic repulsion forces between adjacent ionised groups creates a large osmotic swelling force, which is further enhanced by the glucuronate anions ($C_6H_9O_7^-$) migrating into the gel matrix to balance the charge.

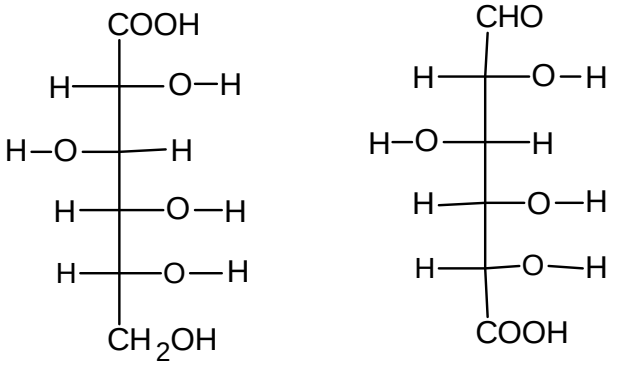

D-gluconic acid (pKa 3.6)

D-glucuronic acid (pKa 3.2)

Figure 3.2 Structure and pKa values of D-gluconic and D-glucuronic acid [236].

It was anticipated that these hydrogels would produce a similar swelling profile in GUS as the glucose-sensitive hydrogels in glucose, as glucuronic and gluconic acid have similar structures and pKa values (Fig 3.2). As previously stated, the hydrogel

volume transition occurs when the pH of the surrounding environment reaches the pK_a of the ionisable moiety, and continues until ionisation is complete. However, as depicted in Fig 3.3, 4-MUG hydrogels displayed a similar swelling response in all GUS solutions irrespective of enzyme concentration. This non-specific response indicates that there is an insignificant (or no) interaction between 4-MUG and GUS within the gel. Consequentially, the swelling behaviour is dominated by water uptake due to the hydrophilic nature of the gel as opposed to network ionisation. It is postulated that glucuronic acid was not produced in the gel due to size exclusion. As the enzyme was contained in the solution in this instance, the cross-linking density and pore size of the hydrogel could have prevented it from entering the matrix and hydrolysing the 4-MUG due to its relatively large size. It is probable that the 4-MUG could still diffuse out of the gel and generate some acid in the surrounding solution. However, it would take significantly longer for the acid concentration to build-up and diffuse into the hydrogel to achieve electrostatic repulsion and the counter-flux of glucoronate anions. Size exclusion is frequently observed in hydrogel-based systems and has previously been applied for interference suppression [111] and ‘capture and release’ separations [237].

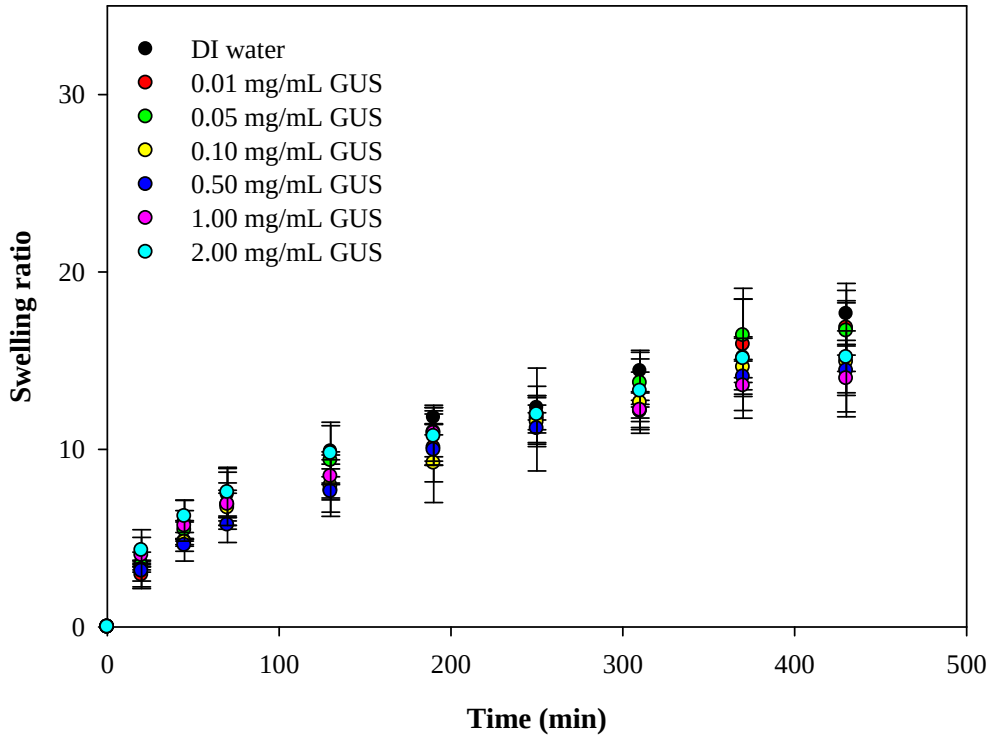

Figure 3.3 Swelling response of 0.5% 4-MUG hydrogels in 0.01-2.00 mg/mL GUS solutions. (n=3)

3.3.2 Gravimetric swelling analysis of GUS hydrogels in 4-MUG

In order to verify that size exclusion was inhibiting the response, the system was inverted and GUS was immobilised in the PEGDGE-Jeffamine® network instead. Subsequently, these GUS hydrogels were immersed in 4-MUG solutions. A schematic depicting this alternative swelling mechanism is provided in Fig 3.4 and the swelling response of 0.5% (w/w) GUS hydrogels in 4-MUG (1-20 mM) is shown in Fig 3.5.

0.5% (w/w) GUS hydrogels displayed a linear swelling response in 4-MUG with clear discrimination between substrate concentrations (Fig. 3.5 (b)). A wide range of swelling ratios were obtained, with greater swelling ratios achieved in higher concentrations of 4-MUG due to increased acid production enhancing network

ionisation and the counter-flux of glucoronate anions. In comparison with the original design, a distinct difference was observed in terms of a concentration-dependant swelling response. The improvement in selectivity suggests that size exclusion was previously inhibiting the enzyme-substrate interaction and the inversion in configuration was sterically favourable. Unfortunately, the hydrogel's cross-linking density could not be reduced to increase pore size, and thereby possibly allow access of GUS into the gel, as high temperatures are required to polymerise gels with excess Jeffamine® which would potentially damage the substrate and gel.

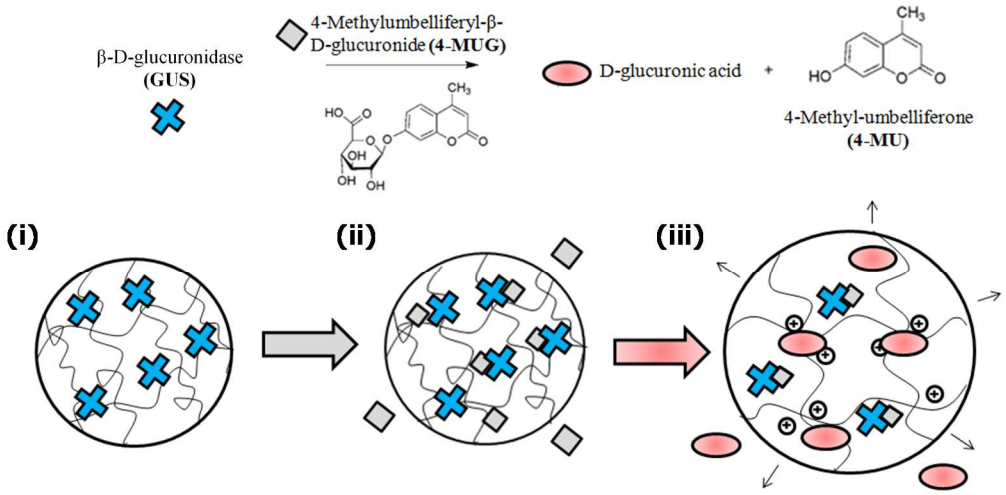

Figure 3.4 Schematic of the alternative swelling mechanism: (i) GUS immobilised within the pH-sensitive polymer network, (ii) 4-MUG diffusion and (iii) production of glucuronic acid/network ionisation.

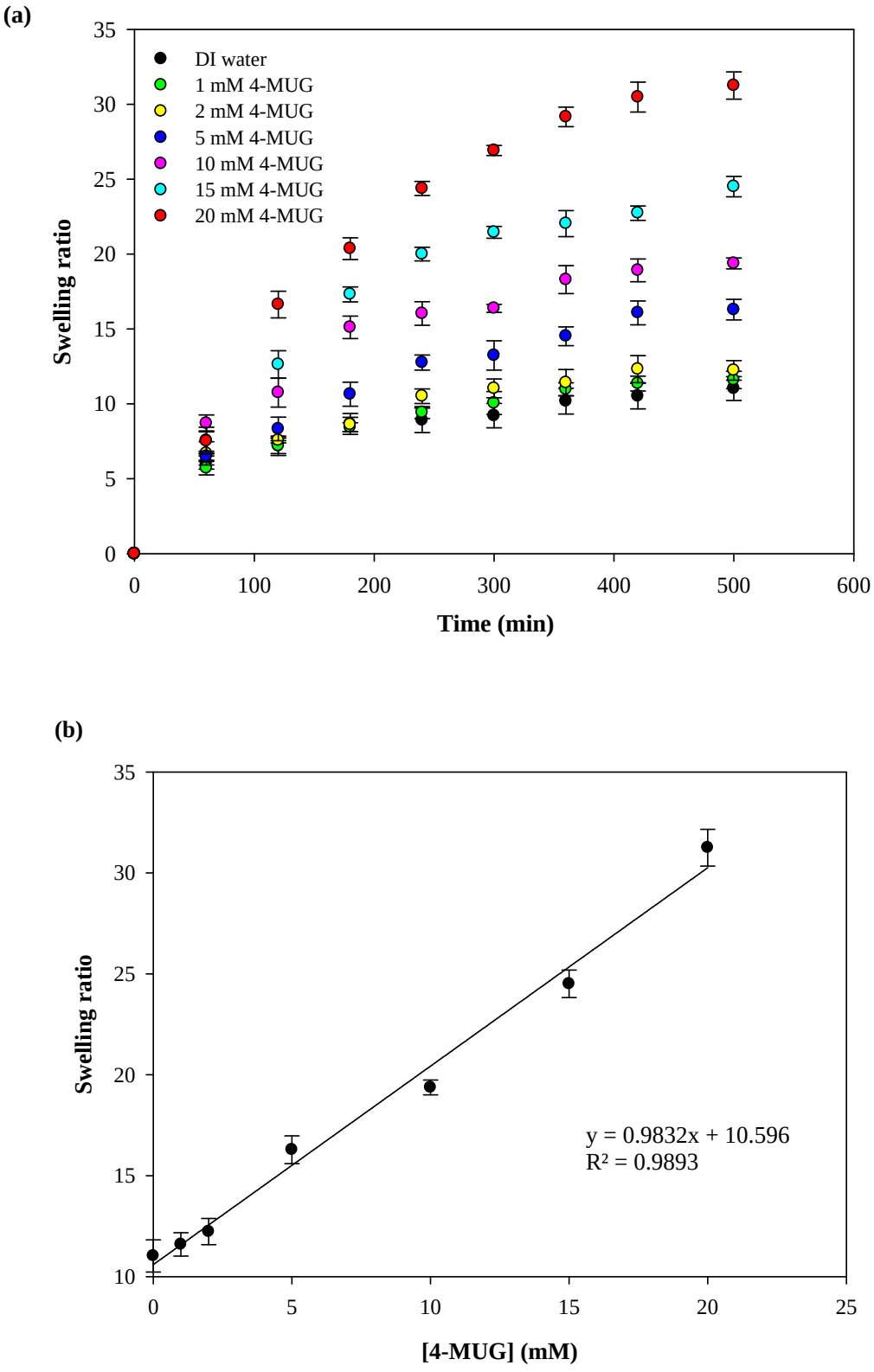

Figure 3.5 (a) Swelling response of 0.5% GUS hydrogels in 1-20 mM 4-MUG solutions and (b) calibration curve of swelling ratio of 0.5% GUS hydrogels in 4-MUG after 500 min. (n=3)

These preliminary results indicated that GUS detection could still be achieved utilising the new design. Therefore, it was decided to vary the loading of GUS in the hydrogels and investigate their swelling response both gravimetrically and impedimetrically in a fixed concentration of 4-MUG. Hydrogels were prepared with GUS loadings between 0.01 and 1.00% (w/w) by dissolving the GUS in the PEGDGE-Jeffamine® precursor solution. 5 mM 4-MUG was selected as an appropriate concentration for this work as the 0.5% GUS hydrogels used previously demonstrated ionisation-induced swelling even at early time points in this concentration and to reduce the cost associated with 4-MUG. Additionally, the 4-MUG swelling solutions were heated at 37^{O}C as this is the optimum temperature for GUS (from *E.coli*) activity and is frequently used as incubation temperature in commercial GUS assays [238, 239]. Fig. 3.6 shows the gravimetric swelling response of these gels in 4-MUG (5 mM) and a calibration curve of swelling response versus GUS concentration generated after 500 min. A linear increase in swelling response was observed upon increasing the GUS loading from 0.01-1.00% with a correlation coefficient of 0.9854 and a limit of detection of 0.0163% GUS (27.17 μM). Microbiological testing would be required to convert this LOD to CFU or MPN and compare with other reported methodologies and commercial technologies. Although this was not done as part of this thesis, these results do indicate that the PEGDGE-Jeffamine® hydrogels possess good potential for detection of GUS, and therefore, possibly *E.coli*.

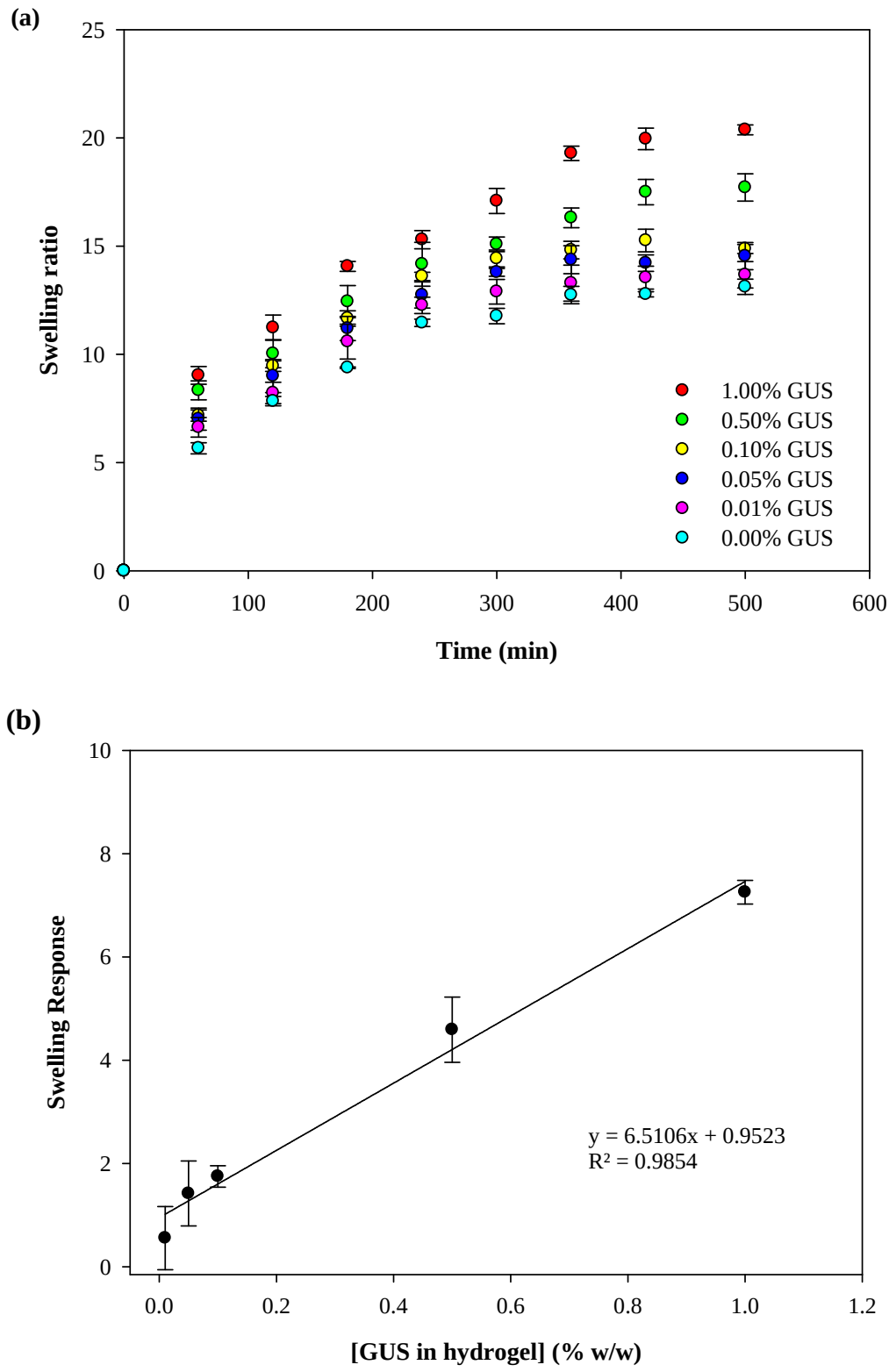

Figure 3.6 (a) Gravimetric swelling response of GUS hydrogels over 500 min and (b) Calibration curve for GUS hydrogels (0.01-1.00%) after 500 min in 4-MUG (5 mM) at 37^{O}C. (n=3)

3.3.3 Impedimetric swelling analysis of GUS hydrogels in 4-MUG

Representative Nyquist spectra of the GUS hydrogels in 4-MUG (5 mM) recorded after 500 min are shown in Fig 3.7. They comprise a high frequency intercept on the real Z' axis and the beginning of a semi-circular arc across the high to low frequency region. The semi-circular arc and imaginary part of the impedance (-Z") is observed to decrease as the loading of GUS in the gel increases. This is attributed to alterations in the resistance and capacitance properties at the electrode-electrolyte interface generated by hydrogel swelling. Within the timescale of the experiment, the resistance of the hydrogels decreases with a higher enzyme loading present. Each GUS molecule functions as an active site for the catalysis of 4-MUG to glucuronic acid, therefore the rate of production of glucuronic acid is faster in the hydrogel containing 1.00% GUS in comparison with the 0.01% GUS gel. Subsequently, the hydrogel is ionised, porosity increases and gel resistance decreases at a faster rate.

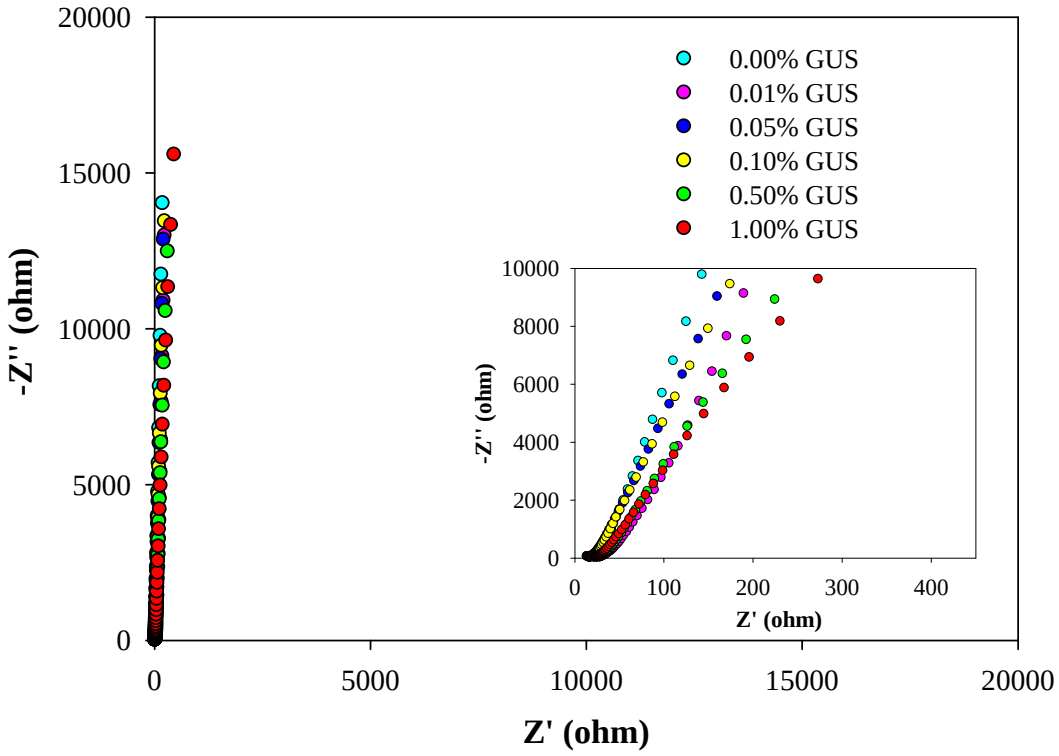

Figure 3.7 Nyquist spectra of GUS hydrogels in 4-MUG (5 mM) at 37^{O}C after 500 min. (n=3)

The impedimetric data was modelled using an electrical equivalent circuit to investigate if the ionisation-induced swelling could be tracked impedimetrically as in Chapter 2. The same equivalent circuit was utilised as there were no additional system components or configuration changes which would necessarily impact circuit design. Additionally, a chi-squared (χ^2) with magnitude of $10^{-4}/10^{-5}$ was observed which indicated good agreement between the experimental data and the model data obtained from the equivalent circuit. Similarly to the impedimetric glucose calibration curve generated in Chapter 2, a GUS calibration curve was produced using the gel resistance values acquired by fitting the data (Fig 3.8). A logarithimic curve provided the best fit for the calibration data. A rapid decrease in gel resistance is visible as the concentration of GUS in the hydrogel increases from 0.01% to 1.00%. This is again

attributed to the increased porosity resulting from enhanced ionisation and demonstrates that concentration of GUS can be determined impedimetrically. The logarithmic fit indicates first-order reaction kinetics as in Chapter 2. However, as the enzyme concentration was changing in this instance, a zero order reaction would be observable if the substrate was present in excess amount, i.e. the reaction would be independent of substrate concentration and the plot would be linear without using a logarithmic transformation (rate = k). Thus, as the rate is proportional to the first power of substrate concentration (rate = k[S]), this implies that the substrate was not in excess and was a limiting factor in the reaction. It is likely that response time and sensitivity could be improved by increasing the amount of 4-MUG present.

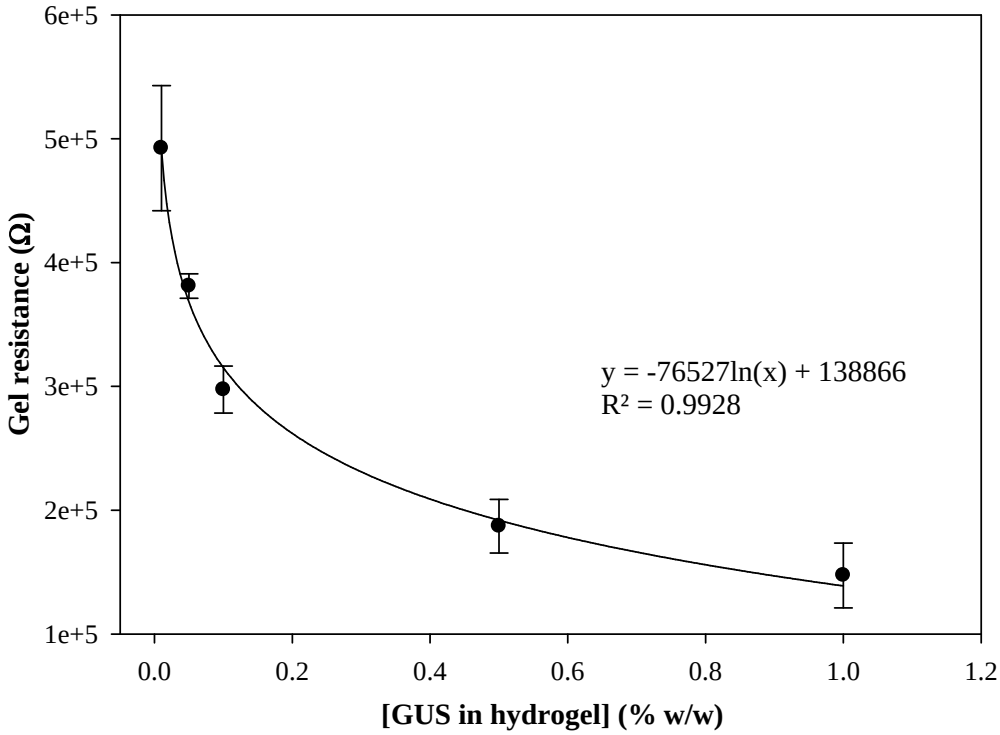

Figure 3.8 Calibration curve for GUS hydrogels (0.01-1.00%) after 500 min in 4-MUG (5 mM) at 37^{O}C using EIS. (n=3)

The limit of detection under these conditions was calculated as 0.006% GUS (10.02 μM) using this method which is an improvement on the limit of detection achieved using the gravimetric method (0.0163% or 27.17 μM GUS). However, a greater improvement in detection limit was anticipated due to the higher sensitivity of EIS. Possible causes of just this small improvement could include temperature effects or issues with the solubility of the substrate. These effects are investigated in the following sections.

3.3.4 Effect of temperature on hydrogel swelling

Both the gravimetric and impedance measurements were performed at 37^{O}C in this chapter, the optimum temperature for GUS activity. Given that the earlier work on glucose was carried out at room temperature, it was of interest to investigate the effect of applied temperature on the swelling ratios and impedance measurements of the hydrogels. Fig 3.9 shows the swelling response of 1:1 PEGDGE-Jeffamine® hydrogels in DI water at different temperatures (0-50^{O}C). The swelling rate of the hydrogels was observed to increase with temperature. This phenomenon has been observed with other hydrogel systems and has been attributed to an increase in the penetration rate of fluid into the gel matrix [240] and/or an increase in the elasticity of the polymer chains as temperature is increased [241]. Additionally, hydrogels swollen at 37^{O}C achieved a higher swelling capacity than hydrogels swollen at room temperature at 500 min (Fig 3.9). This increase in swelling rate and overall capacity at elevated temperatures likely leads to improved sensitivity and hence limit of detection for GUS enzyme detection using gravimetry.

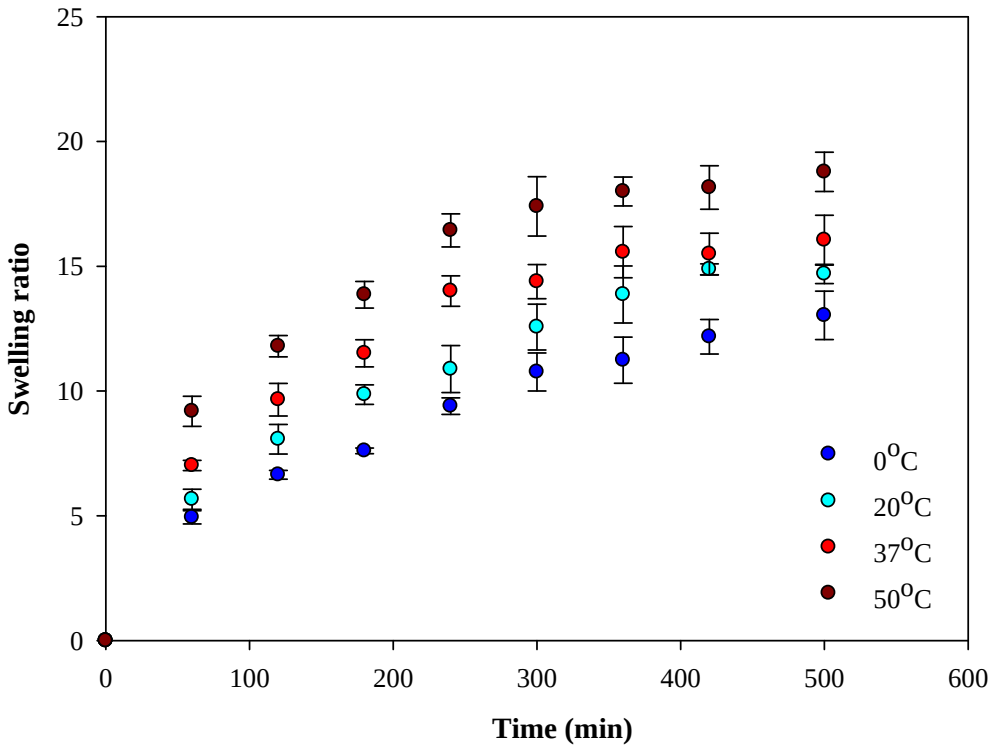

Figure 3.9. Effect of temperature on swelling ratio of 1:1 PEGDGE-Jeffamine® hydrogels in DI H_2O. (n=3)

The effect of temperature on the impedimetric transduction was also investigated. The initial resistance of hydrogels without prior swelling was modelled using the equivalent circuit. The reduction in gel resistance was then recorded after 300 and 500 min of swelling in water at 20^{O}C, 37^{O}C and 50^{O}C, and expressed as a percentage in Table 3.1. One-way ANOVA was performed to determine if the mean reductions in gel resistance were statistically difference upon heating. The p value generated by ANOVA indicates the confidence of the statistical variation. Values below 0.05 express 95% confidence that the populations are considered statistically significantly different. As shown in Table 3.1, the p values produced were greater than 0.05 indicating that there was no statistical difference in the reduction of gel resistance

when swollen at 37^{O}C or 50^{O}C at the selected time points tested. Therefore, this indicates that swelling the hydrogels at 37^{O}C did not impact the impedimetric measurement and consequently, the detection capabilities of this method. However, it is noteworthy that if higher temperatures (>50^{O}C) were applied and the sample population was greater, changes in Rgel may be deemed significant using ANOVA. However, under the current conditions, ANOVA testing found the change to be insignificant at a 95% CI (n=3).

Table 3.1 Effect of temperature on impedimetric change in resistance of 1:1 PEGDGE-Jeffamine® hydrogels over time in PBS (10 mM). (n=3)

	Decrease in Rgel (%)			
Time (min)	Room temp (20^{O}C)	37^{O}C	50^{O}C	ANOVA p value
300	32.3 ± 20.7	35.8 ± 13.3	37.8 ± 11.9	0.913
500	54.9 ± 3.0	50.9 ± 12.2	60.3 ± 3.9	0.373

3.3.5 Investigation into use of 4-NPG as an alternate substrate

In addition to determining the effect of temperature on the swelling response, an alternative substrate to 4-MUG was also investigated, 4-nitrophenol β-D-glucuronide (4-NPG). In comparison with 4-MUG, 4-NPG is much more stable in solution. It has a solubility of approximately 100 mg/mL in water compared with 0.35 mg/mL for 4-MUG. It is possible that even with the sonication and heating the 4-MUG

was not fully dissolved in solution for the previous experiments and therefore, could not interact as efficiently with the GUS to effect ionic repulsion and hence swelling within the gel. Consequently, the gravimetric and impedimetric analyses were repeated using 4-NPG.

Fig 3.10 displays the swelling response of GUS hydrogels in 4-NPG (5 mM) at 37^{O}C and a calibration curve recorded after 500 min (Fig 3.10 (b)). Mirroring the previous swelling study in 4-MUG, a linear increase in swelling ratio was observed as the GUS loading was increased from 0.01% to 1.00%. This again corresponds to the production of glucuronic acid which ionises the pendant amine groups in the hydrogel network and increases the swelling response due to electrostatic repulsion and increased osmotic pressure. However, the GUS hydrogels swelled faster and achieved higher swelling ratios in 4-NPG. For example, after 60 min, 1.00% w/w GUS hydrogels achieved a swelling ratio of 17 in 4-NPG versus 9 in 4-MUG, indicating that the swelling rate had almost doubled at this early time point. After 500 min, these 1.00% w/w GUS hydrogels obtained a swelling ratio of 28 in 4-NPG compared with a swelling ratio of 20 in 4-MUG demonstrating a higher equilibrium swelling ratio. A wider range of swelling ratios was also visible, ranging from 19-28 in 4-NPG versus 13-20 in 4-MUG. This improvement was reflected in the LOD additionally as it decreased from 0.0163% GUS (27.17 μM) to 0.042% GUS (7.00 μM). It is likely that the improvement arises from the higher stability of 4-NPG in solution which increases the efficiency of glucuronic acid generation and hence the degree of ionisation.

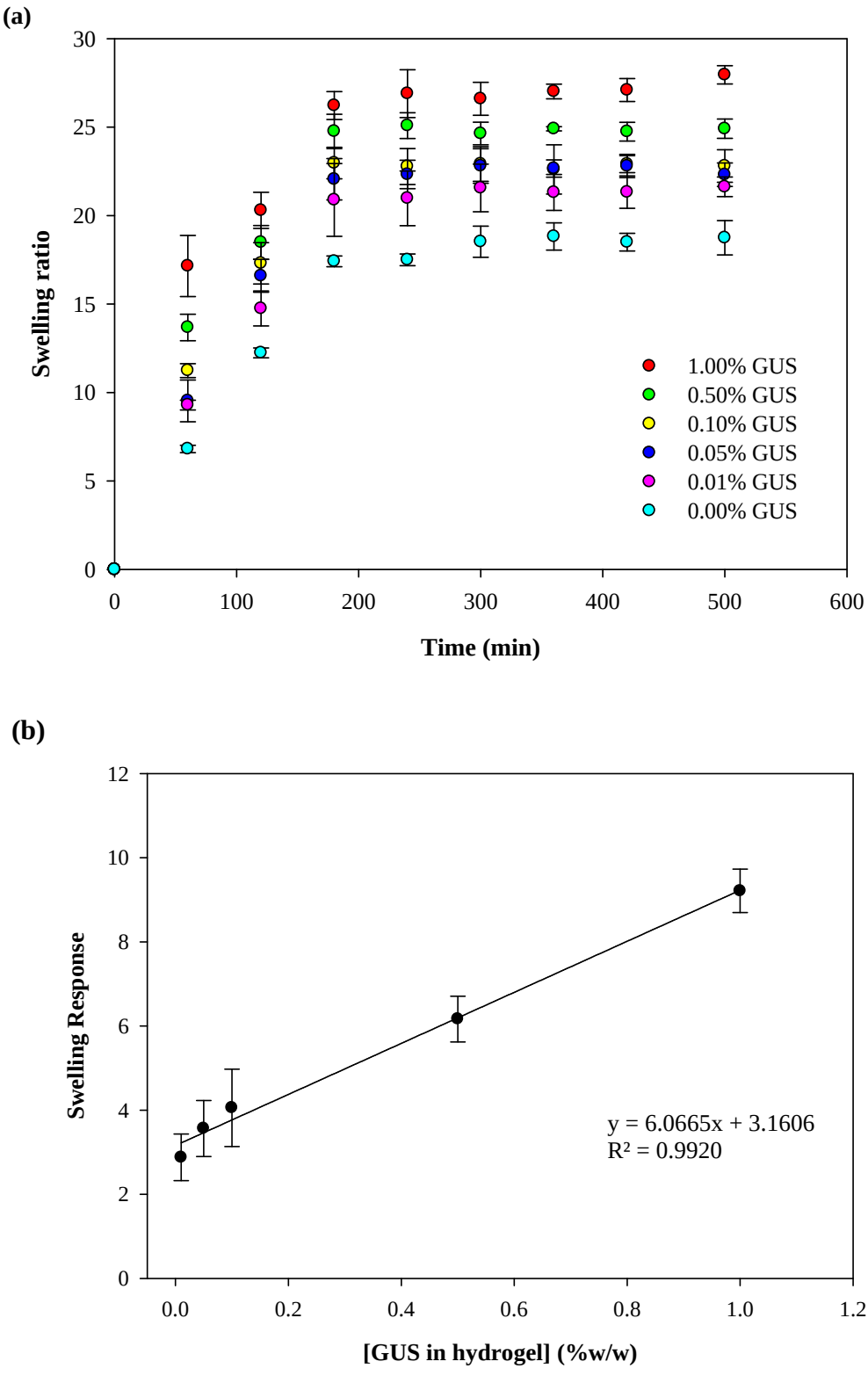

Figure 3.10 (a) Swelling response of GUS hydrogels over 500 min and (b) Calibration curve for GUS hydrogels (0.01-1.00%) in 4-NPG (5 mM) at 37^{O}C after 500 min. (n=3)

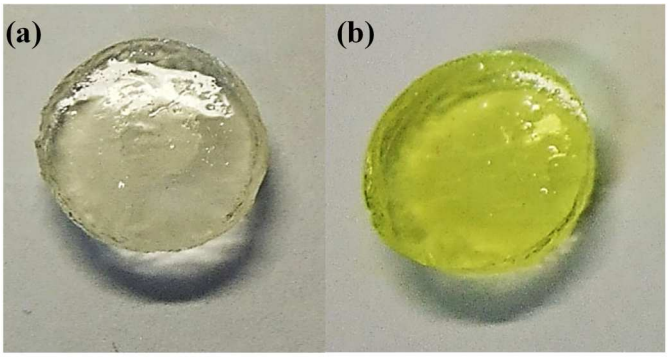

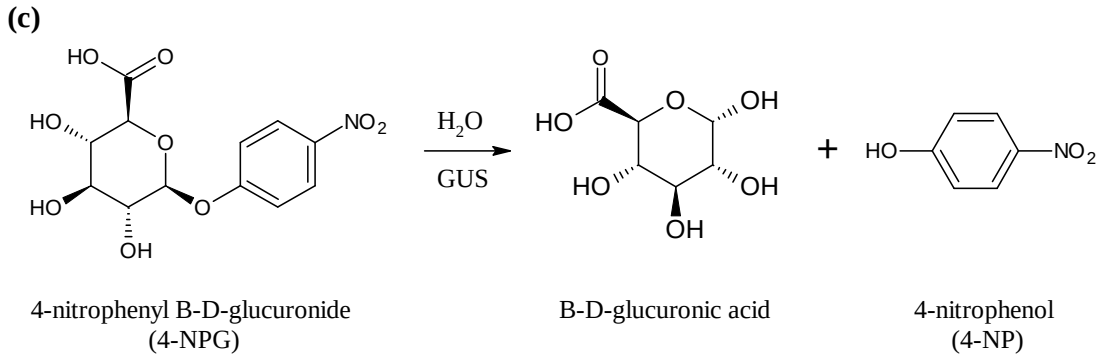

Figure 3.11 Photographs of unmodified hydrogel (0% GUS) (a) and 1.00% (w/w) GUS hydrogel swollen in 4-NPG (5 mM) (b). (c) Enzymatic reaction of GUS with 4-NPG.

As stated previously, GUS catalyses the hydrolysis of β-conjugated D-glucuronides into glucuronic acid and an aglycon. Fig 3.11 (c) shows the catalysis of 4-NPG into D-glucuronic acid and 4-nitrophenol (4-NP). The bright yellow of the GUS hydrogel in Fig 3.11 (b) originates from the generation of 4-NP during this reaction. GUS assays have been developed based on spectrophotometric detection of 4-NP at 415 nm [242]. As the yellow colour is quite vibrant in the hydrogel it is possible that solid-phase spectroscopy could be utilised to measure GUS concentration also. Of particular importance is that, unlike 4-MU, 4-NP is electroactive. Many groups have developed electrochemical sensors for 4-NP with the analytical signal derived from the 4 electron reduction of the nitro group as it is listed as a priority pollutant by the US Environmental Protection Agency (EPA) due to its toxicity [243-

245]. In relation to this work, an investigation into the electroactivity of 4-NP on carbon cloth was required to ascertain if there was activity present at 0 V, the potential used for the impedance measurements. It is likely that any activity present would bias the electrode and alter the swelling response of the hydrogel. For example, polyelectrolyte hydrogels, such as the PEGDGE-Jeffamine® gel, have been reported to bend in an electric field due to a change in osmotic pressure. This change originates from a difference in the ionic concentration inside and outside of the gel as the counterions of the polyions in the gel and the free ions in solution migrate towards their counter-electrodes provoking an ionic gradient along the direction of the electrical field. Specifically, polycationic gels will swell on the cathode side and shrink on the anode side, thereby bending towards the anode [246-248]. Therefore, if the electrode was biased, such a bending effect would alter the swelling and impact the measurement of gel resistance.

3.3.6 Electrochemical response of 4-NP on carbon cloth

Fig 3.12 (a) shows a cyclic voltammogram of bare carbon cloth in 4-NP. Two redox couples were detected A1/C1 (-0.097 V/-0.171 V) and A2/C2 (0.077 V/0.024 V). Additional peaks A’ (0.90 V) and C’ (-0.35 V) were observed. As the number of potential cycles was increased, the A’ and C’ peak currents decreased and the peak currents corresponding to the redox couples increased. A similar phenomenon was reported recently by Sundaram *et al*. [249]. They proposed the reaction pathway shown in Fig 3.12 (b) to explain the electrochemical behaviour of 4-NP (in pH 5.0 to 7.0). Nitrophenol is firstly irreversibly reduced to hydroxyl aminophenol with the transfer of four electrons and four protons. Secondly, the hydroxyl aminophenol loses one H_2O

yielding benzoquinoneimine (C') which can lose two electrons generating aminophenol (A1/C1). An additional electron is transferred forming nitrosophenol (A2/C2). Peak A' was assigned to the irreversible oxidation of 4-NP with no mechanism suggested. This peak was also observed by other authors whom also neglected to provide a mechanism [250]. This complicated reaction pathway would need to be verified through variation of voltammetric parameters (scan rate, potential window etc.) to confirm this mechanism. However, this information is unnecessary for this current study. It was concluded that the impedimetric measurements in 4-NPG would be performed at the open circuit potential (OCP) due to the high amount of electroactivity observed around 0 V. The OCP is the potential of the working electrode relative to the reference electrode i.e. when no current is flowing to the system. This should possibly avoid biasing the electrode and the swelling response subsequently.

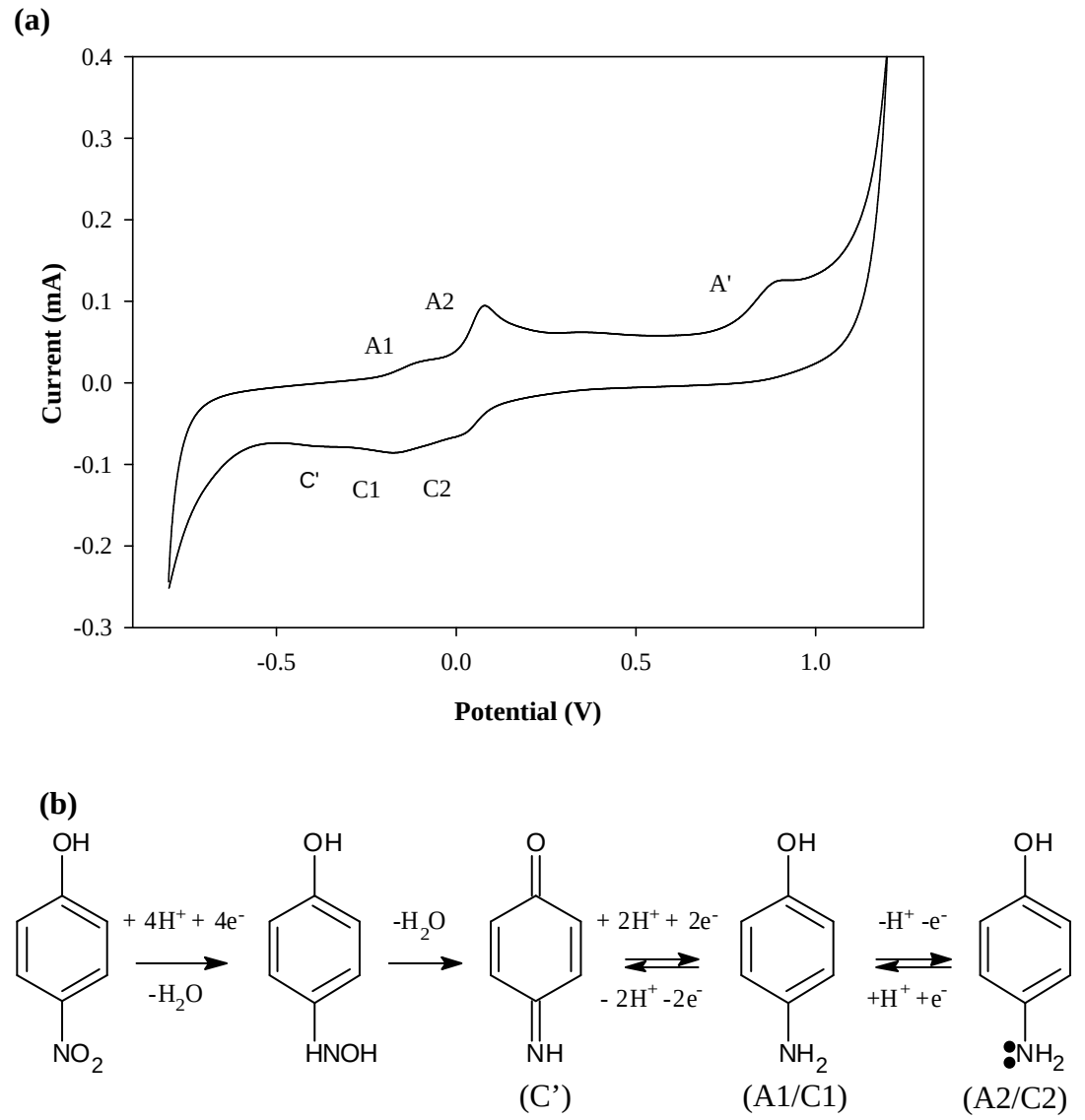

Figure 3.12 (a) Cyclic voltammogram of bare carbon cloth in 4-NP (1 mM) (in 10 mM PBS) at 0.05 V/s and (b) Proposed reaction pathway of the electrochemical behaviour of 4-NP.

The OCP of GUS hydrogel modified carbon cloth electrodes was measured in 4-NP for 300 s (Fig 3.13). A steady state potential of -0.368 (± 0.059) V was reached after 25 s and was utilised for all subsequent impedance measurements with GUS hydrogel modified carbon cloth electrodes. There was no apparent drift detected over

300 s which is approximately the length of time of an impedance scan over the frequency range of interest, indicating no significant changes occurred at the electrode surface during this time and that the potential should remain constant throughout the impedance measurements.

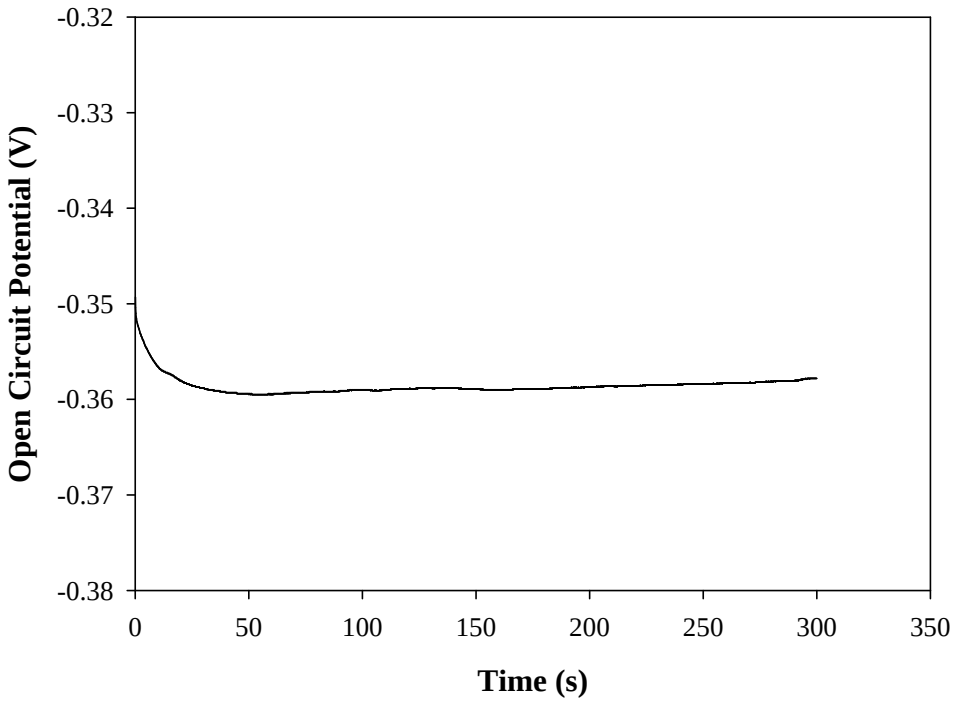

Figure 3.13 Time dependence of the OCP of GUS hydrogel modified carbon cloth electrodes in PBS (10 mM) after equilibrium swelling in 4-NPG (5 mM) in PBS (10 mM).

3.3.7 Impedimetric swelling analysis of GUS hydrogels in 4-NPG

Typical Nyquist spectra for GUS hydrogels recorded at the OCP after 500 min swelling in 4-NPG (5 mM) are shown in Fig 3.14. They comprise a similar shape to the Nyquist spectra recorded after swelling in 4-MUG i.e. a high frequency intercept on the real Z' axis and the beginning of a semi-circular arc across the high to low frequency region. The same trend is also visible as imaginary part of the impedance (-Z") decreases as the loading of GUS in the gel increases due to the faster rate of glucuronic acid production, enhanced ionisation and a greater decrease in gel resistance.

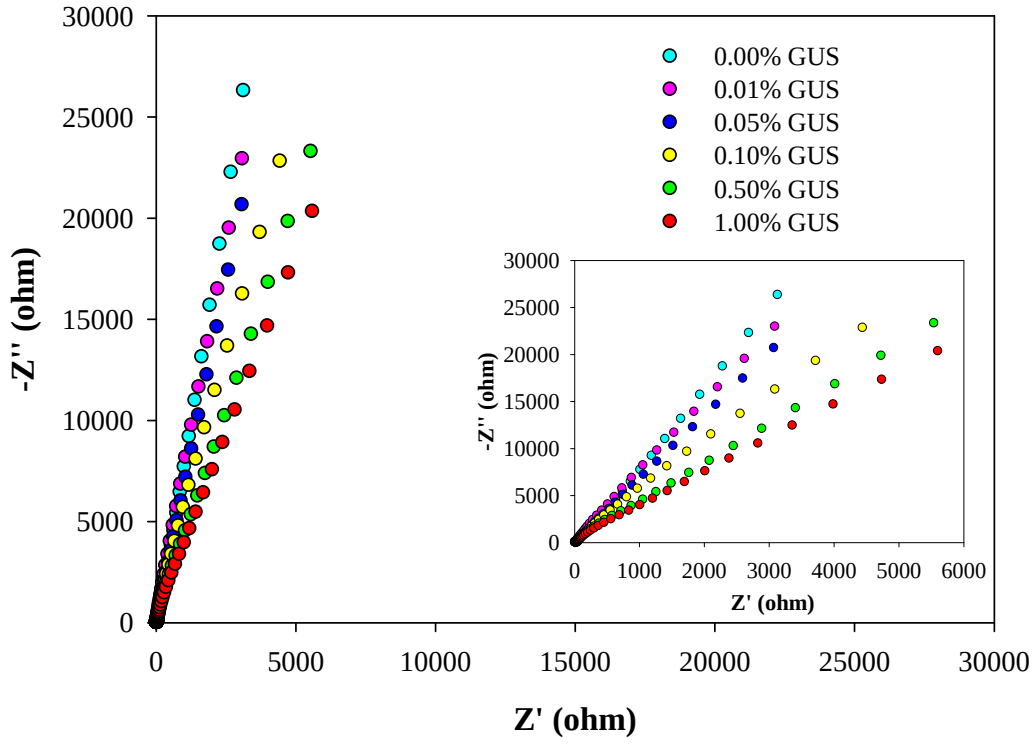

Figure 3.14 Nyquist spectra of GUS hydrogels in 4-NPG (5 mM) at 37^{O}C after 500 min. (n=3)

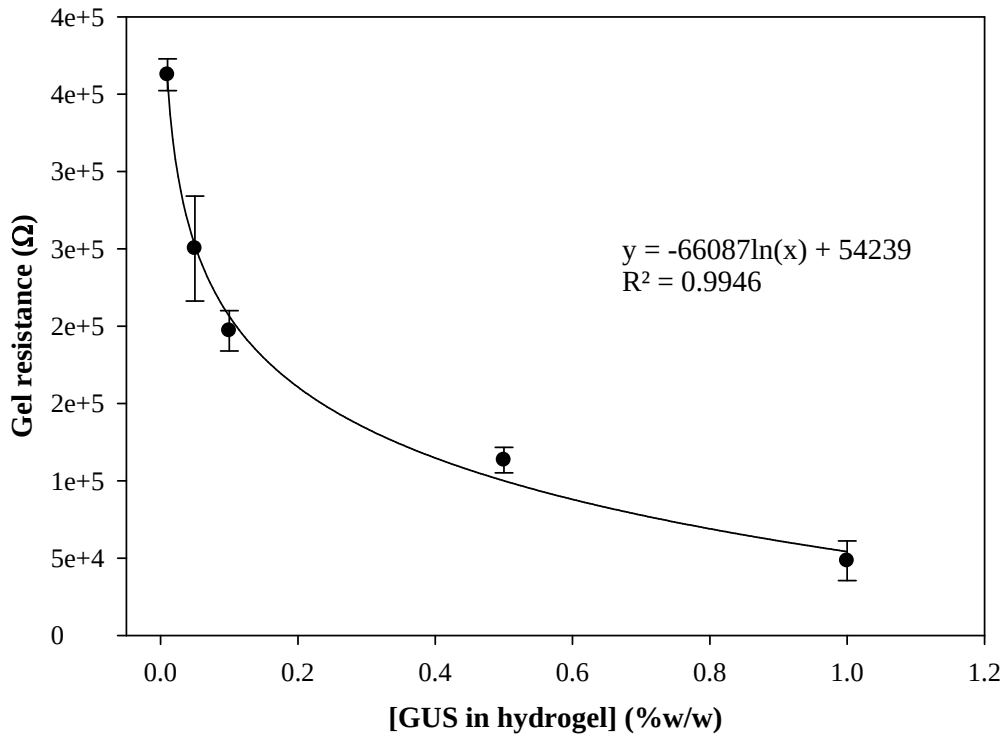

Figure 3.15 Calibration curve for GUS hydrogels (0.01-1.00%) after 500 min in 4-NPG (5 mM) at 37^{O}C using EIS. (n=3)

Fig 3.15 shows the calibration curve for the GUS hydrogels after 500 min swelling in 4-NPG (5 mM). The data was fitted to obtain the gel resistance values for each GUS loading using the same equivalent circuit employed with the 4-MUG data. The data was modelled using a logarithmic trend line and a limit of detection of 0.0007% GUS (1.24 μM) was achieved. In comparison to the GUS sensing using 4-MUG as a substrate, the limit of detection has improved by an order of magnitude with 4-NPG. This improvement is likely attributed to the higher solubility of 4-NPG in solution promoting the efficiency of glucuronic acid production and thus the resulting swelling response. The logarithmic trend line indicates that the concentration of 4-NPG also limited the reaction kinetics and faster, more sensitive detection could be achieved by increasing substrate concentration as seen previously.

In relation to the similarity in detection limits obtained by the gravimetric and impedimetric methods with 4-MUG, it appears that both temperature and substrate solubility were contributing factors. Performing the analyses at 37^{O}C lead to higher swelling ratios using the gravimetric method whilst having no significant impact on the EIS data. Although the two methods are difficult to compare as the samples are in completely different formats, it is possible that temperature had a greater effect on the gravimetric measurements due to the larger sample size (bulk gel discs versus dip coating).

In terms of substrate used, the detection limit of both methods increased with the replacement of 4-MUG with 4-NPG, as summarised in Table 3.2. As stated previously, this improvement arises from the increased solubility of 4-NPG in solution. It is likely that this influenced the EIS data to a greater extent as spectra were only recorded after 2 time points (300 and 500 min) whereas gravimetric measurements were recorded at more regular intervals. Consequently, the swelling solutions were agitated more frequently as the gels were removed/returned for measurements with the gravimetric method. This agitation could have replenished the local concentration of 4-MUG around the hydrogel between readings whereas the EIS swelling solutions were more stationary. Therefore, the increased stability of 4-NPG becomes a bigger contributor to swelling response when the solutions are left stationary. Thus, stirring or shaking the solutions during swelling would possibly have reduced this difference.

Table 3.2 Summary of limit of detections for GUS achieved using 4-MUG, 4-NPG and both methods.

Method / Substrate	Gravimetry	EIS
4-MUG	0.0163% GUS (27.17 μM)	0.006% GUS (10.02 μM)
4-NPG	0.042% GUS (7.00 μM)	0.0007% GUS (1.24 μM)

3.4 Conclusion

This chapter demonstrates that the swelling response of the pH-sensitive hydrogel can be used to sensitively detect the enzyme GUS, an *E.coli* marker. Specifically, it was shown that the enzyme must be located inside the hydrogel matrix, otherwise size-exclusion can prevent concentration-dependant ionisation-induced swelling. Consequently, GUS was entrapped in the hydrogel and two substrates were selected, 4-MUG and 4-NPG, which would generate glucuronic acid upon catalysis. The swelling response of the GUS hydrogels was successfully tracked gravimetrically and impedimetrically using either substrate. However, higher swelling ratios and lower resistance values were achieved with 4-NPG due to its higher solubility in aqueous solutions. Similar limits of detection were achieved for both methods of measurement. Temperature was seen to enhance the swelling which improved the gravimetric signal but didn't alter the resistance change of the gels using EIS. This is possibly attributed to the larger sample size used with the gravimetric method. It is likely that there is another unknown factor contributing to the similarity additionally.

Overall, this chapter shows that the PEGDGE-Jeffamine® hydrogel can be modified to sensitively detect other analytes which can elicit a pH change. Additionally, it demonstrates that size exclusion and electroactivity of by products must be considered when selecting the system configuration and parameters, and that the application of temperature up to $50^{O}C$ does not affect the impedimetric measurements. Despite alterations to the system similar low limits of detection were achieved as demonstrated previously. This illustrates the versatility of the hydrogel system, as well as good potential to be developed into a sensitive detection method for GUS which doesn't require labour-intensive, multiple days of analysis as per the traditional microbiological strategies.

Chapter 4

Electro-Stimulated Release from a Reduced Graphene Oxide Composite Hydrogel

4.1 Introduction

As detailed in Chapters 2 and 3, the pH-sensitive hydrogel coupled with electrochemical transduction has demonstrated excellent potential as a highly sensitive biosensing platform. In addition to sensing, intelligent materials such as the PEGDGE:Jeffamine® hydrogel are desirable in numerous other applications as reviewed in Chapter 1. This chapter investigates use of this hydrogel system as a responsive drug carrier for controlled drug delivery.

As discussed previously, intelligent drug carriers capable of on-demand release would provide safer, more efficient drug distribution than traditional oral and injection methods, by enabling site-specific drug delivery with on-off regulation in real time. This precision could result in improved medical treatments, reduce adverse side-effects and increase patient compliance. Various external stimuli have be employed recently to initiate drug release from smart materials *in vivo*. These include use of ultrasound, radiofrequency, light, NIR and laser radiation, magnetic and electric fields [144, 145]. Use of an electric field as an applied stimulus has many advantages, including reliability and precise control of magnitude, duration and intervals of pulses. The application or removal of an electrical field can trigger drug release similar to the pulsatile release of numerous endogenous chemicals in vivo including insulin, oestrogen and growth hormones. Electric fields can be generated by applying an electro-conducting patch to the skin above the implanted gel. Electrodes are then connected to the patch and the electric field is switched on. Iontophoresis and electroporation have been utilised for drug delivery *in vivo* [146-148].

To fabricate an electroactive hydrogel the addition of a conductive component is often necessary as many hydrogels are inherently non-conductive. They can be

prepared by fabricating the gel directly from conducting polymers [149, 150], incorporating conducting polymers [151, 152] or conductive particles into the hydrogel network [153-155]. When composited together, these materials aim to integrate the unique properties of their constituents i.e. the high water content, biocompatibility and 3D matrix of hydrogels with the electrical conductivity and switchable electrical and optical properties of ICPs. Use of carbon nanomaterials, such as carbon nanotubes (CNTs), graphene, graphene oxide (GO) and rGO (reduced graphene oxide), can attribute a large surface area, high electrical conductivity and enhanced mechanical properties. These properties facilitate a high drug loading, while the sp^2 carbon lattice and active oxygen-containing functional groups of rGO enable modification and functionalisation opportunities for targeted and controlled drug delivery.

Electro-stimulated release from CNTs in a chitosan hydrogel was achieved by Naficy *et al*. [251]. They demonstrated high potential for controlled release based on electrostatic interactions between CNTs and dexamethasone. It has been reported that graphene materials have a larger surface area than CNTs due to their planar structure [252]. This suggests that higher charge could be generated by incorporating graphene materials, leading to faster and possibly higher drug release. Also, passive release could potentially be reduced by additional positive charge and a higher capacity for adsorption. Liu *et al*. [253] investigated electro-modulated release of lidocaine hydrochloride from rGO in a PVA hydrogel. On demand drug release was feasible with release profiles varying from slow elution to rapid release. However, large voltages were required which may not be permitted *in vivo*.

This work describes the synthesis and characterisation of an electroactive hydrogel composite and its potential application in electro-stimulated drug delivery. A

high loading of rGO (20% w/w) was incorporated into the PEGDGE-Jeffamine® hydrogel in a single polymerisation step. For drug delivery experiments, methyl orange (MO) was added as a model drug. As depicted in Fig 4.1, MO is negatively charged and therefore can be expelled/retained according to the applied electrical stimulus. This is attributed to electrostatic interactions between the rGO and MO during charging. The high surface area of rGO permitted use of low applied potentials for electro-stimulation. By selection of the rGO loading, polarity and amplitude of the applied potential electro-modulation of the release profile was achieved.

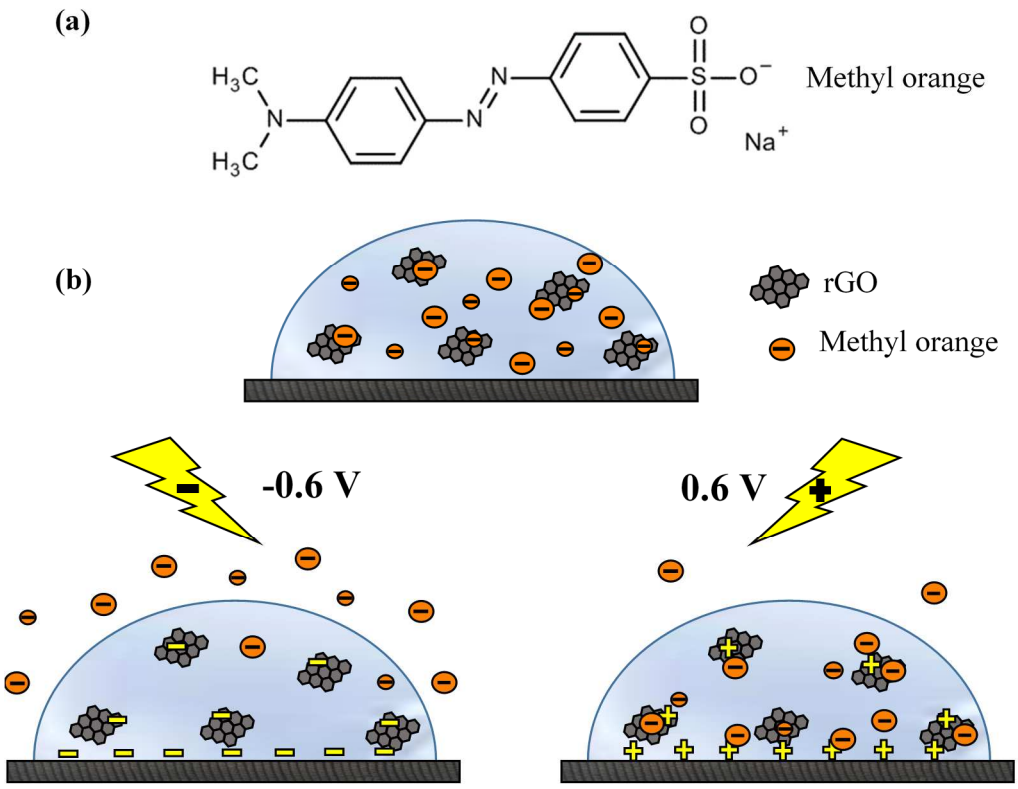

Figure 4.1 (a) Structure of MO and (b) schematic of electro-stimulated release from the rGO-hydrogels.

4.2 Experimental

4.2.1 Materials

As per Materials Section 2.2.1 with the following additions; hyaluronic acid potassium salt from human umbilical cord and PBS tablets pH 7.4 were purchased from Sigma-Aldrich (Australia). Potassium ferricyanide was obtained from Univar (US). Reduced graphene oxide was prepared and supplied by the Intelligent Polymer Research Institute (Wollongong, Australia).

4.2.2 Instrumentation

As per Instrumentation Section 2.2.2 with the following additions; SEM micrographs were obtained using a Jeol JSM-6490LA scanning electron microscope at an accelerating voltage of 15 kV. Equilibrium water-swollen hydrogels were flash frozen in liquid nitrogen (for 45 s) on a brass plate and cryofractured using a scalpel blade to obtain cross-sections of the internal structure. Uniaxial compression measurements were performed using a universal testing machine (EZ-L Shimadzu) fitted with a 10 N load cell. Equilibrium water-swollen hydrogels (5.5 mm width, 15 mm in diameter) were compressed at a strain rate of 2 mm/min until fracture. Force and displacement data were recorded with Trapezium X software and converted into stress-strain curves for analysis. All electrochemical protocols were performed using a CHI660C or CHI660D electrochemical analyser in PBS (10 mM), using cyclic voltammetry or AC impedance modes. UV-Vis spectroscopy was performed using a Shimadzu 1800 UV-vis spectrophotometer. Absorbance measurements were recorded at 493 nm.

4.2.3 rGO hydrogel synthesis

The production and characterisation of the rGO has been reported by Gambhir *et al.* [254]. In brief, GO was prepared by oxidation/exfoliation of natural graphite powder (Bay Carbon) via a modified Hummer's method. The GO was subsequently reduced to rGO with hydrazine, acidified to pH <2 using dilute sulphuric acid, thoroughly washed and dried under vacuum to produce rGO powder.

An aqueous dispersion of rGO (2 mg/mL) was prepared using hyaluronic acid (0.03%) as a dispersing agent. The dispersion remained highly stable after ultrasonication using a Branson Digital Sonifier at 35 % amplitude for 2 h (4 s on and 2 s off pulses) with continuous cooling in an ice bath. Small aliquots were collected regularly and dropped on a glass slide to assess the dispersion quality under a light microscope. A cover slip was placed on top to prevent drying and ensure appropriate viewing thickness.

Various amounts of the rGO dispersion (0.5% - 20% w/w) were incorporated into a 1.0:1.0 molar ratio solution of Jeffamine® EDR-148 and PEGDGE in DI water with vortexing. All hydrogels were polymerised in the refrigerator ($4^{o}C$) overnight to reduce evaporation. The PEGDGE-Jeffamine® hydrogels containing rGO will be referred to as "rGO-hydrogel" and without the rGO simply "bulk hydrogel" from here on in this chapter.

4.2.4 Gravimetric characterisation of the swelling response

Cylindrical discs of rGO-hydrogels were prepared by pouring 4 mL of the hydrogel precursor solution into petri-dishes (53 mm internal diameter) and placing them in the refrigerator ($4^{O}C$) overnight to polymerise. Cylindrical discs (5 mm diameter and 0.8 mm thick) were cut from the polymerised membrane. Their swelling

ratio in DI water was measured at regular time intervals and calculated as per Section 2.2.4.

4.2.5 rGO-hydrogel modified carbon cloth electrodes

Carbon cloth electrodes were cut and insulated as in Section 2.2.5. A single dip-coat of rGO-hydrogel or bulk hydrogel was applied to the working electrode area. Electrodes were swollen for 24 h in solution before electrochemical measurements were taken.

4.2.6 Electrochemical analysis

Cyclic voltammograms were obtained by cycling hydrogel modified carbon cloth electrodes between -0.2 V and +0.7 V (without ferricyanide) or -0.1 V and +0.5 V (in the presence of 2 mM ferricyanide) vs. Ag/AgCl at 50 mV s^{-1}. Electrochemical impedance spectra were collected at the OCP, in a frequency range of 0.1 - 1 x 10^4 Hz, with an alternating current sinusoid of ± 10 mV amplitude.

4.2.7 Drug release

Hydrogel modified carbon cloth electrodes were prepared with dip-coats of 0%, 5% and 20% (w/w) rGO-hydrogels containing 0.654% w/w dissolved MO. PBS (10 mM) at room temperature (ca. 22^{O}C) was used as the release media for all drug release experiments. For passive release, electrodes were placed in PBS (1.5 mL) and moved to fresh PBS solutions at selected time points. For electrically stimulated release, a three electrode configuration was used consisting of the hydrogel modified carbon cloth working electrode, platinum mesh counter electrode and Ag/AgCl reference electrode. The release media (8 mL) was gently stirred. Constant potentials of -0.6 V, -0.2 V and 0.6 V (vs. Ag/AgCl) were applied to the system. At specific time

intervals, 1 mL aliquots of the release media were collected and replenished with 1 mL of fresh PBS. MO release was quantified by measuring the absorbance of the aliquots at 493 nm. Dilution factors and swelling volumes were considered in the drug release calculations. A release profile was generated by plotting the cumulative methyl orange release as a percentage of the initial amount incorporated.

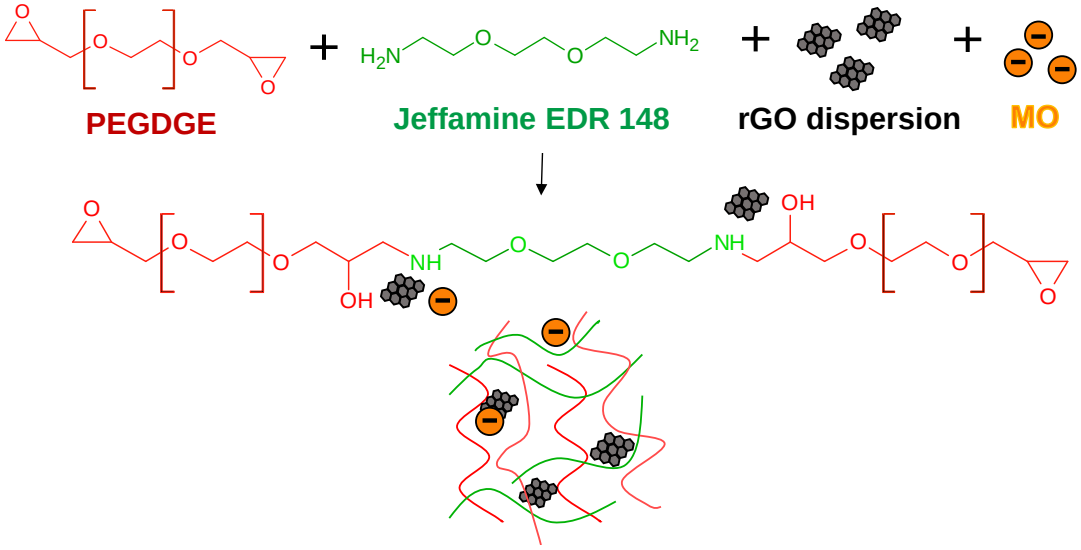

Figure 4.2 Schematic of rGO-hydrogel formation for drug release experiments.

4.3 Results & Discussion

4.3.1 Incorporation of rGO into hydrogels

Hydrogel formation can be a slow process when cross-linking occurs spontaneously (i.e., without use of heat or UV light) such as the hydrogel system described here. Consequently, the rGO solution must be highly stable and remain homogenously dispersed throughout the hydrogel monomer mixture to ensure good distribution of rGO throughout the formed hydrogel network. This is paramount for creating interconnected electrical pathways and increasing the overall conductivity of the gel. Dispersions of rGO in DI water and Jeffamine® were unstable as the rGO began precipitating out in < 2 h (Fig 4.3). Heat, sonication and ultrasonication were utilised in the attempt of increasing the dispersion stability but were unsuccessful. It was decided that a dispersing agent was required to achieve a dispersion stable for the duration of the crosslinking process.

Hyaluronic acid (HA) was utilised as a dispersing agent since HA has been shown to act as an effective dispersing agent for rGO nanosheets and carbon nanotubes [255-258]. Additionally, as a major component of the extracellular matrix, HA is highly biocompatible and contributes to tissue repair by cell proliferation, migration and moderation of the inflammatory response [259, 260]. Only a very small amount of HA (0.03% w/w) was required to obtain a rGO dispersion (at a rGO concentration of 2 mg/mL) which was stable for more than 6 months. The presence of the HA did not hinder the crosslinking process and enabled a high loading capacity of rGO (up to 20% w/w) into the hydrogels.

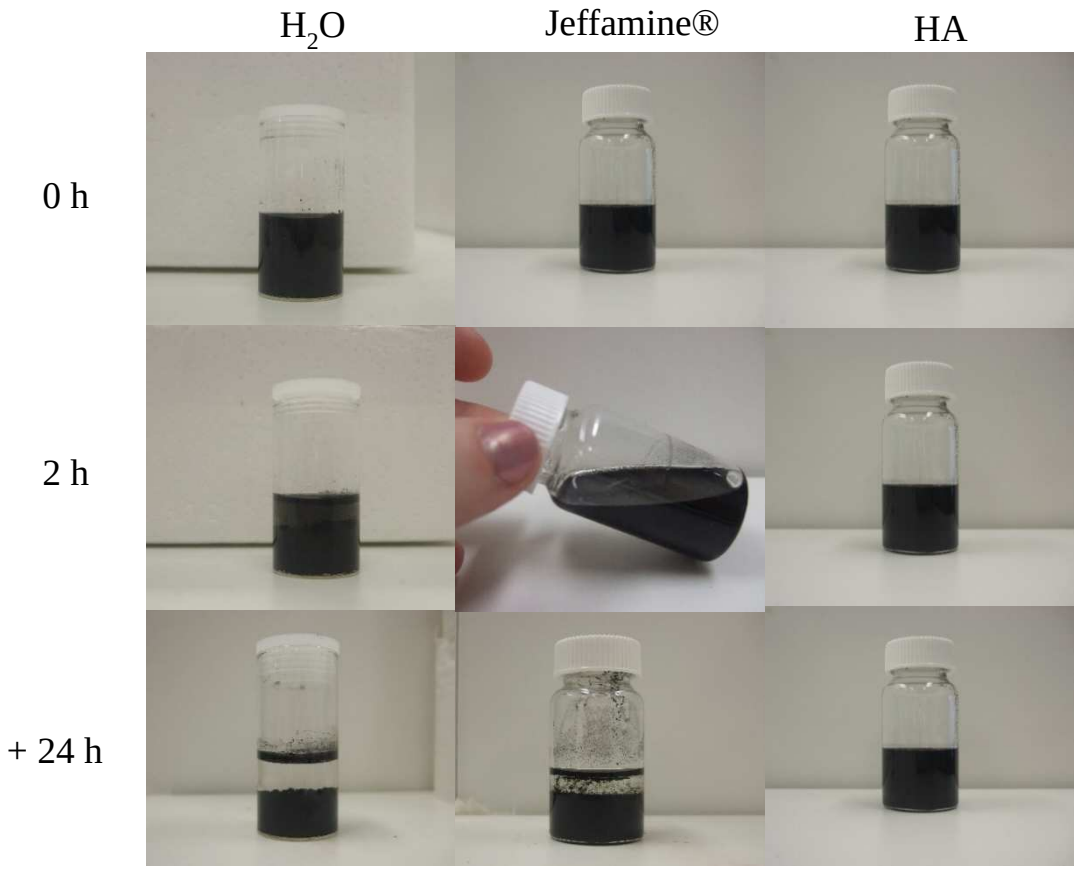

Figure 4.3. rGO dispersions (2 mg/mL) over time in water, Jeffamine® and HA..

Fig 4.4 shows the hydrogels prepared from rGO dispersions with and without HA. It can clearly be seen that without the dispersing agent HA the rGO agglomerates. This is particularly visible in the 0.5% rGO-No HA sample. The aggregation present in the 5% and 20% rGO-No HA hydrogels is not as visible due to their high concentration of rGO. Hydrogels prepared using the HA dispersed rGO appear homogeneous, even at the highest rGO loading of 20%.

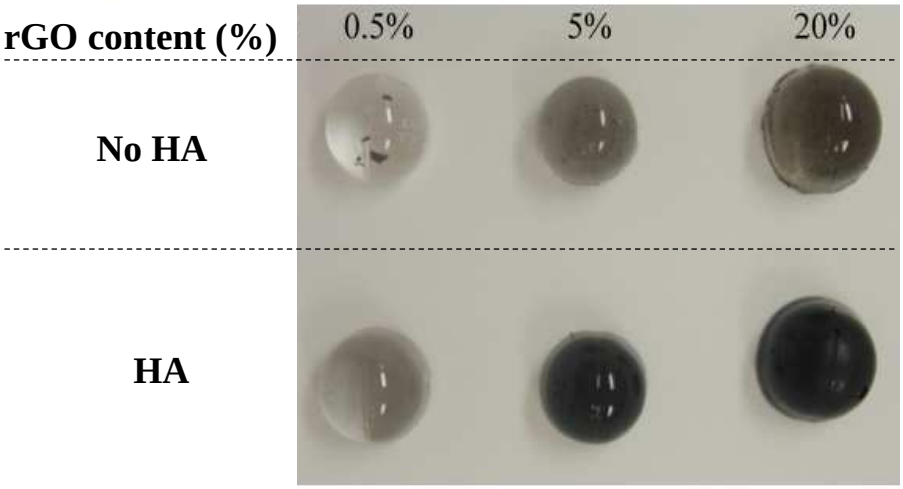

Figure 4.4 Hydrogels with various rGO loadings without a dispersing agent (No HA) and using HA as the dispersing agent (HA).

All rGO-hydrogels retained the rGO in the network even when fully swollen and at prolonged immersion times (longer than 4 days) suggesting strong interactions between the rGO and the PEGDGE-Jeffamine® backbone. It is postulated that strong hydrogen bonds form between the -OH and –COOH groups of rGO and the –OH and $–NH_2$ groups of the Jeffamine-PEGDGE backbone. X-ray diffraction studies and x-ray photoelectron spectroscopy were performed previously to confirm the presence of these oxygen-containing groups on the rGO after its reduction from GO [254].

4.3.2 Gravimetric analysis of the swelling response

The swelling response of rGO-hydrogel discs with rGO loadings from 0.5 - 20% (w/w) was investigated. Fig 4.5 displays the swelling behaviour of these rGO-hydrogels and bulk hydrogels in DI water at room temperature. It is clear that all gels swell rapidly initially and the swelling rate decreases over time. The rGO content had negligible impact on the time required to reach swelling equilibrium (~ 45 h). As

mentioned above no leaching into the solution was observed. The equilibrium swelling ratio decreased gradually with increasing rGO content. This is attributed to negatively charged rGO possibly associating with the positive charge on the Jeffamine® and imparting an ionic cross-linking effect which in turn increases the cross-linking density of the network and the possible formation of defects in the network structure such as meshes and grafts. It is well known that the swelling response of a hydrogel is heavily dependent on its cross-linking density. Additional cross-links and structural defects reduce the swelling capacity of the hydrogels decreasing water uptake and swelling ratios.

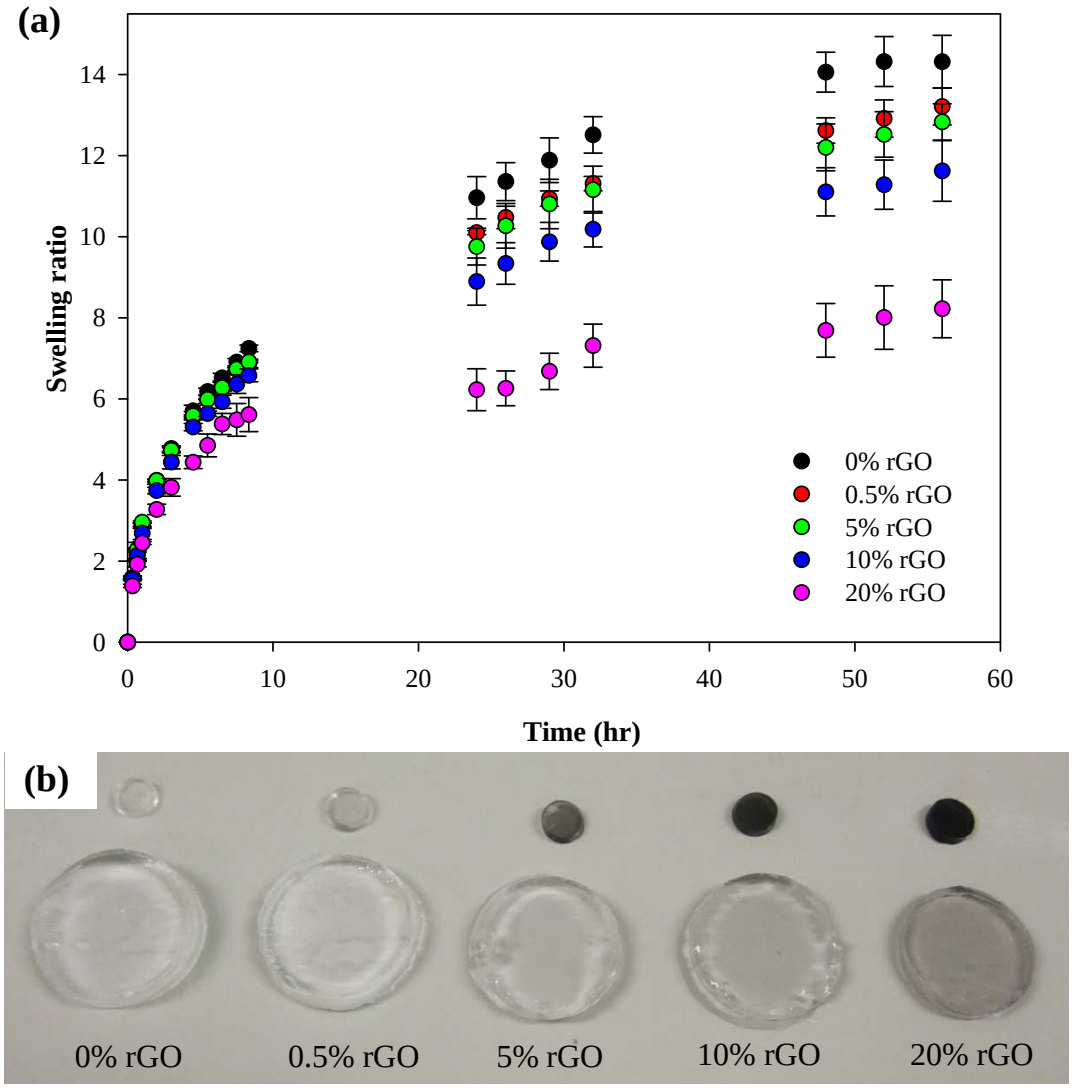

Figure 4.5 Swelling response of rGO-hydrogels and bulk hydrogels in DI water at room temperature with n=3 (a). Photograph of the samples prior to immersion in DI water (top) and after equilibration in DI water at room temperature (bottom) (b).

4.3.3 SEM analysis of rGO-hydrogels

The morphology of the rGO-hydrogels was investigated using low vacuum SEM (Fig 4.6). SEM images of fully swollen rGO-hydrogels containing 20% rGO were recorded and compared with bulk hydrogels. All samples were flash-frozen in

liquid nitrogen for 45 s and fractured to view their internal structure. A smooth sponge-like architecture, with a wide pore size distribution, was observed for all hydrogels with the presence of rGO indistinguishable from the hydrogel network. There were no apparent structural differences in the rGO-hydrogels which could be attributed to the rGO. Fig 4.6 (C) highlights some structures which were found in one sample but thought to be from the HA used for dispersion. This indicates that the rGO does not have a significant impact on the morphology of the hydrogels. However, it is noteworthy that any small change in pore size or in the thickness of the walls would be difficult to determine with confidence in this randomly orientated 3D matrix. Additionally, the structure is quite dynamic and thaws during analysis, particularly under the viewing area where the heat from the electron beam is focussed. As a result, the pores naturally shrink and the walls appear to increase in thickness as the hydrogel loses water and the structure begins to collapse.

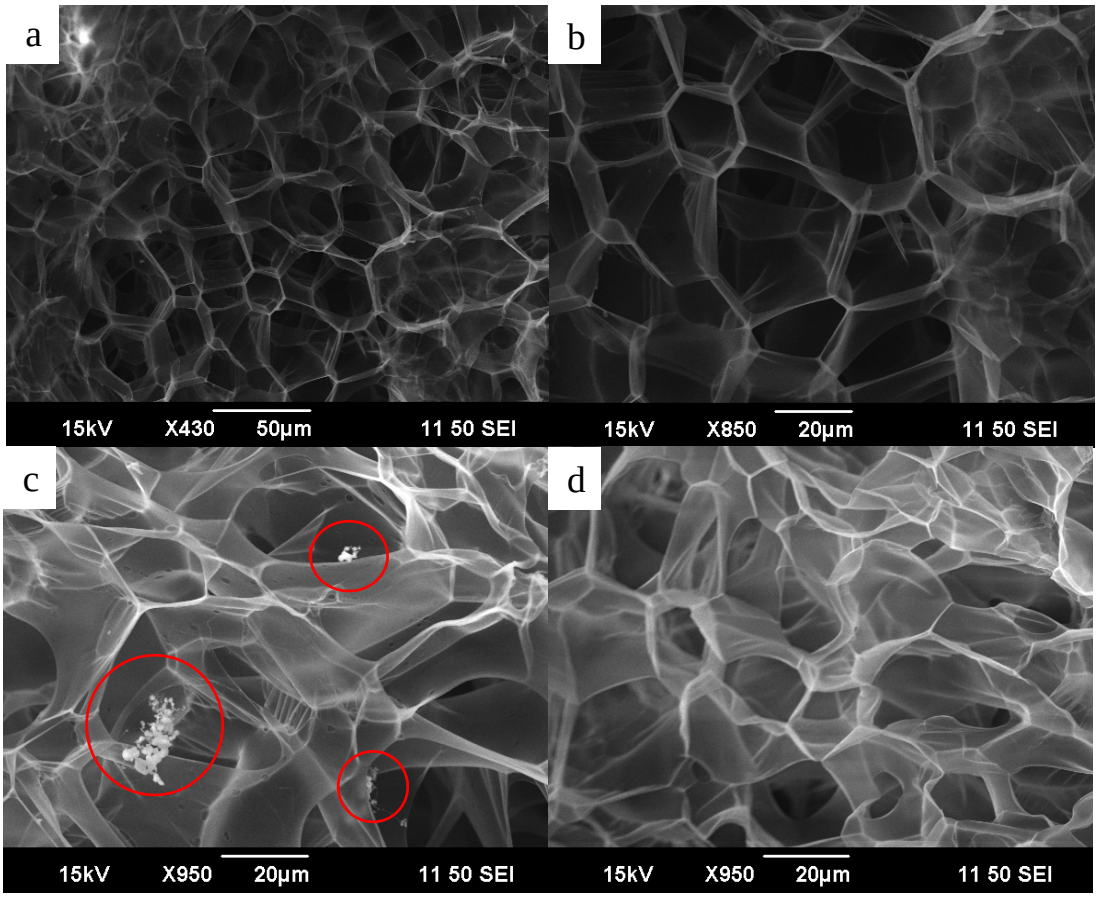

Figure 4.6 (a-c) SEM images of 20% rGO-hydrogels with increasing magnification (x430, x850, x950) and (d) bulk hydrogel at a magnification of x950. Scale bars: 50 µm (a) and 20 µm (b-d).

4.3.4 Mechanical properties of rGO-hydrogels

Typical stress-stain curves of the rGO-hydrogels under compression, and a summary of their compression properties, are presented in Fig 4.7 and Table 4.1 respectively. All hydrogels displayed non-linear hyperelastic stress-strain curves, similar to biological soft tissue. Higher stress and compressive moduli were sustained as the rGO loading in the hydrogels was increased. In comparison with the bulk hydrogel (18.9 ± 7.0 kPa), 5% rGO-hydrogels had compressive strengths of 30.6 (±

7.4) kPa and 20% rGO-hydrogels had compressive strengths of 51.2 (± 7.7) kPa, increasing by 62% and 171% respectively. Additionally, the modulus increased by 136% with the addition of 20% rGO into the hydrogel (1.9 ± 0.7 kPa to 4.5 ± 0.4 kPa). It is widely accepted that graphene is one of the strongest known materials. It has a Young's Modulus of approximately 1 TPa, around five times stronger than structural steel, and an intrinsic strength of ~130 GPa. It can also withstand large bending curvatures without disrupting the electric resistance [261]. These results indicate that incorporation of rGO reinforces the hydrogel network and improves load transfer between the network and the rGO sheets, enhancing the mechanical properties. A similar response has been seen previously with incorporation of GO into PVA and PAA based hydrogels [262-265]. This flexibility and strength make graphene an ideal candidate for 'smart' wearable textiles.

However, while the mechanical properties of the unmodified bulk hydrogels improve when composited with rGO, they may still be regarded as relatively weak in comparison with other hydrogel systems. This is predominately because these hydrogels have been prepared with a 1:1 PEGDGE:Jeffamine® ratio, resulting in a low cross-linking density in the polymer matrix. This design choice yields high swelling ratios, whilst compromising on mechanical strength [203]. High swelling ratios can be advantageous for drug delivery applications as faster release rates can be achieved or higher dosages released. If further strength was required the cross-linking density could be increased, as observed in Chapter 2, or a second polymer network could be incorporated to form a double-network gel.

Table 4.1. Mechanical (compression) properties of rGO hydrogels. (n=3)

Sample	Initial Modulus (kPa)	Modulus before break (kPa)	Breaking Strain (%)	Breaking Stress (kPa)
0% rGO	1.9 (± 0.7)	104.1 (± 21.8)	61.7 (± 6.8)	18.9 (± 7.0)
0.5% rGO	2.2 (± 0.4)	119.4 (± 28.2)	63.9 (± 7.4)	28.2 (± 4.9)
5% rGO	2.8 (± 0.5)	125.9 (± 36.4)	61.1 (± 8.6)	30.6 (± 7.4)
10% rGO	3.7 (± 0.7)	159.8 (± 21.2)	56.2 (± 2.3)	32.3 (± 5.2)
20% rGO	4.5 (± 0.4)	244.9 (± 19.0)	62.1 (± 6.5)	51.2 (± 7.7)

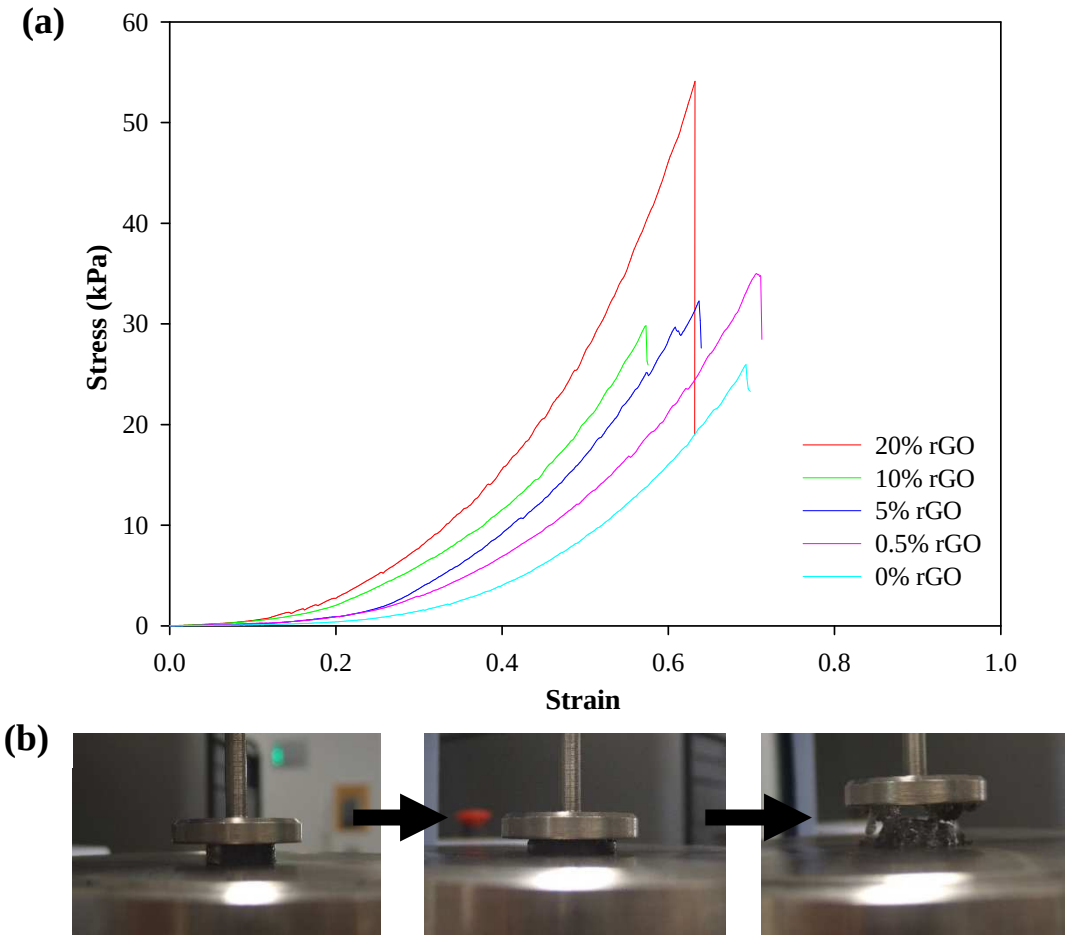

Figure 4.7 (a) Typical stress-strain curves for rGO-hydrogels performed in compressive mode using a 10 N load cell at a strain rate of 2 mm/min until fracture and (b) photographs of the compression of a 20% rGO-hydrogel until failure.

4.3.5 Electrochemical characterisation of rGO-hydrogels

The electrochemical properties of the rGO-hydrogels were evaluated by cyclic voltammetry and EIS. In order to characterise the capacitance and electron transfer properties, voltammetry was assessed both in PBS (10 mM) and in the presence of the ferri/ferrocyanide redox couple (2 mM). Higher currents and increased capacitance were observed as the rGO content increased (Fig 4.8 (a)) corresponding to the rGO providing a larger electroactive surface area. A close to ideal non-Faradaic voltammogram was observed when increasing the potential scan rate from 1 – 200 mV/s (Fig A-3.1), indicating excellent charge propagation and ionic transport within the rGO-hydrogels. Additionally, Fig. 4.8 (b) depicts the peak current (i_p) values increasing and a decrease in the peak-to-peak separation for the oxidation and reduction processes indicating improved redox switching with increasing rGO content. For example, the i_p for the redox couple increased by approximately 43% and the ΔEp value reduced from 0.339 V to 0.205 V when the rGO content in the hydrogel was increased from 0.5% to 20%. It is apparent that the rGO is lowering the electric resistance and enhancing the charge transfer properties.

This result is particularly interesting as in Chapter 2, higher i_p values and lower ΔEp values were observed as the swelling ratio and porosity of the hydrogel network increased. However, despite the 20% rGO-hydrogel having a lower swelling ratio than the 0.5% rGO-hydrogel, it resulted in the best electrochemistry. This indicates that the system with graphene content is no longer diffusion limited and a percolation threshold of the rGO may have been reached, producing charge propagation through a conductive network - a much faster process than diffusion.

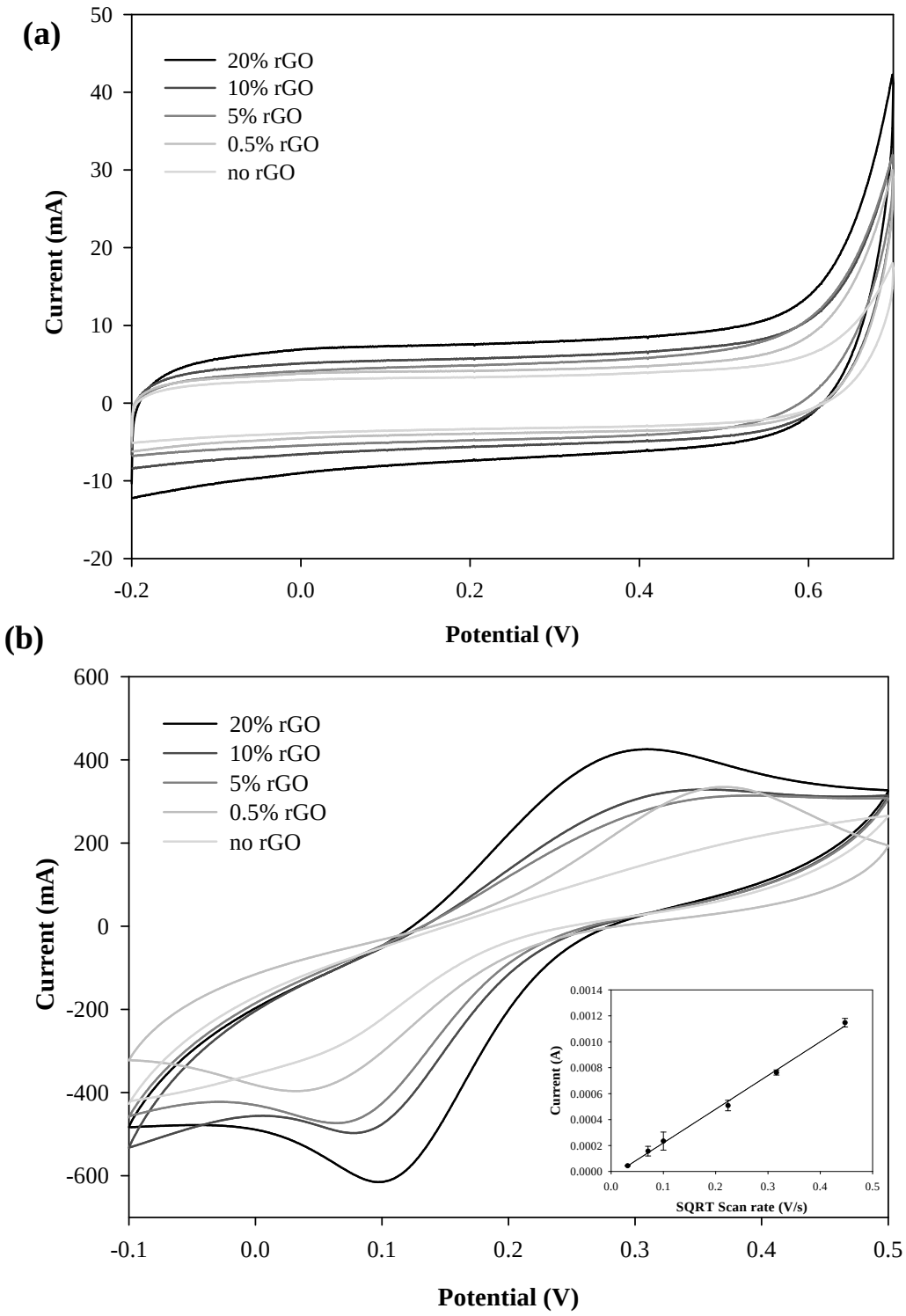

Figure 4.8 Cyclic voltammograms of the bulk hydrogel and rGO-hydrogels with increasing rGO content recorded in PBS (10 mM) (a) and in 2 mM potassium ferrocyanide (in 10 mM PBS) (b) at 0.05 V/s. Inset: Scan rate study of 20% rGO-hydrogel in 2 mM potassium ferrocyanide (in 10 mM PBS) (y=0.0026x – 4E05, R^2=0.9972). (n=3)

Complementary to the voltammetry results, a similar trend was detected using EIS. Fig 4.9 (a) shows representative Nyquist spectra for rGO-hydrogels. They comprise a high frequency intercept on the real Z' axis and the beginning of a semi-circular arc across the high to low frequency range. The high frequency intercept is representative of a combination of electrolyte ionic resistance, the intrinsic resistance of the carbon cloth and the resistance of the contacts to the potentiostat. It intersected the Z' axis at approximately a 45^{O} angle indicative of porous electrode behaviour [266]. The semi-circular arc was representative of the capacitive and resistive behaviour of the rGO-hydrogels with the resistance observed to decrease with increasing rGO content.

The Bode plot (Fig 4.9 (b)) can be divided into two frequency regions indicative of the dominant kinetics within each domain. The domain above 400 Hz shows resistive behaviour (I), while the domain from 400 Hz to 0.1 Hz shows the capacitance behaviour of the rGO-hydrogel is dominant (II). Maximum changes in the magnitude of log Z were seen within this region with the hydrogels with a higher rGO content observed to have lower impedance. This decrease in impedance is attributed to the increase in the electrically connected network as the percentage of rGO increases.

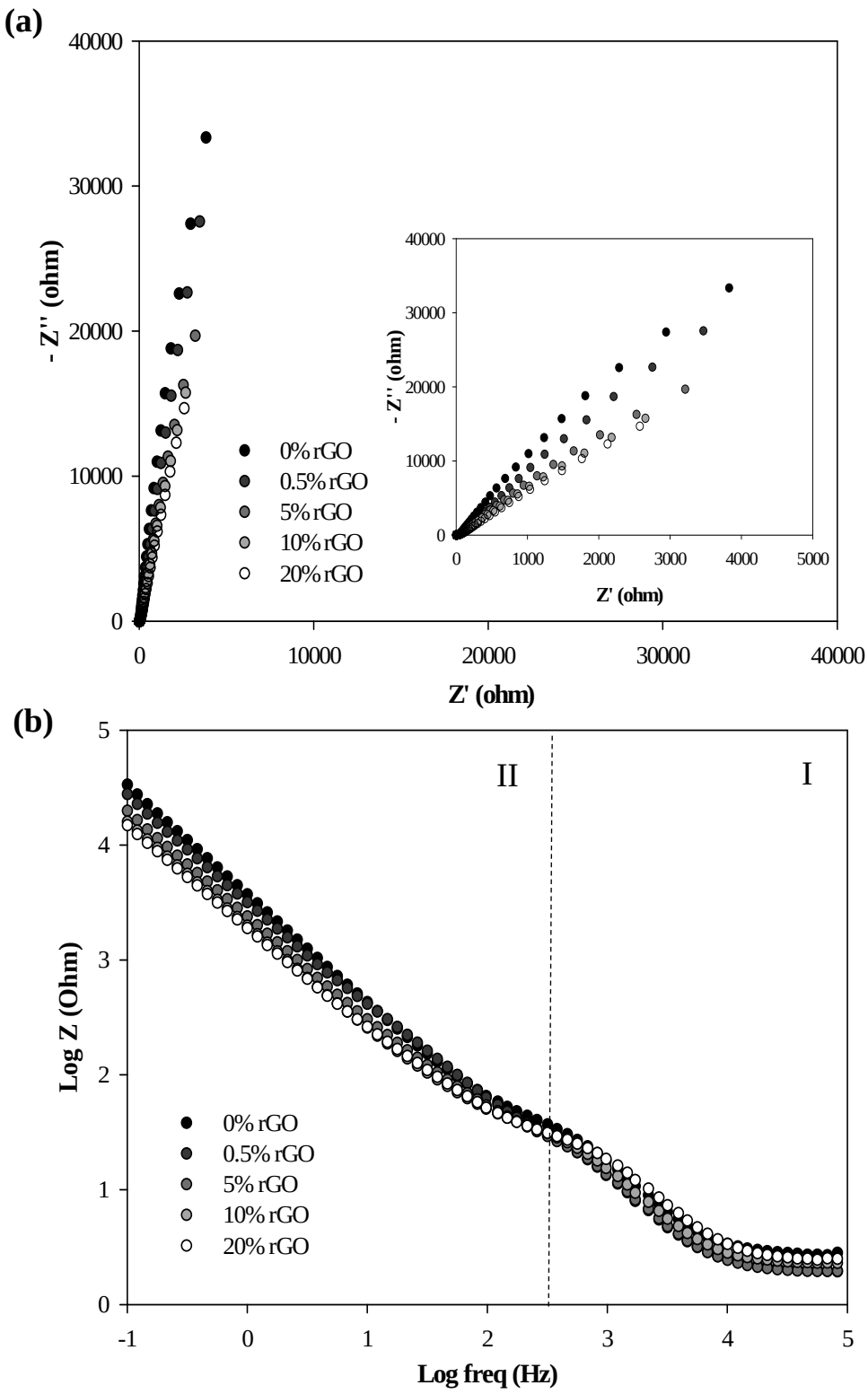

Figure 4.9 Representative Nyquist (a) and Bode spectra (b) of rGO-hydrogels recorded at the OCP in PBS (10 mM).

4.3.6 Methyl orange release

4.3.6.1 Passive release

Methyl orange (MO), an anionic dye with a low molecular weight (327.33 g/mol), was selected as the model drug for evaluating the drug release behaviour of the rGO-hydrogels. Passive release was investigated from rGO-hydrogels containing 5% and 20% rGO, representing a 'low' and 'high' amount of rGO, and compared against the unmodified bulk hydrogel. The cumulative release profile over 4380 min (~ 3 days) in PBS (10 mM, pH 7.4) at room temperature is shown in Fig 4.10. Rapid release of MO was observed for the first 180 min with approximately 70% of the MO being released from the bulk hydrogel (0% rGO). A significant reduction in the release rate occurred subsequently, with the remaining 30% MO requiring 4200 min to be fully released. Since no stimulation was applied to the samples the release rate was governed by passive diffusion of the MO from the hydrogel into the release medium. The initial rapid release occurs from MO located near the surface or loosely bound within the gel. The diffusion path length is much longer for MO molecules located deeper within the hydrogel network leading to prolonged release.

Lower passive release profiles were observed for the rGO-hydrogels with 87% and 72% total cumulative release being obtained for the 5% w/w and 20% w/w rGO-hydrogels respectively. The inclusion of rGO also resulted in slower release rates. After 180 min only 57% and 50% of MO was released from the 20% w/w and 5% w/w samples respectively, compared to 70% for the hydrogel containing no rGO. Previous studies have shown that drug release from hydrogels closely follows the extent of hydrogel swelling, namely the greater the swelling the greater the release [267-269]. This is also the case for these hydrogels indicating that for passive release the presence

of the rGO does not hinder this diffusion process during swelling. Also, the amount released is possibly reduced by MO adsorption onto the rGO sheets as many carbonaceous materials, including graphene, GO and CNTs, display high binding affinities for dyes such as MO [270-273]. Previous work has indicated that this property arises from π-π stacking interactions, oxygen-containing functional groups [273], electrostatic attraction and high specific surface areas [274]. In drug delivery applications, reduced passive diffusion may be highly desirable for administering accurate doses efficiently and minimising potential side-effects.

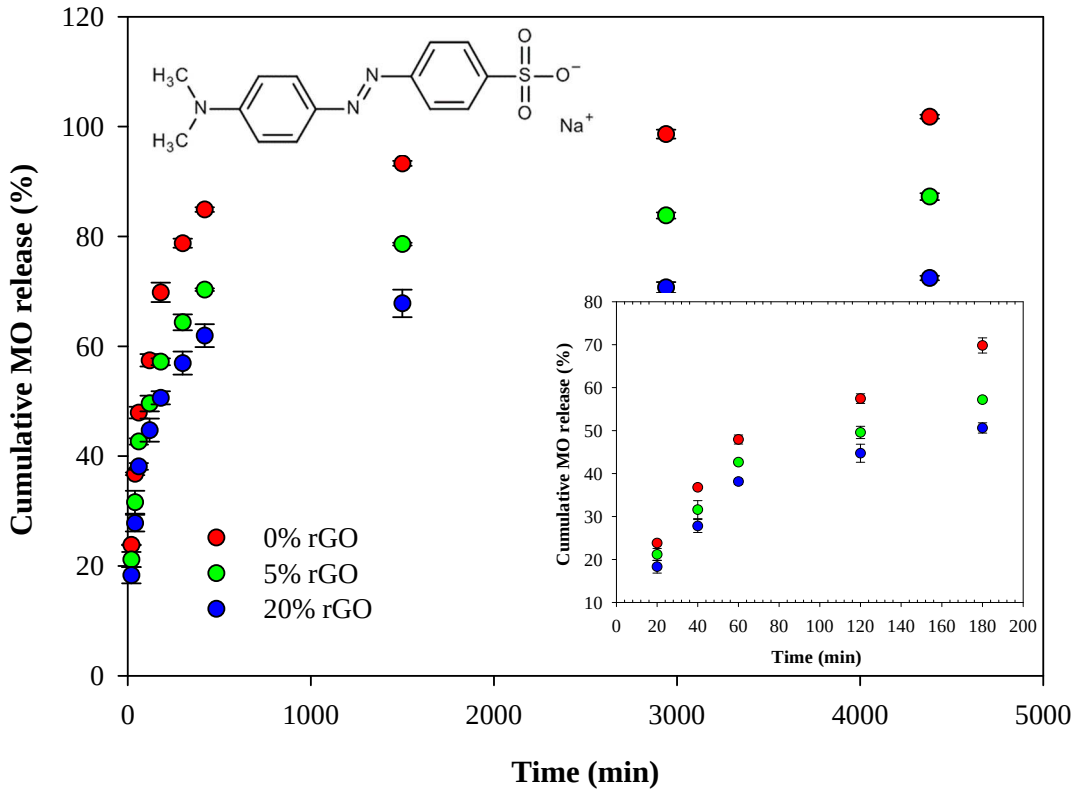

Figure 4.10. Passive release of MO from bulk hydrogels and rGO-hydrogels at room temperature into PBS (10 mM) with n=3. Inset: Early passive release time points and structure of MO.

4.3.6.2 Electro-stimulated release

The electro-stimulated drug release experiments investigated the influence of rGO content, as well as the polarity and amplitude of the applied electric potential on the release characteristics of the MO. The mechanism for this release system is based on electrostatic repulsion between the anionic dye and the rGO during charging. It would be expected that negative potentials would trigger electrostatic repulsion between MO and rGO, accelerating release, whilst positive potentials would induce electrostatic attraction, thereby retarding or suspending the release. In addition to field effects, it is possible that there is also capacitive deionisation associated with the applied voltages contributing to the release. The MO containing rGO-hydrogel samples were prepared using the same methodology described previously for preparing the samples for electrochemical characterisation. The MO was incorporated into the rGO-hydrogel as described above with the release experiments being performed in PBS (10 mM, pH 7.4) at room temperature. A release duration of 180 min was selected as this is where the majority of the release occurred in the passive experiments detailed above. Applied voltages of +0.6 V, -0.2 V and -0.6 V were chosen as the rGO-hydrogels demonstrated excellent charging behaviour in this range during the voltammetry studies (Fig 4.8 (a)). As displayed in Fig 4.11, the cumulative MO release from unmodified bulk hydrogels, under electrostimulation, did not show any variation from the passive release shown for the first 180 min in Fig 4.10. This was anticipated as there was no conductive moiety incorporated into these hydrogels. Application of a dc field can sometimes induce swelling in polyelectrolyte hydrogels, such as these, which could influence drug release but this was not seen in our system as much larger potentials are probably required (~6 V) [203]. Such high potentials may not be permitted *in vivo* and previous studies have shown that GO may be reversibly

oxidised and reduced using electrical stimulation of 2-3 V [275] which would be highly unfavourable for this system.

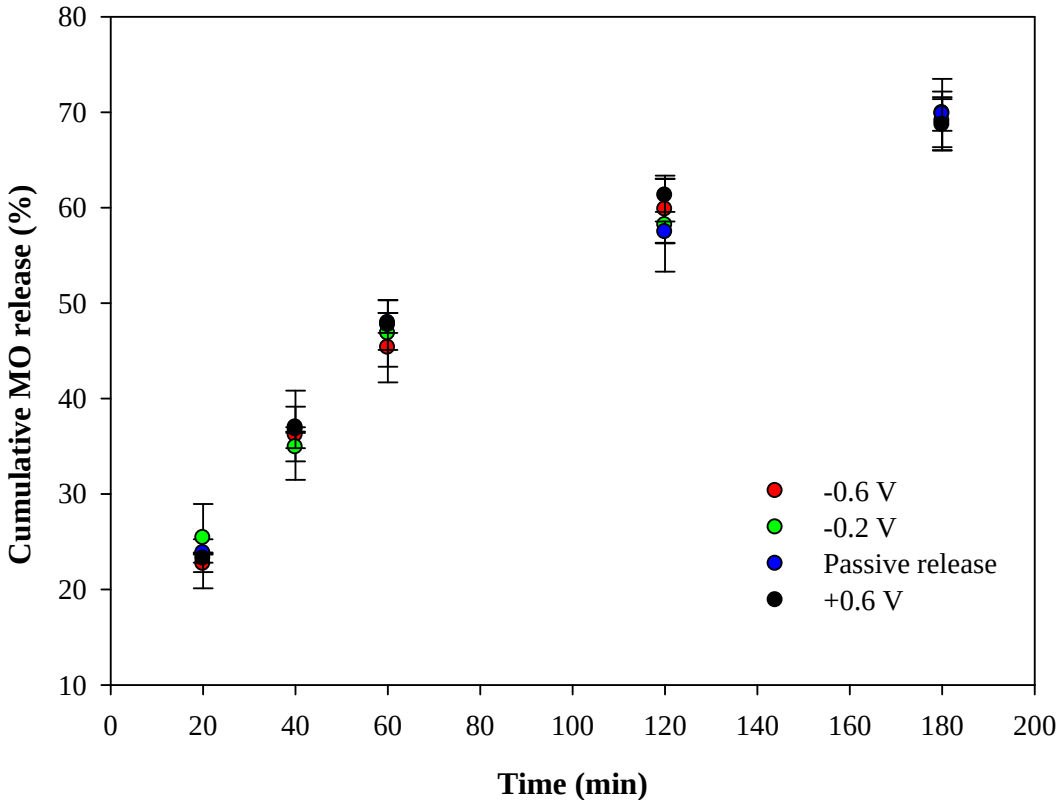

Figure 4.11 Cumulative MO release from unmodified bulk hydrogels (0% rGO) under passive and electro-stimulated conditions.

Fig 4.12 (a) and (b) show the passive and stimulated release profiles for 20% w/w and 5% w/w rGO-hydrogels respectively. The release rate and amount can be modulated by altering the polarity and amplitude of the applied potential, as well as the percent loading of rGO. In terms of electrode polarity, accelerated release was observed upon application of a negative potential. Alternatively when a positive potential is applied the extent of release decreased below that of passive release. These

trends were observed for both the 5% w/w and 20% w/w rGO-hydrogels. After 180 min, 50% release was recorded under passive conditions for the 20% w/w rGO-hydrogel compared to 76% release when a voltage of -0.6 V was applied and this decreased to 24% when +0.6 V is applied. This broad range offers huge control over release quantity over a narrow time period.

Furthermore, the amplitude of the applied stimulus influenced the release profile. Higher release was achieved for rGO-hydrogels at -0.6 V compared to -0.2 V. The 20% rGO-hydrogels released 64% of their MO content at -0.2 V versus 76% at -0.6 V after 3 h. This is attributed to the generation of a higher charge density at more negative voltages, thus increasing the electrostatic repulsion between MO and rGO, leading to an accelerated release. The same trends are visible for 5% rGO-hydrogels in Fig 4.12 (b).

A wider range in the amount of MO released was observed for 20% rGO-hydrogels compared to 5% rGO-hydrogels. This corresponds with the increase in capacitance observed with rGO content in the voltammetry and EIS studies (Fig 4.8 and 4.9). The hydrogels with a higher loading of rGO expel greater amounts of MO at applied negative potentials and lower amounts at positive potentials than hydrogels with low rGO content, corresponding to an increase in electrical conductor density. As previously stated, release from hydrogels is highly dependent on the extent of swelling, however for the rGO-hydrogels developed in this work, the results from Fig 4.12 clearly demonstrate that release can be modulated by the application of an applied voltage. These results strongly indicate that under appropriate electro-stimulated conditions the release is primarily dominated by electrical behaviour of the hydrogels and not the swelling process.

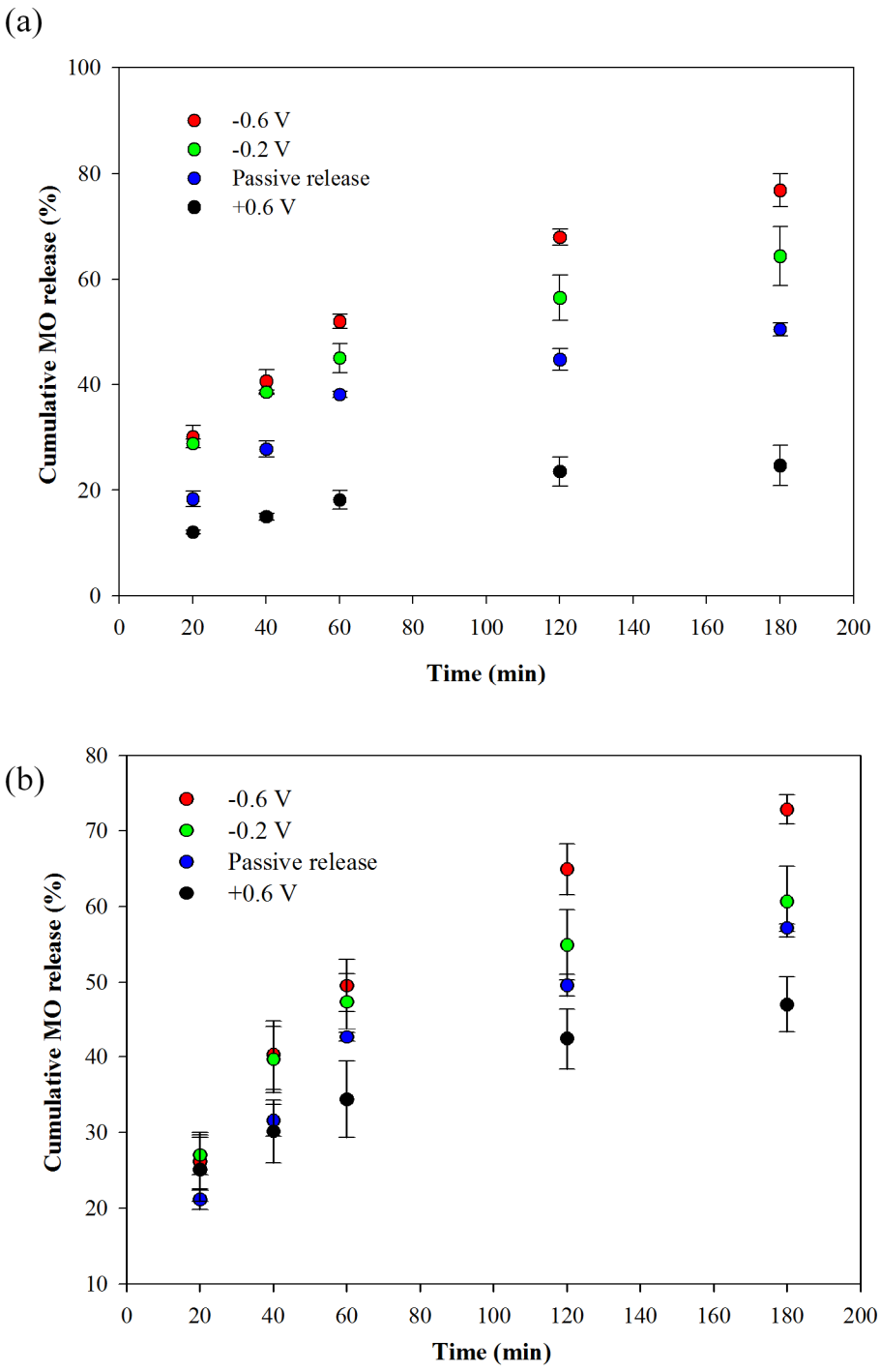

Figure 4.12 (a) Cumulative MO release from 5% rGO- and (b) 20% rGO-hydrogels under passive and electro-stimulated conditions.

4.4 Conclusion

A novel electroconductive hydrogel capable of electro-stimulated drug delivery has been developed. Incorporation of very low concentrations of HA greatly improved the stability of rGO dispersions and allowed the production of high quality, homogeneous rGO-hydrogel composites. The inclusion of rGO attributed new properties and enhanced the inherent characteristics of the PEGDGE-Jeffamine® hydrogel system. Increased mechanical strength and electrochemical properties were also demonstrated.

On-demand controlled drug delivery was achieved with these new composite materials. Through variation of the rGO content, electrode polarity and magnitude, a wide number of drug release profiles were observed, ranging from slow release of low dosages to rapid release of high dosages. This versatile delivery platform has demonstrated great potential towards advancing current delivery systems by exhibiting great control and precision over tuneable release profiles. The pH-responsiveness of this gel that was exploited in Chapters 2 and 3, and its influence on drug delivery, still remains to be explored. However, if present, pH-induced swelling transitions could potentially be exploited for auto-titration of a drug in response to a physiological pH change.

Chapter 5

Strategies to Improve Rates of Hydrogel Swelling

5.1 Introduction

One of the principal limitations of the PEGDGE-Jeffamine® hydrogel, and indeed many hydrogel systems, is their associated slow rate of response. Whilst a slow response is desirable for some applications, such as long-term drug delivery, many applications require rapid swelling responses. Rapid response times are necessary in sensing and drug delivery when immediate intervention may be required. Use of hydrogels as self-actuating pumps and valves in MEMS microfluidic devices also necessitates fast swelling for efficient flow control. Hygiene products such as diapers and sanitary towels also require rapid swelling to quickly imbibe large volumes of fluid. This chapter explores two main strategies for improving the response rate of the PEGDGE-Jeffamine® hydrogel; (i) reduction of the diffusion path length through preparation of hydrogels with smaller dimensions and (ii) eliminating the diffusion limitation by fabrication of superporous gels which can rapidly absorb water by capillary action through open channels in their interconnected pore system.

As discussed in Chapter 1, faster response times can be achieved by reducing the diffusion path length as the swelling rate is primarily diffusion controlled. This is easily achieved via preparation of hydrogels with reduced size dimensions. Baldi *et al*. [166] showed that reduction of the depth of their phenylboronic acid-based hydrogel microvalve from 500 µm to 30 µm decreased the opening time from over 4 h to 7 min in their MEMS device. Bates *et al*. [167] reduced the response time of their piezoresistive pressure sensor from 20 h to 0.34 h by reducing hydrogel thickness from 400 µm to 50 µm. Zhang *et al*. [95] reduced the thickness of their optical glucose sensor by decreasing the amount of hydrogel bilayers incorporated. They observed a decrease in response time from approximately 1.5 to 0.3 min when the bilayer number was reduced from 90 to 30. Micro- and nano-sized gels exhibit fast response times due

to their size reduction in at least one dimension. Several recent reviews are available which discuss their synthesis and areas of application [50, 276-278].

Superporous hydrogels exhibit significantly faster response times than diffusion dependant systems. They possess an interconnected, macro-sized pore system (100-1000 μm) and imbibe water rapidly by capillary action through the open channels [279]. Various synthesis methods exist including gas blowing techniques, ice-templating and surfactant-templating.

Gas blowing techniques are frequently employed to synthesis these hydrogels, typically through generating carbon dioxide bubbles by reacting sodium bicarbonate ($NaHCO_3$) or sodium carbonate (Na_2CO_3) with acid to initiate foaming in the hydrogel precursors. Equations 5.1 shows the reaction equation of $NaHCO_3$ with acetic acid.

$$NaHCO_3 + CH_3COOH \rightarrow CH_3COONa + H_2O + CO_2 \qquad \text{Equation 5.1}$$

Gas foaming with $NaHCO_3$ was used by Gumusderelioglu *et al.* [280] to generate superporous pAAm and p(AAm-co-AA) gels for protein delivery. These hydrogels reached equilibrium swelling in ~ 30 s and completed release of bovine serum albumin (BSA) within 1 h. Interestingly, when a chitosan interpenetrating network was introduced for improving mechanical strength, swelling time increased to 30 min and total release achievable decreased from 80% to 60%. Kuang *et al*. [281] used gas foaming with $NaHCO_3$ and acetic acid to prepare biodegradable polysaccharide-based superporous hydrogels which reached equilibrium swelling in 60-440 s depending on monomer composition. Battig *et al.* [182] also used this approach in the development of an aptamer-functionalised superporous gel for the controlled release of growth factors. The aptamers in the gel could sense and hybridise with fluorescently-labelled complementary strands and produce fluorescence after an incubation time of 5 min.

Another common synthesis method for superporous hydrogels is ice-templating. Also known as cryogelation, this involves polymerising the gel at cold temperatures (~ -18^{O}C) to create large ice crystals which produce large, interconnected pores upon thawing. Cross-linking occurs in non-frozen liquid channels where the soluble monomers/polymers are concentrated. Gels synthesised in this manner are commonly called cryogels. Sahinder *et al.* [282] reported that their pAMPS cryogel reached equilibrium swelling almost 3600 times faster than the corresponding conventional hydrogel. Dinu *et al*. [283] synthesised pHEMA and chitosan-based cryogels which reached equilibrium swelling in 10 s and 70 s respectively. Superporous cryogels have also been composited with metal nanoparticles for H_2 generation from the hydrolysis of $NaBH_4$ due to their fast swelling rates and high catalytic activity [284, 285].

Surfactants have also been used as pore-forming agents. However, pores created using surfactants are typically smaller than those synthesised using the methods discussed above (< 150 μm), resulting in a swelling time in the order of minutes rather than seconds. Shi *et al*. achieved an equilibrium swelling time of approximately 2000 s using sodium n-dodecyl sulfonate (SDS) micelle templating of a hydroxyethyl cellulose-based hydrogel [286] and a sodium alginate-based hydrogel [287]. Bao *et al*. [288] used mechanically agitated surfactants such as sodium n-dodecyl benzene sulfate, cetyltrimethyl ammonium bromide and alkylphenol poly(oxyethylene) to form bubbles to prepare porous poly(sodium acrylic acid) superabsorbent resins which reached equilibrium swelling in approximately 1500 s. Other synthesis methods exist which are used less frequently such as phase separation [289] and microemulsion techniques [290, 291].

This chapter investigates various strategies to improve the swelling rate of the PEGDGE-Jeffamine® hydrogel including preparation of thinner hydrogels and superporous hydrogels. Numerous superporous synthesis methods were explored, such as gas blowing with $NaHCO_3$, ice-templating and a novel gas blowing method involving the catalytic decomposition of hydrogen peroxide using silver nanoparticles to produce oxygen bubbles. The swelling rate of these gels was investigated gravimetrically and impedimetrically to determine the improvement in response time and the possible implications it would have on applications discussed in previous chapters. Pulsatile pH-switching was demonstrated. In addition, the anti-microbial properties were assessed to determine if the gels could control microbial growth for general hygiene purposes if they were to be used in contact with the skin, as well as their potential to be used in a topical dressing for wound care.

5.2 Experimental

5.2.1 Materials

As per Materials Section 2.2.1 with the following additions; silver nanopowder (<100 nm particle size), hydrogen peroxide solution (30% w/w in H_2O), Pluronic® F-127, hexaaminеruthenium (III) chloride (HARC) and sodium hydroxide purchased from Sigma-Aldrich (Ireland). Hydrochloric acid (37%) and polystyrene beads (200-300 μm) were obtained from Fisher Chemical (Ireland) and Polysciences, Inc. (US) respectively. Mueller Hinton agar, and tetracycline (30 μg) and nystatin (100 units) antimicrobial susceptibility discs were purchased from Oxoid™ (UK). All chemicals were used as purchased and all aqueous solutions were prepared using DI water (18 MΩ cm @ 298 K).

5.2.2 Instrumentation

As per Instrumentation Section 2.2.2 with the following additions; optical images were recorded of hydrogels which had reached equilibrium swelling in DI water using a high resolution digital microscope (Keyence VHX-2000). A Deben Coolstage (UK) was attached to the SEM to keep the samples frozen at -10°C throughout the analysis.

5.2.3 Synthesis and swelling measurements of thin hydrogel films

Thin hydrogels were prepared by dropcasting 1:1 Jeffamine:PEGDGE precursor solution onto glass slides and placing cover slips on top. Various amounts of precursor solution (1 mL, 600 μL and 300 μL) were dropcast to prepare hydrogels with different heights (0.8 mm, 0.5 mm and 0.25 mm). All gels were placed in the refrigerator (4°C) overnight to cure. Cylindrical discs (3.5 mm diameter) were cut from

the polymerised membrane with a Harris Uni-Core™ core sampler. Their swelling ratio in DI water was measured at regular time intervals and calculated as per Section 2.2.4

5.2.4 Quantitavtive glucose analysis of thin GOx hydrogel films

Thin hydrogel discs (0.25 mm height x 3.5 mm diameter) were prepared as in Section 5.2.3 with 5% (w/w) glucose oxidase and catalase loading (at an enzyme ratio of 9.4 units catalase per unit glucose) dissolved in the hydrogel precursor solution. A calibration curve of the swelling response in glucose (1-20 mM) was prepared as per Section 2.2.6.

5.2.5 Optimisation of the Pluronic® loading in superporous gels

Superporous hydrogels were prepared by adding 2% (w/w) silver nanoparticles (0.02 g), PEGDGE (0.349 g), 1 M H_2O_2 (0.533 g) and Jeffamine® (0.098 g) sequentially into a glass vial, capping it quickly and vortexing for 10 s. The Pluronic® loading was optimised by measuring the amount of superporous hydrogel versus bulk hydrogel produced after polymerisation using a Workzone® digital caliper. Various Pluronic® loadings were incorporated into the gels (0, 5, 10, 20, 40 and 50% w/w) using a 10% (w/v) Pluronic® solution. The amount of H_2O_2 added was decreased as the Pluronic® loading increased so the cross-linking density of the network remained constant. Solutions of H_2O_2 were prepared fresh daily.

5.2.6 Optimisation of polymerisation temperature of superporous gels

Superporous gels were prepared by adding 2% (w/w) silver nanoparticles (0.02 g), PEGDGE (0.349 g), 40% w/w Pluronic® using a 10% (w/v) solution, 1 M H_2O_2 (0.133 g) and Jeffamine® (0.098 g) into a glass vial, capping it quickly and vortexing

for 10 s. Hydrogels were then heated in an oven at the desired temperature for 20-45 min (depending on temperature investigated) and the proportion of superporous hydrogel versus bulk hydrogel produced after polymerisation was measured using a Workzone® digital caliper.

5.2.7 Anti-microbial testing of superporous gels

The anti-microbial activity of the superporous hydrogels was evaluated against *E.coli* (ATTC 25922), *S.aureus* (ATTC 6538) and *C.albicans* (ATTC 10231) using the disc diffusion method. Overnight grown cultures of *E.coli*, *S.aureus* and *C.albicans* were individually diluted and plated on Mueller Hinton agar inoculated with approximately 10^8 CFU/mL. Superporous gels, prepared as per Section 5.2.6, and 1:1 unmodified PEGDGE:Jeffamine® gels were thoroughly washed by placing the gels in fresh DI water (approx. 100 mL) every day for a week. Hydrogel discs were cut (4 x 2 mm) after washing, placed in a sterile water with the surface exposed to air and sterilised for 15 min each side using a high intensity UV Lamp at 365 nm (Black Ray® B-100AP, 100 Watt). The discs were then gently blotted and placed on the plates in duplicate and incubated at 37°C for 18-24 h. Zones of inhibition were observed. The unmodified PEGDGE:Jeffamine® gels were utilised as negative controls and antibiotic discs were used as positive controls (tetracycline (30 µg) for bacteria and nystatin (100 units) for fungi).

5.2.8 Investigation of swelling rate and response time of superporous gels

Superporous hydrogels were prepared as in Section 5.2.6 and polymerised at 120°C for 20 min. The bulk hydrogel was removed with a scalpel and hydrogel discs with different diameters (3.5, 12 and 20 mm) were cut from the superporous gel. Their swelling ratio in water was calculated as per Section 2.2.4.

5.2.9 Superporous hydrogel modified carbon cloth electrode

Carbon cloth electrodes were cut and insulated as in Section 2.2.5. Parafilm was wrapped around the top of each electrode to prevent gel from polymerising where the potentiostat connections would be attached. Superporous hydrogel was prepared as in Section 5.2.6 with an electrode pinned above the bottom of the glass vial, using the lid, to prevent bulk hydrogel from polymerising on the electrode. Superporous hydrogel modified carbon cloth electrodes were then cut from the polymerised gel with a scalpel. All gels were cut to an area of 9 x 9 x 9 mm when fully swollen.

Cyclic voltammograms were obtained by cycling superporous hydrogel modified carbon cloth electrodes between -0.5 V and 0.2 V in 1 mM HARC (1 M KCl) at 0.1 V s^{-1}. Voltammograms were also recorded with a narrower potential window (-0.5 V to -0.05 V) to eliminate any silver redox activity, and in 1 M KCl to verify that no silver redox activity was visible in the potential window.

5.2.10 Effect of pH on the swelling response of superporous gels

Superporous hydrogels were prepared as in Section 5.2.7. The bulk hydrogel was removed with a scalpel and hydrogel discs were cut (3.5 mm x 4 mm) from the superporous gel using the Harris Uni-Core™ core sampler. The discs were weighed before being washed thoroughly by placing the gels in fresh DI water (approx. 100 mL) every day for a week. The hydrogels were blotted with filter paper and re-weighed to obtain their swelling ratio due to water uptake. The swelling response of the gels was then calculated after 10 min of swelling in solutions with pH ranging from pH 2 to 10 using Equation 5.2. A solution of each pH was prepared by mixing 10 mM stock solutions of HCl (pH 2) and NaOH (pH 12) with the ionic strength kept constant.

$$\text{Swelling response} = \text{Swelling ratio}_{\text{pH}} - \text{Swelling ratio}_{\text{water uptake}} \qquad \text{Equation 5.2}$$

For the pH switching experiments, superporous hydrogels were placed into fresh pH 3 and pH 10 solutions after each measurement. All solutions were gently stirred. The swelling response was calculated after 1 min at each pH.

5.3 Results and Discussion

5.3.1 Reducing response time using thinner hydrogels

Since the swelling rate of bulk hydrogels is primarily governed by diffusion, faster swelling rates can be achieved by reducing the diffusion pathlength. Scaling down the size of the hydrogel through fabrication of smaller or thinner gels is often the simplest method to accomplish this. Consequently, thin hydrogel discs of varying thicknesses were prepared using glass slides and cover slips. Fig 5.1 shows the swelling behaviour of hydrogels with three different thicknesses (0.25, 0.5 and 0.8 mm) in DI water over 360 min. The rate of hydrogel swelling was observed to be highly dependent on the size of the hydrogel. Response time increased as the height was decreased. After 60 min, 0.25 mm hydrogels had a swelling ratio of 13.7 in comparison with 9.7 and 5.7 for 0.5 and 0.8 mm gels respectively. Additionally, after 360 min the 0.25 mm gels appear to be reaching equilibrium swelling whereas the larger gels are still undergoing swelling. Due to their larger size, they possess a greater swelling capacity and would surpass the thinner gels in terms of swelling ratio if permitted enough time. However, as shown in earlier chapters, the bulk hydrogels typically required at least 500 min to reach equilibrium. Thus, fabrication of gels with reduced thickness decreased the diffusion path length in one dimension, and hence improved the rate of response.

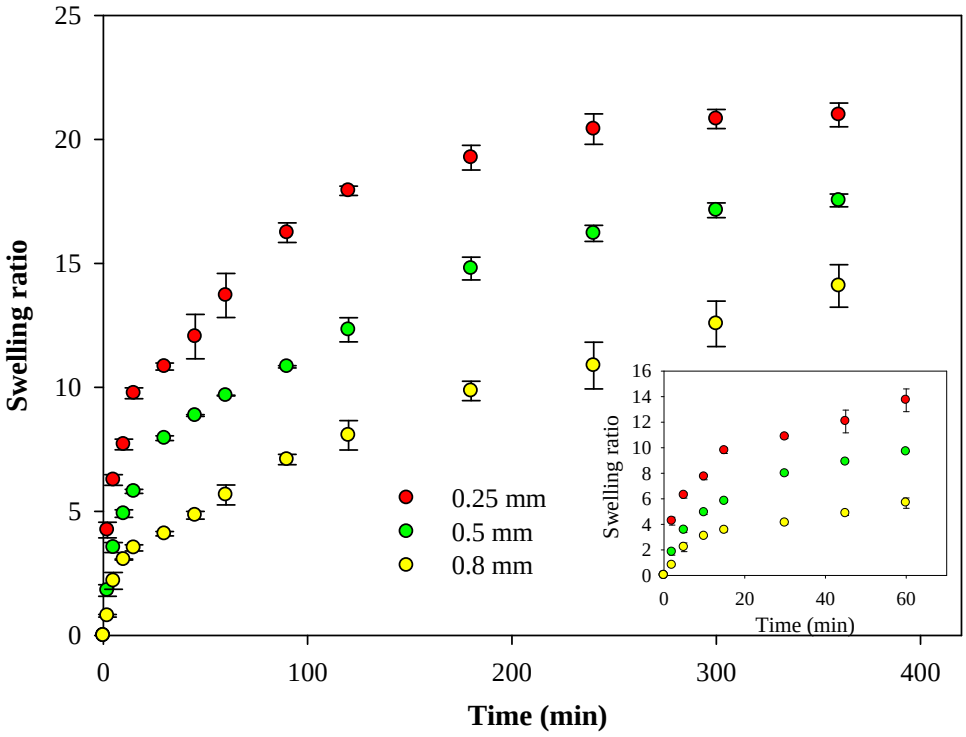

Figure 5.1 Effect of decreasing thickness of hydrogel on swelling response in DI water. Inset: Early time points. (n=3)

As a result of the improvement in the swelling rate with reducing gel thickness, it was decided to repeat the glucose calibration curve prepared in Chapter 2 using the thin hydrogels. This was to determine if the improvement in response rate would translate into increased detection sensitivity. Thin hydrogel discs (0.25 mm height) containing 5% w/w GOx and catalase were immersed in stirred glucose solutions and their swelling response after 100 min was calculated using Equation 2.3. Both the calibration curve of the thin hydrogels and the original data from Chapter 2 with the larger bulk hydrogels are displayed in Fig 5.2. A higher and faster swelling response was observable for the thin hydrogels. The shorter diffusion pathlength within the thin gels resulted in faster solution uptake, thereby increasing the rate of gluconic acid generation and extent of ionisation induced during the timescale of the experiment.

This was reflected in the slope of the calibration plots as it doubled from 1.2 to 2.4 with the thin hydrogels, thus indicating a two-fold improvement in sensitivity. Therefore, a faster swelling rate can lead to an improvement in detection sensitivity.

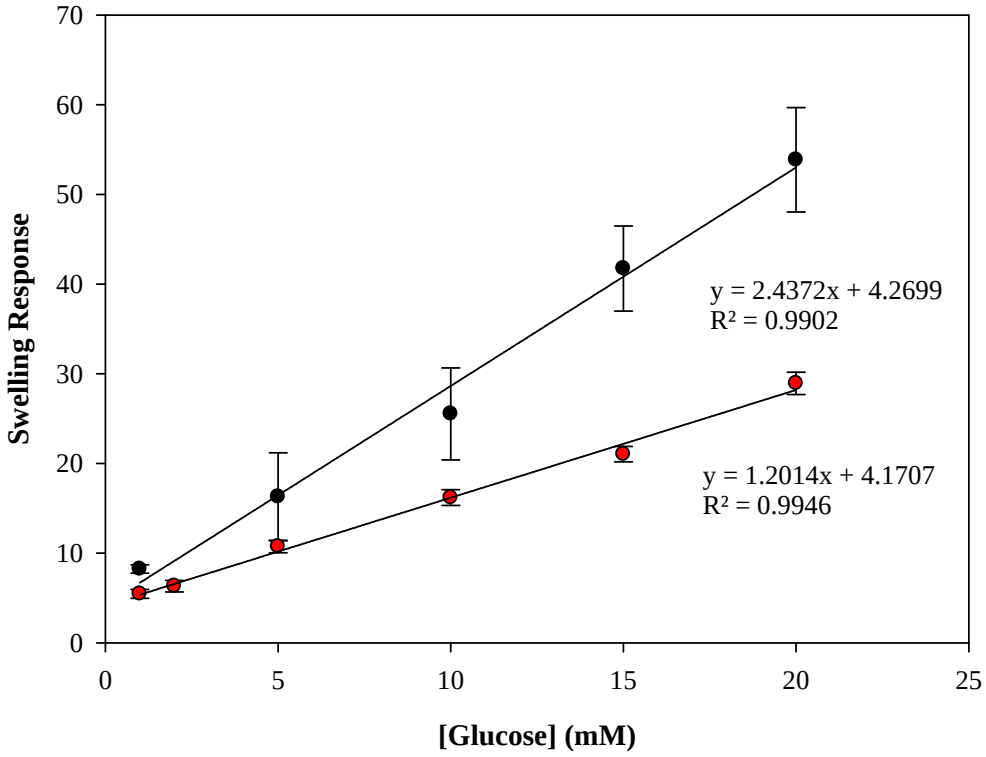

Figure 5.2 Glucose calibration curve of thin hydrogel discs (0.25 mm thick) (black) and bulk discs (11.6 mm x 0.8 mm) (red) with 5% enzyme loading after 100 min swelling time. (n=3)

Despite the reduction in the equilibrium swelling time from approximately 8 to 5 h using the thinner hydrogels, an improvement of 37.5%, this response time is still prohibitively slow for applications such as sensing. Additionally, the hydrogels became very fragile and difficult to handle with reduction in size which would also

limit areas of potential application. As such, the alternative strategy of inducing a macroporous structure into the hydrogels was examined.

5.3.2 Fabrication of superporous hydrogels

Superporous hydrogels containing interconnecting macro-sized pores can rapidly absorb water by capillary action through the open channels. They exhibit significantly faster response times as the swelling is no longer diffusion controlled. Many fabrication methods were investigated to prepare superporous hydrogels with the PEGDGE-Jeffamine® system including gas blowing techniques, templating with macro-sized polystyrene beads and ice-templating.

Gas blowing techniques are frequently employed to synthesis these hydrogels, typically through generating carbon dioxide bubbles by reacting $NaHCO_3$ or Na_2CO_3 with acid to initiate foaming. This strategy was attempted with the PEGDGE-Jeffamine® system. Various amounts of $NaHCO_3$ and acetic acid were added to the PEGDGE-Jeffamine® precursor solution. However, no significant foam was produced with low concentrations of acetic acid ($\leq$ 1 M) and the polymerisation of the gels was not possible in higher concentrations of acetic acid (> 1 M). $NaHCO_3$ reacts with acid to produce a salt and a carbonic acid which decomposes to water and carbon dioxide. When low concentrations of acetic acid were added, the overall pH of the gel precursors solution remained highly alkaline due to the high basic pH of the Jeffamine (pH 11.6). Therefore, the $NaHCO_3$ did not react to produce carbonic acid and subsequent carbon dioxide gas, resulting in no foam. This indicated that sufficient acid must be present to reduce the pH and higher concentrations of acid were required. However, high concentrations of acid resulted in protonation of the amines so they were no longer nucleophilic in nature and able to react with the oxirane groups of the

PEGDGE [292]. Amine nucleophiles require moderate alkaline pH values, usually at least pH 9 [293] to be reactive. Thus, the hydrogel was unable to cross-link and polymerise at low pH. The same behaviour persisted even when strong acids were investigated, including HCl and H_2SO_4. Foaming and crosslinking reactions must occur simultaneously to achieve the well-established porous structures which could not be achieved using this approach.

Due to this pH limitation, several alternative methods for synthesising superporous hydrogels were explored. Polystyrene beads have been used as sacrificial templating agents for hydrogels and are easily removed via dissolution with solvents such as chloroform, dichloromethane and toluene [294-296]. It was postulated that macro-sized polystyrene beads could be incorporated into the PEGDGE-Jeffamine® hydrogel, which would create large pores and possibly open channels, depending on amount, when removed. Macro-sized polystyrene beads (200-300 μm) were incorporated into the PEGDGE-Jeffamine® hydrogel, however the beads remained in the gel even after swelling in chloroform or toluene. Beads were also placed in these solvents in glass vials for extended periods of time (> 1 month) and did not dissolve even with sonication and heating. This is most likely because of the bead stability due to the high level of DVB cross-linker required to synthesise beads of this size.

Ice-templating was the third approach investigated. As stated previously, this involves polymerising the gel at cold temperatures (~ -18 ^{O}C) to create large ice crystals which produce large, interconnected pores upon thawing. Cross-linking occurs in non-frozen liquid channels where the soluble monomers/polymers are concentrated. However, the PEGDGE-Jeffamine® hydrogel would not polymerise at -18 ^{O}C. The gel precursors froze but thawed back to liquid when returned to room temperature. The

cold temperature inhibited the reaction between the amine and epoxy groups, thus inhibiting gelation.

The final approach involved the catalytic decomposition of hydrogen peroxide to produce oxygen bubbles according to Equation 5.3.

$$2H_2O_2 \rightarrow 2H_2O + O_2 \qquad \text{Equation 5.3}$$

Many metals behave as catalysts for the decomposition of hydrogen peroxide including Ag, Fe, Pt, Zn, Cu and Pd [297-301]. Their reaction is often exploited for hydrogen peroxide detection due to its widespread usage in the food industry, pharmaceutical, industrial and environmental analysis. Metal nanoparticles such as Ag, Au, Pt and Pd exhibit excellent catalytic activity for hydrogen peroxide due to their larger specific surface area [302]. Ag nanoparticles (<100 nm) were added to the PEGDGE-Jeffamine® hydrogel precursors. Instead of water, dilute hydrogen peroxide (1 M) was incorporated and produced rapid foaming as it decomposed upon interaction with the Ag nanoparticles. The rate of hydrogen peroxide decomposition also accelerates with increasing pH and temperature [303]. These conditions are provided naturally by the PEGDGE-Jeffamine® system due to the alkaline pH of the Jeffamine® and the heat generated by the oxirane ring-opening of the PEGDGE. Additionally, polymerisation was not affected by the presence of Ag and hydrogen peroxide, thus indicating this to be a viable option for fabricating superporous gels.

Figure 5.3 Photograph of a superporous PEGDGE-Jeffamine® hydrogel prepared via the catalytic decomposition of hydrogen peroxide by silver nanoparticles in the presence of gel precursors.

5.3.3 Optimisation of Pluronic® loading

During the catalytic decomposition of hydrogen peroxide, the generation of oxygen bubbles continues until all the hydrogen peroxide is decomposed. As stated previously hydrogel polymerisation can be a slow process when cross-linking occurs spontaneously (i.e., without use of heat or UV light) such as the hydrogel system described here. Subsequently, due to the rapid decomposition of hydrogen peroxide, it was not surprising that the oxygen generation ceased before the hydrogel polymerised. As a result, the hydrogel produced was not superporous. Therefore, it was decided to incorporate Pluronic® F-127 as a surfactant to stabilise the foam. Pluronic® F-127 is a non-ionic, amphiphilic triblock copolymer of poly(ethylene oxide) and poly(propylene oxide). Spherical micelles are generated in solution as the length of the hydrophilic block is longer than the hydrophobic block of the polymer. Micellisation of these block copolymers occurs as occurs around 10-15^{O}C, thus most of the

molecules are in micellar form at room temperature [304]. It has been used previously as a foam stabiliser in many hydrogel systems [291, 305, 306].

A 10% w/v Pluronic® solution was prepared and incorporated into the PEGDGE-Jeffamine® hydrogel precursor solution with Ag nanoparticles and hydrogen peroxide. The volume of hydrogen peroxide was reduced as the Pluronic® loading was increased to maintain consistency in the overall cross-linking density of the gels. Fig 5.4 consists of a bar chart and photograph showing the proportion of superporous gel versus bulk gel formed upon polymerisation. As the Pluronic® loading increased from 0 to 40%, the depth of superporous gel formed increased from 0.0 (± 0.0) mm to 4.5 (± 0.1) mm and the depth of bulk gel decreased from 4.3 (± 0.1) mm to 2.7 (± 0.2) mm. This indicates that the Pluronic® was behaving as a foam stabiliser and was more efficient at higher loadings. However, when the Pluronic® loading was raised to 50%, the depth of superporous gel decreased to 2.8 (± 0.2) mm and the bulk gel increased to 3.4 (± 0.1) mm. In this instance, in order to achieve such a high Pluronic® loading, the overall concentration of hydrogen peroxide was reduced, hence there was less oxygen produced and available to trap. Additionally, it was apparent that none of the gels were 100% superporous as bulk gel was always present in some proportion. Although this shows that the Pluronic® was successfully stabilising the foam, the polymerisation time was still prohibitively long to fabricate 100% superporous gels.

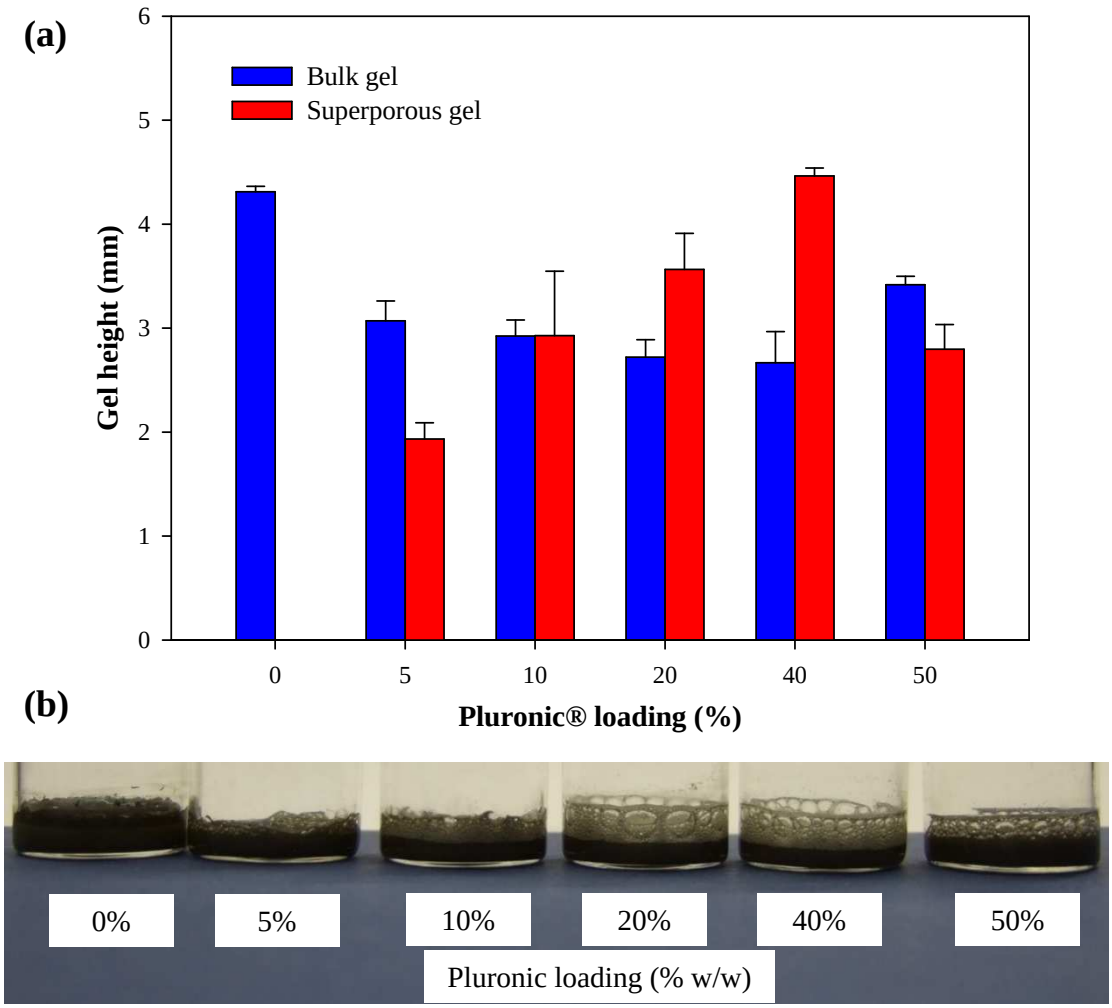

Figure 5.4. (a) Bar chart showing the proportion of bulk versus superporous hydrogel formed with increasing Pluronic® loading (n=3) and (b) corresponding photograph.

5.3.4 Optimisation of polymerisation temperature

PEGDGE-Jeffamine® hydrogels polymerise at room temperature, however higher temperatures can accelerate the epoxy-amine reaction [307-309]. Consequently, polymerisation temperature was investigated to determine if greater amounts of foam (i.e. superporous gel) could be retained if the polymerisation rate was increased. Hydrogels were prepared with a 40% (w/w) Pluronic® loading and placed immediately into a heated oven to polymerise. Fig 5.5 consists of a bar chart and

photograph displaying the proportion of superporous gel versus bulk gel formed upon polymerisation at different temperatures. As the temperature was increased from 20-140^{O}C, the depth of superporous gel increased almost 4 times, from 4.5 (± 0.1) mm to 17.0 (± 0.6) mm. Simultaneously, the depth of bulk gel decreased from 2.7 (± 0.3) mm to 0.4 (± 0.1) mm. The hydrogels also required less time to polymerise as the temperature was increased. Polymerisation time was observed to reduce from ~ 8 h to 15 min with increased temperature. Thus, increasing the temperature accelerates the polymerisation rate, leading to the generation of more superporous gel. Although the hydrogels at 140^{O}C polymerised the fastest and stabilised the greatest amount of superporous gel, the change in gel colour indicated possible thermal degradation of the polymer matrix. Therefore, a polymerisation temperature of 120^{O}C, which required a polymerisation time of 20 min, was used for all subsequent experiments. The superporous and bulk gel were easily separated, to give free-standing superporous gel materials.

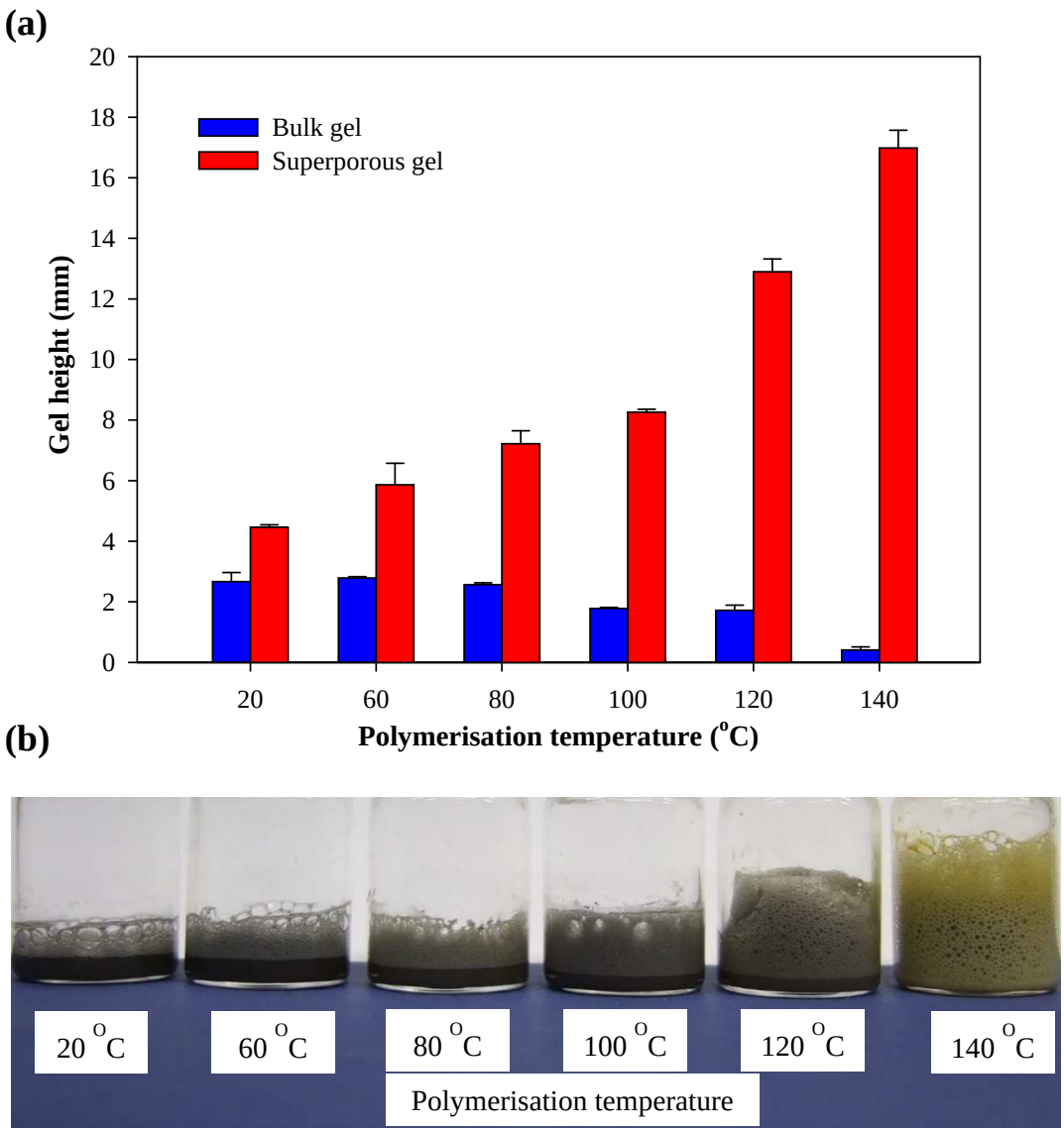

Figure 5.5. (a) Bar chart showing the proportion of bulk and superporous hydrogel formed at various polymerisation temperatures (n=3) and (b) corresponding photograph.

5.3.5 Anti-microbial testing of superporous gels

The control of microorganisms on skin and other surfaces is highly important for maintaining good hygiene standards and health. Consequently, considerable interest has arisen in developing antimicrobial hydrogels for use in consumer products,

as well as protective coatings on medical implants and devices [310, 311]. In particular, hydrogels containing Ag nanoparticles are frequently used in wound and burn dressings [312-314] as Ag possesses the highest bactericidal activity of all known nanoparticles, which increases with decreasing particle size [315].

The anti-microbial properties of the superporous hydrogel and unmodified bulk hydrogel were evaluated against gram-positive bacteria (*S.aureus* 6588), gram-negative bacteria (*E.coli* 25922) and fungi (*C.albicans*) using the disc diffusion method. Hydrogels were fully hydrated in sterile water before analysis as unswollen gels would uptake moisture from the agar and swell, thereby altering their size and contact with the plate. Tetracycline and nystatin antibiotic discs were utilised as positive controls for bacterial and fungal activity respectively. The antibiotic diffuses into the agar, establishing a gradient of antibiotic concentration with high concentration close to the disc and decreasing concentrations further away, and creating a zone of inhibition upon incubation. Fig 5.6 and Fig 5.7 show inhibition zones with a diameter of 35 (± 1) mm for the tetracycline discs on both the *E.coli* and *S.aureus* plates, while the nystatin generated a zone with a diameter of 23 (± 1) mm on the *C.albicans* plate. Both the unmodified bulk hydrogel and superporous hydrogel were ineffective at inhibiting bacterial and fungal growth as no inhibition zones were visible for either gel type. The absence of an inhibition zone for the unmodified bulk hydrogel indicated that the hydrogels were thoroughly cleaned as any unreacted Jeffamine could have potentially leeched from the hydrogel and inhibited growth due to its high pH. All microorganisms have an optimum pH for growth and a pH range where growth is possible, for example *E.coli* is a neutrophile which possesses an optimum pH of 7 and a growth range of pH 5.5 to 8 [316]. Similarly, hydrogen peroxide is biocidal and would inhibit or kill microorganisms if released from the

superporous hydrogels [317]. However, the absence of an inhibition zone around the superporous hydrogels was surprising as the antimicrobial properties of Ag are well-known. Several mechanisms have been proposed for the antimicrobial behaviour of Ag nanoparticles including releasing silver ions which can inactivate vital enzymes, production of free radicals which can damage cell membranes, anchoring to the cell well and penetrating it, or inhibiting growth via modulation of signal transduction [318-321]. As inhibition is dose-dependent, it is possible that the concentration of Ag nanoparticles was too low in the superporous hydrogels to be active against the microorganisms. Alternatively, the hydrogel matrix could be acting as a physical barrier and preventing interaction between the silver and pathogens. In either case, it is probable that a higher loading of Ag nanoparticles would increase activity.

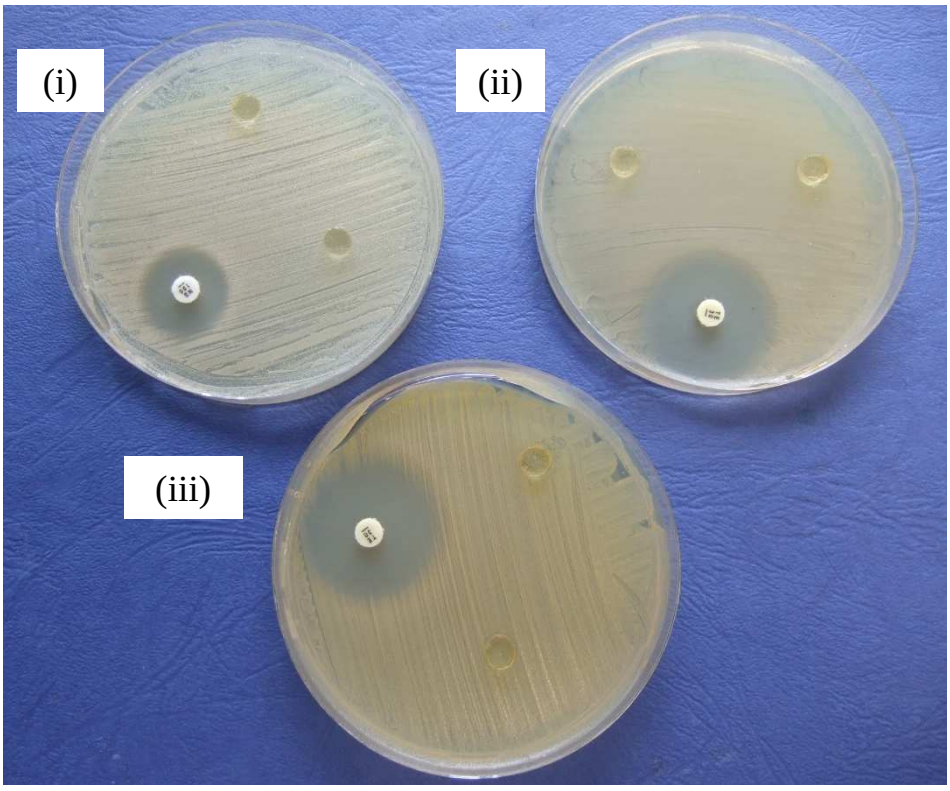

Figure 5.6. Antimicrobial behaviour of unmodified bulk hydrogels against (i) C.albicans (ATTC 10231), (ii) S. aureus (ATTC 6538) and (iii) E.coli (ATTC 25922).

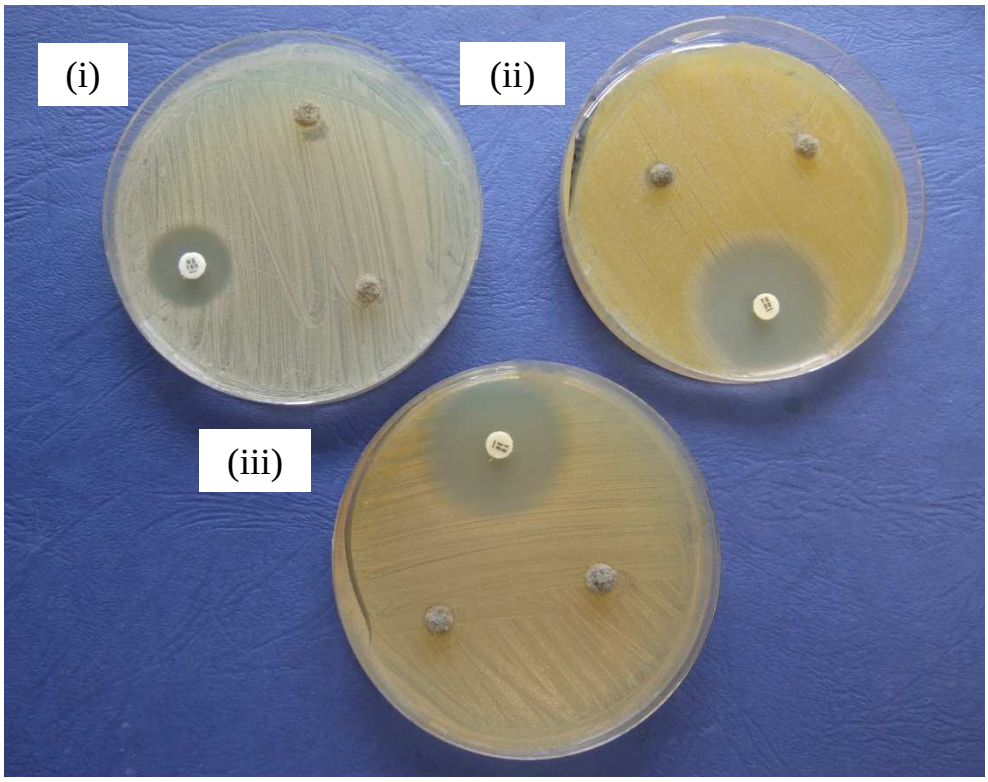

Figure 5.7. Antimicrobial behaviour of superporous hydrogels against (i) C.albicans (ATTC 10231), (ii) S. aureus (ATTC 6538) and (iii) E.coli (ATTC 25922).

5.3.6 Morphology of superporous hydrogels

The morphology of superporous and bulk hydrogels were compared using optical microscopy and SEM. Fig 5.8 shows optical images of fully swollen superporous (a,c) and bulk hydrogels (b,d) at low and high magnifications. The bulk hydrogel appears smooth, with no obvious level of porosity. In comparison, the superporous hydrogel is highly porous, with pores visible at the surface as large as 2500 μm. Due to the low level of magnification used the minimum pore size was too difficult to measure. Although some of the pores appear interconnected, it is difficult be conclusive with these optical images, due to high level of hydration and translucency.

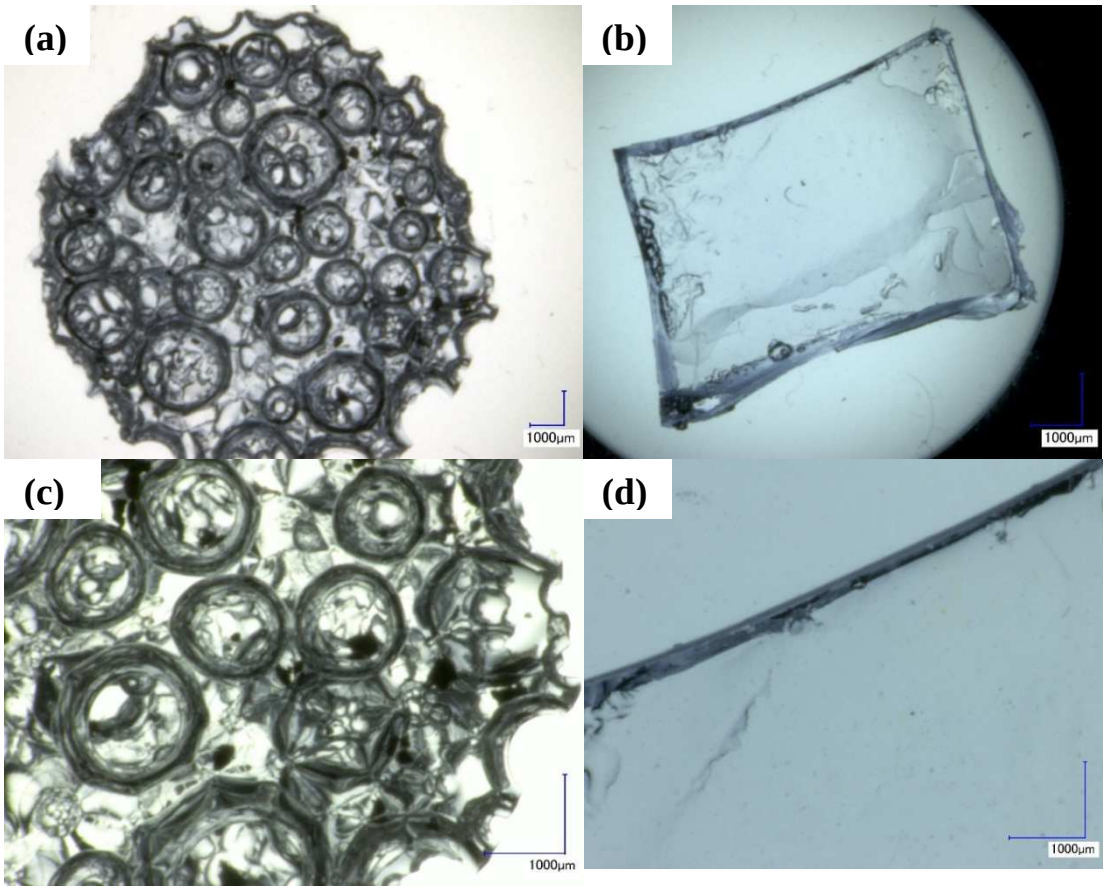

Figure 5.8 Optical microscope images of a superporous hydrogel (a), an unmodified hydrogel (b) and higher magnification images (c,d) respectively. All scale bars = 1000 µm.

Fig 5.9 (a) and (b) display SEM images of an unswollen and fully hydrated superporous hydrogel respectively. These images are at low magnification of x 50. Both images show the superporous structure to be comprised of an interconnecting pore system with typical pore size greater than 100 µm. Pore size ranged from 10-500 µm in the unswollen gel and 200-1000 µm in the swollen hydrogel, with average pore sizes of approximately 100 µm and 550 µm respectively. The thickness of the polymer walls approximately ranged from 200-250 µm in the unswollen gel and 25-40 µm in the swollen hydrogel. Upon swelling, the size of the pores significantly increased, pore

walls became thinner and the channels became wider. The shape of the pores is mainly spherical but some distortion is evident, particularly when swollen. It is likely the distortion occurs due to the rapid pressure changes as the oxygen is generated and travels through the foam. A wide pore size distribution was observable in both gels.

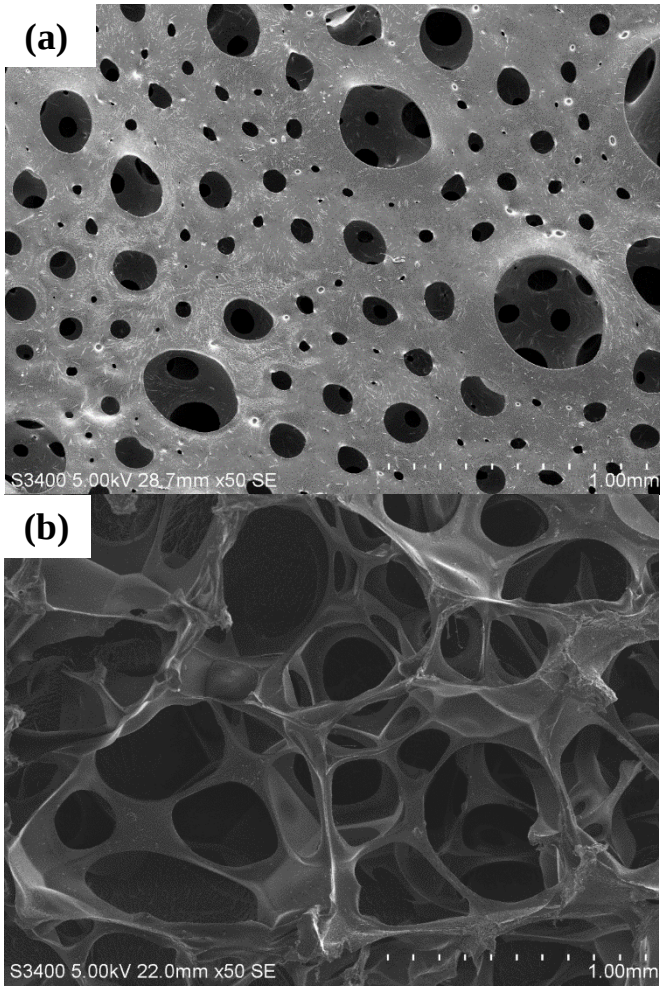

Figure 5.9. SEM images of (a) an unswollen and (b) a fully swollen superporous hydrogel. Mag: x50, scale bar: 1 mm

.

Fig 5.10 (a) and (b) display images of an unswollen and fully hydrated bulk hydrogel. In comparison with the superporous gel, there are no pores visible in the dry

state and much smaller pores present when fully swollen. The pore size ranged from 5-60 μm, with an average size of 20 μm. Thus, the pores of the swollen superporous gels are almost 28 times larger than the corresponding bulk gel. Due to this open structure and increased network capacity the swelling time is likely to significantly decrease.

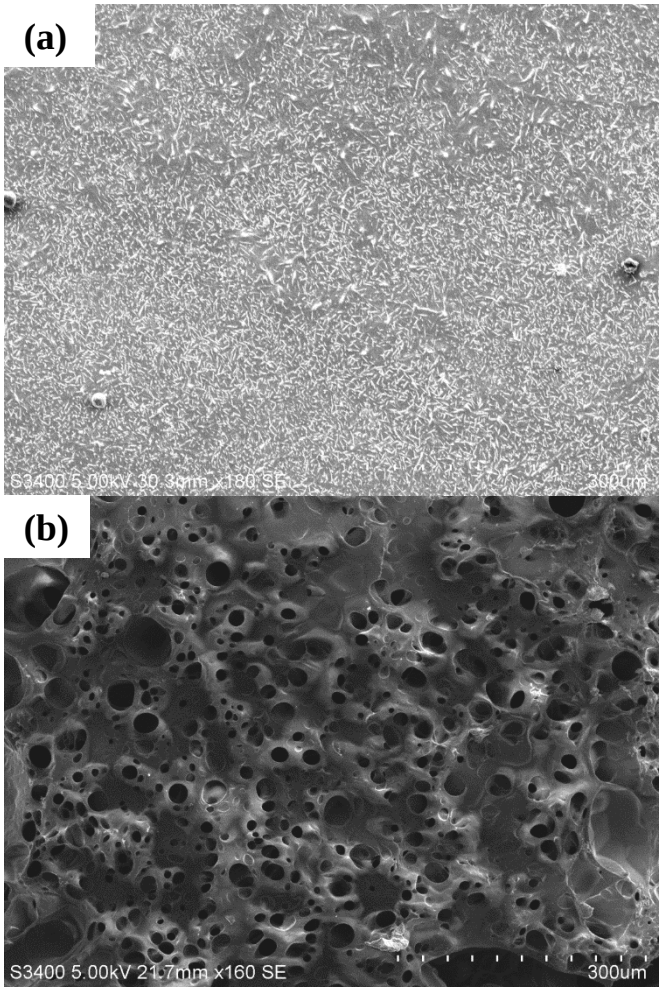

Figure 10. SEM images of (a) an unswollen and (b) a fully swollen bulk hydrogel. Mag: x160, scale bar: 300 μm.

5.3.7 Effect of gel size on swelling time and rate

The swelling behaviour of these superporous hydrogels was monitored to investigate the time required to achieve equilibrium swelling and to determine its relationship with gel size. Fig 5.11 shows the swelling response of superporous hydrogels of three different sizes in water. All hydrogels have an initial height of 4 mm and a diameter of 3.5, 12 or 20 mm. The hydrogels were observed to swell rapidly regardless of their size. An equivalent swelling rate was noted for all three sizes, demonstrating that the swelling rate of these superporous hydrogels does not depend on size. This size-independent fast swelling has been observed in other superporous hydrogel systems and is attributed to the open, macroporous structure of the gel networks [291, 304]. The overall time required to reach equilibrium swelling increased with gel size but all gels were fully swollen in less than 20 s. A swelling time of 10-15 s was required for gels with a 3.5 mm diameter whereas the larger gels with diameters of 12 and 20 mm required 15-20 s. Due to the extremely fast swelling change it was difficult to obtain precise values. Equilibrium swelling ratio also increased with gel size. The largest gel, with a diameter of 20 mm, obtained a swelling ratio of 20.3 compared with 15.3 achieved by the 3.5 mm diameter gel. Swelling ratio and time for equilibrium swelling increase with size as larger gels possess a greater swelling capacity. A larger network signifies that the gel can absorb more water which requires additional time to reach equilibrium swelling. Most applications, including sensing, drug delivery and microfluidics, wouldn’t necessitate a gel larger than 20 mm so the response time will be less than 20 s with these gels. This has decreased dramatically from 5 h achieved with the thin bulk gel discs, an improvement of greater than 1500 fold, and demonstrates the huge advantage in introducing macroporosity.

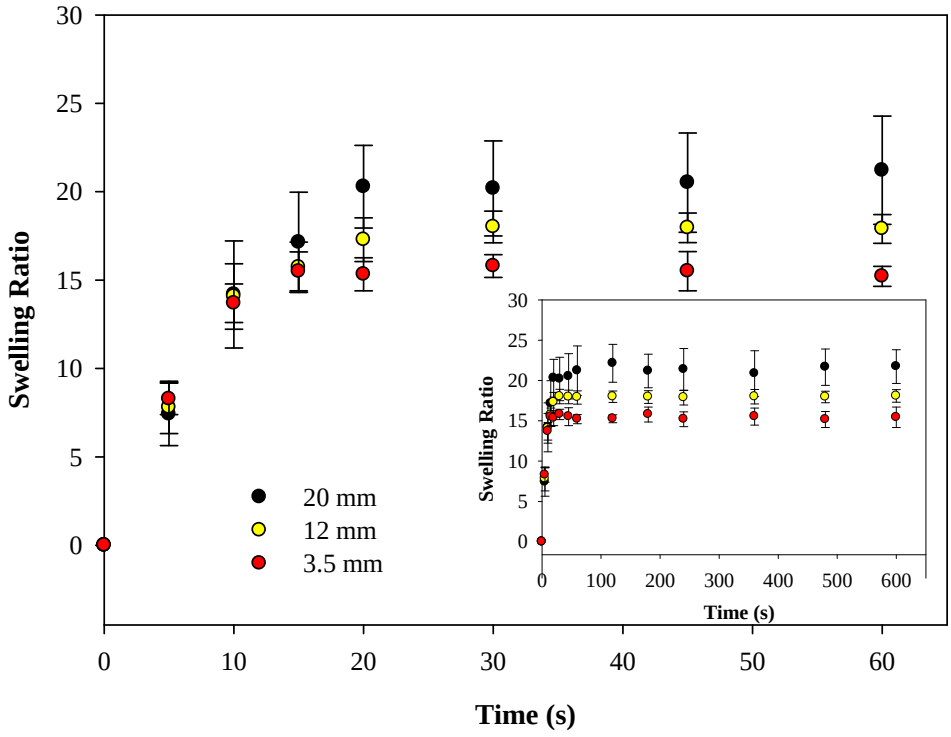

Figure 5.11 Effect of gel diameter on the gravimetric swelling response of superporous hydrogels in water. (n=5)

5.3.8 Comparison of the voltammetric performance with bulk gels

In previous chapters, electrochemical sensing and characterisation has been performed with a single dip-coat of PEGDGE-Jeffamine® due to the resistive nature of the gel. Consequently this section compares the electrochemical properties of the superporous hydrogel with the typical dip-coated films of bulk hydrogel that were prepared in earlier chapters. Dip-coated films of superporous hydrogels couldn't be prepared as it was not possible to trap the oxygen in these thin hydrogel layers on top of the electrode surface. Therefore, superporous hydrogels were prepared in a solution as before, where the carbon cloth was also present in solution. The adhered gel was then cut to the desired size. Due to this increased thickness compared with a dip-coat,

thick bulk gels were also polymerised on carbon cloth electrodes in the same manner as the superporous gels for comparison. Upon swelling, thick bulk and superporous hydrogels were 9 x 9 x 9 mm. Fig 5.12 shows a photograph of the three types of hydrogel for clarification.

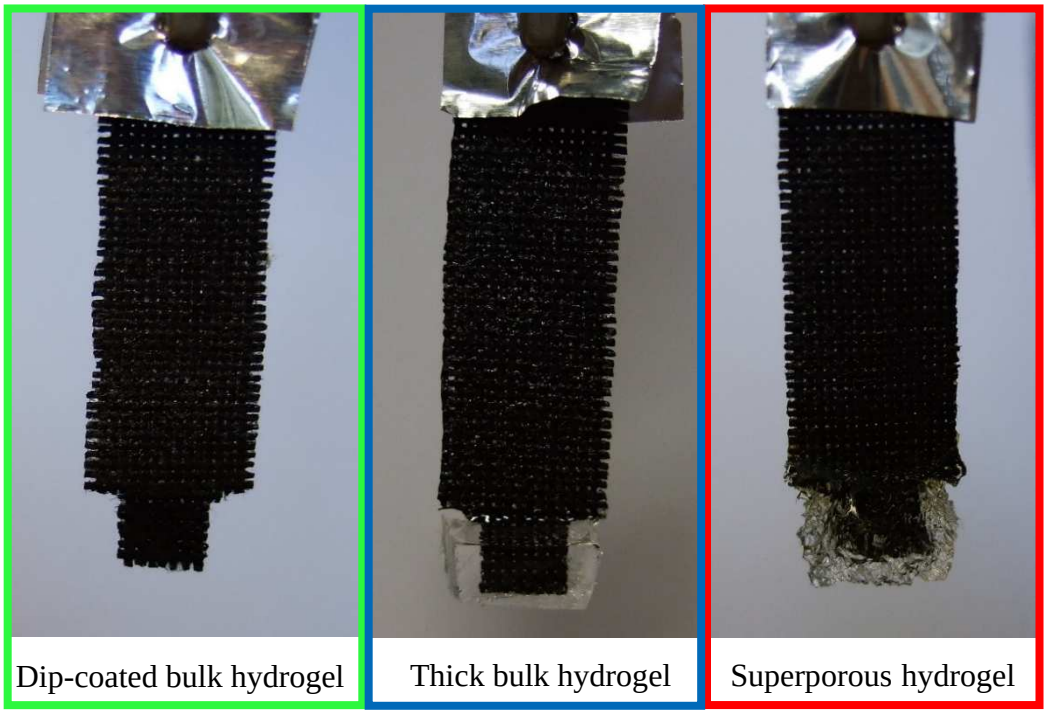

Figure 5.12 Photographs of carbon cloth electrodes modified with dip-coated bulk hydrogel, thick bulk hydrogel and superporous hydrogel.

Silver electrochemistry was observed in the cyclic voltammograms of the superporous hydrogel on carbon cloth electrodes recorded in 1 M KCl (Fig 5.13). The redox couple A1/C1 (0.012/-0.155V) corresponded to the electroformation of Ag^{+} via oxidation (A1) and from the electroreduction of Ag^{+} back to Ag^{0} (C1) arising from the presence of the Ag nanoparticles in the gel [322]. The Ag nanoparticles generated high redox peak currents due to their large electroactive surface area which dominated the

voltammetry between -0.2 and +0.2 V. Consequently, the potential window was narrowed from -0.5 to +0.2 V to -0.5 to -0.1 V to eliminate the silver electrochemistry. Fig 5.14 shows a voltammogram of the superporous hydrogel modified carbon cloth electrodes in this narrower potential window in 1 M KCl. The voltammogram shows only non-Faradaic charging, demonstrating that the silver redox electrochemistry can be eliminated by avoiding the electroformation of Ag+ at the potential of approx. +0.01 V vs Ag/Ag/Cl. Without oxidation, there's no generation of Ag^+ ions to reduce, hence the reduction peak disappears also. Therefore, the diffusion properties of the gel can be investigated in this new potential window.

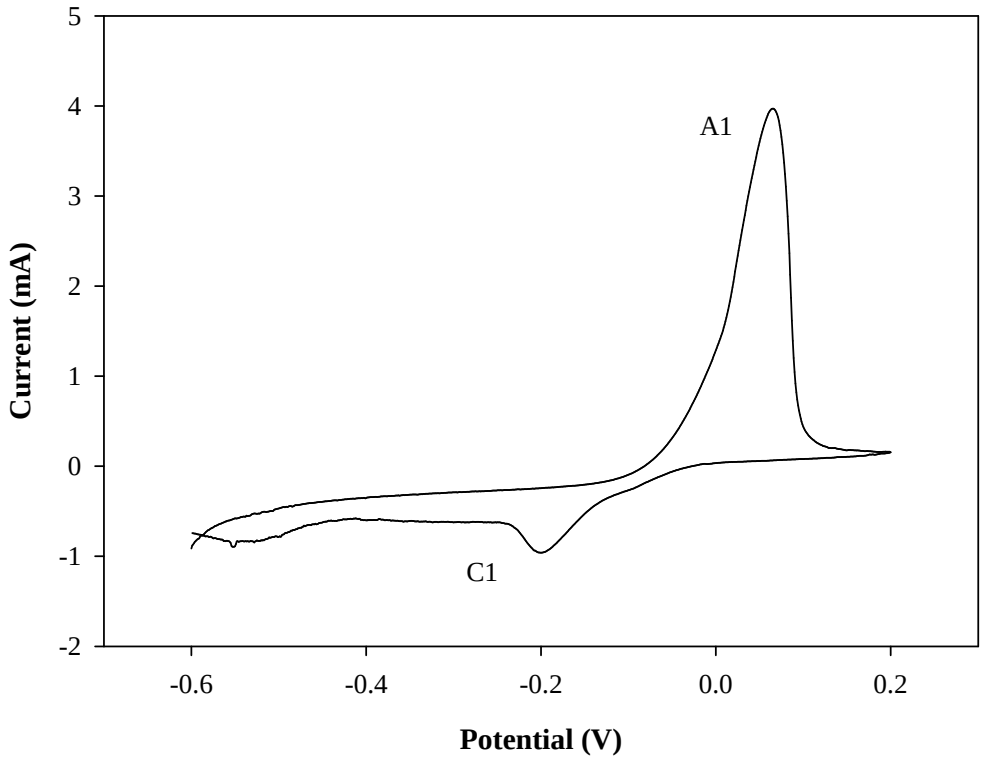

Figure 5.13 Cyclic voltammogram of superporous hydrogel in 1 M KCl at 0.1 Vs^{-1}.

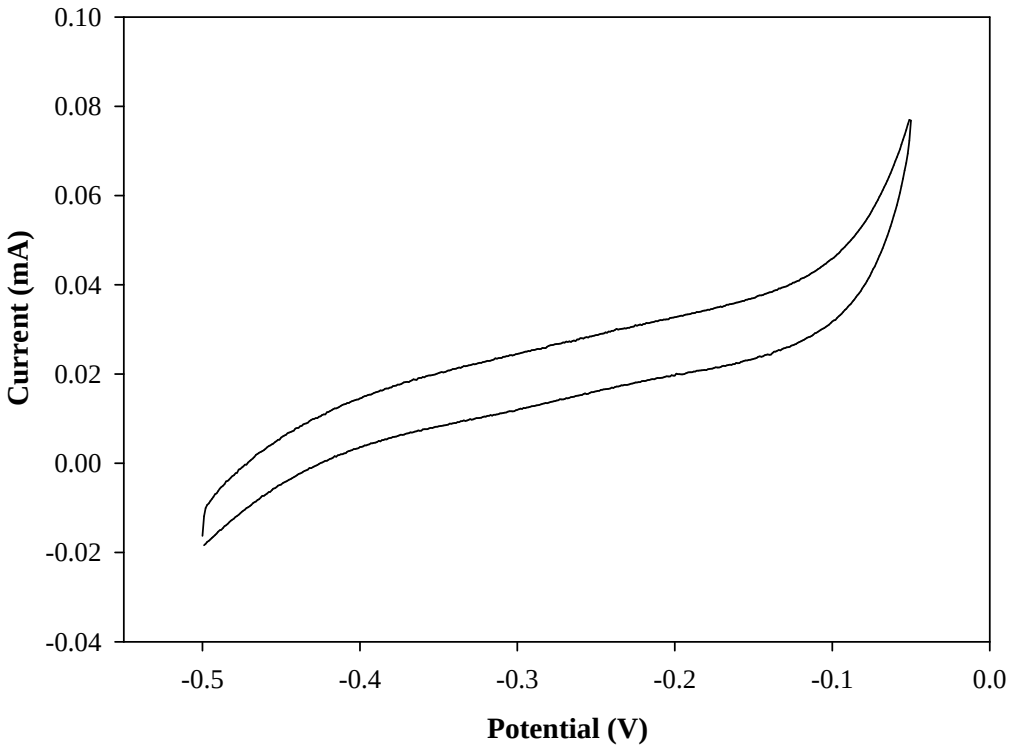

Figure 5.14 Cyclic voltammogram of superporous hydrogel in 1 M KCl at 0.05 Vs^{-1}.

Fig 5.15 shows representative cyclic voltammograms of the electrochemical response of bare carbon cloth, a dip-coat of bulk hydrogel, thick bulk and superporous hydrogel in HARC (1 mM) using the narrow potential window to avoid the silver electrochemistry. Despite the presence of a thick looking gel coating, the redox couple showed very similar voltammetric behaviour with the superporous hydrogel modified electrode compared to at the bare electrode. As summarised in Table 5.1, a high rate of electron transfer was demonstrated with only a very small reduction in peak current and increase in ΔEp evident. In comparison, the thick bulk hydrogel completely inhibited the electroactivity of the bulk solution $[Ru(NH_3)_6]^{3+/2+}$ redox couple. This was unsurprising as it was demonstrated in Chapter 2 that 5 dip-coats of gel was sufficient to inhibit the electroactivity of the carbon cloth due to the resistive nature of

hydrogel. However, this indicates that the macroporosity and thin polymer walls of the superporous hydrogel matrix significantly improve electron transfer and diffusion rates. It is also likely that the Ag nanoparticles in the superporous gel also contribute to this enhancement in electron transfer by increasing the conductivity of the gel.

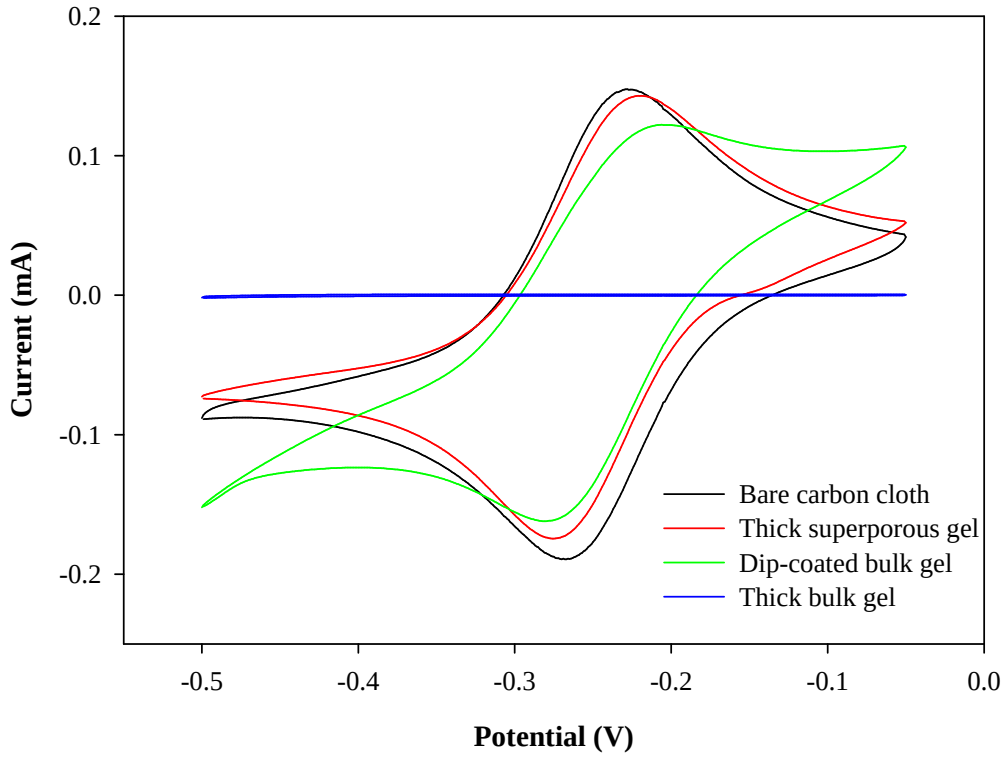

Figure 5.15 Cyclic voltammograms of hydrogels and bare carbon cloth in 1 mM HARC (1 M KCl) at 0.01 Vs^{-1}.

Table 5.1 Summary of peak potential separation values (ΔEp) and current values ($i_{p,a}$ and $i_{p,c}$) for hydrogel modified electrodes (at 0.01 Vs^{-1} in 1 mM HARC in 1 M KCl). (n=3)

Electrode	Average ΔEp (mV)	Average $i_{p,a}$ (mA)	Average $i_{p,c}$ (mA)
Bare carbon cloth	45 ± 6	0.17 ± 0.02	-0.20 ± 0.02
Thick superporous hydrogel	58 ± 5	0.15 ± 0.02	-0.18 ± 0.04
Dip-coated bulk hydrogel	88 ± 15	0.09 ± 0.02	-0.13 ± 0.03

**Values could not be included for thick bulk hydrogel as no redox activity was observed*

At slower scan rates (≤ 25 mV/s), the ΔEp decreased below 59 mV at the bare carbon cloth and superporous hydrogel modified electrode systems which could indicate an influence of thin layer voltammetry due to a surface confined species. It is possible that there was some surface adsorption of the redox species onto the carbon cloth due to its high porosity. However, the values are relatively high, indicating that the process is still primarily diffusion controlled. Additionally, a scan rate study was performed (1 - 250 mV/s) and the three systems, the bare carbon cloth, superporous hydrogel- and dip-coated bulk hydrogel modified carbon cloth electrodes, all displayed a linear correlation between peak current (i_p) and square root of scan rate, indicative of a diffusion controlled process (Fig 5.16). At faster scan rates (> 25 mV), this effect is less apparent potentially because the ΔEp increases due to non-linear diffusion, uncompensated solution resistance and/or slower electron transfer kinetics. Thus, there

is possibly an adsorption effect occurring at slower scan rates but overall the system is diffusion-controlled.

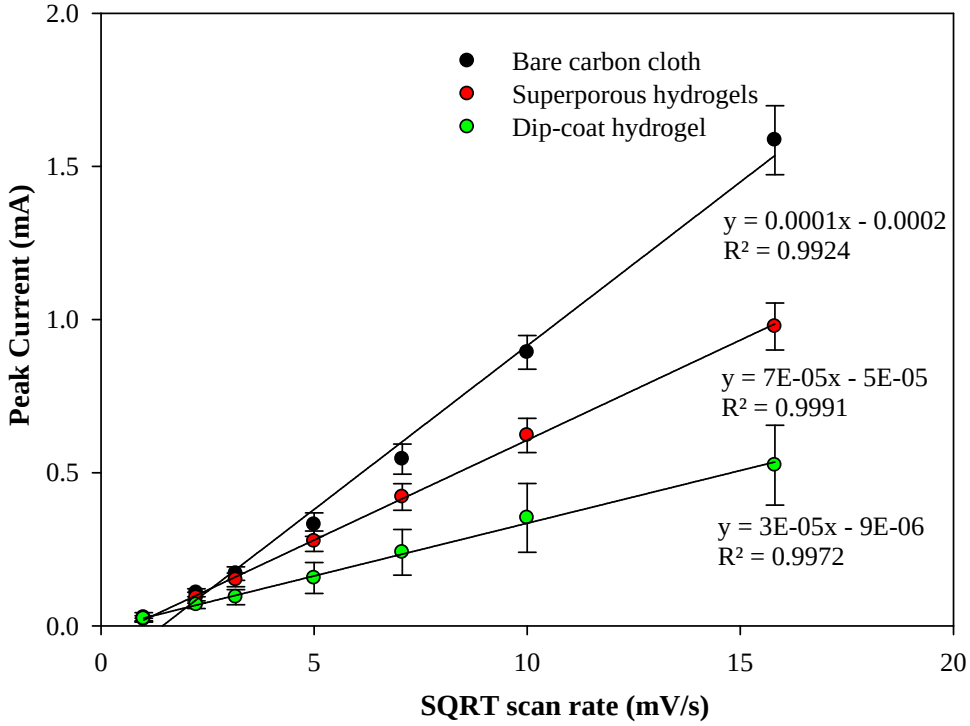

Figure 5.16 Scan rate study of bare carbon cloth, superporous hydrogel- and dip-coated bulk hydrogel modified carbon cloth electrodes in 1 mM HARC (1 M KCl). (n=3)

5.3.9 Effect of macroporosity on impedimetric swelling measurements

The significant improvement in response time of the superporous hydrogels in comparison with bulk hydrogels was tracked with gravimetry previously in this chapter. It was decided to investigate the effect of macroporosity on swelling response time using EIS. Significant benefits could be envisaged if the fast response times could be coupled with impedimetric transduction including rapid and sensitive detection of analytes such as those investigated in Chapters 2 and 3. Nyquist spectra were recorded

of single dip-coated bulk hydrogel and superporous hydrogel modified carbon cloth electrodes at specific time intervals during swelling to determine their equilibrium swelling response time (Fig 5.17). Previously, dip-coated bulk hydrogel modified carbon cloth electrodes were placed in electrolyte solution overnight to ensure they were fully swollen before measurements were recorded for maximum sensitivity. Fig 5.17 (a) shows that these hydrogels required 5-6 h to reach equilibrium swelling. Additional spectra were recorded at 8 and 24 h to confirm the hydrogels were fully swollen. In comparison, the superporous hydrogel modified carbon cloth electrodes were reaching equilibrium swelling in less than 1 min, which was shorter than the timeframe of an impedance measurement (0.13 h) over the frequency range of interest (Fig 5.17 (b)). Therefore, the impedance of the gel at t = 0 could not be measured. Consequently, the swelling was allowed to take place and then an impedance spectrum was recorded. The superporous gels were observed to be less resistive than the dip-coated bulk hydrogel. Gel resistance values of 13,563 (± 189) Ohms and 341,933 (± 73314) Ohms were obtained respectively when the EIS data was fitted using the electrical equivalent circuit applied in Chapters 2 and 3. This reduction in gel resistance and fast swelling time are attributed again to the macroporosity and thin polymer walls of the superporous hydrogel matrix. The improvement in swelling rate also removes the need for overnight swelling prior to analysis, therefore significantly reducing the analysis time and increasing the attractiveness of these materials for sensing applications. The possibility of single frequency measurement or analysis of 2 or 3 frequencies remains to be explored, but if feasible, may permit tracking of the swelling with respect to impedance.

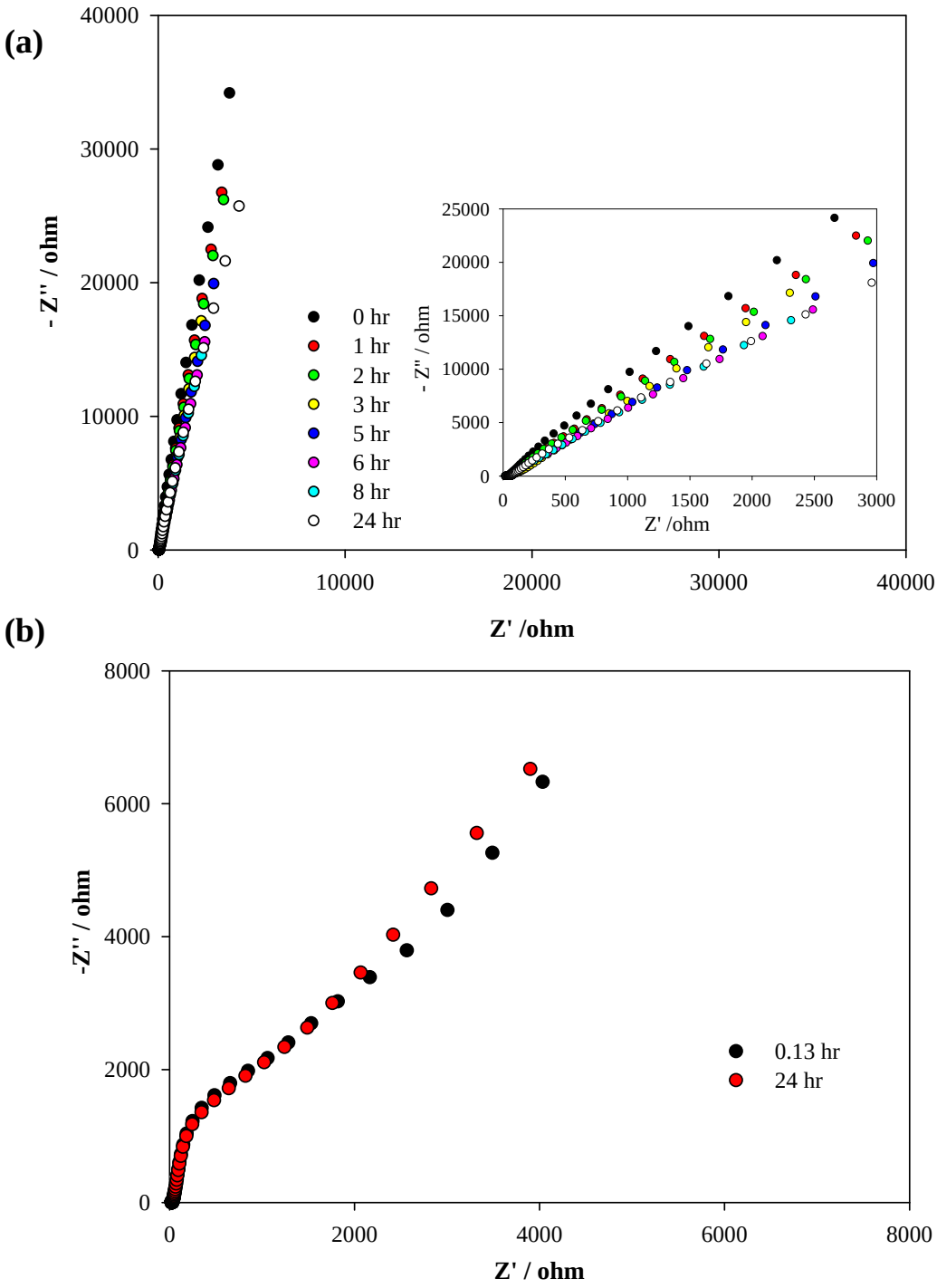

Figure 5.17. Nyquist spectra of (a) PEGDGE-Jeffamine® bulk hydrogel and (b) superporous hydrogel swelling over time (at the OCP in 10 mM PBS).

5.3.10 Effect of pH on swelling response of superporous gels

Ionisation-induced swelling was demonstrated previously with the PEGDGE-Jeffamine® hydrogel in the presence of acid due to the pendant amine groups on the polymer backbone. A pH study was performed to determine if the superporous hydrogels were also pH-sensitive. Superporous hydrogels were allowed reach equilibrium swelling in water before being placed into solutions of different pHs ranging from pH 2 to 10. Stock HCl (pH 2) and NaOH (pH 12) solutions were prepared and mixed to achieve the desired pH. Buffer solutions were not used as no single buffer system would cover the entire pH scale. Therefore, multiple different buffers would be required. This was avoided as buffer composition and additional ions are reported to strongly influence the swelling properties of polyelectrolyte gels [323]. The swelling response was calculated by subtracting the swelling ratio due to water uptake from the swelling ratio at the specified pH, thereby observing swelling solely due to ionisation. As displayed in Fig 5.18, the swelling response is characterised by a peak maximum at pH 3. This maximum swelling at this pH corresponds to maximum ionisation of the amine groups. As discussed in Chapter 2, the majority of the amines exist as secondary amines in the polymer matrix and theoretically possess a pKa of 4.9. According to the Henderson Hasselbach equation (Equation 5.4), these groups are therefore 98.8% ionised at pH 3, 88.8% at pH 4 and 44.3% at pH 5. This corresponds with the apparent pKa of 4.5 visible in Fig 5.18 as the midpoint of the curve.

$$pH = pKa + \log [A^-/HA] \qquad \text{Equation 5.4}$$

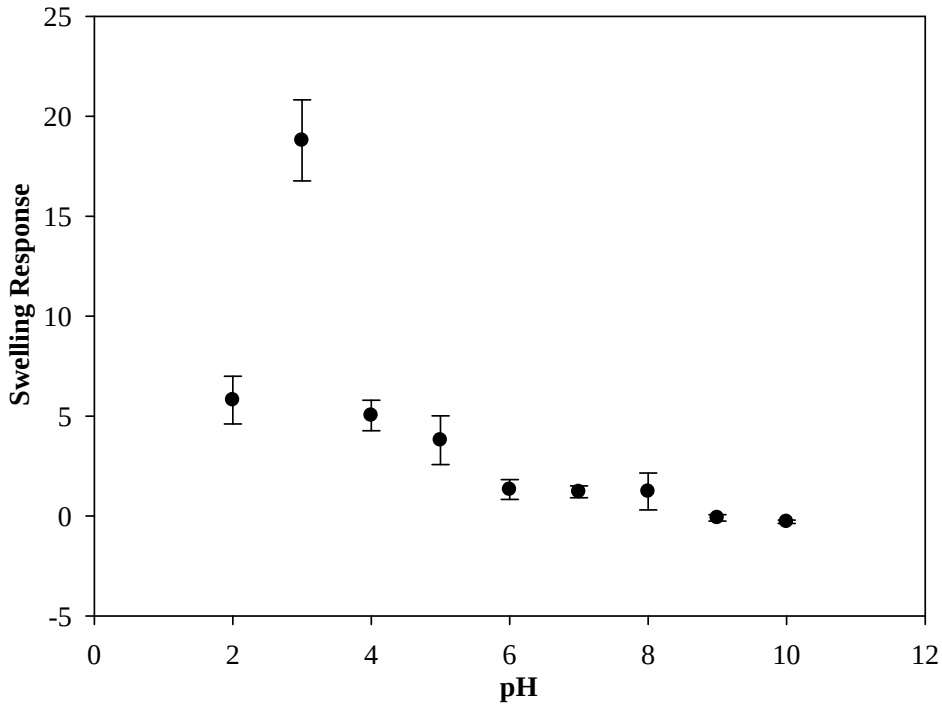

Figure 5.18 Effect of pH on swelling response of superporous hydrogels after 10 min (Swelling response calculated as swelling ratio in pH solution minus swelling ratio in water). (n=3)

Increased swelling capacity was observed at pH 3 because of increased electrostatic repulsion between adjacent charged amines and increased osmotic pressure as counter ions migrate into the gel to balance the charge. At lower pHs (pH <3) the swelling response decreased sharply. Although the amines are theoretically 100% ionised in this region, this phenomenon has been seen previously with polyelectrolyte gels and is attributed to a screening effect of the counter ion (e.g. Cl^-) shielding the charge of the ammonium cations and reducing repulsion efficiency [323]. It can occur additionally if the ionic strength is increased as the osmotic pressure will decrease and the hydrogel will collapse [59]. In this system, it is likely resulting from the screening effect as the ionic strength remained constant. At higher pHs (pH >3), the amines are either partially protonated or unprotonated leading to a lower degree of

ionisation and lower swelling responses. The extent of ionisation observed at pH 3, however was surprisingly high and therefore it is possible that there is another unknown factor contributing to this enhancement in ionisation and swelling response. However, this data point should be verified by repeating the experiment with smaller increments between pH 2 and 4, such as 0.2 of a pH unit, to confirm that this result is indeed real and reproducible.

Pulsatile pH-dependant swelling was evaluated between pH 3 and 10 solutions with 1 min intervals (Fig 5.19). Reversible, consistent swelling was observed for the 10 cycles investigated. The superporous hydrogel was capable of rapidly absorbing and desorbing the swelling medium upon alteration of the pH due to its macroporous, open structure. Compared with Fig 5.18, the hydrogels achieved the maximum swelling response of 18.3 (± 0.5) in pH 3 but only partially deionised and deswelled in pH 10 as the swelling response decreased to 12.8 (± 0.3) instead of 0. This becomes more apparent when the swelling response is expressed as percent change (Fig 5.20). When the hydrogels where switched from a pH 10 solution to pH 3 the swelling response increased by 42.7 (± 5.0) %. Alternatively when they were returned to pH 10 the swelling response decreased by 29.9 (± 2.3) %. Neutralisation effects could be responsible as the hydrogels absorb the pH 3 solution and then release it into the pH 10 solution as they equilibrate in the new environment and vice versa. Alternatively, often times the rate of swelling and deswelling in hydrogel systems are not equal. In this instance, the deswelling rate was slower than the swelling rate. This has been seen previously in other macroporous gel systems [283]. If confirmation was required, testing could be performed in buffered solutions or using longer interval times. These fast and reproducible swelling transitions are highly desirable in hydrogel-based sensors and as intelligent self-actuating valves and pumps in MEMS devices.

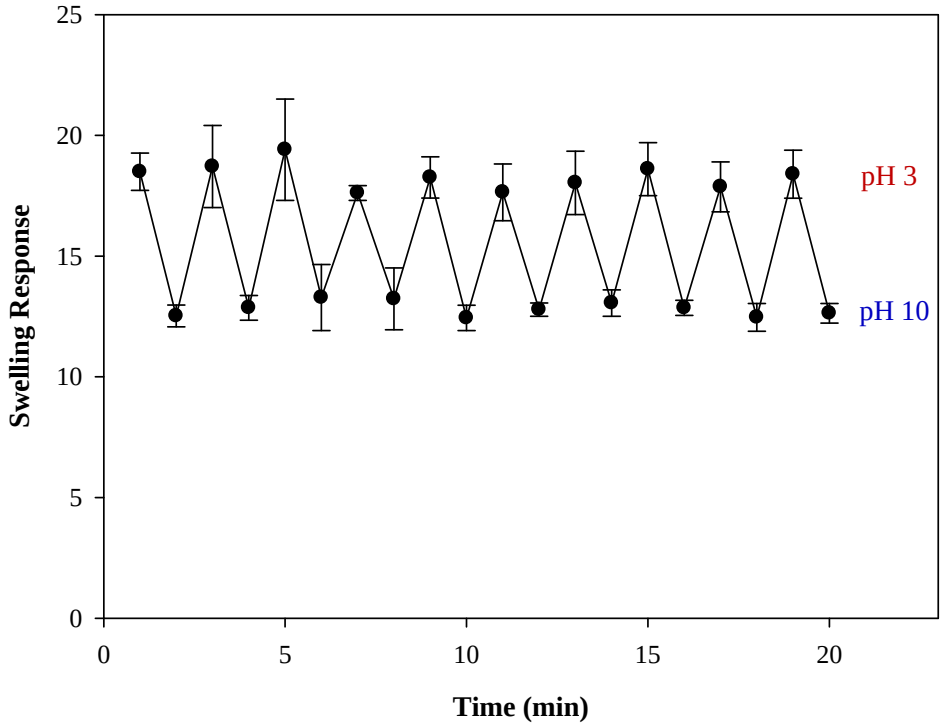

Figure 5.19 Pulsatile pH-dependant swelling (pH 3) and deswelling (pH 10) behaviour of superporous hydrogels (1 min intervals). (n=3)

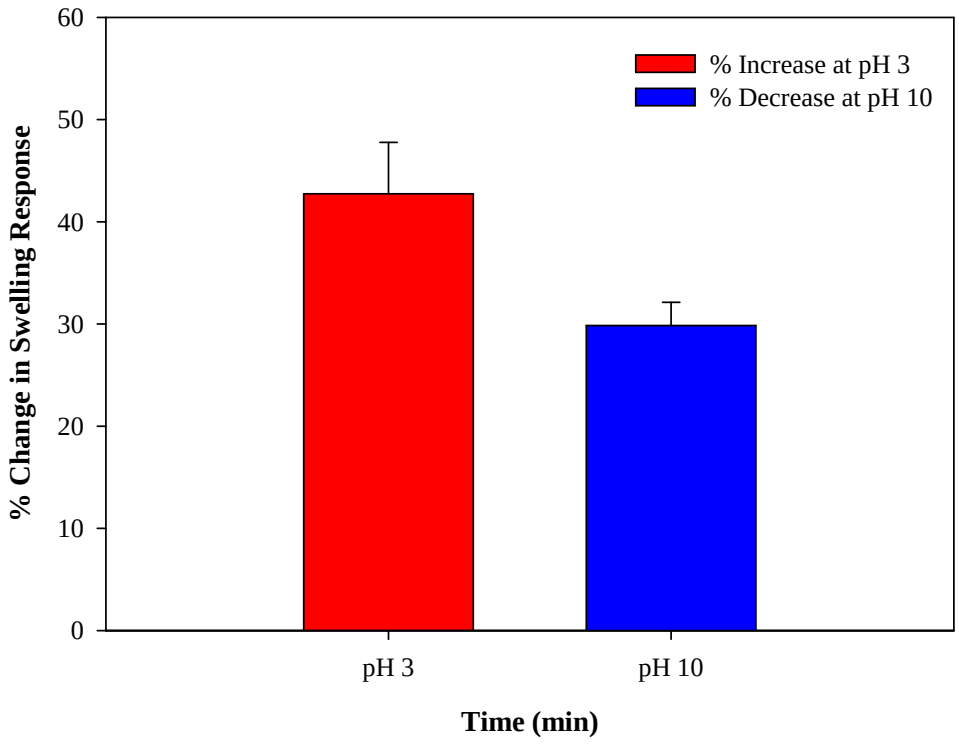

Figure 5.20 Bar chart of the increase and decrease in swelling response, observed at pH 3 and pH 10 respectively, expressed as a percentage. (n=10)

5.4 Conclusion

Overall, this chapter has discussed different strategies to increase the rate of swelling of the PEGDGE-Jeffamine® hydrogel. Although fabrication of thinner gels had many advantages including ease of preparation and reduction of the equilibrium swelling time of bulk gels from approximately 8 to 5 h, which doubled the sensitivity of glucose detection, the resulting gels were very fragile and prohibitively slow for sensing and drug applications when immediate intervention is required.

Superporous hydrogels were successfully prepared using in situ generated oxygen bubbles produced via the catalytic decomposition of hydrogen peroxide by silver nanoparticles. To the author's knowledge, this approach has not been investigated previously and thus has been shown for the first time as a viable synthesis method for hydrogel systems which may be limited by pH or templating restrictions. An interconnected macropore system, with pore size of 200-1000 μm and wall thickness of 25-40 μm, was established. The hydrogels retained their pH-sensitivity and displayed reproducible, well-behaved swelling transitions upon pulsatile pH switching. Additionally, in comparison with bulk hydrogel, the superporous gels significantly improved electron transfer and diffusion rates in the voltammetric studies demonstrating elimination of the diffusion barrier, due to their macroporosity, thin polymer walls and Ag content.

Most importantly, the equilibrium swelling time of superporous gels was found to be in the order of about 20 s. This is a dramatic improvement of more than 1500-fold in terms of time required to reach swelling equilibrium when compared to the bulk gels. Additionally, it was demonstrated that EIS measurements could be performed on equilibrium swollen superporous gels on carbon cloth electrodes after less than 1

minute pre-swelling. This means that overnight pre-swelling in electrolyte solution or 500 min swelling in the solution of interest are no longer necessary to achieve maximum sensitivity. In addition to increasing the practicality of these materials in sensing, the rapid pH-sensitive response could easily be exploited in drug delivery, as intelligent valves in MEMS devices or in numerous other applications.

Chapter 6

Conclusions & Future Work

6.1 Conclusions

Stimuli-sensitive hydrogels are highly attractive materials for sensing and controlled drug delivery applications due to their versatility, high water content, 3D matrix and ability to swell/deswell in response to small environmental or physiological changes. As reviewed in Chapter 1, commonly used transduction systems for hydrogel swelling are based on optical, gravimetric and mechanical methods. They function by detecting changes in the properties of the polymer network, including cross-linking density, volume and tensile strength, or on the mechanical work produced by the swelling mechanism. In comparison, apart from a few conductimetric sensors, electrochemical transduction has not been as thoroughly investigated. Chapter 2 of this work explored use of non-Faradaic EIS to sensitively track hydrogel swelling in response to a target analyte. The swelling response of a cationic PEGDGE-Jeffamine® hydrogel was optimised for glucose detection in terms of cross-linking density and enzyme loading. These hydrogels were dip-coated onto carbon cloth electrodes to investigate their electrochemical properties. Carbon cloth was determined to be a suitable electrode material for investigating the swelling response of the hydrogel due to its high porosity and flexibility which provided extra support to the swollen hydrogel without restricting the swelling response. Using EIS, a linear range of 1 to 100 μM and detection limit of 0.08 μM glucose were observed based on changes in gel resistance upon swelling. This limit of detection was a 6-fold improvement over the traditional gravimetric method and illustrated the feasibility of using EIS as a transduction method to monitor hydrogel swelling.

As this system demonstrated good potential as a sensing platform, Chapter 3 investigated its applicability for other relevant analytes that could be challenging in terms of limit of detection requirements. Consequently, the pH-sensitive hydrogel was

modified to detect GUS, a marker compound for *E.coli*. Changes from the glucose platform configuration included the placement of the enzyme, and use of elevated temperature, and similar low limits of detection were achieved.

Chapter 4 explored the synthesis and characterisation of an electroactive hydrogel composite and its potential application in electro-stimulated drug delivery. Incorporation of very low concentrations of HA greatly improved the stability of rGO dispersions and allowed the production of high quality, homogeneous rGO-hydrogel composites. The inclusion of rGO attributed new properties and enhanced the inherent characteristics of the PEGDGE-Jeffamine® hydrogel system. On-demand controlled drug delivery of a model drug was successfully demonstrated with these new composite materials. Through variation of the rGO content, electrode polarity and magnitude, a wide number of drug release profiles were observed, ranging from slow release of low dosages to rapid release of high dosages.

Chapter 5 discussed various strategies for increasing the swelling rate of the PEGDGE-Jeffamine® hydrogel. Thinner hydrogels were prepared to reduce the diffusion path length which consequently reduced the swelling time from approximately 8 to 5 h. However, this is still prohibitively slow and the gels were very fragile, limiting their potential applications. An alternative approach involved fabrication of superporous gels to remove the diffusion limitation by rapid absorption of water by capillary action through interconnected, macro-sized channels. Superporous hydrogels were successfully prepared using *in situ* generated oxygen bubbles produced via the catalytic decomposition of hydrogen peroxide by Ag nanoparticles. The hydrogels retained their pH-sensitivity and displayed reproducible, well-behaved swelling transitions upon pulsatile pH switching. Swelling equilibrium

time was determined to be in the order of about 20 s using these gels, a dramatic improvement of more than 1500-fold in comparison with the bulk gels.

This work has advanced use of stimuli-sensitive hydrogels for sensing and drug delivery applications. While many research groups have developed various optical and mechanical transduction methods for hydrogel swelling, electrochemical transduction has not been investigated in such detail. This work illustrated that EIS can be used as a viable and sensitive transduction method for tracking hydrogel swelling in response to an analyte. Electrochemical transduction has many advantages including reliability, direct coupling with microelectronics, and ease of interfacing with intricate systems as well as mass-production of low-cost, disposable electrode devices amenable to miniaturisation and widespread application. Relevant, low detection limits were achieved for glucose and GUS demonstrating that this technology is versatile and can adapted for different analytes. A novel electroactive hydrogel capable of electro-stimulated release was developed. Additionally, a new approach was investigated for preparing superporous hydrogels and was shown for the first time as a viable synthesis method for hydrogel systems which may be limited by pH or templating restrictions. This new sensitive transduction method, responsive materials and unique synthesis options offer significant benefits for sensing and drug delivery, as well as numerous other potential applications.

6.2 Future work

The following section presents recommendations to future directions of studies following the work outlined in Chapters 2-5. The high sensitivity of non-Faradaic EIS, coupled with the textile-based electrode approach, opens the potential of this system for monitoring glucose concentration via the skin in sweat or ISF. To realise these

applications, future study should initially focus on investigation of possible interferences, such as common organic acids in sweat including lactic and pyruvic acid, and minimising their impact on sensor response. Brahim *et al*. [111] reported that the cross-linking density of their p(HEMA) hydrogel acted as a 'molecular sieve' by screening larger interferents. Incorporation of cationic PPy led to anion exclusion as anionic species in the buffer migrated to balance the charge on the PPy and behaved as a barrier against the diffusion of other anionic species into the film. As altering the cross-linking density of the hydrogel might reduce sensitivity of the PEGDGE-Jeffamine® system, incorporation of an additional membrane (e.g. cellulose acetate or Nafion) could provide the same effect and reduce interference using electrostatic repulsion or size exclusion. However, this could possibly lead to a reduction in sensitivity and an increase in response time. Alternatively, an affinity-based hydrogel could be explored instead. Phenylboronic acid has a high affinity for diol-containing molecules like glucose and can be functionalised into the polymer backbone to induce volumetric changes in the gel upon exposure to glucose [196]. Through functionalising the polymer backbone with complementary pairs, self-assembling hydrogels can be generated based on specific interactions between antibody-antigen, aptamer-substrate and peptide-peptide pairs [14-16]. These gels are known for their highly selective swelling response which is induced due to competitive binding upon exposure to unbound species. An example of an antigen-sensitive hydrogel is illustrated in Fig 6.1. This network will swell upon addition of free antigen (Ag) as competitive binding will result in dissociation of the Ag-antibody (Ab) crosslinks by exchange of the grafted Ag for free Ag. Additionally, EIS could be performed at the OCP to minimise oxidation of common electroactive interferents, like ascorbic acid, which have the potential to act as interfering species.

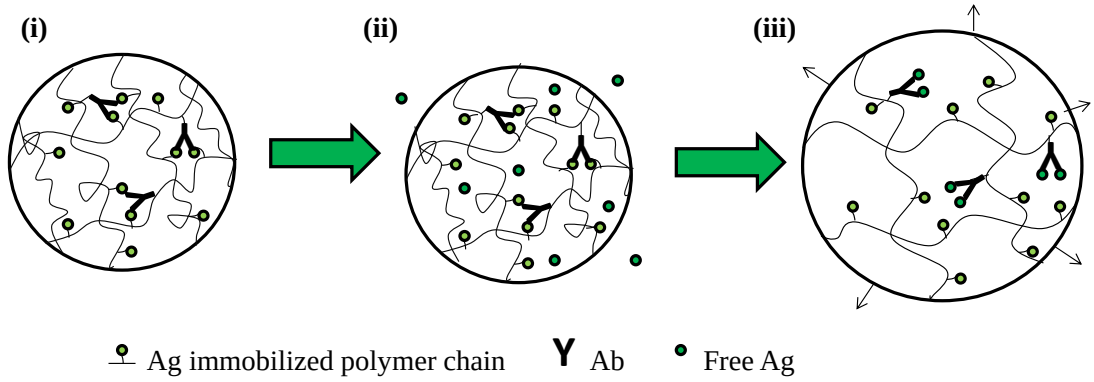

Figure 6.1. Schematic of the swelling mechanism: (i) Grafted Ag and Ab in polymer network, (ii) addition of free Ag and (iii) binding disruption/swelling.

In this thesis, EIS analysis involved measurement of a wide frequency range and fitting the data using an electrical equivalent circuit to obtain gel resistance values. For sensing applications, single frequency measurement, or analysis of the total impedance at two or three frequencies, in the mid to low frequency region would simplify this method as well as reducing cost and analysis time.

To further develop the GUS hydrogel so that it could be applied into an *E.coli* sensor, the detection limits and linear ranges achieved in this work need to be correlated with CFU/mL to compare with existing technologies for *E.coli* detection using GUS. One strategy could involve analysing an *E.coli* standard using the impedimetric method. A particular pathogenic strain of *E.coli* would be cultured and its concentration determined by plate counting. A fixed volume of this *E.coli* suspension would then be filtered to concentrate the sample and improve test sensitivity. The filter would then be exposed to aqueous solution of Triton X-100 or sodium lauryl sulfate to lyse the bacteria and release the GUS. The released GUS

would then be incorporated into the hydrogel and analysed as done in this chapter. As the *E.coli* standard concentration is known it would then be correlated with the impedimetric method using the equation of the calibration line.

A schematic of a microfluidic chip housing this technology for *E.coli* detection is illustrated in Fig 6.2. Pretreatment of the contaminated water sample occurs off-chip and involves filtering the water to isolate and concentrate the bacteria, followed by washing the filter with a detergent solution to lyse the bacteria. This solution is then injected into the device and the PEGDGE and Jeffamine® released from their wells. The inlet can be sealed before the device is shaken to mix all the components. A well is present below the working electrode where the hydrogel can polymerise (~ 1 h) to isolate it from the counter and reference electrodes. All three electrodes consist of sputtered gold. In the case of the working electrode, the gold is present as a conduction path for the carbon cloth electrode used previously. It is important that the hydrogel has sufficient space to swell freely in the channel. This can be controlled by careful calculation of the volumes used. The inlet can be reopened to introduce an aqueous solution containing the substrate (4-NPG) and allow the hydrogel to swell. This solution could be removed via the outlet before the electrolyte solution is introduced for the electrochemical measurements and the device is connected to a potentiostat via the exposed electrodes.

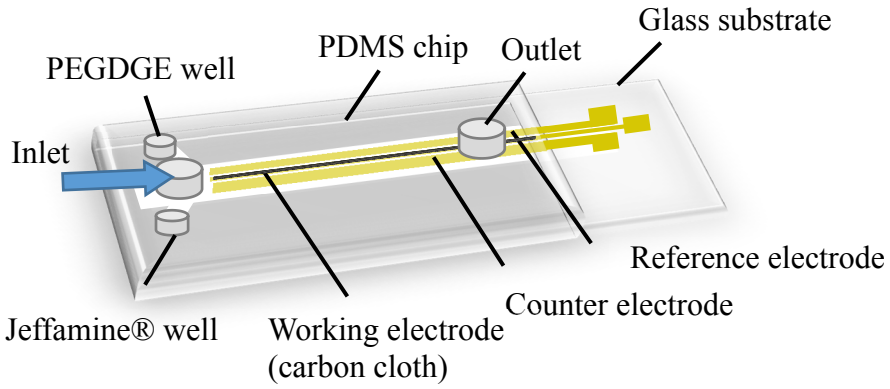

Figure 6.2 Schematic of possible microfluidic design for sensing E.coli on-chip.

A primary aim of this thesis was the development of hydrogel materials for sensing and drug delivery applications. Due to the pH sensitivity of these gels and their ability to rapidly swell, they possess the potential to be developed as an intelligent drug delivery system capable of sensing a physiological pH change and auto-titrating a drug autonomously, without application of an external stimulus. As discussed previously, this combination of sensing and drug delivery is highly desirable and has many advantages including safer, more efficient drug distribution by enabling site-specific drug delivery with on-off regulation in real time. Adverse side-effects would be dramatically reduced and patient compliance would increase. Numerous potential applications could be envisaged including auto-titration of insulin for diabetic patients using the glucose-sensitive gel or in the treatment of various skin conditions.

If the hydrogels were biocompatible, insulin could be incorporated into the glucose-sensitive gel and its role as an artificial pancreas could be explored for insulin delivery. Upon exposure to glucose, pore size would increase as the hydrogel swelled, initiating release of insulin. Release would be suspended when the concentration of glucose decreased and the gel deswelled. This would circumvent the need for multiple

daily injections of insulin and continuous monitoring but would be highly challenging. In addition to biocompatibility studies, stability and long term reversibility would necessitate investigation. Due to the relatively large size of insulin, macro-sized pores would likely be required. The cross-linking density of the hydrogel would require optimisation as it would need to be high enough to maintain insulin delivery over longer time periods but still low enough for insulin to be released from the gel.

Healthy skin has an acidic pH (~5-6) which contributes to the optimal barrier function of this tissue. In comparison, skin pH is significantly elevated in patients with dermatitis. For example, surface skin pH increases up to 7.3–7.4 with acute eczema. This pH discrepancy could be exploited for the delivery of corticosteroids or other drugs by exploiting the swelling/deswelling of pH-sensitive hydrogels.

The fast swelling of the superporous gels also presents a promising avenue for improving the response time and sensitivity of the glucose and *E.coli* detection investigated in Chapters 2 and 3. In relation to the drug delivery explored in Chapter 4, it is probable that the release rate would increase and development of a drug delivery system for rapid intervention could be envisaged. Other areas of potential application include use as self-actuating valves and pumps in MEMS devices or in hygiene products such as diapers and sanitary products due to their pH sensitivity, rapid response and high swelling ratios. Additionally, application of this superporous fabrication strategy into other gel systems could potentially increase their swelling rate and/or capacity (e.g. affinity-based systems such as the phenylboronic acid hydrogel). Due to the high tunability of these materials, their responsive properties and the wide number of potential applications, they possess great potential to become an important contributor in the future development of new technologies and smart devices.

6.3 References

1. Wichterle, O. and D. Lim, *Hydrophilic gels for biological use.* Nature, 1960. **185**(4706): p. 117-118.
2. Ionov, L., *Hydrogel-based actuators: possibilities and limitations.* Materials Today, 2014. **17**(10): p. 494-503.
3. Sirousazar, M. and M. Kokabi, *Intelligent Nanomaterials*. 2012, Massachusetts: Scrivener Publishing LLC.
4. Omidian, H. and K. Park, *Hydrogels*. Fundamentals and applications of controlled release drug delivery. 2012, New York, NY: Springer.
5. Mulyasasmita, W., J.S. Lee, and S.C. Heilshorn, *Molecular-Level Engineering of Protein Physical Hydrogels for Predictive Sol–Gel Phase Behavior.* Biomacromolecules, 2011. **12**(10): p. 3406-3411.
6. Brassinne, J., et al., *Hydrogels with Dual Relaxation and Two-Step Gel–Sol Transition from Heterotelechelic Polymers.* Macromolecules, 2013. **46**(22): p. 9134-9143.
7. Van Tomme, S.R., G. Storm, and W.E. Hennink, *In situ gelling hydrogels for pharmaceutical and biomedical applications.* International Journal of Pharmaceutics, 2008. **355**(1–2): p. 1-18.
8. Hiemstra, C., et al., *Hydrogels: biological properties and applications*. 2009, Milan: Springer.
9. Karacan, P., H. Cakmak, and O. Okay, *Swelling behavior of physical and chemical DNA hydrogels.* Journal of Applied Polymer Science, 2013. **128**(5): p. 3330-3337.
10. Deligkaris, K., et al., *Hydrogel-based devices for biomedical applications.* Sensors and Actuators B: Chemical, 2010. **147**(2): p. 765-774.
11. Ratner, B.D., et al., *Biomaterials Science: An Introduction to Materials in Medicine*. 2004, San Diego, CA: Elsevier Press.
12. Ahmed, E.M., *Hydrogel: Preparation, characterization, and applications.* Journal of Advanced Research, 2013. **6**(2): p. 105-121.
13. Ottenbrite, R., K. Park, and T. Okano, *Biomedical Applications of Hydrogels Handbook.* 2010, New York: Springer.
14. Thompson, M., et al., *Self-Assembling Hydrogels Crosslinked Solely by Receptor-Ligand Interactions.* Chemistry-A European Journal, 2015. **21**(8): p. 3178-3182.
15. Sonmez, C., K.J. Nagy, and J.P. Schneider, *Design of self-assembling peptide hydrogelators amenable to bacterial expression.* Biomaterials, 2015. **37**: p. 62-72.
16. Miyata, T., N. Asami, and T. Uragami, *Structural Design of Stimuli-Responsive Bioconjugated Hydrogels That Respond to a Target Antigen.* Journal of Polymer Science Part B-Polymer Physics, 2009. **47**(21): p. 2144-2157.
17. Kavanagh, A., et al., *Stimuli Responsive Ionogels for Sensing Applications—An Overview.* Membranes, 2012. **2**(1): p. 16-39.
18. Vintiloiu, A. and J.-C. Leroux, *Organogels and their use in drug delivery — A review.* Journal of Controlled Release, 2008. **125**(3): p. 179-192.
19. Goksu, E.I., et al., *Silica xerogel/aerogel-supported lipid bilayers: Consequences of surface corrugation.* Biochimica et Biophysica Acta (BBA) - Biomembranes, 2010. **1798**(4): p. 719-729.

20. Du, A., et al., *A Special Material or a New State of Matter: A Review and Reconsideration of the Aerogel.* Materials, 2013. **6**(3): p. 941-968.
21. Hoffman, A.S., *Hydrogels for biomedical applications.* Advanced Drug Delivery Reviews, 2002. **54**(1): p. 3-12.
22. Eichler, S., et al., *Swelling and contraction driven mass transfer processes during osmotic dehydration of uncharged hydrogels.* International Journal of Food Science & Technology, 2002. **37**(3): p. 245-253.
23. Kumar, C., *Naomaterials for medical diagnosis and therapy*. 2007, Weinheim: Wiley-VCH.
24. Soleimani, F., et al., *Drug Release Study from Superabsorbent Hydrogel Based on Poly-2-acrylamido-2-methylpropanesulfonic Acid Grafted Collagen.* Asian Journal of Chemistry, 2013. **25**(8): p. 4619-4623.
25. Ischakov, R., et al., *Peptide-based hydrogel nanoparticles as effective drug delivery agents.* Bioorganic & Medicinal Chemistry, 2013. **21**(12): p. 3517-3522.
26. Mirzaei, B.E., et al., *Studies on Glutaraldehyde Crosslinked Chitosan Hydrogel Properties for Drug Delivery Systems.* International Journal of Polymeric Materials and Polymeric Biomaterials, 2013. **62**(11): p. 605-611.
27. Lee, S.H., et al., *Hydrogel Nanoparticles for Drug Delivery System.* Tissue Engineering and Regenerative Medicine, 2009. **6**(1-3): p. 57-62.
28. Kim, J.K., et al., *Thermo-reversible injectable gel based on enzymatically-chopped low molecular weight methylcellulose for exenatide and FGF 21 delivery to treat types 1 and 2 diabetes.* Journal of Controlled Release, 2014. **194**: p. 316-322.
29. Lu, H.D., et al., *Injectable shear-thinning hydrogels engineered with a self-assembling Dock-and-Lock mechanism.* Biomaterials, 2012. **33**(7): p. 2145-2153.
30. Orive, G., et al., *Cell encapsulation: Promise and progress.* Nature Medicine, 2003. **9**(1): p. 104-107.
31. Huang, G.Y., et al., *Microfluidic hydrogels for tissue engineering.* Biofabrication, 2011. **3**(1): p. 012001.
32. Tan, H.P. and K.G. Marra, *Injectable, Biodegradable Hydrogels for Tissue Engineering Applications.* Materials, 2010. **3**(3): p. 1746-1767.
33. Zhao, W., et al., *Degradable natural polymer hydrogels for articular cartilage tissue engineering.* Journal of Chemical Technology and Biotechnology, 2013. **88**(3): p. 327-339.
34. Ferruti, P., et al., *Novel poly(amido-amine)-based hydrogels as scaffolds for tissue engineering.* Macromolecular Bioscience, 2005. **5**(7): p. 613-622.
35. Sun, J.C., et al., *Covalently crosslinked hyaluronic acid-chitosan hydrogel containing dexamethasone as an injectable scaffold for soft tissue engineering.* Journal of Applied Polymer Science, 2013. **129**(2): p. 682-688.
36. Zustiak, S.P. and J.B. Leach, *Hydrolytically Degradable Poly(Ethylene Glycol) Hydrogel Scaffolds with Tunable Degradation and Mechanical Properties.* Biomacromolecules, 2010. **11**(5): p. 1348-1357.
37. Kopecek, J., *Hydrogels: From Soft Contact Lenses and Implants to Self-Assembled Nanomaterials.* Journal of Polymer Science Part a-Polymer Chemistry, 2009. **47**(22): p. 5929-5946.
38. Lee, K.Y. and D.J. Mooney, *Alginate: Properties and biomedical applications.* Progress in Polymer Science, 2012. **37**(1): p. 106-126.

39. Kopecek, J. and J.Y. Yang, *Review - Hydrogels as smart biomaterials.* Polymer International, 2007. **56**(9): p. 1078-1098.
40. Park, H. and K. Park, *Hydrogels in bioapplications*. ACS Symposium Series. Vol. 627. 1996, Washington: American Chemical Society.
41. Hejcl, A., et al., *Biocompatible Hydrogels in Spinal Cord Injury Repair*. Physiological Research, 2008. **57**: p. S121-S132.
42. Kabiri, K., et al., *Superabsorbent Hydrogel Composites and Nanocomposites: A Review.* Polymer Composites, 2011. **32**(2): p. 277-289.
43. Raafat, A.I., M. Eid, and M.B. El-Arnaouty, *Radiation synthesis of superabsorbent CMC based hydrogels for agriculture applications.* Nuclear Instruments and Methods in Physics Research Section B: Beam Interactions with Materials and Atoms, 2012. **283**: p. 71-76.
44. Buenger, D., F. Topuz, and J. Groll, *Hydrogels in sensing applications.* Progress in Polymer Science, 2012. **37**(12): p. 1678-1719.
45. Gawel, K., et al., *Responsive Hydrogels for Label-Free Signal Transduction within Biosensors.* Sensors, 2010. **10**(5): p. 4381-4409.
46. Hezaveh, H. and I.I. Muhamad, *Controlled drug release via minimization of burst release in pH-response kappa-carrageenan/polyvinyl alcohol hydrogels.* Chemical Engineering Research & Design, 2013. **91**(3): p. 508-519.
47. Klouda, L. and A.G. Mikos, *Thermoresponsive hydrogels in biomedical applications.* European Journal of Pharmaceutics and Biopharmaceutics, 2008. **68**(1): p. 34-45.
48. Andreopoulos, F.M., E.J. Beckman, and A.J. Russell, *Light-induced tailoring of PEG-hydrogel properties.* Biomaterials, 1998. **19**(15): p. 1343-1352.
49. Li, W., et al., *Synthesis and characterisation of a polyacrylamide-polyacrylic acid copolymer hydrogel for environmental analysis of Cu and Cd.* Reactive & Functional Polymers, 2002. **52**(1): p. 31-41.
50. Doring, A., W. Birnbaum, and D. Kuckling, *Responsive hydrogels - structurally and dimensionally optimized smart frameworks for applications in catalysis, micro-system technology and material science.* Chemical Society Reviews, 2013. **42**(17): p. 7391-7420.
51. Sarmad, S., et al., *Electric field responsive chitosan-poly(N,N-dimethyl acrylamide) semi-IPN gel films and their dielectric, thermal and swelling characterization.* Smart Materials and Structures, 2013. **22**(5): p. 055010.
52. Wang, Y., et al., *Fabrication and characterization of temperature-, pH- and magnetic-field-sensitive organic/inorganic hybrid poly (ethylene glycol)-based hydrogels.* Colloids and Surfaces a-Physicochemical and Engineering Aspects, 2012. **415**: p. 68-76.
53. Miyata, T., T. Uragami, and K. Nakamae, *Biomolecule-sensitive hydrogels.* Advanced Drug Delivery Reviews, 2002. **54**(1): p. 79-98.
54. Li, L.L., X.D. Xing, and Z.L. Liu, *Triply-responsive (thermo/light/pH) copolymeric hydrogel of N-isopropylacrylamide with an azobenzene-containing monomer.* Journal of Applied Polymer Science, 2012. **124**(2): p. 1128-1136.
55. Wei, Q.B., et al., *Synthesis, characterization, and swelling kinetics of pH-responsive and temperature-responsive carboxymethyl chitosan/polyacrylamide hydrogels.* Journal of Applied Polymer Science, 2013. **129**(2): p. 806-814.
56. Zhao, C.W., et al., *Synthesis of biodegradable thermo- and pH-responsive hydrogels for controlled drug release.* Polymer, 2009. **50**(18): p. 4308-4316.

57. Hendrickson, G.R. and L.A. Lyon, *Bioresponsive hydrogels for sensing applications.* Soft Matter, 2009. **5**(1): p. 29-35.
58. Richter, A., et al., *Characterization of a microgravimetric sensor based on pH sensitive hydrogels.* Sensors and Actuators B: Chemical, 2004. **99**(2–3): p. 579-585.
59. Richter, A., et al., *Review on hydrogel-based pH sensors and microsensors.* Sensors, 2008. **8**(1): p. 561-581.
60. Sun, L., et al., *A pH Gated, Glucose-Sensitive Nanoparticle Based on Worm-Like Mesoporous Silica for Controlled Insulin Release.* Journal of Physical Chemistry B, 2013. **117**(14): p. 3852-3860.
61. Herber, S., et al., *A Miniaturized Carbon Dioxide Gas Sensor Based on Sensing of pH-Sensitive Hydrogel Swelling with a Pressure Sensor.* Biomedical Microdevices, 2005. **7**(3): p. 197-204.
62. Beebe, D.J., et al., *Functional hydrogel structures for autonomous flow control inside microfluidic channels.* Nature, 2000. **404**(6778): p. 588-+.
63. Ward, M.A. and T.K. Georgiou, *Thermoresponsive Polymers for Biomedical Applications.* Polymers, 2011. **3**(3): p. 1215-1242.
64. Peppas, N.A., J.Z. Hilt, and J.B. Thomas, *Nanotechnology in Therapeutics-Current Technology and Applications*. 2007, Norfolk, UK: Horizon Bioscience.
65. Tokarev, I. and S. Minko, *Stimuli-responsive hydrogel thin films.* Soft Matter, 2009. **5**(3): p. 511-524.
66. Hacker, M.C., et al., *Synthesis and characterization of injectable, thermally and chemically gelable, amphiphilic poly(N-isopropylacrylamide)-based macromers.* Biomacromolecules, 2008. **9**(6): p. 1558-1570.
67. Yang, X.D., et al., *Thermo-responsive photoluminescent polymer brushes device as a platform for selective detection of Cr(VI).* Polymer Chemistry, 2013. **4**(22): p. 5591-5596.
68. Yin, J., et al., *Metal-Chelating and Dansyl-Labeled Poly(N-isopropylacrylamide) Microgels as Fluorescent Cu2+ Sensors with Thermo-Enhanced Detection Sensitivity.* Langmuir, 2009. **25**(19): p. 11367-11374.
69. Singh, N.K. and D.S. Lee, *In situ gelling pH- and temperature-sensitive biodegradable block copolymer hydrogels for drug delivery.* Journal of Controlled Release, 2014. **193**: p. 214-227.
70. He, C.L., S.W. Kim, and D.S. Lee, *In situ gelling stimuli-sensitive block copolymer hydrogels for drug delivery.* Journal of Controlled Release, 2008. **127**(3): p. 189-207.
71. Lyon, L.A., et al., *Thermoresponsive microgel-based materials.* Chemical Society Reviews, 2009. **38**(4): p. 865-874.
72. Kawaguchi, H., *Thermoresponsive microhydrogels: preparation, properties and applications.* Polymer International, 2014. **63**(6): p. 925-932.
73. Matricardi, P., et al., *Interpenetrating Polymer Networks polysaccharide hydrogels for drug delivery and tissue engineering.* Advanced Drug Delivery Reviews, 2013. **65**(9): p. 1172-1187.
74. Bawa, P., et al., *Stimuli-responsive polymers and their applications in drug delivery.* Biomedical Materials, 2009. **4**(2): p. 022001
75. Roy, S.G. and P. De, *Swelling properties of amino acid containing cross-linked polymeric organogels and their respective polyelectrolytic hydrogels with pH and salt responsive property.* Polymer, 2014. **55**(21): p. 5425-5434.

76. Molla-Abbasi, P. and S.R. Ghaffarian, *Decoration of carbon nanotubes by chitosan in a nanohybrid conductive polymer composite for detection of polar vapours.* RSC Advances, 2014. **4**(58): p. 30906-30913.
77. McDonald, T.O., et al., *Branched peptide actuators for enzyme responsive hydrogel particles.* Soft Matter, 2009. **5**(8): p. 1728-1734.
78. Ravaine, V., C. Ancla, and B. Catargi, *Chemically controlled closed-loop insulin delivery.* Journal of Controlled Release, 2008. **132**(1): p. 2-11.
79. Uva, M., et al., *Influence of Alternating and Static Magnetic Fields on Drug Release from Hybrid Hydrogels Containing Magnetic Nanoparticles.* Journal of Biomaterials and Nanobiotechnology, 2014. **5**: p. 116-127.
80. Zahn, R., J. Vörös, and T. Zambelli, *Tuning the Electrochemical Swelling of Polyelectrolyte Multilayers toward Nanoactuation.* Langmuir, 2014. **30**(40): p. 12057-12066.
81. Venegas-Sanchez, J.A., et al., *Sono-respond on thermosensitive polymer microgels based on cross-linked poly(N-isopropylacrylamide-co-acrylic acid).* Ultrasonics Sonochemistry, 2013. **20**(5): p. 1271-1275.
82. Miyata, T., et al., *Controlled permeation of model drugs through a bioconjugated membrane with antigen-antibody complexes as reversible crosslinks.* Polymer Journal, 2010. **42**(10): p. 834-837.
83. Wang, X.Q., G. Ye, and X.G. Wang, *Hydrogel diffraction gratings functionalized with crown ether for heavy metal ion detection.* Sensors and Actuators B-Chemical, 2014. **193**: p. 413-419.
84. Wang, X.Q., X.Y. Liu, and X.G. Wang, *Hydrogel diffraction grating as sensor: A tool for studying volume phase transition of thermo-responsive hydrogel.* Sensors and Actuators B-Chemical, 2014. **204**: p. 611-616.
85. Ye, G., C.Q. Yang, and X.G. Wang, *Sensing Diffraction Gratings of Antigen-Responsive Hydrogel for Human Immunoglobulin-G Detection.* Macromolecular Rapid Communications, 2010. **31**(15): p. 1332-1336.
86. Wang, X. and X. Wang, *Aptamer-functionalized hydrogel diffraction gratings for the human thrombin detection.* Chemical Communications, 2013. **49**(53): p. 5957-5959.
87. Kang, J.H., et al., *Thermoresponsive hydrogel photonic crystals by three-dimensional holographic lithography.* Advanced Materials, 2008. **20**(16): p. 3061-3065.
88. Yao, C., et al., *Hydrogel Improved the Response in the Titania/Graphene Oxide One-Dimensional Photonic Crystals.* Acs Applied Materials & Interfaces, 2014. **6**(19): p. 16727-16733.
89. Xue, F., et al., *A 2-D photonic crystal hydrogel for selective sensing of glucose.* Journal of Materials Chemistry A, 2014. **2**(25): p. 9559-9565.
90. Zhang, J.T., et al., *Two-Dimensional Photonic Crystal Sensors for Visual Detection of Lectin Concanavalin A.* Analytical Chemistry, 2014. **86**(18): p. 9036-9041.
91. Yetisen, A.K., et al., *Light-Directed Writing of Chemically Tunable Narrow-Band Holographic Sensors.* Advanced Optical Materials, 2014. **2**(3): p. 250-254.
92. Yang, X., et al., *Towards the real-time monitoring of glucose in tear fluid: Holographic glucose sensors with reduced interference from lactate and pH.* Biosensors and Bioelectronics, 2008. **23**(6): p. 899-905.

93. Naydenova, I., et al., *Characterisation of the humidity and temperature responses of a reflection hologram recorded in acrylamide-based photopolymer.* Sensors and Actuators B: Chemical, 2009. **139**(1): p. 35-38.
94. Bhatta, D., et al., *Development of a holographic sensor for the detection of calcium dipicolinate—A sensitive biomarker for bacterial spores.* Sensors and Actuators B: Chemical, 2008. **134**(2): p. 356-359.
95. Zhang, X., Y. Guan, and Y. Zhang, *Ultrathin Hydrogel Films for Rapid Optical Biosensing.* Biomacromolecules, 2011. **13**(1): p. 92-97.
96. Peng, R.P., et al., *Highly Sensitive and Selective Fluoride Ion Sensors Based on Microcantilevers Modified with Hydrogels.* Journal of Nanoscience and Nanotechnology, 2014. **14**(9): p. 6632-6637.
97. Orthner, M.P., et al., *Hydrogel based sensor arrays (2 x 2) with perforated piezoresistive diaphragms for metabolic monitoring (in vitro).* Sensors and Actuators B: Chemical, 2010. **145**(2): p. 807-816.
98. Orthner, M.P., et al., *Development, fabrication, and characterization of hydrogel based piezoresistive pressure sensors with perforated diaphragms.* Sensors and Actuators a-Physical, 2010. **161**(1-2): p. 29-38.
99. Cho, S.H., et al., *Effect of Chemical Composition on the Response of Zwitterionic Glucose Sensitive Hydrogels Studied by Design of Experiments.* Journal of Applied Polymer Science, 2014. **131**(17).
100. Sorber, J., et al., *Hydrogel-Based Piezoresistive pH Sensors: Investigations Using FT-IR Attenuated Total Reflection Spectroscopic Imaging.* Analytical Chemistry, 2008. **80**(8): p. 2957-2962.
101. Bates, J., *pH-responsive hydrogel-based chemomechanical sensors designed for disposable bioreactor applications*, in *Department of Materials Science and Engineering*2013, University of Utah.
102. Wang, R. and Y. Li, *Hydrogel based QCM aptasensor for detection of avian influenzavirus.* Biosensors and Bioelectronics, 2013. **42**: p. 148-155.
103. Sheppard, N.F., M.J. Lesho, and P. McNally, *Microfabricated conductimetric pH sensor* Sensors and Actuators B-Chemical, 1995. **28**(2): p. 95-102.
104. Guan, T., F. Ceyssens, and R. Puers, *Conductometric and optical sensing of stimuli sensitive hydrogels inside microfluidic channels.* Solid-State Sensors, Actuators and Microsystems Conference 2011: p. 1264-1267.
105. Cui, H.F., et al., *Modification of carbon nanotubes with redox hydrogel: Improvement of amperometric sensing sensitivity for redox enzymes.* Biosensors & Bioelectronics, 2009. **24**(6): p. 1723-1729.
106. Niculescu, M., S. Sigina, and E. Csoregi, *Glycerol dehydrogenase based amperometric biosensor for monitoring of glycerol in alcoholic beverages.* Analytical Letters, 2003. **36**(9): p. 1721-1737.
107. Liu, H.M., et al., *Osmium redox hydrogel mediated biosensor for measurement of low concentration glucose extracted by reverse iontophoresis.* Electroanalysis, 2008. **20**(2): p. 170-177.
108. Justin, G., et al., *Biomimetic hydrogels for biosensor implant biocompatibility: electrochemical characterization using micro-disc electrode arrays (MDEAs).* Biomedical Microdevices, 2009. **11**(1): p. 103-115.
109. Lin, C.-C. and K. Anseth, *PEG Hydrogels for the Controlled Release of Biomolecules in Regenerative Medicine.* Pharmaceutical Research, 2009. **26**(3): p. 631-643.

110. Montero, L., et al., *Increasing biosensor response through hydrogel thin film deposition: Influence of hydrogel thickness.* Vacuum, 2012. **86**(12): p. 2102-2104.
111. Brahim, S., D. Narinesingh, and A. Giuseppi-Elie, *Interferent suppression using a novel polypyrrole-containing hydrogel in amperometric enzyme biosensors.* Electroanalysis, 2002. **14**(9): p. 627-633.
112. Vashist, A., et al., *Recent advances in hydrogel based drug delivery systems for the human body.* Journal of Materials Chemistry B, 2014. **2**(2): p. 147-166.
113. Singh, B., L. Varshney, and V. Sharma, *Design of sterile mucoadhesive hydrogels for use in drug delivery: Effect of radiation on network structure.* Colloids and Surfaces B-Biointerfaces, 2014. **121**: p. 230-237.
114. Deat-Laine, E., et al., *Efficacy of Mucoadhesive Hydrogel Microparticles of Whey Protein and Alginate for Oral Insulin Delivery.* Pharmaceutical Research, 2013. **30**(3): p. 721-734.
115. Gupta, A.K. and A.W. Siddiqui, *Environmental Responsive Hydrogels: A Novel Approach in Drug Delivery System.* Journal of Drug Delivery & Therapeutics, 2012. **2**(1): p. 1-8.
116. Karmali, P.P., et al., *Different Effect of Hydrogelation on Antifouling and Circulation Properties of Dextran-Iron Oxide Nanoparticles.* Molecular Pharmaceutics, 2012. **9**(3): p. 539-545.
117. Lin, C.-C. and A.T. Metters, *Hydrogels in controlled release formulations: Network design and mathematical modeling.* Advanced Drug Delivery Reviews, 2006. **58**(12–13): p. 1379-1408.
118. Peppas, N.A., et al., *Hydrogels in pharmaceutical formulations.* European Journal of Pharmaceutics and Biopharmaceutics, 2000. **50**(1): p. 27-46.
119. Amsden, B., *Solute diffusion within hydrogels. Mechanisms and models.* Macromolecules, 1998. **31**(23): p. 8382-8395.
120. Kanjickal, D.G. and S.T. Lopina, *Modeling of drug release from polymeric delivery systems - A review.* Critical Reviews in Therapeutic Drug Carrier Systems, 2004. **21**(5): p. 345-386.
121. Lamberti, G., I. Galdi, and A.A. Barba, *Controlled release from hydrogel-based solid matrices. A model accounting for water up-take, swelling and erosion.* International Journal of Pharmaceutics, 2011. **407**(1–2): p. 78-86.
122. Brandl, F., et al., *Hydrogel-based drug delivery systems: Comparison of drug diffusivity and release kinetics.* Journal of Controlled Release, 2010. **142**(2): p. 221-228.
123. Agrawal, A.K., M. Das, and S. Jain, *In situ gel systems as 'smart' carriers for sustained ocular drug delivery.* Expert Opinion on Drug Delivery, 2012. **9**(4): p. 383-402.
124. Kushwaha, S.K., P. Saxena, and A. Rai, *Stimuli sensitive hydrogels for ophthalmic drug delivery: A review.* International Journal of Pharmaceutical Investigation, 2012. **2**(2): p. 54-60.
125. Liu, L., et al., *Camptothecine encapsulated composite drug delivery system for colorectal peritoneal carcinomatosis therapy: Biodegradable microsphere in thermosensitive hydrogel.* Colloids and Surfaces B-Biointerfaces, 2013. **106**: p. 93-101.
126. Popescu, I., et al., *Phosphorylated curdlan microgels. Preparation, characterization, and in vitro drug release studies.* Carbohydrate Polymers, 2013. **94**(2): p. 889-898.

127. Ali, L., et al., *Controlled release of highly water-soluble antidepressant from hybrid copolymer poly vinyl alcohol hydrogels.* Polymer Bulletin, 2014. **71**(1): p. 31-46.
128. Dong, L.C. and A.S. Hoffman, *A Novel-Approach for Preparation of pH-Sensitive Hydrogels for Enteric Drug Delivery.* Journal of Controlled Release, 1991. **15**(2): p. 141-152.
129. Patton, J.N. and A.F. Palmer, *Engineering temperature-sensitive hydrogel nanoparticles entrapping hemoglobin as a novel type of oxygen carrier.* Biomacromolecules, 2005. **6**(4): p. 2204-2212.
130. Feng, Q., et al., *Frontal polymerization synthesis and drug delivery behavior of thermo-responsive poly(N-isopropylacrylamide) hydrogel.* Colloid and Polymer Science, 2010. **288**(8): p. 915-921.
131. Constantin, M., et al., *Poly(NIPAAm-co-β-cyclodextrin) microgels with drug hosting and temperature-dependent delivery properties.* Reactive and Functional Polymers, 2014. **84**: p. 1-9.
132. Ruel-Gariépy, E., et al., *A thermosensitive chitosan-based hydrogel for the local delivery of paclitaxel.* European Journal of Pharmaceutics and Biopharmaceutics, 2004. **57**(1): p. 53-63.
133. Johnson, T.D. and K.L. Christman, *Injectable hydrogel therapies and their delivery strategies for treating myocardial infarction.* Expert Opinion on Drug Delivery, 2013. **10**(1): p. 59-72.
134. Gong, C., et al., *Thermosensitive Polymeric Hydrogels As Drug Delivery Systems.* Current Medicinal Chemistry, 2013. **20**(1): p. 79-94.
135. Ko, D.Y., et al., *Recent progress of in situ formed gels for biomedical applications.* Progress in Polymer Science, 2013. **38**(3-4): p. 672-701.
136. Khutoryanskiy, V.V., *Hydrogen-bonded interpolymer complexes as materials for pharmaceutical applications.* International Journal of Pharmaceutics, 2007. **334**(1–2): p. 15-26.
137. Huynh, C.T., et al., *Controlled release of human growth hormone from a biodegradable pH/temperature-sensitive hydrogel system.* Soft Matter, 2011. **7**(19): p. 8984-8990.
138. Loh, X.J. and J. Li, *Biodegradable thermosensitive copolymer hydrogels for drug delivery.* Expert Opinion on Therapeutic Patents, 2007. **17**(8): p. 965-977.
139. Jeong, B., S.W. Kim, and Y.H. Bae, *Thermosensitive sol–gel reversible hydrogels.* Advanced Drug Delivery Reviews, 2002. **54**(1): p. 37-51.
140. Traitel, T., Y. Cohen, and J. Kost, *Characterization of glucose-sensitive insulin release systems in simulated in vivo conditions.* Biomaterials, 2000. **21**(16): p. 1679-1687.
141. Guan, Y. and Y. Zhang, *Boronic acid-containing hydrogels: synthesis and their applications.* Chemical Society Reviews, 2013. **42**(20): p. 8106-8121.
142. Kikuchi, A., et al., *Glucose-Sensing Electrode Coated with Polymer Complex Gel Containing Phenylboronic Acid.* Analytical Chemistry, 1996. **68**(5): p. 823-828.
143. Matsumoto, A., R. Yoshida, and K. Kataoka, *Glucose-responsive polymer gel bearing phenylborate derivative as a glucose-sensing moiety operating at the physiological pH.* Biomacromolecules, 2004. **5**(3): p. 1038-1045.
144. Mura, S., J. Nicolas, and P. Couvreur, *Stimuli-responsive nanocarriers for drug delivery.* Nature Materials, 2013. **12**(11): p. 991-1003.
145. LaVan, D.A., T. McGuire, and R. Langer, *Small-scale systems for in vivo drug delivery.* Nature Biotechnology, 2003. **21**(10): p. 1184-1191.

146. Murdan, S., *Electro-responsive drug delivery from hydrogels.* Journal of Controlled Release, 2003. **92**(1–2): p. 1-17.
147. Denet, A.R., R. Vanbever, and V. Preat, *Skin electroporation for transdermal and topical delivery.* Advanced Drug Delivery Reviews, 2004. **56**(5): p. 659-674.
148. Brown, M.B., et al., *Dermal and transdermal drug delivery systems: Current and future prospects.* Drug Delivery, 2006. **13**(3): p. 175-187.
149. Pan, L.J., et al., *Hierarchical nanostructured conducting polymer hydrogel with high electrochemical activity.* Proceedings of the National Academy of Sciences of the United States of America, 2012. **109**(24): p. 9287-9292.
150. Shi, Y., et al., *Nanostructured conductive polypyrrole hydrogels as high-performance, flexible supercapacitor electrodes.* Journal of Materials Chemistry A, 2014. **2**(17): p. 6086-6091.
151. Naficy, S., et al., *Electrically Conductive, Tough Hydrogels with pH Sensitivity.* Chemistry of Materials, 2012. **24**(17): p. 3425-3433.
152. Brahim, S. and A. Guiseppi-Elie, *Electroconductive hydrogels: Electrical properties of polypyrrole-poly(HEMA) and electrochemical composites.* Electroanalysis, 2005. **17**(7): p. 556-570.
153. Ahadian, S., et al., *Hybrid hydrogels containing vertically aligned carbon nanotubes with anisotropic electrical conductivity for muscle myofiber fabrication.* Scientific Reports, 2014. **4**: p. 4271.
154. Dvir, T., et al., *Nanowired three-dimensional cardiac patches.* Nature Nanotechnology, 2011. **6**(11): p. 720-725.
155. Whiteside, N.J., G.G. Wallace, and M. in het Panhuis, *Preparation and characterisation of graphene composite hydrogels.* Synthetic Metals, 2013. **168**: p. 36-42.
156. Guiseppi-Elie, A., *Electroconductive hydrogels: Synthesis, characterization and biomedical applications.* Biomaterials, 2010. **31**(10): p. 2701-2716.
157. Lira, L.M. and S.I. Córdoba de Torresi, *Conducting polymer–hydrogel composites for electrochemical release devices: Synthesis and characterization of semi-interpenetrating polyaniline–polyacrylamide networks.* Electrochemistry Communications, 2005. **7**(7): p. 717-723.
158. Niamlang, S., et al., *Controlled Aloin Release from Crosslinked Polyacrylamide Hydrogels: Effects of Mesh Size, Electric Field Strength and a Conductive Polymer.* Materials (1996-1944), 2013. **6**(10): p. 4787-4800.
159. Wadhwa, R., C.F. Lagenaur, and X.T. Cui, *Electrochemically controlled release of dexamethasone from conducting polymer polypyrrole coated electrode.* Journal of Controlled Release, 2006. **110**(3): p. 531-541.
160. Ali, A.E.H., et al., *Characterization and potential application of electro-active acrylamido-2-methyl propane sulfonic acid/acrylic acid copolymer prepared by ionizing radiation.* Journal of Macromolecular Science Part a-Pure and Applied Chemistry, 2007. **44**(1): p. 91-98.
161. Liu, K.-H., et al., *Drug release behavior of chitosan–montmorillonite nanocomposite hydrogels following electrostimulation.* Acta Biomaterialia, 2008. **4**(4): p. 1038-1045.
162. Sawahata, K., et al., *Electrically Controlled Drug Delivery System Using Polyelectrolyte Gels.* Journal of Controlled Release, 1990. **14**(3): p. 253-262.
163. Kwon, I.C., Y.H. Bae, and S.W. Kim, *Electrically Erodible Polymer Gel for Controlled Release of Drugs.* Nature, 1991. **354**(6351): p. 291-293.

164. Tanaka, T. and D.J. Fillmore, *Kinetics of Swelling of Gels.* Journal of Chemical Physics, 1979. **70**(3): p. 1214-1218.
165. Gemeinhart, R.A. and C. Guo, *Fast swelling hydrogel systems*. Reflexive Polymers and Hydrogels-Understanding and Designing Fast Responsive Polymeric Systems. 2004, Florida: CRC Press LLC.
166. Baldi, A., et al., *A hydrogel-actuated environmentally sensitive microvalve for active flow control.* Journal of Microelectromechanical Systems, 2003. **12**(5): p. 613-621.
167. Bates, J., et al., *An Improved Design for Chemomechanical Sensors: A Piezoresistive Pressure Sensor with a Mechanical Boss.* Chemosensors, 2013. **1**(3): p. 33-42.
168. Yue, L.-L., et al., *Nano-gel containing thermo-responsive microspheres with fast response rate owing to hierarchical phase-transition mechanism.* Journal of Colloid and Interface Science, 2012. **377**(1): p. 137-144.
169. Xiao, X.C., et al., *Preparation of submicrometer-sized monodispersed thermoresponsive core-shell hydrogel microspheres.* Langmuir, 2004. **20**(13): p. 5247-5253.
170. Hasanzadeh, M., N. Shadjou, and M. de la Guardia, *Electrochemical biosensing using hydrogel nanoparticles.* TrAC Trends in Analytical Chemistry, 2014. **62**: p. 11-19.
171. Xia, L.-W., et al., *Nano-structured smart hydrogels with rapid response and high elasticity.* Nature communications, 2013. **4**: p. 2226.
172. Zhang, J., et al., *Rapid pH/temperature-responsive cationic hydrogels with dual stimuli-sensitive grafted side chains.* Polymer, 2009. **50**(11): p. 2516-2525.
173. Demirel, G.B., et al., *Effect of Pore-Forming Agent Type on Swelling Properties of Macroporous Poly(N-3-(dimethylaminopropyl)-methacrylamide-co-acrylamide) Hydrogels.* Journal of Macromolecular Science Part a-Pure and Applied Chemistry, 2009. **46**(1): p. 58-64.
174. Kato, N. and S.H. Gehrke, *Microporous, fast response cellulose ether hydrogel prepared by freeze-drying.* Colloids and Surfaces B-Biointerfaces, 2004. **38**(3-4): p. 191-196.
175. Halim, S.A.A., S.A. Yehia, and M.A. El-Nabarawi, *Chromium picolinate loaded superporous hydrogel and superporous hydrogel composite as a controlled release device: in vitro and in vivo evaluation.* Journal of Drug Delivery Science and Technology, 2014. **24**(4): p. 326-337.
176. Kumar, A., et al., *Synthesis of Fast Swelling Superporous Hydrogel: Effect of Concentration of Crosslinker and Acdisol on Swelling Ratio and Mechanical Strength.* International Journal of Drug Delivery, 2010. **2**(2): p. 135-140.
177. Yang, S., et al., *Application of poly(acrylic acid) superporous hydrogel microparticles as a super-disintegrant in fast-disintegrating tablets.* Journal of Pharmacy and Pharmacology, 2004. **56**(4): p. 429-436.
178. Omidian, H., K. Park, and J.G. Rocca, *Recent developments in superporous hydrogels.* Journal of Pharmacy and Pharmacology, 2007. **59**(3): p. 317-327.
179. Yin, L.C., et al., *Polymer integrity related absorption mechanism of superporous hydrogel containing interpenetrating polymer networks for oral delivery of insulin.* Biomaterials, 2010. **31**(12): p. 3347-3356.
180. Chavda, H., et al., *Topical Vaginal Drug Delivery System Based on Superporous Hydrogel Hybrids.* Protein and Peptide Letters, 2014. **21**(11): p. 1176-1184.

181. Cetin, D., A.S. Kahraman, and M. Gumusderelioglu, *Novel Scaffolds Based on Poly(2-hydroxyethyl methacrylate) Superporous Hydrogels for Bone Tissue Engineering.* Journal of Biomaterials Science-Polymer Edition, 2011. **22**(9): p. 1157-1178.
182. Battig, M.R., et al., *Aptamer-functionalized superporous hydrogels for sequestration and release of growth factors regulated via molecular recognition.* Biomaterials, 2014. **35**(27): p. 8040-8048.
183. Brett, C.M. and A.M.O. Brett, *Electrochemistry: principles, methods, and applications*. Vol. 4. 1993, Oxford: Oxford University Press.
184. Wang, J., *Analytical Electrochemistry*. 2 ed. 2000, New York: Wiley-VCH.
185. Ebrahimi, A., et al., *Nanotextured superhydrophobic electrodes enable detection of attomolar-scale DNA concentration within a droplet by non-faradaic impedance spectroscopy.* Lab on a Chip, 2013. **13**(21): p. 4248-4256.
186. Daniels, J.S. and N. Pourmand, *Label-Free Impedance Biosensors: Opportunities and Challenges.* Electroanalysis, 2007. **19**(12): p. 1239-1257.
187. Wang, J., *Electrochemical glucose biosensors.* Chemical Reviews, 2008. **108**(2): p. 814-825.
188. Moyer, J., et al., *Correlation between sweat glucose and blood glucose in subjects with diabetes.* Diabetes Technology & Therapeutics, 2012. **14**(5): p. 398-402.
189. Falk, M., et al., *Miniature Direct Electron Transfer Based Enzymatic Fuel Cell Operating in Human Sweat and Saliva.* Fuel Cells, 2014. **14**(6): p. 1050-1056.
190. Strambini, L.M., et al., *Self-powered microneedle-based biosensors for pain-free high-accuracy measurement of glycaemia in interstitial fluid.* Biosensors & Bioelectronics, 2015. **66**: p. 162-168.
191. Vezouviou, E. and C.R. Lowe, *A near infrared holographic glucose sensor.* Biosensors & Bioelectronics, 2015. **68**: p. 371-381.
192. Liu, C., et al., *A glucose oxidase-coupled DNAzyme sensor for glucose detection in tears and saliva.* Biosensors & Bioelectronics, 2015. **70**: p. 455-61.
193. Soni, A. and S.K. Jha, *A paper strip based non-invasive glucose biosensor for salivary analysis.* Biosensors & Bioelectronics, 2015. **67**: p. 763-768.
194. Matzeu, G., L. Florea, and D. Diamond, *Advances in wearable chemical sensor design for monitoring biological fluids.* Sensors and Actuators B: Chemical, 2015. **211**: p. 403-418.
195. Corrie, S.R., et al., *Blood, sweat, and tears: developing clinically relevant protein biosensors for integrated body fluid analysis.* The Analyst, 2015. **140**(13): p. 4350-64.
196. Zhang, C., M.D. Losego, and P.V. Braun, *Hydrogel-Based Glucose Sensors: Effects of Phenylboronic Acid Chemical Structure on Response.* Chemistry of Materials, 2013. **25**(15): p. 3239-3250.
197. Matsumoto, A., et al., *Swelling and Shrinking Kinetics of Totally Synthetic, Glucose-Responsive Polymer Gel Bearing Phenylborate Derivative as a Glucose-Sensing Moiety.* Macromolecules, 2004. **37**(4): p. 1502-1510.
198. Lee, Y.J., S.A. Pruzinsky, and P.V. Braun, *Glucose-sensitive inverse opal hydrogels: Analysis of optical diffraction response.* Langmuir, 2004. **20**(8): p. 3096-3106.
199. Miyata, T., et al., *Preparation of reversibly glucose-responsive hydrogels by covalent immobilization of lectin in polymer networks having pendant glucose.* Journal of Biomaterials Science - Polymer Edition, 2004. **15**(9): p. 1085-1098.

200. Zhang, R., et al., *Synthesis and characterization of a D-glucose sensitive hydrogel based on CM-dextran and concanavalin A.* Reactive & Functional Polymers, 2006. **66**(7): p. 757-767.
201. Yin, R., et al., *Photo-crosslinked glucose-sensitive hydrogels based on methacrylate modified dextran–concanavalin A and PEG dimethacrylate.* Carbohydrate Polymers, 2010. **82**(2): p. 412-418.
202. Jeong, S.H., K.T. Oh, and K. Park, *Polymeric Biomaterials: Medicinal and Pharmaceutical Applications, Volume 2*. Vol. 2. 2013, Florida: CRC Press.
203. Yoshioka, Y. and P. Calvert, *Epoxy-based electroactive polymer gels.* Experimental Mechanics, 2002. **42**(4): p. 404-408.
204. Teodorescu, M., B. Cursaru, and P.O. Stanescu, *Swelling and Diffusion Characteristics of Hydrogels Synthesized from Diepoxy-terminated Poly(ethylene glycol)s and Aliphatic Polyamines.* Soft Materials, 2010. **8**(3): p. 288-306.
205. Teodorescu, M., et al., *Novel hydrogels from diepoxy-terminated poly(ethylene glycol)s and aliphatic primary diamines: synthesis and equilibrium swelling studies.* Polymers for Advanced Technologies, 2009. **20**(12): p. 907-915.
206. Hild, G., *Model networks based on `endlinking' processes: synthesis, structure and properties.* Progress in Polymer Science, 1998. **23**(6): p. 1019-1149.
207. Peppas, N.A., *Hydrogels in Medicine and Pharmacy: Fundamentals*. 1986: CRC Press.
208. Palanisamy, S., A.T.E. Vilian, and S.-M. Chen, *Direct Electrochemistry of Glucose Oxidase at Reduced Graphene Oxide/Zinc Oxide Composite Modified Electrode for Glucose Sensor.* International Journal of Electrochemical Science, 2012. **7**(3): p. 2153-2163.
209. Barsan, M.M., et al., *Carbon nanotube modified carbon cloth electrodes: Characterisation and application as biosensors.* Electrochimica Acta, 2012. **85**: p. 203-209.
210. Pell, W.G., A. Zolfaghari, and B.E. Conway, *Capacitance of the double-layer at polycrystalline Pt electrodes bearing a surface-oxide film.* Journal of Electroanalytical Chemistry, 2002. **532**(1–2): p. 13-23.
211. Li, J., Q. Yang, and I. Zhitomirsky, *Composite Electrodes for Electrochemical Supercapacitors.* Nanoscale Research Letters, 2010. **5**(3): p. 512-517.
212. Doran, P.M., *Bioprocess Engineering Principles*. 1995, UK: Academic Press.
213. Bandodkar, A.J., et al., *Tattoo-Based Noninvasive Glucose Monitoring: A Proof-of-Concept Study.* Analytical Chemistry, 2014. **87**(1): p. 394-398.
214. Sun, T.P., et al., *Carbon nanotube composites for glucose biosensor incorporated with reverse iontophoresis function for noninvasive glucose monitoring.* International Journal of Nanomedicine, 2010. **5**: p. 343-349.
215. Ching, C.T.S., et al., *A Mediated Glucose Biosensor Incorporated with Reverse Iontophoresis Function for Noninvasive Glucose Monitoring.* Annals of Biomedical Engineering, 2010. **38**(4): p. 1548-1555.
216. Kostov, Y., et al., *Portable system for the detection of micromolar concentrations of glucose.* Measurement Science & Technology, 2014. **25**(2): p. 025701.
217. Chung, J., et al., *Fast and continuous microorganism detection using aptamer-conjugated fluorescent nanoparticles on an optofluidic platform.* Biosensors and Bioelectronics, 2015. **67**: p. 303-308.

218. Zhang, W., et al., *Amperometric method for rapid detection of Escherichia coli by flow injection analysis using a bismuth nano-film modified glassy carbon electrode.* Electrochemistry Communications, 2007. **9**(4): p. 833-838.
219. Krishnan, S., et al., *Dual labeled Ag@SiO2 core–shell nanoparticle based optical immunosensor for sensitive detection of E. coli.* Materials Science and Engineering: C, 2014. **45**: p. 337-342.
220. Huang, Y., et al., *Graphene-based biosensors for detection of bacteria and their metabolic activities.* Journal of Materials Chemistry, 2011. **21**(33): p. 12358-12362.
221. Mondani, L., et al., *Simultaneous enrichment and optical detection of low levels of stressed Escherichia coli O157:H7 in food matrices.* Journal of Applied Microbiology, 2014. **117**(2): p. 537-546.
222. Maalouf, R., et al., *Label-Free Detection of Bacteria by Electrochemical Impedance Spectroscopy: Comparison to Surface Plasmon Resonance.* Analytical Chemistry, 2007. **79**(13): p. 4879-4886.
223. Manafi, M., *Fluorogenic and chromogenic enzyme substrates in culture media and identification tests.* International Journal of Food Microbiology, 1996. **31**(1-3): p. 45-58.
224. Geary, J.R., et al., *Hydrolysis of the soluble fluorescent molecule carboxyumbelliferyl-beta-d-glucuronide by E. coli beta-glucuronidase as applied in a rugged, in situ optical sensor.* Enzyme and Microbial Technology, 2011. **49**(1): p. 6-10.
225. Huang, S.-H., *Detection of Escherichia coli using CMOS array photo sensor-based enzyme biochip detection system.* Sensors and Actuators B: Chemical, 2008. **133**(2): p. 561-564.
226. Pérez, F., et al., *Rapid detection of Escherichia coli in water by a culture-based amperometric method.* Analytica Chimica Acta, 2001. **427**(2): p. 149-154.
227. Majid, E., K.B. Male, and J.H.T. Luong, *Boron Doped Diamond Biosensor for Detection of Escherichia coli.* Journal of Agricultural and Food Chemistry, 2008. **56**(17): p. 7691-7695.
228. Togo, C., et al., *Novel detection of Escherichia coli β-d-glucuronidase activity using a microbially-modified glassy carbon electrode and its potential for faecal pollution monitoring.* Biotechnology Letters, 2007. **29**(4): p. 531-537.
229. Mulchandani, P., et al., *Amperometric microbial biosensor for p-nitrophenol using Moraxella sp.-modified carbon paste electrode.* Biosensors & Bioelectronics, 2005. **21**(3): p. 523-527.
230. Honarbakhsh, M., et al., *Development of a thermostable beta-glucuronidase-based reporter system for monitoring gene expression in hyperthermophiles.* Biotechnology and Bioengineering, 2012. **109**(7): p. 1881-1886.
231. Tao, Y.B., et al., *Isolation and characterization of an ubiquitin extension protein gene (JcUEP) promoter from Jatropha curcas.* Planta, 2015. **241**(4): p. 823-836.
232. Sahoo, D.K., et al., *Comparative analysis of synthetic DNA promoters for high-level gene expression in plants.* Planta, 2014. **240**(4): p. 855-875.
233. Aich, S., L.T.J. Delbaere, and R. Chen, *Expression and Purification of Escherichia coli β-Glucuronidase.* Protein Expression and Purification, 2001. **22**(1): p. 75-81.
234. Feng, S. and J.D. Song, *Relationship of beta-glucuronidase to differentiation and invasion of human colorectal carcinoma.* Chinese Medical Journal, 1999. **112**(9): p. 854-857.

235. Waszkiewicz, N., et al., *Serum beta-glucuronidase as a potential colon cancer marker: a preliminary study.* Postepy Higieny I Medycyny Doswiadczalnej, 2015. **69**: p. 436-439.
236. Lemke, T.L. and D.A. Williams, *Foye's Principles of Medicinal Chemistry*. 2012, PA, United States: Lippincott Williams & Wilkins.
237. Castellanos, A., et al., *Size-Exclusion "Capture and Release" Separations Using Surface-Patterned Poly(N-isopropylacrylamide) Hydrogels.* Langmuir, 2007. **23**(11): p. 6391-6395.
238. Tsujikawa, K., et al., *Optimized conditions for the enzymatic hydrolysis of alpha-hydroxytriazolam-glucuronide in human urine.* Journal of Health Science, 2004. **50**(3): p. 286-289.
239. Kamata, T., et al., *Optimized glucuronide hydrolysis for the detection of psilocin in human urine samples.* Journal of Chromatography B, 2003. **796**(2): p. 421-427.
240. Ganji, F., S. Vasheghani-Farahani, and E. Vasheghani-Farahani, *Theorectical Description of Hydrogel Swelling: A Review.* Iranian Polymer Journal, 2010. **19**(5): p. 375-398.
241. Kaith, B., et al., *Temperature, pH and electric stimulus responsive hydrogels from Gum ghatti and polyacrylamide-synthesis, characterization and swelling studies.* Der Chemica Sinica, 2010. **1**(2): p. 44-54.
242. Falciatore, A., F. Formiggini, and C. Bowler, *Reporter Genes and In Vivo Imaging*. Molecular Plant Biology, ed. P.M. Gilmartin and C. Bowler. Vol. 2. 2002, United Kingdom: Oxford University Press.
243. Gu, Y.-e., et al., *Investigation of photoelectrocatalytic activity of Cu2O nanoparticles for p-nitrophenol using rotating ring-disk electrode and application for electrocatalytic determination.* Electrochimica Acta, 2010. **56**(2): p. 953-958.
244. Zhu, S., et al., *Single-walled carbon nanohorn as new solid-phase extraction adsorbent for determination of 4-nitrophenol in water sample.* Talanta, 2009. **79**(5): p. 1441-1445.
245. Lupu, S., et al., *Electrochemical sensors based on platinum electrodes modified with hybrid inorganic-organic coatings for determination of 4-nitrophenol and dopamine.* Electrochimica Acta, 2009. **54**(7): p. 1932-1938.
246. Shang, J., Z. Shao, and X. Chen, *Chitosan-based electroactive hydrogel.* Polymer, 2008. **49**(25): p. 5520-5525.
247. O'Grady, M.L., P.-l. Kuo, and K.K. Parker, *Optimisation of Electroactive Hydrogel Actuators.* ACS Applied Materials & Interfaces, 2010. **2**(2): p. 343-346.
248. Engel, L., et al., *Actuation of a novel Pluronic-based hydrogel: Electromechanical response and the role of applied current.* Sensors and Actuators B: Chemical, 2014. **191**: p. 650-658.
249. Sundaram, S., et al., *In situ stabilization of hydroxylamine via electrochemical immobilization of 4-nitrophenol on GCE/MWCNT electrodes: NADH electrocatalysis at zero potential.* Analytical Methods, 2014. **6**(22): p. 8894-8900.
250. Yin, H., et al., *Electrochemical oxidative determination of 4-nitrophenol based on a glassy carbon electrode modified with a hydroxyapatite nanopowder.* Microchimica Acta, 2010. **169**(1-2): p. 87-92.
251. Naficy, S., et al., *Modulated release of dexamethasone from chitosan–carbon nanotube films.* Sensors and Actuators A: Physical, 2009. **155**(1): p. 120-124.

252. Bussy, C., H. Ali-Boucetta, and K. Kostarelos, *Safety Considerations for Graphene: Lessons Learnt from Carbon Nanotubes.* Accounts of Chemical Research, 2012. **46**(3): p. 692-701.
253. Liu, H.-W., et al., *Characterization and drug release behavior of highly responsive chip-like electrically modulated reduced graphene oxide-poly(vinyl alcohol) membranes.* Journal of Materials Chemistry, 2012. **22**(33): p. 17311-17320.
254. Gambhir, S., et al., *Anhydrous organic dispersions of highly reduced chemically converted graphene.* Carbon, 2014. **76**: p. 368-377.
255. Filip, J., et al., *A hyaluronic acid dispersed carbon nanotube electrode used for a mediatorless NADH sensing and biosensing.* Talanta, 2011. **84**(2): p. 355-361.
256. Miao, W., G. Shim, and K. Choong Mo, *Cholesteryl hyaluronic acid-coated, reduced graphene oxide nanosheets for anti-cancer drug delivery.* Biomaterials, 2013. **34**(37): p. 9638-9647.
257. Lynam, C., S.E. Moulton, and G.G. Wallace, *Carbon-nanotube biofibers.* Advanced Materials, 2007. **19**(9): p. 1244-1248.
258. Razal, J.M., K.J. Gilmore, and G.G. Wallace, *Carbon nanotube biofiber formation in a polymer-free coagulation bath.* Advanced Functional Materials, 2008. **18**(1): p. 61-66.
259. Moulton, S.E., et al., *Liquid crystal behavior of single-walled carbon nanotubes dispersed in biological hyaluronic acid solutions.* Journal of the American Chemical Society, 2007. **129**(30): p. 9452-9457.
260. Jiang, D., J. Liang, and P.W. Noble, *Hyaluronan in tissue injury and repair*, in *Annual Review of Cell and Developmental Biology*. 2007, Annual Reviews: Palo Alto. p. 435-461.
261. Zhang, Q., et al., *Synthesis of amphiphilic reduced graphene oxide with an enhanced charge injection capacity for electrical stimulation of neural cells.* Journal of Materials Chemistry B, 2014. **2**(27): p. 4331-4337.
262. Xu, Y., et al., *Strong and ductile poly(vinyl alcohol)/graphene oxide composite films with a layered structure.* Carbon, 2009. **47**(15): p. 3538-3543.
263. Zhang, L., et al., *High strength graphene oxide/polyvinyl alcohol composite hydrogels.* Journal of Materials Chemistry, 2011. **21**(28): p. 10399-10406.
264. Yang, X., et al., *Well-dispersed chitosan/graphene oxide nanocomposites.* ACS Applied Materials and Interfaces, 2010. **2**(6): p. 1707-1713.
265. Faghihi, S., et al., *Graphene oxide/poly(acrylic acid)/gelatin nanocomposite hydrogel: Experimental and numerical validation of hyperelastic model.* Materials Science and Engineering: C, 2014. **38**: p. 299-305.
266. Suss, M.E., et al., *Impedance-based study of capacitive porous carbon electrodes with hierarchical and bimodal porosity.* Journal of Power Sources, 2013. **241**: p. 266-273.
267. Amin, M., et al., *Synthesis and characterization of thermo- and pH-responsive bacterial cellulose/acrylic acid hydrogels for drug delivery.* Carbohydrate Polymers, 2012. **88**(2): p. 465-473.
268. Gupta, P., K. Vermani, and S. Garg, *Hydrogels: from controlled release to pH-responsive drug delivery.* Drug Discovery Today, 2002. **7**(10): p. 569-579.
269. Omidian, H. and K. Park, *Swelling agents and devices in oral drug delivery.* Journal of Drug Delivery Science and Technology, 2008. **18**(2): p. 83-93.

270. Yao, Y.J., et al., *Equilibrium and kinetic studies of methyl orange adsorption on multiwalled carbon nanotubes.* Chemical Engineering Journal, 2011. **170**(1): p. 82-89.
271. Tsai, T.H., S.C. Chiou, and S.M. Chen, *Enhancement of Dye-Sensitized Solar Cells by using Graphene-TiO2 Composites as Photoelectrochemical Working Electrode.* International Journal of Electrochemical Science, 2011. **6**(8): p. 3333-3343.
272. Ma, J., et al., *Enhanced Adsorptive Removal of Methyl Orange and Methylene Blue from Aqueous Solution by Alkali-Activated Multiwalled Carbon Nanotubes.* Acs Applied Materials & Interfaces, 2012. **4**(11): p. 5749-5760.
273. Wang, Y., et al., *Microporous spongy chitosan monoliths doped with graphene oxide as highly effective adsorbent for methyl orange and copper nitrate (Cu(NO3)2) ions.* Journal of Colloid and Interface Science, 2014. **416**: p. 243-251.
274. Wang, Y.L., et al., *Graphite Oxide: Preparation and Removal Ability of Cationic Dyes.* Chinese Journal of Inorganic Chemistry, 2012. **28**(2): p. 391-397.
275. Ekiz, O.Ö., et al., *Reversible Electrical Reduction and Oxidation of Graphene Oxide.* ACS Nano, 2011. **5**(4): p. 2475-2482.
276. Ganguly, K., et al., *Polysaccharide-based micro/nanohydrogels for delivering macromolecular therapeutics.* Journal of Controlled Release, 2014. **193**: p. 162-173.
277. Shewan, H.M. and J.R. Stokes, *Review of techniques to manufacture micro-hydrogel particles for the food industry and their applications.* Journal of Food Engineering, 2013. **119**(4): p. 781-792.
278. Mudassir, J., Y. Darwis, and P.K. Khiang, *Prerequisite Characteristics of Nanocarriers Favoring Oral Insulin Delivery: Nanogels as an Opportunity.* International Journal of Polymeric Materials and Polymeric Biomaterials, 2015. **64**(3): p. 155-167.
279. Chavda, H.V., et al., *Preparation and characterization of superporous hydrogel based on different polymers.* International Journal of Pharmaceutical Investigation, 2012. **2**(3): p. 134-9.
280. Gumusderelioglu, M., D. Erce, and T.T. Demirtas, *Superporous polyacrylate/chitosan IPN hydrogels for protein delivery.* Journal of Materials Science-Materials in Medicine, 2011. **22**(11): p. 2467-2475.
281. Kuang, J., K.Y. Yuk, and K.M. Huh, *Polysaccharide-based superporous hydrogels with fast swelling and superabsorbent properties.* Carbohydrate Polymers, 2011. **83**(1): p. 284-290.
282. Sahiner, N. and F. Seven, *Energy and environmental usage of super porous poly(2-acrylamido-2-methyl-1-propan sulfonic acid) cryogel support.* RSC Advances, 2014. **4**(45): p. 23886-23897.
283. Dinu, M., et al., *Morphogical and swelling properties of porous hydrogels based on poly(hydroxyethyl methacrylate) and chitosan modulated by ice-templating process and porogen leaching.* Journal of Polymer Research, 2013. **20**(11): p. 1-10.
284. Sahiner, N., F. Seven, and H. Al-Lohedan, *Super-fast hydrogen generation via super porous Q-P(VI)-M cryogel catalyst systems from hydrolysis of NaBH4.* International Journal of Hydrogen Energy, 2015. **40**(13): p. 4605-4616.
285. Sahiner, N. and F. Seven, *The use of superporous p(AAc (acrylic acid)) cryogels as support for Co and Ni nanoparticle preparation and as reactor in*

H-2 production from sodium borohydride hydrolysis. Energy, 2014. **71**: p. 170-179.
286. Shi, X., Jietang, and A. Wang, *Development of a superporous hydroxyethyl cellulose-based hydrogel by anionic surfactant micelle templating with fast swelling and superabsorbent properties.* Journal of Applied Polymer Science, 2015. **132**(23): p. 42027.
287. Shi, X., W. Wang, and A. Wang, *pH-responsive sodium alginate-based superporous hydrogel generated by an anionic surfactant micelle templating.* Carbohydrate Polymers, 2013. **94**(1): p. 449-455.
288. Bao, J., et al., *A novel foaming approach to prepare porous superabsorbent poly(sodium acrylic acid) resins.* Journal of Applied Polymer Science, 2015. **132**(3): p. 41298.
289. Elbert, D.L., *Liquid–liquid two-phase systems for the production of porous hydrogels and hydrogel microspheres for biomedical applications: A tutorial review.* Acta Biomaterialia, 2011. **7**(1): p. 31-56.
290. Spiller, K.L., et al., *Superporous hydrogels for cartilage repair: Evaluation of the morphological and mechanical properties.* Acta Biomaterialia, 2008. **4**(1): p. 17-25.
291. Omidian, H., J.G. Rocca, and K. Park, *Advances in superporous hydrogels.* Journal of Controlled Release, 2005. **102**(1): p. 3-12.
292. Bruice, P.Y., *Organic Chemistry 7th Edition*. 2013, NJ, United States: Prentice Hall.
293. Hermanson, G.T., *Bioconjugate Techniques*. Vol. 3rd edition. 2013, UK: Academic Press.
294. Xue, F., et al., *Two-dimensional inverse opal hydrogel for pH sensing.* Analyst, 2014. **139**(23): p. 6192-6196.
295. Li, T., et al., *Voltammetric behavior of carboxyl hydrogel particles on a cavity electrode surface.* Electrochimica Acta, 2014. **130**: p. 22-28.
296. Texter, J., *Templating hydrogels.* Colloid and Polymer Science, 2009. **287**(3): p. 313-321.
297. Wang, G.-L., et al., *The pH-dependent interaction of silver nanoparticles and hydrogen peroxide: A new platform for visual detection of iodide with ultra-sensitivity.* Talanta, 2013. **107**: p. 146-153.
298. Neumann, C.C.M., et al., *Performance of silver nanoparticles in the catalysis of the oxygen reduction reaction in neutral media: Efficiency limitation due to hydrogen peroxide escape.* Nano Research, 2013. **6**(7): p. 511-524.
299. Gudarzi, D., et al., *Factors affecting catalytic destruction of H2O2 by hydrogenation and decomposition over Pd catalysts supported on activated carbon cloth (ACC).* Catalysis Today, 2015. **248**: p. 69-79.
300. Ding, J., Q. Zhong, and S.L. Zhang, *Catalytic efficiency of iron oxides in decomposition of H2O2 for simultaneous NOX and SO2 removal: Effect of calcination temperature.* Journal of Molecular Catalysis a-Chemical, 2014. **393**: p. 222-231.
301. Lee, H., et al., *pH-Dependent reactivity of oxidants formed by iron and copper-catalyzed decomposition of hydrogen peroxide.* Chemosphere, 2013. **92**(6): p. 652-658.
302. Yin, J., et al., *A hydrogen peroxide electrochemical sensor based on silver nanoparticles decorated silicon nanowire arrays.* Electrochimica Acta, 2011. **56**(11): p. 3884-3889.

303. Blanco-Brieva, G., et al., *Selective decomposition of hydrogen peroxide in the epoxidation effluent of the HPPO process.* Catalysis Today, 2012. **187**(1): p. 168-172.
304. Omidian, H. and K. Park, *Experimental design for the synthesis of polyacrylamide superporous hydrogels.* Journal of Bioactive and Compatible Polymers, 2002. **17**(6): p. 433-450.
305. Omidian, H., D. Mastropietro, and U. Kandalam, *Swelling, strength, and biocompatibility of acrylate-based superporous hydrogel hybrids.* Journal of Bioactive and Compatible Polymers, 2014. **29**(1): p. 66-80.
306. Park, K., J. Chen, and H. Park, *Hydrogel composites and superporous hydrogel composites having fast swelling, high mechanical strength, and superabsorbent properties*, 2001, US Patent US6271278 B1: United States.
307. Zhao, C., G. Zhang, and L. Zhao, *Effect of curing agent and temperature on the rheological behavior of epoxy resin.* Molecules, 2012. **17**(7): p. 8587-8594.
308. Pramanik, M., E. Fowler, and J. Rawlins, *Cure kinetics of several epoxy–amine systems at ambient and high temperatures.* Journal of Coatings Technology and Research, 2014. **11**(2): p. 143-157.
309. Calvert, P.D., S.Z. Erhan, and Z. Liu, *Extrusion freeform fabrication of soybean oil-based composites by direct deposition, 2002*, in *WO2002042391 A2*2002: United States.
310. Li, P., et al., *A polycationic antimicrobial and biocompatible hydrogel with microbe membrane suctioning ability.* Nature Materials, 2011. **10**(2): p. 149-156.
311. Ng, V.W.L., et al., *Antimicrobial hydrogels: A new weapon in the arsenal against multidrug-resistant infections.* Advanced Drug Delivery Reviews, 2014. **78**: p. 46-62.
312. Archana, D., et al., *Chitosan-PVP-nano silver oxide wound dressing: In vitro and in vivo evaluation.* International Journal of Biological Macromolecules, 2015. **73**: p. 49-57.
313. Boonkaew, B., et al., *Development and Characterization of a Novel, Antimicrobial, Sterile Hydrogel Dressing for Burn Wounds: Single-Step Production with Gamma Irradiation Creates Silver Nanoparticles and Radical Polymerization.* Journal of Pharmaceutical Sciences, 2014. **103**(10): p. 3244-3253.
314. Abou-Yousef, H. and S. Kamel, *High efficiency antimicrobial cellulose-based nanocomposite hydrogels.* Journal of Applied Polymer Science, 2015. **132**(31): p. 42327.
315. Malmsten, M., *Antimicrobial and antiviral hydrogels.* Soft Matter, 2011. **7**(19): p. 8725-8736.
316. Madigan, M.T., et al., *Brock Biology of Microorganisms 13th Edition*. 2010, San Francisco, CA: Benjamin Cummings.
317. Linley, E., et al., *Use of hydrogen peroxide as a biocide: new consideration of its mechanisms of biocidal action.* Journal of Antimicrobial Chemotherapy, 2012. **67**(7): p. 1589-1596.
318. Kim, J.S., et al., *Antimicrobial effects of silver nanoparticles.* Nanomedicine: Nanotechnology, Biology and Medicine, 2007. **3**(1): p. 95-101.
319. Sondi, I. and B. Salopek-Sondi, *Silver nanoparticles as antimicrobial agent: a case study on E. coli as a model for Gram-negative bacteria.* Journal of Colloid and Interface Science, 2004. **275**(1): p. 177-182.

320. Shrivastava, S., et al., *Characterization of enhanced antibacterial effects of novel silver nanoparticles.* Nanotechnology, 2007. **18**(22): p. 225103.
321. Feng, Q.L., et al., *A mechanistic study of the antibacterial effect of silver ions on Escherichia coli and Staphylococcus aureus.* Journal of Biomedical Materials Research, 2000. **52**(4): p. 662-668.
322. Giovanni, M. and M. Pumera, *Size Dependant Electrochemical Behavior of Silver Nanoparticles with Sizes of 10, 20, 40, 80 and 107 nm.* Electroanalysis, 2012. **24**(3): p. 615-617.
323. Pourjavadi, A. and G.R. Mahdavinia, *Superabsorbency, pH-sensitivity and swelling kinetics of partially hydrolyzed chitosan-g-poly(acrylamide) hydrogels.* Turkish Journal of Chemistry, 2006. **30**(5): p. 595-608.

Appendix

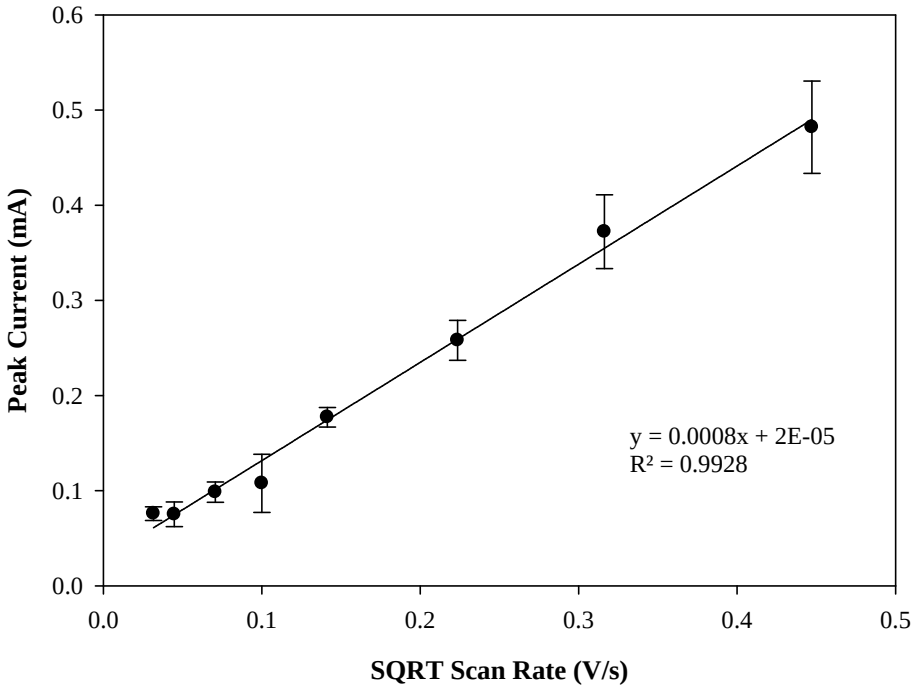

Figure A-1.1 Scan rate study of a carbon cloth electrode modified with a single dipcoat of hydrogel in ferri/ferrocyanide (2 mM) in KCl (1 M). (n=3)

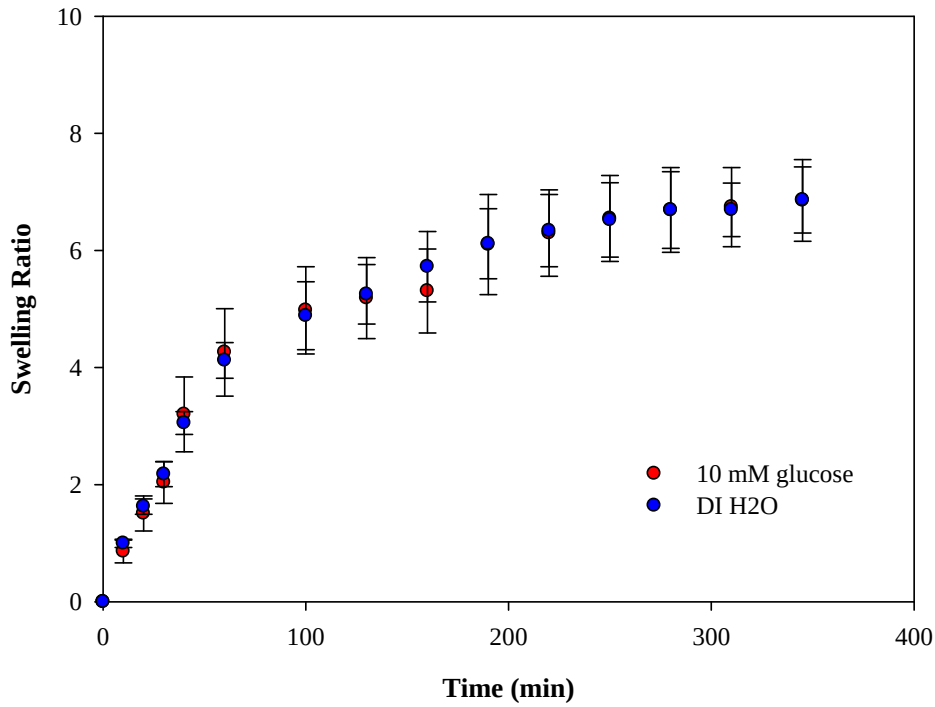

Figure A-1.2 Swelling profile of hydrogels without GOx incorporated over time. (n=3)

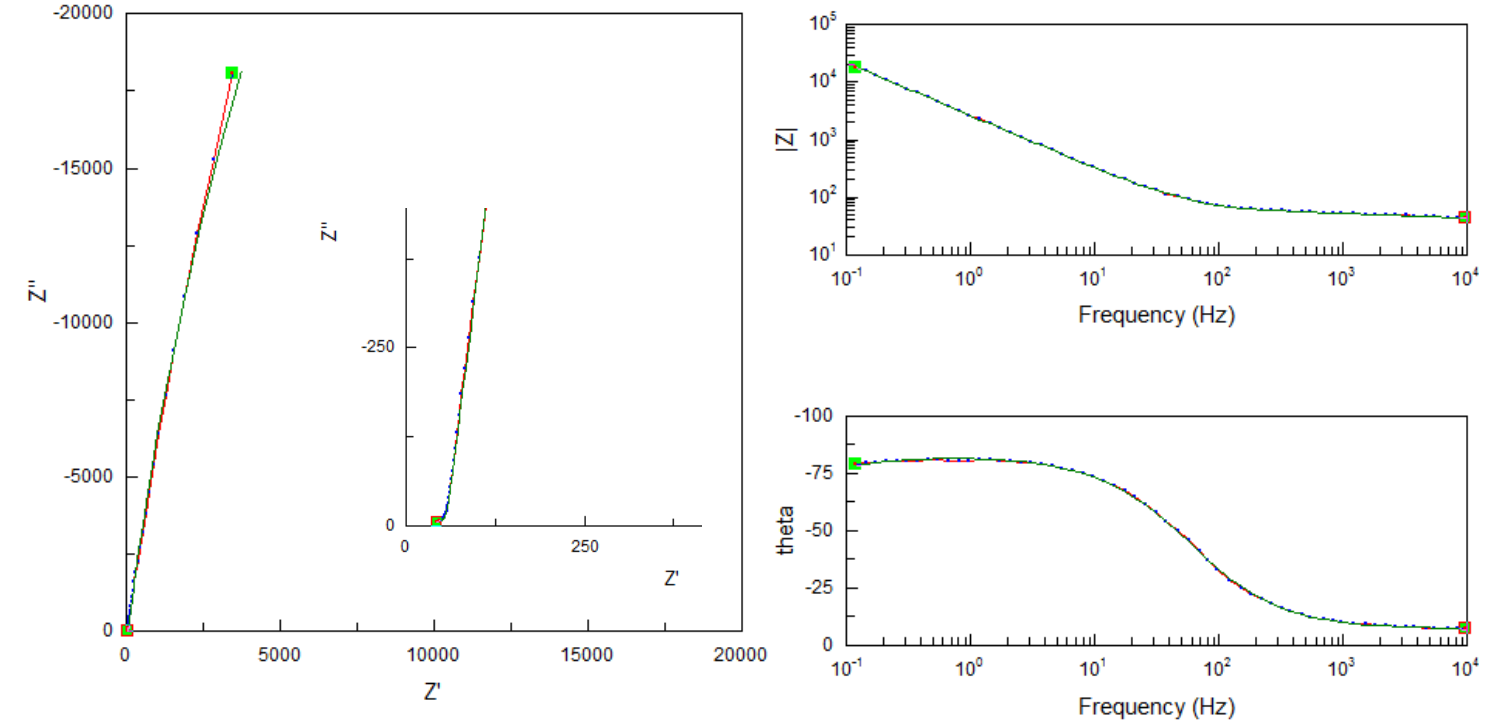

Figure A-1.3 Example of fitted impedance spectra of a glucose-sensitive hydrogel after swelling in 50 µM glucose using ZView. (Data points are blue, interconnected with a red line, and the fit is shown in green)

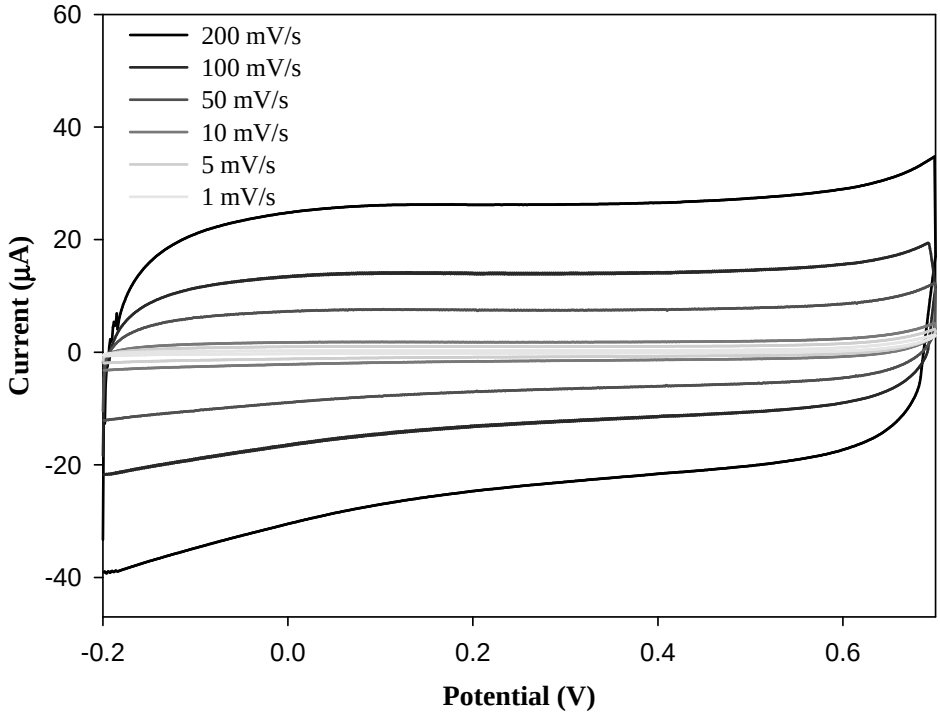

Figure A-3.1 Cyclic voltammograms of a 5% (w/w) rGO-hydrogel modified carbon cloth electrode in PBS (10 mM).